

# Supramolecular assembly of functionalized polymers

Straightforward synthesis and dynamic investigations of individual nanostructures

## Dissertation

zur Erlangung des akademischen Grades  
doctor rerum naturalium (Dr. rer. nat.)



---

seit 1558

vorgelegt dem Rat der  
Chemisch-Geowissenschaftlichen Fakultät  
der Friedrich-Schiller-Universität Jena

von Diplom-Chemiker Ulrich Mansfeld  
geboren am 07.08.1982 in Lutherstadt Eisleben

Gefördert durch das Dutch Polymer Institute (DPI), Projekt #622.

Gutachter:

1. Prof. Dr. Ulrich S. Schubert (Friedrich-Schiller-Universität Jena)
2. Prof. Dr. Felix H. Schacher (Friedrich-Schiller-Universität Jena)

Tag der öffentlichen Verteidigung: 14.05.2014

*Für meine Familie*





# Table of content

Table of content.....	5
Documentation of authorship.....	7
1 Introduction.....	11
2 Functionalization of polymers via “click” binding sites polymerized by NMP.....	13
3 Assembly of telechelics with supramolecular binding sites polymerized by NMP in a one-step procedure.....	19
3.1 Homotelechelic towards supramolecular polymers.....	21
3.2 Heterotelechelic towards orthogonal supramolecular polymers.....	23
3.3 Heterotelechelic towards A(B) <sub>2</sub> A quasi-triblock copolymers.....	25
4 Assembly of fluorinated copolymers in solution.....	27
5 Investigation of polymer assemblies in ionic liquids by electron microscopy.....	31
5.1 Ionic liquids as intrinsic staining media.....	33
5.2 Investigation of motion and dynamics of polymeric assembly.....	36
Summary.....	43
Zusammenfassung.....	47
References.....	51
Supplementary information.....	59
List of abbreviations.....	65
Publication list.....	67
Curriculum vitae.....	71
Acknowledgment.....	73
Declaration of authorship/Selbstständigkeitserklärung.....	75
Publications P1– P7.....	77



## Documentation of authorship

This section contains a list of the individual authors' contributions to the publications reprinted in this thesis.

P1) U. Mansfeld, C. Pietsch, R. Hoogenboom, C. R. Becer, U. S. Schubert, "Clickable initiators, monomers and polymers in controlled radical polymerizations – a prospective combination in polymer science", *Polym. Chem.* **2010**, *1*, 1560-1598.

U. Mansfeld:	Conceptual development, preparation of the manuscript: chapters 2, 3, 4.3 and parts of chapters 4.1, 5 and 6
C. Pietsch:	Conceptual development, preparation of the manuscript: chapters 4.2, 7 and parts of chapters 3.3, 4.1, 5 and 6
R. Hoogenboom:	Correction of the manuscript, supervision
C. R. Becer:	Preparation of the manuscript: introduction, conclusion
U. S. Schubert:	Correction of the manuscript, supervision

P2) U. Mansfeld, A. Winter, M. D. Hager, R. Hoogenboom, W. Günther, U. S. Schubert, "Orthogonal self-assembly of stimuli-responsive supramolecular polymers using one-step prepared heterotelechelic building blocks", *Polym. Chem.* **2013**, *4*, 113-123.

U. Mansfeld:	Synthesis and characterization of compounds, conception and preparation of the manuscript
A. Winter:	Supervision, preparation and correction of the manuscript
M. D. Hager:	Supervision, preparation and correction of the manuscript
W. Günther:	1D and 2D NMR experiments
R. Hoogenboom:	Correction of the manuscript, supervision
U. S. Schubert:	Correction of the manuscript, supervision

P3) U. Mansfeld, A. Winter, M. D. Hager, W. Günther, E. Altuntas and U. S. Schubert, "A homotelechelic bis-terpyridine macroligand: One-step synthesis and its metallo-supramolecular self-assembly" *J. Polym. Sci., Part A: Polym. Chem.* **2013**, *51*, 2006-2015.

U. Mansfeld:	Synthesis and characterization of compounds, conception and preparation of the manuscript
A. Winter:	Supervision, preparation and correction of the manuscript
M. D. Hager:	Supervision, preparation and correction of the manuscript
W. Günther:	1D and 2D NMR experiments
E. Altuntas:	ESI-MS measurement
U. S. Schubert:	Correction of the manuscript, supervision

P4) U. Mansfeld, A. Winter, M. D. Hager, G. Festag, S. Hoepfener and U. S. Schubert, "Amphiphilic supramolecular A(B)<sub>2</sub>A quasi-triblock copolymers", *Polym. Chem.* **2013**, *4*, 3177-3181.

U. Mansfeld: Synthesis and characterization of compounds, TEM measurements, conception and preparation of the manuscript  
A. Winter: Supervision, preparation and correction of the manuscript  
M. D. Hager: Supervision, preparation and correction of the manuscript  
G. Festag: SEC measurements  
S. Hoepfener: AFM measurements  
U.S. Schubert: Correction of the manuscript, supervision

P5) U. Mansfeld, S. Hoepfener, K. Kempe, J.-M. Schumers, J.-F. Gohy and U. S. Schubert, "Tuning the morphology of triblock terpoly(2-oxazoline)s containing a 2-phenyl-2-oxazoline block with varying fluorine content", *Soft Matter* **2013**, *9*, 5966-5974.

U. Mansfeld: TEM measurements, conception and preparation of the manuscript  
S. Hoepfener: TEM measurements, conception, preparation and correction of the manuscript, supervision  
K. Kempe: Synthesis and characterization of the compounds  
J.-M. Schumers: DLS measurements  
J.-F. Gohy: DLS measurements and correction of the manuscript  
U. S. Schubert: Supervision, correction of the manuscript

P6) U. Mansfeld, S. Hoepfener, C. Guerrero-Sanchez, J.-F. Gohy and U. S. Schubert, "Polymer nanostructures in ionic liquids: From staining to motion", *Microsc. Microanal.* **2013**, submitted.

U. Mansfeld: TEM measurements and preparation of the manuscript: chapter 3  
S. Hoepfener: TEM measurements and preparation of the manuscript: chapters 1, 2  
C. Guerrero-Sanchez: Synthesis of the polymers: chapters 1, 2  
J.-F. Gohy: DLS measurements  
U. S. Schubert: Supervision, correction of the manuscript

P7) U. Mansfeld, S. Hoepfner and U. S. Schubert, “Investigating the motion of diblock copolymer assemblies in ionic liquids by *in-situ* electron microscopy”, *Adv. Mater.* **2013**, *25*, 761-765.

U. Mansfeld:	TEM measurements, analysis of results, preparation of the manuscript
S. Hoepfner:	Analysis of results, preparation of the manuscript, correction of the manuscript
U. S. Schubert:	Supervision, correction of the manuscript

Declaration of the supervisor:

---

(Prof. Dr. Ulrich S. Schubert)



# 1. Introduction

Supramolecular assembly of matter on the nanoscale is one of the key issues to understand processes in biological systems and to advance the control over novel properties such as reversibility and responsiveness in modern materials' science.<sup>1</sup> Thereon, the preparation of well-defined adaptive macromolecular architectures is a main challenge in today's polymer science with respect to materials with potential self-healing and responsive properties.<sup>2-4</sup>

The immense progress in controlled polymerization techniques over the last 18 years provides these days straightforward access to advanced macromolecules.<sup>5-6</sup> Following the invention of the living anionic polymerization by Szwarc *et al.* in the 1950s,<sup>7</sup> controlled radical polymerizations have been widely studied.<sup>5-6,8</sup> One of the most significant controlled radical polymerization (CRP) techniques is the nitroxide-mediated radical polymerization (NMP). This technique tolerates a wide range of functional groups while providing polymers for various applications without traces of metal ions.<sup>9</sup> Moreover, a crucial challenge is to expand the range of side- and endfunctional groups that can be implemented to the macromolecules while maintaining the control over the polymerization. Recent attention is focussed on "click" functionalities as introduced by Sharpless *et al.*<sup>10</sup> that are under certain precautions compatible with CRPs to gain access to a variety of multifunctional well-defined polymeric architectures *via* efficient, high-yield linking reactions under mild conditions.<sup>11-12</sup>

Although excellent control over the molecular structure is thereby generally assured, these systems lack intramolecular adaptivity and do not allow to control a more complex 3D order when compared to natural macromolecules. This ordered self-assembly and adaptivity to the environment of natural systems is based on non-covalent interactions as reversible linkages caused by the highly dynamic binding equilibrium.<sup>1</sup> Such non-covalent interactions are represented by solvophobic and ionic interactions as well as hydrogen bonding and metal-to-ligand coordination.<sup>3</sup> The incorporation of such interactions into polymers enable the responsiveness against external stimuli, *e.g.* changes in temperature, pH value, redox potential and concentration.<sup>13-14</sup> Among the non-covalent interactions, metal-to-ligand coordination and hydrogen bonding can offer both, reversibility and directionality – essential features for the formation of complex supramolecular polymers.<sup>15-17</sup> Prominent examples are 2,2':6',2''-terpyridine<sup>18-19</sup> (tpy) as a tridentate ligand for metal coordination and 2-ureido-4[1*H*]-pyrimidinone<sup>20</sup> (UPy) as a self-complementary quadruple hydrogen bonding that are orthogonal to each other. The incorporation of different non-covalent interactions expands thereby the range of responsiveness of such a system against external stimuli and offers the opportunity to selectively address the interactions, if they are orthogonal to each other.<sup>4,21-22</sup>

Beyond the self-assembly of polymers by spatial-defined non-covalent binding sites such as hydrogen bonding or metal complexation entities, supramolecular assembly can be driven by more general attractive and/or repulsive forces between covalently linked polymer segments with each other or with selective solvents.<sup>23</sup> Thereby the self-assembly is driven by the unfavorable mixing enthalpy in combination with low mixing entropy, which is classified by the Flory-Huggins parameters.<sup>24-25</sup> In addition, the morphology is also determined by the volume fractions of the polymer segments classified by the packing parameters introduced by Israelachvili.<sup>26</sup> Already well-known diblock polymers exhibit multiple morphologies in solution ranging from multi-shaped micellar, lamellar, and bicontinuous structures.<sup>23</sup> Due to

their stability these assemblies represent appealing nanostructures for biomaterials, templating and catalytic applications.<sup>27-31</sup> The assembly of triblock copolymers in solution introduces additional assembly parameters and, thus, even more complexity that expands the morphologies towards multicompartmentalized aggregates (*e.g.* raspberry-like micelles<sup>32-33</sup> or tube walled vesicles<sup>34</sup>) and enables hierarchical super-assembly.<sup>35</sup> These advanced morphologies require incompatibility of the solvophobic blocks to each other and are of particular interest for multifunctional carriers in drug delivery.<sup>36</sup> Promising candidates for well-defined core domain segregation are fluoro-functionalized triblock terpolymers due to their intrinsic incompatibility against lipophilic and hydrophilic segments. Different types of fluoro-functionalized polymers were reported with fluorine *e.g.* (i) in the side chain (*e.g.* perfluorinated alkyl chains<sup>37-38</sup> or fluorinated phenyl rings<sup>39</sup>) or in the main chain.<sup>33</sup> In some cases the tremendous interfacial tension prevails the entropic penalty leading to “super strong segregation”<sup>40-41</sup> which enables, *e.g.*, flattening of interfaces<sup>42</sup> or unusual aggregation<sup>43</sup> leading to advanced morphologies including raspberry-like micelles, hamburger-like micelles or segmented worms.<sup>36</sup>

For high resolution imaging of such individual nanostructure, transmission electron microscopy represents a powerful characterization tool, in particularly, for morphologies in solution.<sup>44-45</sup> However, since solutions of common-used organic solvents have to be vitrified upon investigation to sustain the high vacuum conditions required for TEM, drawbacks arise from, *e.g.*, time-consuming preparation, low contrast of organic structures and cryogenic (cryo) artifacts. Furthermore, the investigation of dynamic processes *via* cryoTEM only allows for “snap-shots” leading to tentative models of hierarchical self-assembly and the evolution of morphology transitions. To overcome this drawbacks a liquid environment compatible with the high vacuum of TEM would be necessary. A class of neoteric liquids that gained popularity in many applications in the last decade are ionic liquids (IL). They exhibit unique characteristics such as negligible vapor pressure, high electroconductivity and provide tunable properties (*e.g.* viscosity, proticity and polarity) by a distinct anion-cation combination.<sup>46-48</sup> Among the possible applications, IL can be used as matrices for high vacuum analyses<sup>49</sup> and as potential selective solvents for the assembly of *e.g.* block copolymers.<sup>50-51</sup> The combination is promising for dynamic investigations of individual polymer assemblies in liquid TEM.

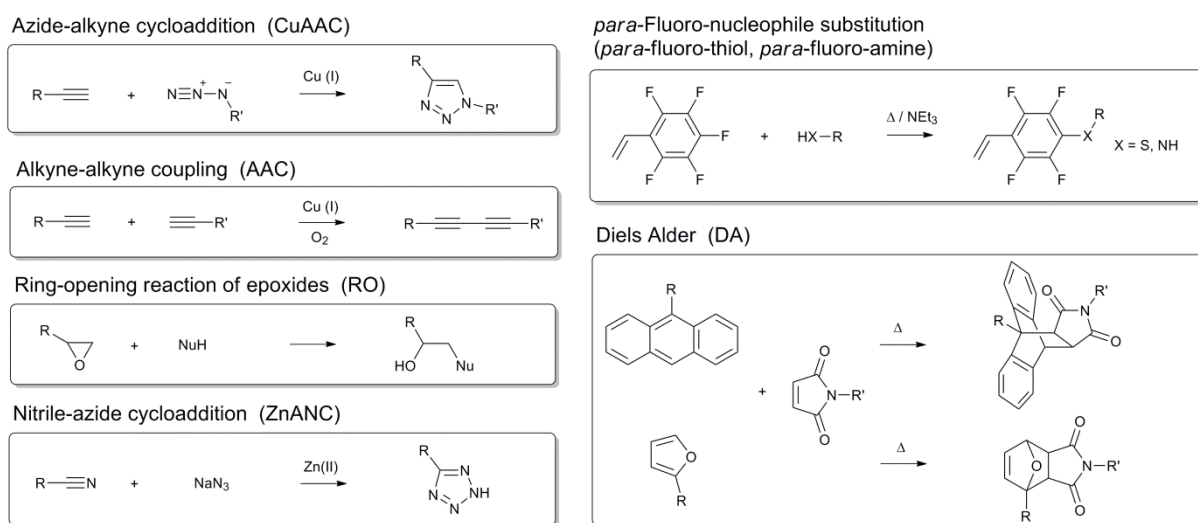
In this thesis, different strategies to implement functional groups into macromolecular structures polymerized by NMP in a controlled way are elucidated and the most promising paths are evaluated in comparison to the reversible addition fragmentation chain transfer (RAFT) polymerization and the atom transfer radical polymerization (ATRP) (Chapter 2). Using these concepts, different kinds of supramolecular assemblies of precise functionalized polymers were investigated including: (i) Responsive linear supramolecular assembly of spatial-defined homotelechelic or heterotelechelic polymers in non-selective solvents (Chapter 3.1 and 3.2), (ii) advanced supramolecular self-assembly of side-chain functionalized ABC triblock terpolymers in selective solvents (Chapter 4) and (iii) a combination of both, *i.e.* supramolecular block copolymers in selective solvents (Chapter 3.3). Moreover, ionic liquids were introduced as liquid matrices in TEM acting as selective solvents for various block copolymers (Chapter 5). This combination could be used to investigate for the first time motional and dynamic processes of individual assemblies on the nanometer scale.



## 2. Functionalization of polymers via “click” binding sites polymerized by NMP

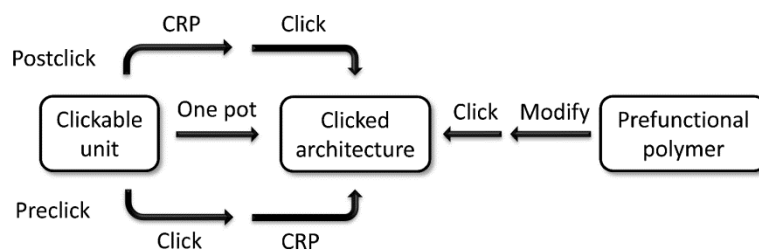
Parts of this chapter have been published: A1) U. Mansfeld, C. Pietsch, R. Hoogenboom, C. R. Becer, U. S. Schubert, *Polym. Chem.* **2010**, *1*, 1560-1598.

One of the most prominent controlled radical polymerization (CRP) techniques is the nitroxide-mediated radical polymerization (NMP) tolerating a wide range of functional groups while providing metal-free polymers for various applications.<sup>9</sup> A crucial challenge is to expand the range of side- and end-functional groups that can be implemented to the macromolecules while maintaining the control over the polymerization. The vast developments of diverse click reactions motivated the combination of such reactions and precursor units with controlled radical polymerization techniques as they are found to be stable under certain conditions.<sup>12</sup> In particular, metal-free click reactions have attracted attention in recent years since they are lacking metal-catalysts representing the main disadvantage of the prominent copper-catalyzed azide-alkyne cycloaddition.<sup>52</sup> This opens new avenues to rapid and efficient reactions that can be employed, *e.g.*, in biological systems.<sup>53</sup> An overview over the click-like reactions that are reported with NMP is given in Scheme 2.1.



**Scheme 2.1** Schematic representation of the click reactions that have been used in combination with NMP.

The prominent copper-catalyzed azide-alkyne 1,3-dipolar cycloaddition (CuAAC) has been employed in various fields of synthetic chemistry, in particular, in organic chemistry.<sup>10</sup> In addition, Glaser coupling was applied as a copper-catalyzed alkyne-alkyne homocoupling reaction (AAC).<sup>54</sup> Beside alkynes, also nitriles can react with azides in a zinc-catalyzed cycloaddition (ZnANC) that can be used in combination with NMP.<sup>55</sup> Furthermore, thiol compounds are employed for new click reactions due to their high reactivity towards common functional groups.<sup>12</sup> Among those is the efficient nucleophilic substitution of the *para*-fluorine of pentafluorophenyl under ambient conditions that is reported for thiols.<sup>56</sup> Commonly, the Diels-Alder reaction (DA) has been employed to construct star polymers or to engineer self-healing polymers.<sup>57-58</sup> The ring-opening reaction of epoxides as well-known



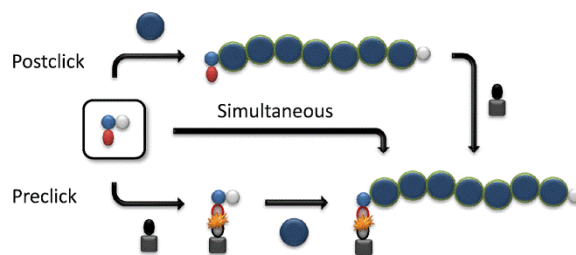
**Figure 2.1** Schematic overview of the different pathways towards clicked architectures.

spring-loaded reaction<sup>10</sup> is used in combination with NMP mostly to introduce other clickable functionalities or for the attachment to surfaces.<sup>59</sup> Besides, other metal-free click-like reactions such as cycloalkyne-azide cycloaddition,<sup>60</sup> thiol-maleimide addition,<sup>61</sup> thiol-alkene radical addition,<sup>62</sup> thiol-alkyne radical addition,<sup>63</sup> thiol-isocyanate addition,<sup>62</sup> cycloaddition of alkynes with nitrile oxides,<sup>64</sup> or *O*-hydroxylamine-carbonyl addition<sup>65</sup> are recently reported with ATRP or RAFT and might be also applicable with NMP in near future.

There are at least four common ways to combine NMP and click chemistry (Figure 2.1). In a postclick strategy (poC), functional initiators or monomers with clickable moieties are polymerized towards clickable polymers that can be clicked post to the polymerization. As a limitation, the clickable moiety must not interfere with the polymerization process or has to be protected. Hereon, this approach has a wide scope by means of construction flexibility in comparison to the preclick approach. The postclick approach offers high functional group fidelity compared to the postmodification approach. In the preclick strategy (prC), functional initiators or monomers with clickable moieties are clicked prior to the polymerization. This strategy is used if the clickable unit interferes with the polymerization and cannot be sufficiently protected. However, in contrast to the stable triazole ring, the Diels-Alder product may undergo a retro Diels-Alder during polymerization.<sup>66</sup> This procedure provides the highest control over the incorporation of the clicked functionality into polymeric architectures, while having the lowest scope by means of construction flexibility. The simultaneous/one pot strategy, where the polymerization and click reaction can happen at the same time, is up to now only relevant for ATRP.<sup>67</sup> The main advantage compared to the other strategies is the small number of purification steps.

By postmodification, prefunctional polymers with latent groups can be modified with clickable moieties to obtain clickable polymers. The modification reaction must be efficient, since it correlates to the fidelity of functional groups in the modified polymer. In this case, modification as well as clicking is carried out at the polymer, which in principle might complicate the purification and analysis, in particular for side-chain functionalization.

The use of functional initiators in CRP leads to terminal-functionalized polymers in one step, whereby the click reactions can be performed either after (postclick) or prior to the polymerization (preclick) (Figure 2.2). By using unimolecular initiators such as phenylethyl-alkylated (PhEt) 2,2,6,6-tetramethylpiperidinylnitroxide (TEMPO) and 2,2,5-trimethyl-4-phenyl-3-azahexane-3-nitroxide (TIPNO) functionalization on both the initiating and the mediating fragment is possible without influencing the control over the polymerization allowing for  $\omega$ -clickable and  $\alpha,\omega$ -clickable polymers in a one-step procedure.<sup>68-69</sup> Until now, clickable moieties are only attached to the initiating fragment due to the intrinsic higher end-

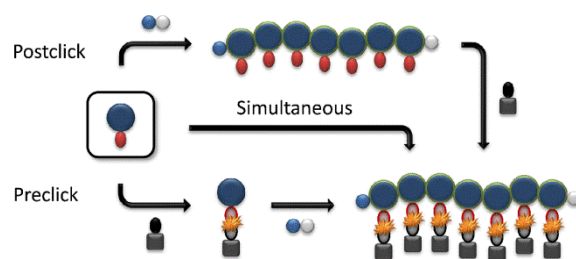


**Figure 2.2** Schematic representation of the different pathways using clickable initiators.

group fidelity. In contrast to the clickable monomer route (Figure 2.3), lower concentrations of the clickable units reduce side reactions upon polymerization, allowing for controlled polymerizations with high end-group fidelity.

Although for NMP only few examples were described up to now which is related to the higher reaction temperatures compared to other CRPs, it is the perfect match for the polymerization of styrene: An  $\alpha$ -alkyne-functionalized PhEt-TIPNO was used in the homopolymerization of styrene (St) resulting in  $\alpha$ -clickable PS.<sup>70</sup> Thereby, the *p*-phenylic-attached alkyne was trimethylsilyl-protected to inhibit side reactions during polymerization, *e.g.* H-abstraction, polymerization along the triple bond,<sup>71</sup> and addition of nitroxide radicals to the alkyne.<sup>72</sup> In addition,  $\alpha$ -alkyne-functionalized PhEt-TEMPO initiators were reported for the controlled homopolymerization of St without protecting the alkyne.<sup>73</sup> The higher stability of the alkyne is ascribed to the alkyl-spacer that avoids conjugation with the aromatic ring. Since NMP does not interfere with the azide-alkyne cycloaddition, either simultaneously (one-pot/one-step) or subsequently (one-pot/two-step) clicking an azide-functionalized polymer can be performed.<sup>74</sup> In contrast, *p*-(azidomethyl)phenylethyl-TIPNO was used in prC polymerization or postmodification of St due to the side reactions of the azide at 120 °C with the vinylic double bond of the monomer.<sup>70</sup> However, the preclicked triazole moiety revealed an influence on the polymerization of NiPAM and *n*-BA and required a rigid spacer to the alkoxyamine to suppress electronic and hydrogen bonding interactions.<sup>75</sup> Besides, also anthracene or furan-protected maleimide can be attached to TEMPO-initiators for Diels-Alder reactions, but can be only used in prC polymerization of St due to side reactions (*i.e.* retro-Diels Alder reaction) under NMP conditions.<sup>76</sup>

**Clickable monomers** can be used to synthesize pendant functionalized polymers (Figure 2.3) that can be easily modified in a grafting-onto approach *via* click chemistry. Thereby, the clickable monomer can be homopolymerized or copolymerized to obtain versatile random-, block- or comb polymers. In contrast to the initiator approach, side reactions involving the reactive click functionality are pronounced by the higher concentration of the monomer compared to the initiator. To circumvent such side reactions, either the clickable unit has to be protected or the polymerization time has to be reduced. According to this, the alkyne-functionalized monomers have to be protected by, *e.g.*, the trimethylsilyl group (TMS), because the terminal alkyne is known to be thermally unstable under NMP conditions causing radical addition to the triple bond.<sup>77</sup> Thereon, TMS-protected alkyne-functionalized styrene was copolymerized with St using PhEt-TIPNO as initiator in a controlled way with contents of the alkyne monomer up to 20%.



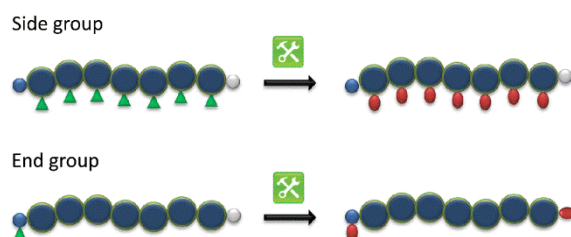
**Figure 2.3** Schematic representation of the different pathways using clickable monomers.

This post-click approach was used to prepare various random copolymers and amphiphilic diblock copolymers with acrylates.<sup>59,78</sup> By increasing the content of the protected alkyne monomer, control was lost, due to sterical hindrance and/or recombination of the nitroxide and the TMS group. This can be circumvented by either using an excess of free nitroxide or (ii) by implementing a methoxy group as a flexible spacer between the styrene and the alkyne moiety allowing for low molar mass homopolymers and diblock copolymers with pendant alkyne groups.<sup>79</sup> Furthermore TMS-protected propargyl acrylate and acrylamide can be randomly copolymerized with their parent monomers using PhEt-TIPNO as initiator,<sup>78</sup> while acrylonitrile that can be clicked *via* 1,3-dipolar cycloaddition with azide to the tetrazole ring can be polymerized with TEMPO/dibenzoylperoxide as a bimolecular initiator.<sup>80</sup> Due to the high temperature in NMP no azide-functionalized monomers were polymerized by NMP.

As a potential styrene derivative, pentafluorostyrene can be polymerized by NMP using the commercial available  $\beta$ -phosphonylated alkoxyamine (BlocBuilder) or a terpyridine-functionalized PhEt-TIPNO towards homopolymers and random or diblock copolymers with styrene. In a post-click approach, the *para*-fluorine can be substituted by functionalized amines or thiols under mild conditions.<sup>56</sup>

In addition, commercial available glycidyl methacrylate is thermally stable under NMP conditions and can be copolymerized with St using PhEt-TIPNO as initiator. Although subsequent ring opening of epoxides represents an efficient click reaction it is lacking selectivity and is mostly used as an efficient reaction to introduce more selective click binding sites.<sup>59</sup>

Postmodification reactions are used to transform latent functional groups into clickable units, whereby the polymer can be modified either at pendant or at terminal positions (Figure 2.4). The  $\alpha$ -terminus of the polymer is more preferred for modification in comparison to the  $\omega$ -terminus due to the intrinsic higher end-group fidelity caused by radical termination reactions during polymerization for the latter. As a consequence, polymerizations intended for  $\omega$ -postmodification were kept at low conversions.



**Figure 2.4** Schematic representation of the postmodification of the polymers side-chains or end-groups.

The most prominent approach for a postmodification on the  $\alpha$ -terminus in NMP (Figure 2.4) uses upon polymerization functionalized PhEt-TIPNO alkoxyamines with a *para*-benzylic chloro-group on the initiating fragment (Cl-CH<sub>2</sub>-PhEt-TIPNO) prior the substitution of the chlorine against azide with sodium azide.<sup>81</sup>

In contrast, modifications on the  $\omega$ -terminus deal with the exchange of the nitroxide moiety. In first experiments the propagating radical of polystyrene, polyisoprene and poly(*n*-butylacrylate) was trapped by *N*-functional maleimide at elevated temperatures.<sup>82</sup> In related experiments it was shown that *N*-pentafluorophenyl maleimide or protected *N*-propargyl maleimide could be incorporated into ATRP polymers.<sup>83</sup> Beside thermal cleavage of the nitroxide, oxidative cleavage of TIPNO-/TEMPO-terminated PS can be achieved under ambient conditions by single electron oxidation, where the resulting cation-terminated polymer can be trapped by nucleophiles such as propargyl alcohol.<sup>81</sup> Due to specific interactions neither BlocBuilder-terminated nor acrylates can be postmodified by this technique. The azide functionality could be introduced by modification of the TIPNO- or BlocBuilder-terminated PS at the  $\omega$ -terminus in a one-step procedure using an excess of an activated azide or in a two-step procedure, where the  $\omega$ -terminus is prior azidation activated by bromination.<sup>84</sup> Hereon, the azidation of nitroxide-terminated acrylates is not possible by the one-step technique.<sup>81</sup>

In contrast to modify end-groups, modification of pendant groups is more influenced by steric or electronic effects, in particular for homopolymers. Nonetheless, this method is applied if the direct polymerization of the desired clickable monomers is not possible. Thereon, acetyl-protected poly[styrene-*r*-(4-hydroxystyrene)] could be functionalized after deprotection with propargyl bromide in a Williamson ether reaction to yield the clickable styrenic copolymer.<sup>85</sup> Another efficient method is the carbodiimide-mediated condensation with functional amines. In a two-step reaction, a *t*-butyl protected diblock polymer poly(acrylic acid-*b*-styrene) was – after deprotection to the free poly(acrylic acid) – activated by a carbodiimide and under ambient conditions reacted with propargyl- or azido-functionalized amines.<sup>86</sup>

In a one-step reaction, succinimide-functionalized acrylates can be copolymerized with styrene, *t*-butylacrylate or acrylamide followed by the condensation with azide- or alkyne-functionalized amines, where the succinimide acts as a protecting and an activating group.<sup>78</sup> However the most prominent method to introduce azides in the side-chain is the substitution of benzylic chloride with sodium azide in polar media at room temperature. This approach was used to postmodify homopolymers as well as random and block copolymers of 4-(chloromethyl)styrene to the pendant azido derivatives.<sup>87</sup> Furthermore, the pendant benzylic chloro-group is also accessible for the etherification at room temperature with 9-(oxymethyl)anthracene in poly(styrene-*r*-4-(chloromethyl)styrene) towards the diene-functionalized polymer acting as the precursor for subsequent Diels Alder reactions.<sup>88</sup>

Click chemistry and NMP emerge as a potential combination: By utilizing the approaches of clickable initiator, clickable monomer and postmodification versatile types of highly functional tailor-made polymers become accessible such as (i) end-functional polymers on one or on both sites, (ii) mid-chain functional polymers, (iii) side-chain functional polymers and (iv) combinations of them that can act as selective building blocks for the preparation of more complex structures for potential applications in material science and

biology, *e.g.* cycles, star-shape polymers, dendrimers, networks as well as selective grafting, surface attachments and bioconjugation.

Although, the most prominent combinations of click chemistry and CRPs are nowadays (i) ATRP in combination with azide cycloaddition<sup>11</sup> and (ii) RAFT with thio-click chemistry,<sup>89</sup> NMP can be combined with various click reactions and has its own advantages in specific cases.<sup>9</sup> Thereon, NMP provides the most facile approaches for polymerization of styrene derivatives, while avoiding the sometimes inconvenient sulphur chemistry of the RAFT technique. Furthermore, it represents an alternative if the monomer interacts with the metal catalyst in ATRP or the absence of any traces of metal is required in combination with the upcoming metal-free click reactions, *e.g.*, for biological applications. In addition, with the use of alkoxyamines as unimolecular initiators in NMP, where functionalization of both the initiating as well as the mediating fragment do not disturb the polymerization, a versatile platform is at hand *via* the clickable/clicked initiator approach for the synthesis of tailor-made telechelic polymers with click binding sites.

### 3. Assembly of telechelics with supramolecular binding sites polymerized by NMP in a one-step procedure

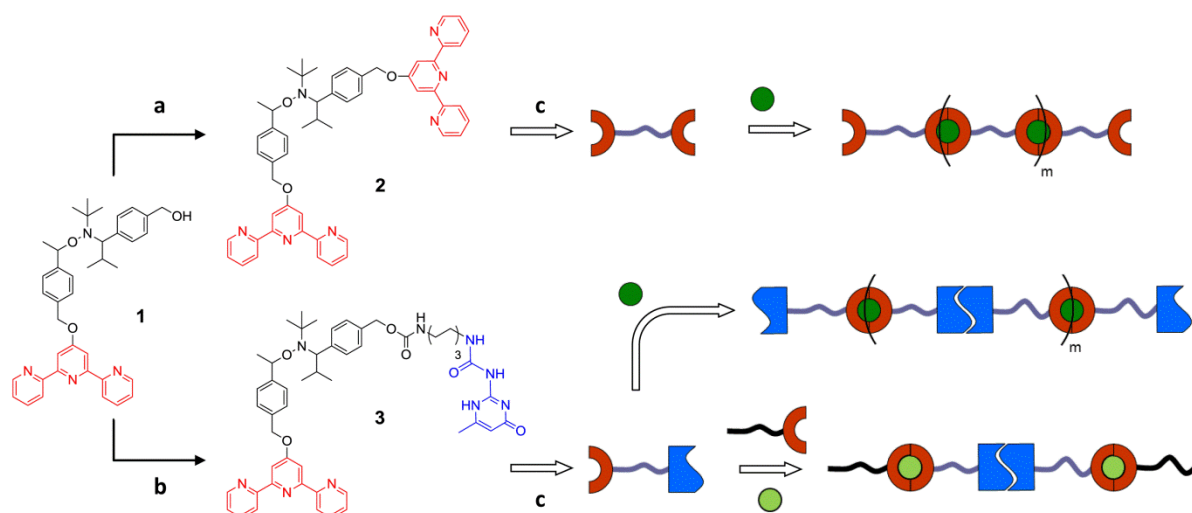
Parts of this chapter have been published: A2) U. Mansfeld, A. Winter, M. D. Hager, R. Hoogenboom, W. Günther, U. S. Schubert, *Polym. Chem.* **2013**, *4*, 113-123. A3) U. Mansfeld, A. Winter, M. D. Hager, W. Günther, E. Altuntas, U. S. Schubert, *J. Polym. Sci., Part A: Polym. Chem.* **2013**, *51*, 2006-2015. A4) U. Mansfeld, A. Winter, M. D. Hager, G. Festag, S. Hoepfner, U. S. Schubert, *Polym. Chem.* **2013**, *4*, 3177-3181.

The preparation of precise macromolecular architectures that contain spatial-defined supramolecular bonding sites is a main challenge in today's polymer science in particular with respect to self-healing and stimuli-responsive materials with controlled properties.<sup>2-4</sup> Prominent classes of non-covalent interactions that are orthogonal to each other are metal-to-ligand coordination, *e.g.* 2,2':6',2''-terpyridine,<sup>18-19</sup> (tpy) and hydrogen bonding, *e.g.* 2-ureido-4[1*H*]-pyrimidinone,<sup>20</sup> (UPy) that can offer both, reversibility and directionality representing crucial features for the formation of well-ordered supramolecular polymers.<sup>15-17</sup> The presence of orthogonal non-covalent interactions expands the range of responsiveness against external stimuli and enables the opportunity to selectively address them.<sup>4,21-22</sup>

As it was already discussed in Chapter 2 NMP-initiators tolerate a variety of functional or reactive groups. Functionalized TIPNO derivatives were initially reported by Hawker *et al.* as universal initiators in NMP featuring high end-group fidelity and high tolerance towards a broad range of functional groups.<sup>5,90</sup> This was proven to be also the case for tpy and UPy: Lohmeijer *et al.* expanded the scope of functional TIPNOs by using tpy-TIPNO, as initiator, for the synthesis of tpy-functionalized block copolymers *via* NMP.<sup>91</sup> The initial synthetic strategies towards telechelic polymers was based on a monofunctionalized initiator<sup>92</sup> with a postmodification to attach the second moiety. In contrast to ATRP and RAFT initiators, TIPNO-based alkoxyamines are even potential initiators in NMP if they bear bulky functional groups on both the initiating as well as the mediating fragment.<sup>68-69</sup> Hence, they can be used as difunctional initiators for the one-step preparation of  $\alpha,\omega$ -functionalized polymers. Hereon, we already reported the synthesis of the heterodifunctional alkoxyamine **3** as initiator for NMP bearing tpy and UPy as end-groups (Scheme 3.1).<sup>93</sup>

The functional initiator approach provides, compared to a postmodification approach, a higher versatility by means of construction flexibility, as the chain length and composition between the supramolecular binding sites can be varied in less reaction steps without compromising the end-group fidelity and purification can be simply performed by precipitation. This makes it appealing for studying the influence of the polymer spacer within supramolecular architectures.





**Scheme 3.1** Schematic representation of the investigated linear supramolecular architectures using the one-step procedure of difunctional initiators: (a)  $\text{Ph}_3\text{P}$ , DIAD, 2,2':6',2''-terpyridin-4'(1'*H*)-one, MeOH, 12 h, r.t.; (b) cat.  $\text{Sn}^{\text{II}}$ ,  $\text{CHCl}_3$ , 18 h, 65 °C; (c) styrene, anisole, 2 to 6 h, 125 °C.

In the summarized work, the formation of different types of linear supramolecular architectures were investigated using the strategy of difunctionalized initiators in NMP to construct complex structures in a minimum number of steps (Scheme 3.1): Homotelechelic macroligands polymerized by alkoxyamine **2** bearing two tpy units were used for the preparation of a linear homoleptic metallo-supramolecular polymers (Chapter 3.1). Heterotelechelic macroligands that were polymerized by alkoxyamine **3** bearing UPy and tpy as end-groups were used to engineer either linear orthogonal supramolecular polymers held together by homoleptic *bis*-tpy complexes and self-complementary UPy-dimers in an alternating fashion (Chapter 3.2) or quasi-triblock copolymers held together by heteroleptic *bis*-tpy complexes and self-complementary UPy-dimers (Chapter 3.3).



### 3.1 Homotelechels towards supramolecular polymers

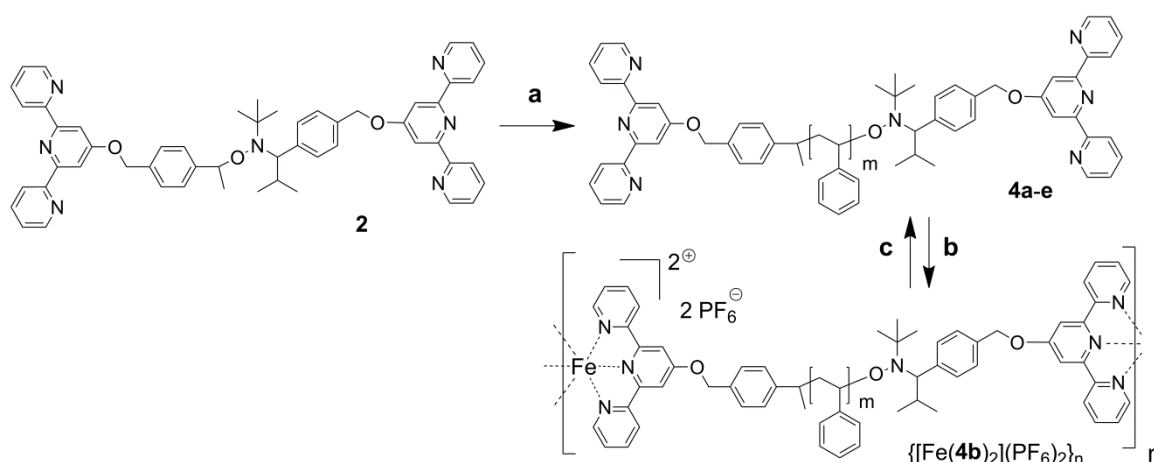
The homodifunctional alkoxyamine tpy-TIPNO-tpy (**2**, Scheme 3.1) was synthesized *via* Mitsunobu coupling<sup>94-95</sup> of 2,2':6',2''-terpyridin-4'(1'*H*)-one with the benzylic hydroxyl group of the nitroxide framework **1** (Scheme 3.1, reaction a) that was prepared in a multi-step procedure as reported previously.<sup>93</sup> The structure of tpy-TIPNO-tpy was confirmed by 1D/2D NMR spectroscopy and by mass spectrometry (MALDI-TOF MS, HR-ESI MS). The polymerization of styrene was investigated using **2** as initiator (Scheme 3.2, reaction a). The polymerization process was investigated up to a conversion of 40%, to ensure high end-group fidelity (Table 3.1).

**Table 3.1** Telechelic polystyrenes using alkoxyamine **2** as initiator at 125 °C with a monomer to initiator ratio of 200:1 and a monomer concentration of 3 mol L<sup>-1</sup>.

	time [min]	conv. [%] (GC)	$M_n$ [g/mol] (theo.) <sup>a</sup>	$M_n$ [g/mol] ( <sup>1</sup> H NMR)	$M_n$ [g/mol] (SEC) <sup>b,c</sup>	PDI (SEC)
<b>4a</b>	320	--	--	9,500	7,200	1.18
<b>4b</b>	380	40	9,300	12,100	10,100	1.17
<b>4c</b>	105	15	4,450	--	4,500	1.15
<b>4d</b>	245	23	6,150	--	6,000	1.18
<b>4e</b>	335	39	10,100	--	9,900	1.16

<sup>a</sup>  $M_n$  (theo.) represents the targeted  $M_n$  with respect to the conversion (GC); <sup>b</sup> after precipitation of the polymer into methanol; <sup>c</sup> a linear polystyrene calibration with DMA as eluent was used.

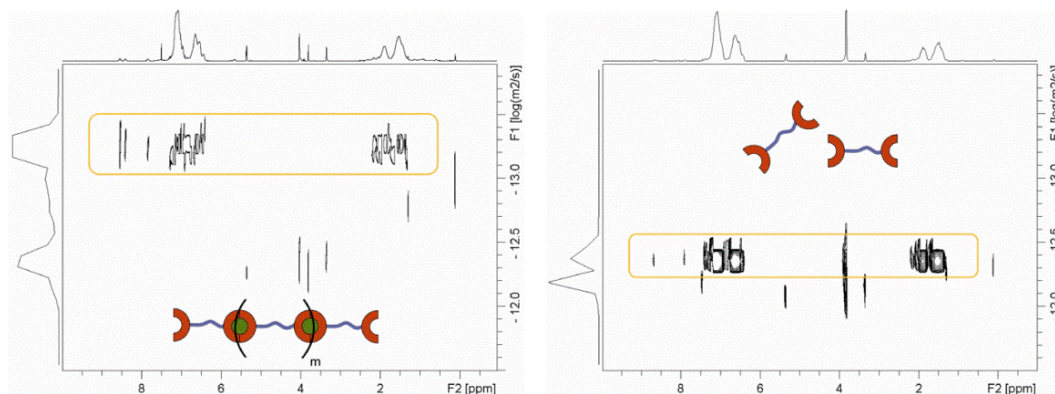
The polymerizations were controlled with  $M_n$  up to 10,000 g mol<sup>-1</sup> and PDI values below 1.2 which was confirmed by kinetic investigations, *i.e.* the semilogarithmic plot of the polymerization index ( $\ln([M_0]/[M])$ ) as a function of time and the plot for the molar mass *vs.* conversion revealed a linear dependency. The  $M_n$  values calculated from NMR seem to be overestimated while the values by SEC fit to the theoretical values (Table 3.1). For the end-group analysis, the structure of homotelechelic **4a** was confirmed by ESI-TOF MS revealing distributions of the fragment tpy-PS-TIPNO with an unusual cleavage of the second tpy at the benzylic bond that is ascribed to the ESI process rather than to thermal degradation during



**Scheme 3.2** Schematic representation of the polymerization with functional initiator **2** (a: styrene, anisole, 125 °C), homoleptic complexation with Fe<sup>II</sup> (b: (i) FeCl<sub>2</sub>, SnCl<sub>2</sub>, CHCl<sub>3</sub>/MeOH (ii) NH<sub>4</sub>PF<sub>6</sub>) and *in-situ* decomplexation (c: Na<sub>3</sub>(HEEDTA), MeOH).

polymerization. Moreover, a small distribution can indeed be related to the non-fragmented species proving the incorporation of both tpy onto the PS. In addition, 2D ( $^1\text{H}$ - $^1\text{H}$ ) diffusion-ordered spectroscopy (DOSY) confirmed that the tpy units were covalently attached to the polystyrene chain (Figure 3.1).

The complexation of divalent transition metal ions with tpy of the telechelic PS is used as a strong supramolecular driving force to engineer responsive high molar mass suprapolymers.<sup>96</sup> Hereon, Fe(II) is the most favored metal ion, since it forms *bis*-tpy complexes characterized by large binding constant with  $\log K_2 \gg \log K_1$ .<sup>97-98</sup> Despite the high complex stability constants the Fe(II) complexes are considered to be labile.<sup>99</sup> These characteristics ensure the formation of both responsive and high molar mass suprapolymers with insensitivity against deviating from the metal-to-ligand ratio of 1:1, which is likely by using macroligands with averaged masses. Metallopolymer  $\{[\text{Fe}(\mathbf{4b})_2](\text{PF}_6)_2\}_n$  was synthesized in the presence of stannous chloride to avoid oxidation of Fe(II) prior to coordination (Scheme 3.2, reaction b). An excess of the metal ion was used to ensure quantitative coordination of the macroligand and to suppress the formation of rings, as a ring-chain equilibrium is assumed for the flexible polymeric spacer.<sup>100</sup> 2D DOSY measurements revealed that PS and tpy signals arise from one macromolecular species, due to the same relative diffusion coefficients (Figure 3.1, left). The responsiveness of the metal complex linkages against an external stimuli was proven by *in-situ* addition of  $\text{Na}_3(\text{HEEDTA})$ , as strong competitive ligand (Scheme 3.2, reaction c): A tremendous decrease in molar mass due to the decomplexation of the metallopolymer  $\{[\text{Fe}(\mathbf{4b})_2](\text{PF}_6)_2\}_n$  towards  $\mathbf{4b}$  could be concluded from the significant decrease in the relative diffusion coefficients for the tpy and PS signals pointing to the absence of monomeric or low molar mass metallopolymer (Figure 3.1, right). However, no molar mass estimation could be performed *via* the Stoke-Einstein equation since the correlation between hydrodynamic radius and molar mass differ for the metallopolymer compared to the macroligand due to the partially ionic backbone. Moreover  $M_n$  can also not be determined by SEC since the Fe(II) *bis*-tpy complex is not stable under the conditions used for PS.<sup>101</sup> A theoretical  $M_n$  estimation of the coordination polymer in solution suggests  $M_n \approx 10^6 \text{ g mol}^{-1}$ , which is based on a ring-chain equilibrium model<sup>100</sup> and binding constants in organic solvents.<sup>98,102</sup> The presented model provides the construction of metallopolymeric architectures in a minimum number of steps, which makes it appealing for studying the influence of the polymeric spacer within complex supramolecular architectures with respect to the development of efficient stimuli-responsive materials.



**Figure 3.1** 2D  $^1\text{H}$ - $^1\text{H}$  DOSY spectra of  $\{[(\mathbf{4b})\text{Fe}(\mathbf{4b})](\text{PF}_6)_2\}_n$  (left) and  $\mathbf{6b}$  (right) (400 MHz,  $\text{CD}_2\text{Cl}_2$ , 298 K).

### 3.2 Heterotelechelic towards orthogonal supramolecular polymers

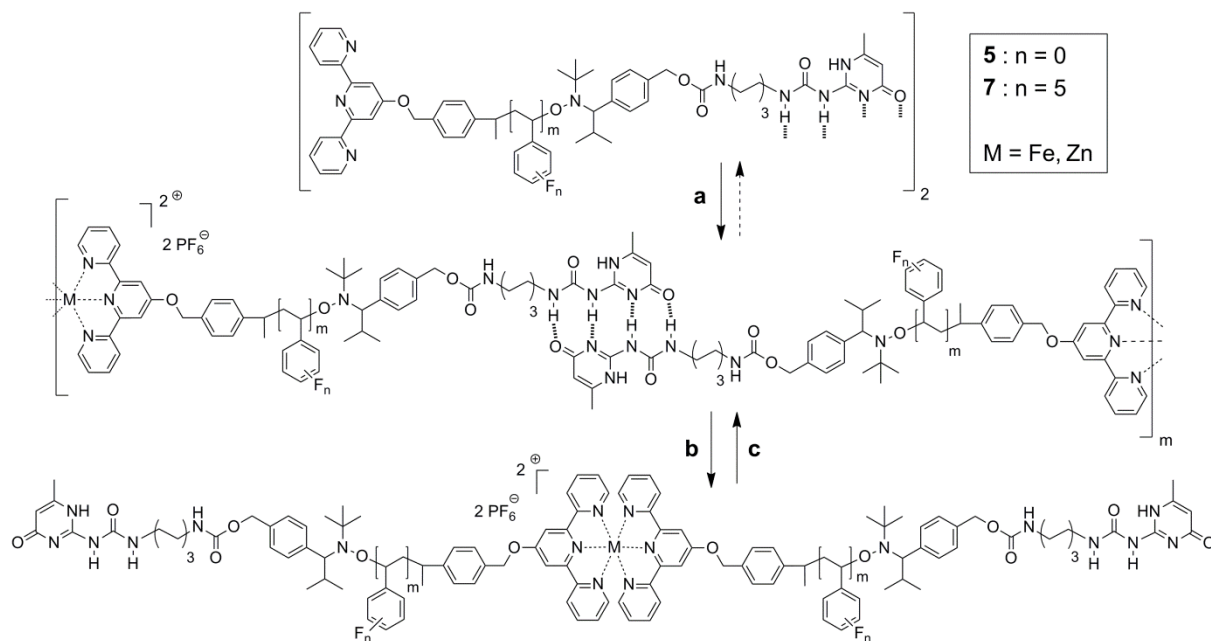
The synthesis of the heterodifunctional alkoxyamine tpy-TIPNO-Upy (**3**, Scheme 3.1) *via* stepwise functionalization has already been published using the isocyanate coupling of UPy with the key building block **1** in the last step (Scheme 3.1, reaction b).<sup>93</sup> The alkoxyamine **3** is proven to be an efficient initiator for the NMP of styrene up to  $M_n = 15,000 \text{ g mol}^{-1}$  and conversions up to 45% (Scheme 3.1, reaction c) while retaining both end-groups.<sup>103</sup> The focus of the present work was to built up linear supramolecular polymers using the heterotelechelic and to prove the orthogonal assembly and addressability (Scheme 3.3).

**Table 3.2** Details for nitroxide-mediated polymerizations using alkoxyamine **3** as initiator.

	time [min]	monomer	M/I	conv. [%] (GC)	$M_n$ [g/mol] theor. <sup>a</sup>	$M_n$ [g/mol] (SEC) <sup>b</sup>	PDI (SEC)
<b>5</b>	300	St	200	35	8,700	9,000	1.17
<b>6</b>	300	St	200	41	9,400	9,300	1.17
<b>7</b>	300	PFSt	200	-- <sup>c</sup>	-- <sup>c</sup>	10,500 <sup>d</sup>	1.11

<sup>a</sup>  $M_n$  (theor.) calc. from GC; <sup>b</sup> linear polystyrene calibration with DMAc; <sup>c</sup> bulk polymerization; <sup>d</sup> linear polystyrene calibration with chloroform.

For the present investigations heterotelechelic polystyrene **5** polymerized with tpy-TIPNO-Upy as initiator was used (Table 3.2). In addition, pentafluorostyrene (PFSt) was applied as monomer in NMP, yielding tpy-PPFS-UPy (**7**) (Table 3.2). As for styrene, good control over the polymerization was observed after 5 h in bulk with a  $M_n$  value of 10,500  $\text{g mol}^{-1}$  and a PDI value of 1.13. <sup>1</sup>H NMR spectroscopy confirmed the incorporation of both end-groups into the polymer in a 1:1 ratio, while in dichloromethane hydrogen-bonding signals point to the dimeric form (**6**)<sub>2</sub>. Molar mass calculations from <sup>1</sup>H NMR ( $M_n = 21,500 \text{ g mol}^{-1}$ ) confirm the UV-vis titration value ( $M_n = 18,500 \text{ g mol}^{-1}$ ) which shows, beside the formation of the

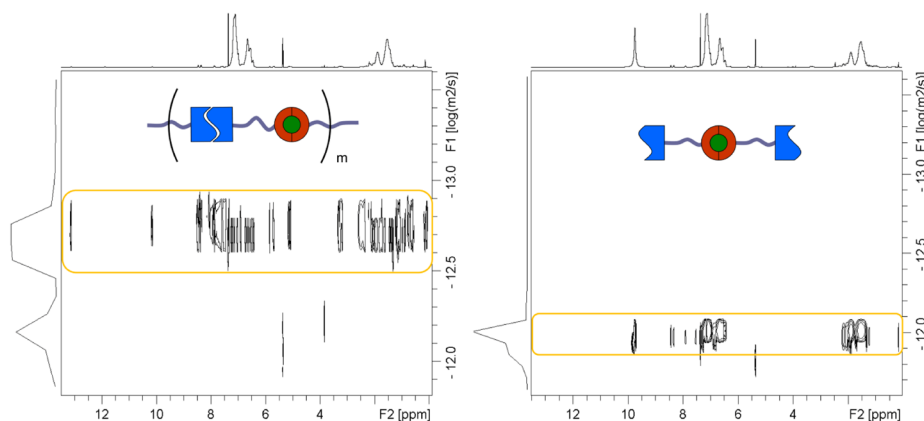


**Scheme 3.3** Schematic representation of the orthogonal assembly of  $\{[(\mathbf{5})\text{M}(\mathbf{5})](\text{PF}_6)_2\}_n$  and  $\{[(\mathbf{7})\text{Fe}(\mathbf{7})](\text{PF}_6)_2\}_n$ : (a) (i)  $\text{MCl}_2$ ,  $\text{SnCl}_2$ ,  $\text{CHCl}_3/\text{MeOH}$  (ii)  $\text{NH}_4\text{PF}_6$ ; (b) TFA and (c) washing with water.

metallopolymer with a PFSt spacers (Scheme 3.3, reaction a), the underestimation of  $M_n$  by SEC due to the unavailability of a suitable calibration standard. PFSt was polymerized to show that the initiator is suitable to prepare functionalized styrenes, while additional value arises in particular from the potential of a click-like side-chain modification *via* the *para*-fluoro position within supramolecular architectures.<sup>56,104-105</sup>

For the chain-extension *via* metal-ion coordination Fe(II) was chosen as the candidate since it can be characterized by NMR spectroscopy and is believed to form high molar mass suprapolymers upon complexation due to the characteristics mentioned in Chapter 3.1. Although such high molar mass polymers are not expected with zinc(II) compared to Fe(II), it was also used, as (i) it does not suffer from oxidation, (ii) can be characterized by NMR and (iii) is a candidate for self-healing materials due to its labile character. The metallo-polymers  $\{[(\mathbf{5})M(\mathbf{5})](PF_6)_2\}_n$  ( $M = Fe(II), Zn(II)$ ) were synthesized in a chloroform/methanol mixture at a 2:1 stoichiometry of macroligand to metal ions. In case of Fe(II) ions, an equimolar amount of stannous(II) chloride was added to the reaction mixture to prevent oxidation of Fe(II) to paramagnetic Fe(III) (Scheme 3.3, reaction a). SEC could not be performed, due to instability of Fe(II) or Zn(II) *bis*-tpy complexes under the measurement conditions used for PS.<sup>101</sup>  $^1H$  NMR spectra revealed quantitative shifts of the tpy signals while the hydrogen-bonding signals remained unchanged proving the orthogonal formation in dichloromethane.

More importantly, 2D DOSY measurements confirmed the presence of the two types of supramolecular bonds within the chain-extended polymer: The same relative diffusion coefficients was observed for the tpy, PS and UPy signals of  $\{[(\mathbf{5})Fe(\mathbf{5})](PF_6)_2\}_n$  (Figure 3.2, left). In contrast to the metallopolymer  $\{[Fe(\mathbf{4})_2](PF_6)_2\}_n$  in Chapter 3.1 the range of diffusion is broader, which can be related to the incorporation of the hydrogen bond junction within the backbone that is less stable in nature than the metal complex. Hereon, the molar mass of the suprapolymer could be neither calculated nor estimated since in the case of  $\{[Fe(\mathbf{5})_2](PF_6)_2\}_n$  an interplay of multiple kinetic and thermodynamic stabilities with respect to H-bonding and metal complexation has to be taken into account. The orthogonal responsiveness of the supramolecular entities was tested by *in-situ* addition of trifluoroacetic acid (TFA) (Scheme 3.3, reaction b): The H-bonding of the UPy dimer was cleaved without affecting the more pH-robust metal complex or the alkoxyamine as confirmed by  $^1H$  NMR spectroscopy. In fact, the disappearance of only the H-bonding signals and a significant change in the diffusion behavior confirmed the selective responsiveness that results in the disassembly of the

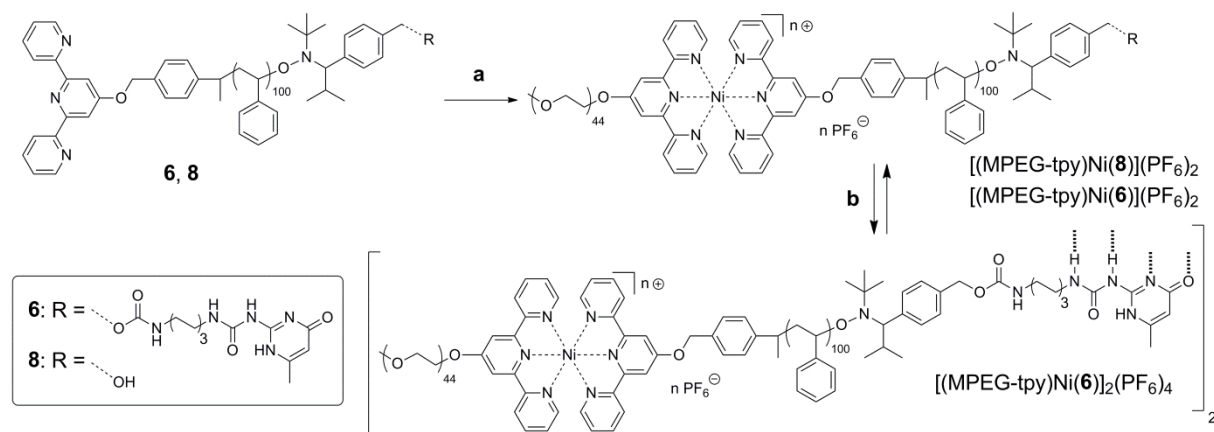


**Figure 3.2** 2D  $^1H$ - $^1H$  DOSY of  $\{[(\mathbf{5})Fe(\mathbf{5})](PF_6)_2\}_n$  (left) and  $[(\mathbf{5})Fe(\mathbf{5})](PF_6)_2$  (right) (400 MHz,  $CD_2Cl_2$ , 298 K).

suprapolymer  $\{[(\mathbf{5})\text{Fe}(\mathbf{5})](\text{PF}_6)_2\}_n$  towards the dimer  $[\text{Fe}(\mathbf{5})_2](\text{PF}_6)_2$  (Figure 3.2). The dimer  $[\text{Fe}(\mathbf{5})_2](\text{PF}_6)_2$  could be further decomplexed *in situ* towards the monomeric telechelic  $\mathbf{5}$  according to the decomplexation of  $\{[\text{Fe}(\mathbf{4})_2](\text{PF}_6)_2\}_n$  with  $\text{Na}_3(\text{HEEDTA})$  in Chapter 3.1, where the metal complex was addressed without affecting the alkoxyamine. The dimer  $[\text{Fe}(\mathbf{5})_2](\text{PF}_6)_2$  can be also assembled in reverse towards  $\{[(\mathbf{5})\text{Fe}(\mathbf{5})](\text{PF}_6)_2\}_n$  by washing the dichloromethane solution with water to remove the TFA (Scheme 3.3, reaction c). The self-assembly of the prepared building blocks towards linear supramolecular polymers with alternating metal-ion complex and hydrogen-bonding linkage was investigated showing beside stepwise assembly the selective addressability of the hydrogen bonding against pH value as an external stimulus since the hydrogen-bonding linkage were switched off without affecting the metal-ion complex.

### 3.3 Heterotelechelic towards A(B)<sub>2</sub>A quasi-triblock copolymers

The heterotelechelic macroligand tpy-PS<sub>m</sub>-UPy ( $\mathbf{6}$ ) was further used for the orthogonal assembly *via* self-complementary hydrogen bonding and heteroleptic metal-ion complexation with a monofunctional tpy-PEG to built up responsive amphiphilic supramolecular quasi-triblock copolymers PEG-PS||PS-PEG. While the route of heteroleptic Ru<sup>II</sup> tpy *bis*-complexes *via* stepwise self-assembly is established, relatively harsh reaction conditions are required.<sup>96</sup> Alternatively, a one-pot heteroleptic complexation with Ni(II) systems can be applied at room temperature due to an combination of an activated precursor and the characteristic kinetic stabilities of the Ni(II) mono-complexes in polar organic solvents.<sup>97-99,106-108</sup> The Ni complexation is, thus, suitable for the present one-pot strategy as it preserves the UPy end-group that is linked to the PS *via* the temperature-labile alkoxyamine. For comparison, a heterotelechelic tpy-PS<sub>m</sub>-OH ( $M_n = 11,400 \text{ g mol}^{-1}$ ; PDI 1.14) ( $\mathbf{8}$ ) was synthesized with alkoxyamine  $\mathbf{1}$  as initiator (Scheme 3.1, reaction c). This telechelic was used as a reference system that avoids the assembly *via* hydrogen bonding and, thus, maintains the AB diblock assembly in an aprotic, apolar environment. Scheme 3.4 represents the synthesized supramolecular block copolymers  $[(\text{MPEG-tpy})\text{Ni}(\mathbf{6})_2\text{Ni}(\text{tpy-MPEG})](\text{PF}_6)_n$  or  $[(\text{MPEG-tpy})\text{Ni}(\mathbf{8})](\text{PF}_6)_2$  following the procedure by Mugemana *et al.* (Scheme 3.4, reaction a).<sup>106</sup>



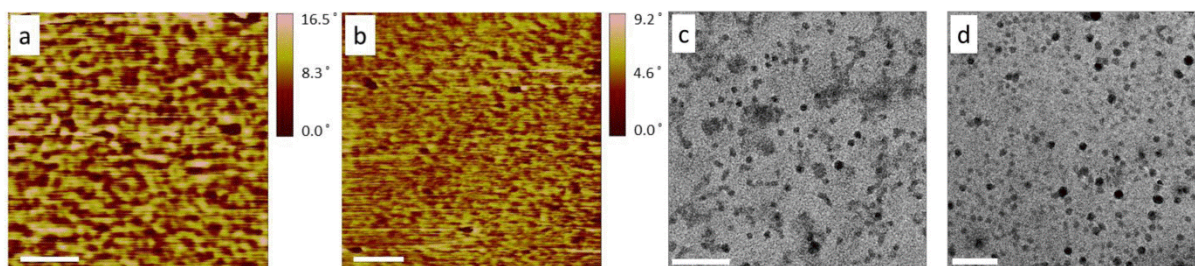
**Scheme 3.4** Schematic representation of the synthesis and assembly of the supramolecular quasi-triblock copolymer A(B)<sub>2</sub>A  $[(\text{MPEG-tpy})\text{Ni}(\mathbf{6})_2](\text{PF}_6)_4$  and the reference AB diblock copolymer  $[(\text{MPEG-tpy})\text{Ni}(\mathbf{8})](\text{PF}_6)_2$  [a: (i)  $\text{NiCl}_2$ , DMF (ii) MPEG-tpy,  $\text{NH}_4\text{PF}_6$ ; b: in  $\text{CH}_2\text{Cl}_2$ ].



The formation of the heteroleptic Ni(II) complexes is confirmed by SEC revealing a distinct shift of the RI traces and characteristic UV-vis absorption bands at 315 and 329 nm. Hydrogen bonding for the [(MPEG-tpy)Ni(**6**)](PF<sub>6</sub>)<sub>2</sub>, however, is suppressed by using DMAc/NH<sub>4</sub>PF<sub>6</sub> as a polar eluent to maintain the metal complexes. In contrast, <sup>1</sup>H NMR spectroscopy confirmed both: (i) The presence of hydrogen bonding forming dimers of [(MPEG-tpy)Ni(**6**)](PF<sub>6</sub>)<sub>2</sub> and (ii) the quantitative formation of Ni(II) complexes in dichloromethane (Scheme 3.4, reaction b). While the hydrogen bonding signals are observed at 10 to 13 ppm, the tpy signals cannot be observed due to the vicinity of the paramagnetic Ni(II) in the complex. The hydrogen bonding can be cleaved by adding an acid to the solution neither affecting the alkoxamine<sup>103</sup> nor the pH-insensitive Ni<sup>II</sup> *bis*-tpy complex.<sup>109</sup> The morphology of thin films of the metallopolymers were investigated by performing atomic force microscopy (AFM) on spin-coated films without prior annealing.<sup>110-112</sup> The films were spin-coated from a 2 wt% solution of toluene as an unpolar aprotic solvent allowing the self-complementary hydrogen bonding of the UPy moieties to form the quasi triblock copolymers (Figure 3.3a,b).

A non-ordered but visible phase separation was present for [(MPEG-tpy)Ni(**8**)](PF<sub>6</sub>)<sub>2</sub> (Figure 3.3a), while for [(MPEG-tpy)Ni(**6**)](PF<sub>6</sub>)<sub>2</sub> (Figure 3.3b) only a poor phase separation with smaller length scale was observed suggesting an influence of the hydrogen bonding on the solid state morphology and, thus, the formation of dimers towards [(MPEG-tpy)Ni(**6**)<sub>2</sub>Ni(tpy-MPEG)](PF<sub>6</sub>)<sub>n</sub>. The formation of the amphiphilic polymers *via* heteroleptic complexation was also confirmed for both polymers by the formation of micelles in a mixture of DMAc/water. Since these solvents are strong competitors for hydrogen bondings, both polymer systems are expected to assemble equally as AB amphiphiles (Figure 3.3c,d).

Attempts to assemble the systems in less polar and less protic solvents allowing for self-complementary hydrogen bonding *via* the UPy units are rather complex due to multiple interlinked parameters: The solubility of the metal complexes, selective solubility for PEG/PS, proticity, polarity combined with TEM preparation parameters such as freezing ability for film formation in cryoTEM and vapor pressure for dryTEM investigations. Therefore, different alternative molecular solvents were tested. While polymer assemblies were found in some solvents, no significant differences in assembly for the two systems were observed as it would be expected for AB and A(B)<sub>2</sub>A block copolymers (Figure S1). However, the system represents a model for the strategy of combining one-step polymerized telechelic building blocks with one-pot orthogonal assembly of supramolecular binding sites. This is promising for studying the influence of multiple supramolecular linkages on the self-assembly behavior of amphiphilic copolymers as the polymeric spacers can be easily varied.



**Figure 3.3** Morphology investigations in a spin-coated non-annealed film *via* AFM (phase images, hard tapping) of (a) [(MPEG-tpy)Ni(**8**)](PF<sub>6</sub>)<sub>2</sub> and (b) [(MPEG-tpy)Ni(**6**)<sub>2</sub>](PF<sub>6</sub>)<sub>4</sub> as well as in solution *via* dryTEM of (c) [(MPEG-tpy)Ni(**8**)](PF<sub>6</sub>)<sub>2</sub> and [(MPEG-tpy)Ni(**6**)](PF<sub>6</sub>)<sub>2</sub> (scale bars = 200 nm).

## 4. Assembly of fluorinated copolymers in solution

Parts of this chapter have been published: A5) U. Mansfeld, S. Hoepfener, K. Kempe, J.-M. Schumers, J.-F. Gohy, U. S. Schubert, *Soft Matter* **2013**, *9*, 5966–5974.

Beyond the self-assembly of polymers by spatial-defined non-covalent binding sites such as hydrogen-bonding or metal-complexation entities, supramolecular assembly can be driven by more general attractive and/or repulsive forces between covalently linked polymer segments with each other or with selective solvents.<sup>23</sup> Beside the simplest model of AB diblock copolymers, ABC triblock copolymers lead to even more complexity of morphologies if the solvophobic blocks are incompatible to each other. Promising candidates for well-defined core domain segregation are fluoro-functionalized triblock terpolymers due to their intrinsic incompatibility against the lipophilic and hydrophilic segments.<sup>36,42</sup>

In this respect, 2-oxazolines represent a well-suited monomer class for cationic ring-opening polymerization tolerating among a wide variety of functional groups<sup>113-114</sup> also fluorinated groups that result in well-defined polymeric architectures.<sup>115-116</sup> Recently, a linear fluorinated ABC terpoly(2-oxazoline) was reported consisting of 2-ethyl-2-oxazoline (EtOx), a 2-(1-ethylpentyl)-2-oxazoline (EPOx) and a 2-(2,6-difluorophenyl)-2-oxazoline block (DiFPhOx) (PDiFPhOx-*b*-PEPOx-*b*-PEtOx) that results in unique spiral disk-like structures.<sup>43</sup>

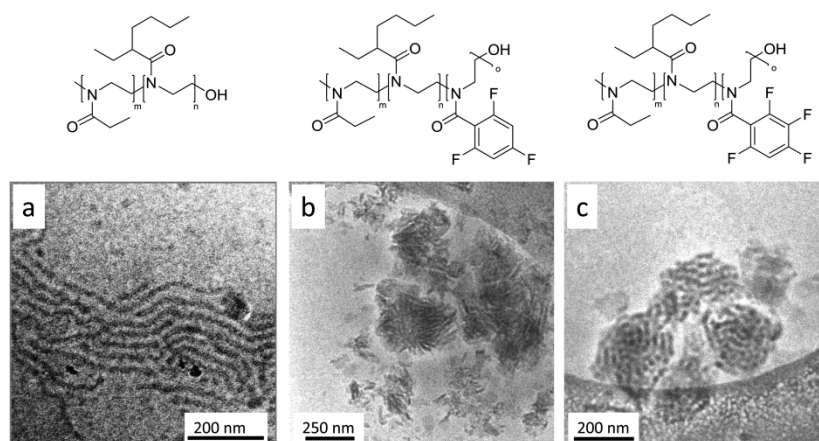
Based on the unique assembly of the fluorinated ABC terpoly(2-oxazoline) the influence of the fluorine content within the phenyl-2-oxazoline block on the morphology of the ABC terpolymer was investigated. For this purpose, a series of poly[2-ethyl-2-oxazoline-*block*-2-(1-ethylpentyl)-2-oxazoline-*block*-2-(*X*fluorophenyl)-2-oxazoline] (PEtOx-*b*-PEPOx-*b*-P*X*FPhOx) structure (*X* = tri, tetra, penta) was synthesized. Starting from PEtOx-*b*-PEPOx, the degree of fluorination of the p*X*FPhOx block was varied by polymerizing the related 2-(*X*fluorophenyl)-2-oxazoline according to literature procedures (Table 4.1).<sup>115,117</sup>

**Table 4.1** Series of the investigated fluorinated terpoly(2-oxazoline)s.

Copolymer	$M_n^a$ [g mol <sup>-1</sup> ]	PDI <sup>a</sup>	Molecular composition <sup>b</sup>		$R_h^c$ [nm]	PDI <sup>c</sup>
			theor.	exp.		
PEtOx- <i>b</i> -PEPOx	11,440	1.14	66/33/0	69/31/0	72	0.35
PEtOx- <i>b</i> -PEPOx- <i>b</i> -PTriFPhOx	14,900	1.15	50/25/25	52/34/14	209	0.21
PEtOx- <i>b</i> -PEPOx- <i>b</i> -PTetFPhOx	15,600	1.15	50/25/25	55/24/21	219	0.22
PEtOx- <i>b</i> -PEPOx- <i>b</i> -PPFPhOx	12,900	1.14	50/25/25	57/34/9	69/440	-/-

<sup>a</sup> SEC results (eluent: *N,N*-dimethylacetamide with 2.1 g L<sup>-1</sup> LiCl; PS standards); <sup>b</sup> determined using <sup>1</sup>H NMR spectroscopy; <sup>c</sup> from DLS measurements.

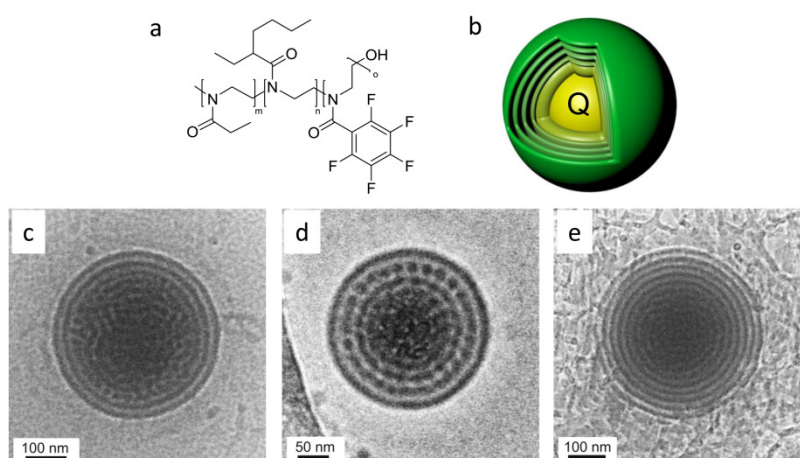
A direct comparison of the fluorinated terpolymers with each other has to be critically evaluated in this case. All investigated systems have slightly different block length ratios, which is why the difference in assembly can not be exclusively related to the degree of fluorination, but might also rely on, *e.g.*, the distinct block lengths. The assemblies of the oxazoline systems in aqueous solution (1 g L<sup>-1</sup>) was investigated by cryoTEM. Firstly, the cryoTEM of the diblock solution reveals spherical and cylindrical assemblies partially densely packed with dimensions of core and corona suggesting rod-like micelles (Figure 4.1a).



**Figure 4.1** Representative chemical structures and cryoTEM images of assemblies in 1 wt% aqueous solution of a) PEtOx-*b*-PEPOx, b) PEtOx-*b*-PEPOx-*b*-PTriFPhOx and c) PEtOx-*b*-PEPOx-*b*-PTetFPhOx.

By introducing the PTriFPhOx block, rod-like but mainly sheet-like features were observed that tend to stack towards extended aggregates of 200 nm to decrease the surface tension (Figure 4.1b). The transition from cylindrical assemblies of the diblock to the sheet-like assemblies of the fluorinated triblock can be promoted by the superstrong segregation behavior of fluorinated blocks which increases interfacial tension becoming the predominant assembly force.<sup>42</sup> The dimensions and the dark contrast of the core suggest a dense packing of the fluorinated blocks due to the superphobic character and stacking of the fluorinated phenyl rings caused by dipole interactions of the C-F bonds.<sup>118</sup> By increasing the fluorine content within PEtOx-*b*-PEPOx-*b*-PTetFPhOx, more defined super-aggregates of either entangled rod-like assemblies or stacked sheet-like features were found with the same dimensions as observed for PEtOx-*b*-PEPOx-*b*-PTriFPhOx (Figure 4.1c).

By further increasing the fluorine content of the PhOx block within PEtOx-*b*-PEPOx-*b*-PPFPhOx (Figure 4.2a), unique round-shaped super-aggregates were found (Figure 4.2c-e). In addition, a large number of worm-like micelles were observed that are attributed to kinetically frozen preformed structures<sup>119</sup> or a coexistent assembly due to small difference in

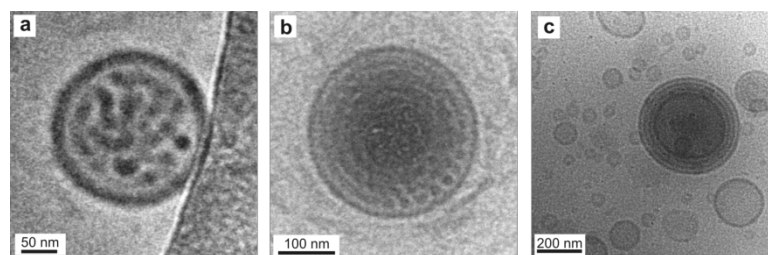


**Figure 4.2** Assembly studies of PEtOx-*b*-PEPOx-*b*-PPFPhOx in aqueous solution (1 wt%): a) Schematic representation of the chemical structure, b) the model of the coexistent lamellar/cubic phases (green/yellow) and c-e) representative cryoTEM images.



free energy.<sup>120</sup> The assembly of side products or educts can be excluded as the formation of the triblock was characterized by a low PDI value, a monomodal shape and a quantitative shift of the SEC traces. The spherical aggregates show different structural interiors ranging from assemblies similar to onion-like multilamellar vesicles, segregated concentric lamellar features to bicontinuous structures. A full characterization of the interior would require tomography series for 3D reconstruction, but the structures were not stable enough suffering from beam damage (see interior in Figure 4.2d). However, analysis of a large number of aggregates revealed that only spherical structures have been formed excluding cylindrical, disk-like or elliptical assemblies, since only round-shaped projections were observed. An explanation can be given by an angle-depended superstructure, described by a “ball of yarn” model: In contrast to the planar role-up in case of the spiral-assembled PDiFPhOx-*b*-PEPOx-*b*-PEtOx, the rod-like micelles role up spherically along a distinct orientation axis. This leads to either projections of multilamellar vesicles or to dotted structures by perpendicular orientation facing the axis of the rod-like vesicles. The thickness of the lamellar core area (12 nm) is in the same range as the dot core area (16 nm) (Figure 4.2d,e), while the corona areas are of similar thickness (10 nm). In addition, deviation from the ideal model angles are likely and were often observed by irregular structures showing asymmetric projection features (Figure 4.3b). Another explanation suggests transitions between lamellar and bicontinuous structures within the spherical nanostructures. While multilamellar vesicles are well-known,<sup>23</sup> the existence of bicontinuous phases in solution is rarely reported<sup>121-123</sup> but theoretically predicted for small surfactant molecules by self-consistent-field simulation.<sup>124</sup> Furthermore, the coexistence of multilamellar vesicles and a cubic phase (Figure 4.2b) for block copolymers in solution is practically<sup>125-126</sup> rarely reported but theoretically predicted.<sup>127-129</sup>

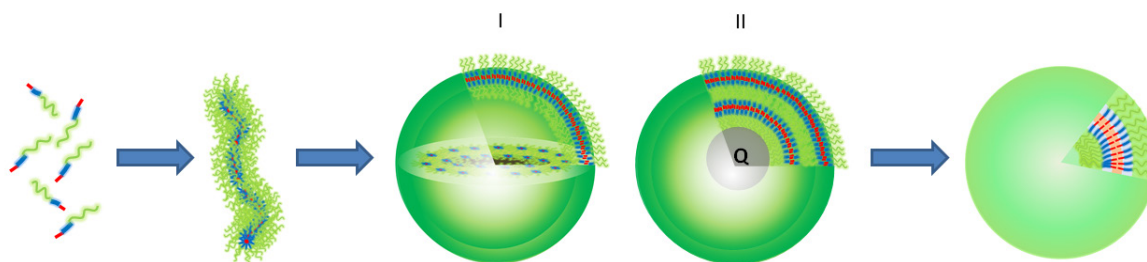
In the present case, the interiors of the round-shaped assemblies range from multilamellar and bicontinuous structures to mixtures where a centered bicontinuous structure is surrounded by multilamella. The interfacial layer of segregated dotted bands could be ascribed to a transition between lamellar and bicontinuous morphologies (Figure 4.2d).<sup>130-133</sup> Within all multilamellar structures (Figure 4.2e) an additional morphology is found in the very center pointing to either a water content depended morphology<sup>134</sup> and/or to a dependency on the curvature, which increases towards the center. To minimize frustration of the latter, interfacial tension is decreased by the formation of cubic phases as minimal surfaces, which generally leads to bicontinuous morphologies.<sup>135-136</sup> This coexistence within a vesicular assembly was theoretically described for a small amphiphile.<sup>130</sup> The avoidance of high curvature is also observed for aggregates with diameters below 200 nm showing only non-regular structures (Figure 4.3a). In addition, all aggregates are surrounded by an envelope



**Figure 4.3** TEM images of PEtOx-*b*-PEPOx-*b*-PPFPhOx in water show a) small spherical assembly with irregular interiors, b) asymmetric structure and c) assemblies after preheating the solution for two days at 70 °C.

lamella, which is thermodynamically favored as the hydrophilic PEtOx block points completely out to the solvent reducing interfacial tension of the hydrophobic blocks as it was predicted by Fraaje and Sevink.<sup>124</sup>

According to the spiral-like assembly of PDiFPhOx-*b*-PEPOx-*b*-PEtOx the lamellar-bicontinuous assemblies of PEtOx-*b*-PEPOx-*b*-PPFPhOx are suggested to be transient morphologies. Therefore the solution was heated at 70 °C for 2 days to support the thermodynamically most favorable morphology: Beside predominantly unilamellar vesicles, only some multilamellar vesicles were observed proving the transient nature of the segregated vesicular structures (Figure 4.3c). For all investigated triblock and diblock copolymers, the formation of rod-like micelles is seen as the preassembly that leads, upon introduction of a fluorinated block, to additional interactions, *e.g.* interfacial tension or stacking. This subsequently causes the self-assembly of the rod-like micelles into transient superstructure such as spirals, bicontinuous or multilamellar spheres that merge upon heating into vesicles representing the ultimate equilibrium state of aggregation (Figure 4.4). This rod-to-vesicle transition is in accordance to classical phase diagrams of surfactants, where this transition is observed by increasing the concentration of the amphiphile<sup>23,137-138</sup> and is explained *via* packing of rods merging into vesicles.<sup>119,133</sup> In this respect, the presented fluorinated terpolymers introduce the degree of fluorination as a key parameter to tune the complexity of multi-compartmentalized supramolecular aggregates.



**Figure 4.4** Schematic representation of the structural evolution of the rod-to-vesicle transformation of penta-fluorophenyl-functionalized triblock terpoly(2-oxazoline)s in aqueous solution: The PEtOx block is shown in green, the PEPOx block in blue and the PPFPhOx in red. The transient assembly can be explained by either (I) a “ball of yarn” assembly of rod-like micelles and/or a (II) coexistence of lamellar and cubic phases (Q) within the same spherical aggregate.

As a major limitation of cryoTEM, the static nature of the investigation allows only “snapshots” of the existing morphologies. Thus, hierarchical self-assembly and the direction of morphology transitions can be only tentatively assumed. For example, it cannot be proven in the present case if the interior morphology transition starts from the bicontinuous towards multilamellar vesicles or vice versa. For such dynamic investigations of individual nanostructures a combined method of the spatial resolution of TEM with a liquid environment would be necessary, for which initial investigations are the subject of Chapter 5.2.

## 5. Investigation of block copolymer assemblies in ionic liquids by electron microscopy

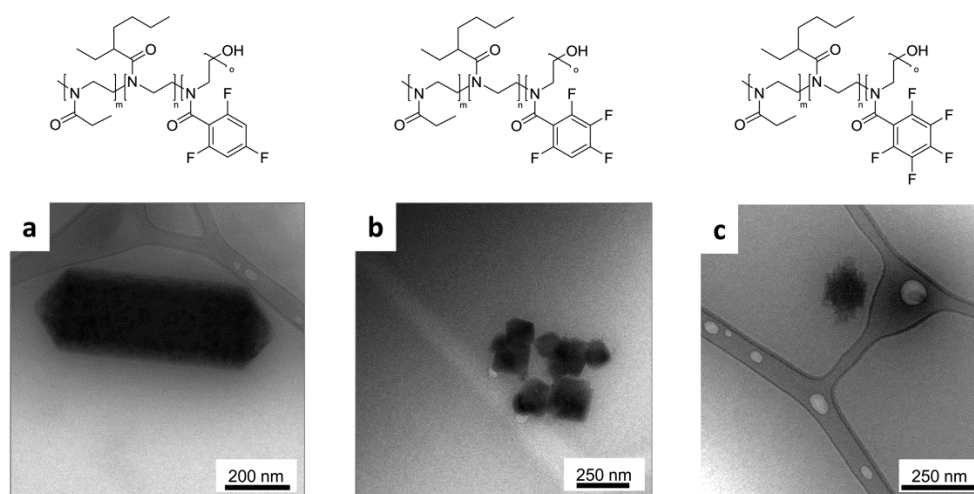
Parts of this chapter have been published: A6) U. Mansfeld, S. Hoepfner, C. Guerrero-Sanchez, J.-F. Gohy and U. S. Schubert, *Microsc. Microanal.* **2013**, submitted. A7) U. Mansfeld, S. Hoepfner and U. S. Schubert, *Adv. Mater.* **2013**, *25*, 761-765.

Transmission Electron microscopy is a powerful tool in polymer science for high resolution imaging of individual nanostructures, in particular, in solution.<sup>44-45</sup> However, as solutions of commonly used organic solvents have to be vitrified upon investigation to sustain the high vacuum, drawbacks arise including low contrast of organic structure and the lack of studies of dynamic processes. Ionic liquids (IL) represent hereon promising alternative matrices that benefits from, *e.g.*, negligible vapor pressure and their tunable properties (*e.g.* viscosity, proticity and polarity) by a certain combination of anion and cation.<sup>46-48</sup> According to this, IL can be used as selective solvents for the assembly of block copolymers<sup>50-51</sup> as well as matrices for high vacuum analyses<sup>49</sup> which paves the way for the investigation of polymer assembly in a liquid environment by TEM.

In this chapter, different possibilities to utilize IL for the visualization of self-assembled polymer structures by TEM will be discussed. The studies focus on polymer nanostructures in different ionic liquids. Thereby, the influence of the ILs is discussed with respect to the observed structures. Additionally, alternative staining procedures that can be applied by utilizing ILs as solvents are discussed in Chapter 5.1. Moreover, a novel approach is introduced by using ILs as liquid media for TEM that permit the investigation of particle motion and first observation of dynamic processes which will be discussed in Chapter 5.2. These studies were performed on different block copolymers by a facile blotting technique of the IL/polymer solution onto lacey carbon copper grids.<sup>139</sup> The resulting free-standing liquid films were investigated at room temperature up to 92 °C. Thereby, 16 commercially available IL were tested considering liquid film formation and electron beam durability (Table S1). The most suitable ILs forming durable liquid films were imidazolium-based ILs with triflate (TfO<sup>-</sup>) and bis(trifluoromethylsulfonyl)imide (Tf<sub>2</sub>N<sup>-</sup>) as counterions, which are known for their low viscosity and high thermal stability.<sup>48</sup>

Suitable ILs were first used to screen the assembly of diblock copolymers, *e.g.* PS-*b*-PMMA, PS-*b*-P2VP, PS-*b*-PEG and PS-*b*-PEtOx (Table S2), that were partially investigated by cryoTEM characterization by several research groups.<sup>50,139-140</sup> In the present case, different assemblies could be visualized at room temperature showing micelles, worm-like micelles, vesicles and stomatocyte-type vesicles (Figure S2). It was shown in literature that the polymer solubility is mainly governed by the anion.<sup>50</sup> In addition, different triblock copolymers were screened in the IL. Among those were the fluorinated triblock terpoly(2-oxazoline)s that are also investigated in aqueous solution (Chapter 4). Thereby, unique nanostructures of the polymers were observed in BMIm BF<sub>4</sub> (Figure 5.1) that are rather different compared to the nanoaggregates observed in water. As shown for the assembly of the PS-*b*-PEtOx polymer (Figure S2) and PEtOx-*b*-R-PBuEtOx (Figure S7b), the PEtOx represents a soluble block in polar ILs. The PEtOx-*b*-PEPOx-*b*-PTriFPhOx revealed angular rod-like features that are

partially dark contrasted depending on the illumination angle, which suggests crystalline assembly (Figure 5.1a). Also for PEtOx-*b*-PEPOx-*b*-PTetFPhOx angular-shaped structures were observed and were ascribed to crystallisation (Figure 5.1b). In contrast, PEtOx-*b*-PEPOx-*b*-PPFPhOx revealed sheet-like assemblies that tend to stack to each other (Figure 5.1c). The anisotropic angular shapes are ascribed to partial crystallization of the fluorinated side-chains that influence the shape of the assembly.<sup>141-142</sup> In fact, crystallization of blocks within copolymers can drive the shape of assemblies in solution.<sup>143</sup> In this vein, fluorinated blocks are potential candidates for crystallization, due to the high polarity and low polarizability,<sup>144</sup> which results in stacking of the fluorinated phenyl rings due to dipole-dipole interactions between C-F bonds.<sup>118</sup>



**Figure 5.1** TEM images of polymers in BMIm BF<sub>4</sub> (1 wt%) of a) PEtOx-*b*-PEPOx-*b*-PTriFPhOx shows crystal-like rods, b) PEtOx-*b*-PEPOx-*b*-PTetFPhOx reveals angular structures and c) PEtOx-*b*-PEPOx-*b*-PPFPhOx shows stacked sheet-like assemblies, respectively.

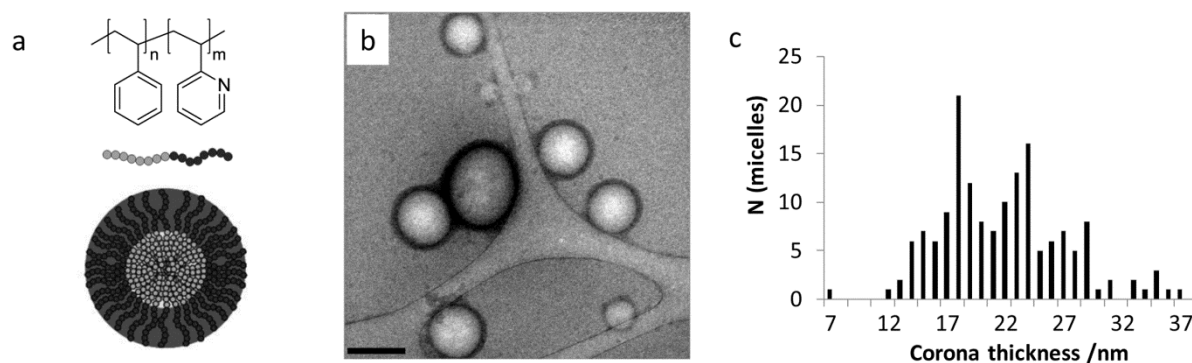
In contrast to the assembly in aqueous solution, the degree of order increases towards the trifluorinated triblock teroxazoline indicating, beside different block solubility, different degree of crystallization of the fluorinated side-chains. By comparing the length of the fluorinated blocks (Table 4.1) for the three triblock oxazolines, the pentafluorinated block is rather small and crystallization might not govern the assembly structure like in the case of the tri- and tetrafluorinated terpolymer. Thus, using IL as selective solvents for polymer assembly expand the range of diversity towards novel nanostructures while using the same polymer pool.

## 5.1 Ionic liquids as intrinsic staining media

TEM investigations of organic assemblies in commonly used organic solvents generally suffer from a severe lack of contrast. This is caused by the same density of matter as well as the same elements (*e.g.* C, N, O, H) within the object and the medium that are characterized by low atomic numbers and, thus, low electron scattering abilities.<sup>45</sup> Therefore, contrast generation is a crucial issue for characterization of organic nanometric objects.<sup>145</sup> This can be overcome by adding compounds of high atomic number as staining agents generating contrast either on the substrate (negative staining) or on compatible assembly areas. However, staining artifacts and influence on the assembly behavior are common problems.<sup>45,145</sup>

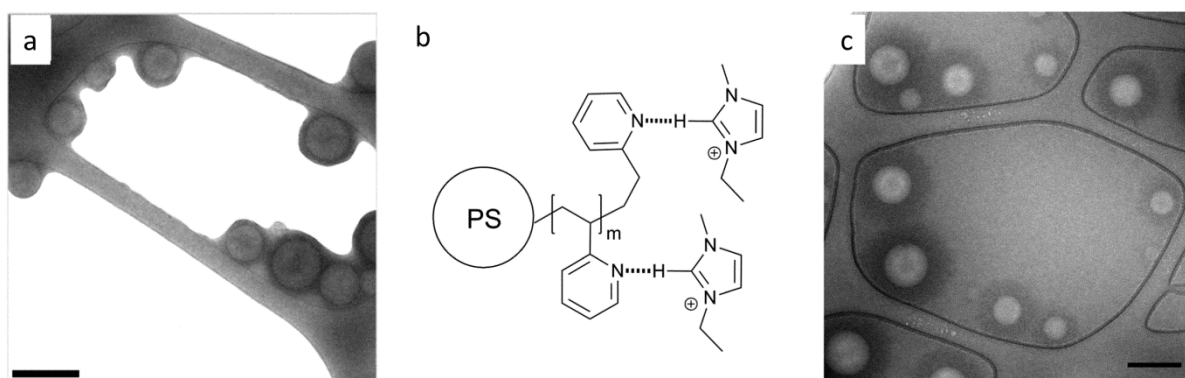
ILs offer intrinsic staining capabilities that provide high contrast to organic assemblies by negative staining, since they inherently provide high electron scattering through high atom number elements of their inorganic anions. By using different methods, selective areas such as core and corona dimensions of micellar assemblies can be determined without using additional staining agents. In this context, the core of micelles can be directly visualized by negative staining. A complementary washing method can be additionally utilized to visualize selectively the corona of the micelle system as it could be shown for PS-*b*-PMMA and PNonOx-*b*-PEtOx.<sup>146</sup>

An unusual selective intrinsic staining was observed for the assembly of polystyrene-*block*-poly-2-vinylpyridine ( $M_n$  [kg mol<sup>-1</sup>] = PS<sub>440</sub>-*b*-P2VP<sub>353</sub>) in 1-ethyl-3-methylimidazolium ethyl sulfate (EMIm EtOSO<sub>3</sub>). CryoTEM investigations visualize both core and corona already in the ionic liquid film (Figure 5.2a,b). PS as an hydrophobic block represents the core and P2VP as the more hydrophilic block represents the corona area which is soluble in imidazolium-based IL<sup>50</sup> although distinct interactions with the IL are reported.<sup>147-151</sup> The core shows a negative contrast, while the corona shows an unusual darker contrast compared to the surrounding. Although dichloromethane was used as cosolvent, non-spherical micelles were found pointing to non-equilibrium assembly conditions. This is caused by an unusual precipitation of the polymer in the solvent mixture even though P2VP is soluble in dichloromethane and the IL. The corona thickness of 15 up to 40 nm (Figure 5.2c) suggests a high contraction of the corona as the fully stretched P2VP<sub>353k</sub> block is theoretically about 800 nm in length.



**Figure 5.2** Assembly of PS-*b*-P2VP in EMIm EtOSO<sub>3</sub>: a) Schematic representation of the chemical structure and micellar assembly; b) cryoTEM image (scale bar 200 nm) and c) statistical analysis of the corona thickness.

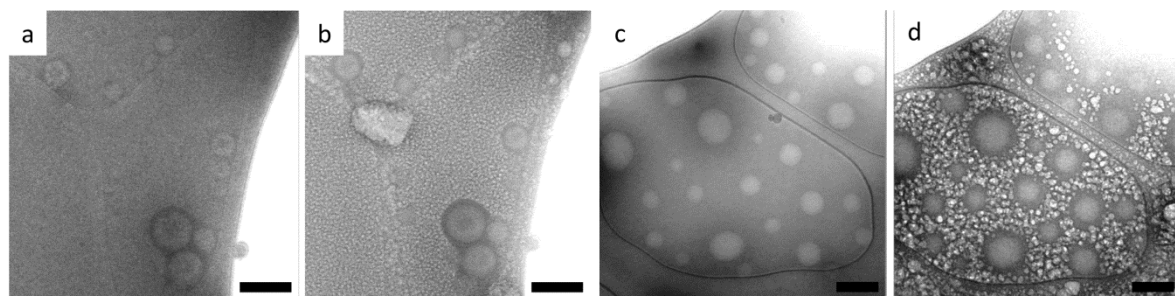




**Figure 5.3** a) RtTEM images of burst free-standing IL film shows contrast of the coronae; b) Schematic representation of hydrogen bonding of imidazolium cations with the nitrogen atom of P2VP; c) the TEM image reveals expanded coronae at 92 °C and at a high electron dose (scale bars = 200 nm).

Subsequently, several potential origins for the dark contrast were elucidated. Matter thickness can be an issue if, *e.g.*, the objects are not completely embedded within the IL films. This could be excluded as the corona contrast was also visualized in burst films by rtTEM, where the structure is expected to be completely surrounded by the IL (Figure 5.3a). The dark contrast is ascribed to an interplay of (i) high atom number of the material's containing elements and (ii) the high density of matter. Concentration of high atom number elements (S of the anion) within the corona can be caused by supramolecular interactions of the IL with 2VP represented by hydrogen bonding where the imidazolium cation acts as hydrogen donor<sup>152-154</sup> with the pyridine nitrogen<sup>155-156</sup> (Figure 5.3b) or by cation- $\pi$  interactions with the pyridine ring.<sup>157-158</sup> As a consequence, the  $\text{EtOSO}_3^-$  is attracted to the positively charged corona causing the contrast.<sup>151,159</sup> The unusual precipitation in the cosolvent/IL mixture is tentatively ascribed to the formation of a charged corona upon addition of the IL, causing the incompatibility with the organic solvent. Charged coronae are up to now not reported in ionic liquids, but the contraction of a polyelectrolyte corona<sup>160-161</sup> as well as a phase separation into a densely packed inner corona with a diluted outer part<sup>161-162</sup> were reported upon salt addition in molecular solvents. In this case, the contrast of the corona in TEM is supported by the high density of matter. The corona contraction can also be caused by nonionic temperature-dependent solubility, which was observed for P2VP in BMIm TfO<sup>149-150</sup> and BMIm Tf<sub>2</sub>N<sup>148</sup> leading to chain stretching. In the present case, larger corona thickness of 60 to 80 nm in free-standing IL film at 92 °C and at high electron doses were observed (Figure 5.3c). The temperature-dependency does not necessarily contradict the term of corona charging upon hydrogen bonding, because the elevated temperature supports chain flexibility. This increases the possibility of interactions with the IL-cation resulting in charging, which leads to a higher solubility in a polar medium. Although this method is restricted to polymer-IL systems with distinct interactions between corona block and the ionic liquid, the intrinsic staining enables the visualization of the corona in their liquid environment avoiding drying or staining artifacts and is applicable for flexible/labile assemblies.

In the course of larger irradiation times it was found that vitrified IL films of EMIm EtOSO<sub>3</sub> and 1-butyl-3-methylimidazolium triflate (BMIm TfO) melt in a heterogenic way



**Figure 5.4** CryoTEM images of PS-*b*-P2VP: The contrasted corona in EMIm EtOSO<sub>3</sub> (a) was confirmed after electron irradiation *via* melting (b); for BMIM TfO the corona is not visible in cryoTEM (c) but shows contrast after electron irradiation (d) (scale bars = 200 nm).

while maintaining the core and coronal areas of PS-*b*-P2VP (Figure 5.4). Such visualization upon electron irradiation was recently described by Talmon *et al.* for PS-*b*-P4VP in DMF.<sup>163</sup> For both ILs, no alteration of the PS core diameter was observed upon electron irradiation. Furthermore, the thickness of the contrasted corona in EMIm EtOSO<sub>3</sub> could be confirmed (Figure 5.4a,b) making the melting of ILs in cryo-TEM reliable for the determination of the corona thickness. Analogue heterogenic melting was observed in 1-ethyl-3-methylimidazolium bis(trifluoromethylsulfonyl)imide (Emim Tf<sub>2</sub>N) and 1-butyl-pyridinium bis(trifluoromethyl-sulfonyl)imide (Bpy Tf<sub>2</sub>N) (Figure S3).

Interestingly, no corona contrast was observed for PS-*b*-P2VP in BMIm TfO (Figure 5.4c). This can be caused by a different solubility and/or by reduced H-bonding interactions between the cation and the P2VP compared to EMIm EtOSO<sub>3</sub>. This is ascribed to a competition between the formation of polymer–cation (inter-solvent) and cation–anion (intra-solvent) hydrogen bonds, where the latter is promoted by additional hydrogen bonds of the cation to the fluorine atoms of the triflate anion in the case of BMIm TfO.<sup>153,164</sup> The strong influence of the competition of hydrogen bonds (*e.g.* inter- vs. intra-solvent/polymer, between polymer and solvent) is illustrated by comparing the polymer solubility in imidazolium-based ionic liquids that increases by H-bonding between solvent and polymer: P2VP is soluble due to weak intra-polymer H-bonding, while P4VP is insoluble due to strong intra-polymer H-bonding.<sup>50,165</sup> Nonetheless, in both ILs (TfO<sup>-</sup> and EtOSO<sub>3</sub><sup>-</sup>) the micelles were separated to each other suggesting the stabilization of the coronal blocks by charging. In contrast, assemblies in IL with Tf<sub>2</sub>N<sup>-</sup> tend to agglomerate (Figure S3), which indicates less charged coronae and, thus, even more pronounced intra-solvent hydrogen bonding of EMIm<sup>+</sup> to Tf<sub>2</sub>N<sup>-</sup>.

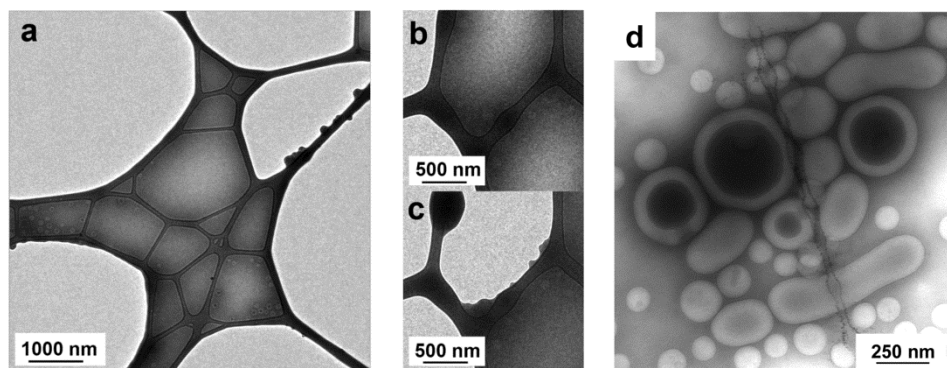
Upon electron irradiation the corona areas become visible in all cases (Figure 5.4d, Figure S3) with similar thicknesses suggesting high contraction equal to the coronae in EMIm EtOSO<sub>3</sub>. The non-contrasted corona in BMIm TfO, although similar contracted, supports the assumption of distinct interactions between EMIm EtOSO<sub>3</sub> and P2VP, since the physical density cannot be the only reason in this case. Electron irradiation of the cryogenic IL film may be used as a method for visualization of distinct polymer areas in its liquid-like state avoiding drying artifacts as long as the assembly dimensions are not influenced by the radiation damage.

## 5.2 Investigation of motion and dynamics of polymeric assembly

Dynamic processes on the nanometer scale are important phenomena in liquids and fluids representing key questions in many biological<sup>166-170</sup> and technological processes.<sup>171</sup> Among those are self-assembly processes of natural and synthetic molecules into supramolecular structures.<sup>172-173</sup> Most of the investigations of such processes rely nowadays on NMR spectroscopy<sup>174-175</sup> and scattering techniques (*e.g.* static and dynamic light scattering, small- and wide-angle X-ray scattering and small-angle neutron scattering),<sup>162,176-178</sup> which provide only average information over a large number of structures. These techniques lack the observation of individual processes on the level of nano-objects in liquids. Although TEM permits a sufficiently high spatial resolution, the incompatibility of the inherently high vacuum conditions with commonly used liquid matrices restricts to consecutive cryoTEM investigations.<sup>179-180</sup> This allows only for vitrified “snapshots” of solution-like states that may be altered by cryogenic artifacts and lacks the real-time observation of nano-object dynamics. Recently, TEM-compatible liquid cells were employed to provide a sealed environment for liquid samples that allows for continuous observation of objects, but contrast is a critical issue for organic material at film thicknesses at which unperturbed motion is assured.<sup>181-184</sup>

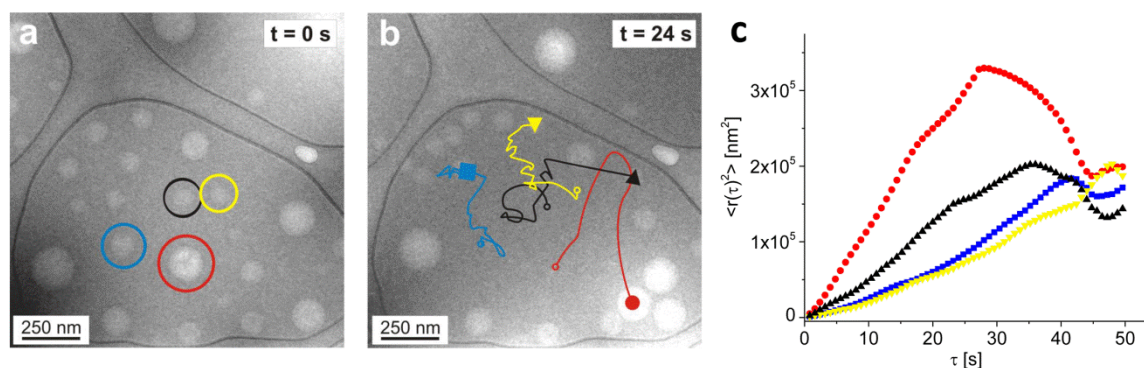
By using suitable ILs as liquid matrices most of the restrictions described above can be omitted due to their negligible vapor pressure,<sup>49</sup> electronconductivity and wide liquid phase range.<sup>48</sup> Thereon, ionic liquids were up to now used in TEM for *in-situ* observation of dynamic processes of inorganic materials on the nanometer scale.<sup>185-186</sup> Due to the intrinsic staining ability (Chapter 5.1) and their selective solvation of block copolymers,<sup>50,139</sup> IL are also promising for dynamic investigations of polymer assemblies. However, up to now, the investigation of motional or dynamic processes of polymeric assemblies in IL has been rarely reported.<sup>187-188</sup> The present work describes the assemblies of, *e.g.*, PS<sub>440k</sub>-*b*-P2VP<sub>353k</sub> and PS<sub>100k</sub>-*b*-PEG<sub>34k</sub> in selective solvents for P2VP and PEG such as 1-ethyl-3-methylimidazolium ethylsulfate (EMIm EtOSO<sub>3</sub>) or 1-butyl-3-methyl-imidazolium tetrafluoroborate (BMIm BF<sub>4</sub>) by the cosolvent method.<sup>139</sup> Ionic liquids can form, stable free-standing films over different length scales<sup>186</sup> due to their characteristic surface tension.<sup>48</sup> As such, sufficiently thin free-standing IL films can be prepared by standard blotting procedures onto lacey-carbon grids with varying hole diameters ranging from 200 nm up to micrometers which are stable under electron irradiation (Figure 5.5a). At high electron doses the liquid character of the films becomes obvious by bursting, while drops remain on the lacey carbon support (Figure 5.5b,c). In this liquid media, micellar and vesicular assemblies of PS<sub>440k</sub>-*b*-P2VP<sub>353k</sub> could be resolved by TEM with good contrast, caused by the intrinsic staining of IL as described in Chapter 5.1 (Figure 5.5d). In addition, the durability of the free-standing films allow for high electron doses with minor beam damage as compared to common cryoTEM investigations. However, for the visualization of motion, relatively low electron doses have to be applied, as high doses result in inhibition of motion after a certain amount of time. An explanation for the “solidification” of the IL might be the radiation-induced radical generation and redox reactions of cation and anion,<sup>189-190</sup> which might lead upon recombination to IL oligomers and, thus, to an increased viscosity.<sup>191-192</sup> Alternative explanations for this effect might be seen in (i) the adhesion of particles to bars by charging effects and (ii) the film





**Figure 5.5** RtTEM images of free-standing films of EMIm EtOSO<sub>3</sub> (a), proving the liquid phase by bursting (b,c) and assembly of PS<sub>440k</sub>-*b*-P2VP<sub>350k</sub>.

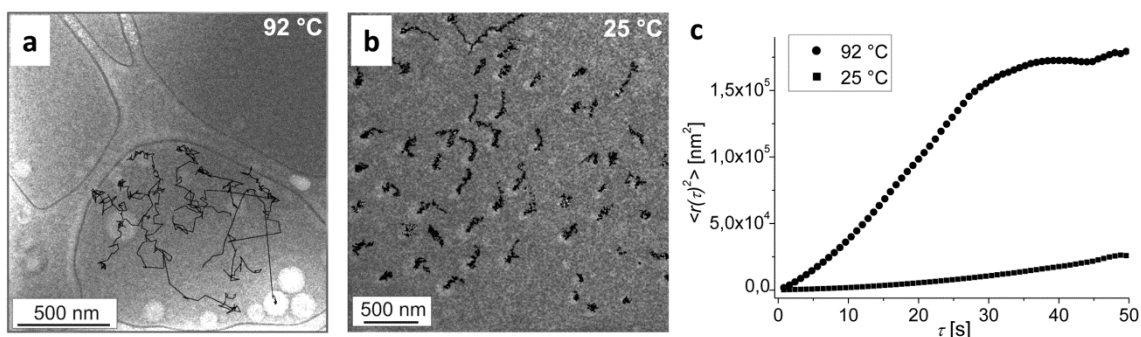
thinning caused by material flowing of the IL due to charge or heat heterogeneity upon irradiation.<sup>44,181</sup> However, at sufficiently low electron doses, particle movement of PS<sub>440k</sub>-*b*-P2VP<sub>350k</sub> in EMIm EtOSO<sub>3</sub> could be followed continuously over an image sequence of up to 140 measurements with a time resolution down to 450 ms (300 ms acquisition; 150 ms read-out) until the motions stop. The film thickness seems to play a crucial role. It was observed for thick films of PEG-*b*-PS in BMIm BF<sub>4</sub> that even at high electron doses motion could be observed up to 500 measurements with a time resolution of 800 ms (Figure S6). However, a sufficiently thin film is required for high resolution. Although objects in thick films were observed to move from the top to the bottom surface, the motion in the films is practically reduced to two dimensions and depends crucially on the viscosity of the IL that can be influenced by temperature. Thereon, heating the sample increases the velocity of the objects within a device-limited temperature range of 20 up to 92 °C. In this vein, different pathways of individual assemblies of PS<sub>440k</sub>-*b*-P2VP<sub>350k</sub> in EMIm EtOSO<sub>3</sub> were followed at 92 °C (Figure 5.6a,b) and the motion of the encircled micelles was analyzed by mean-square-displacement (MSD) calculations<sup>193-195</sup> represented by related MSD plots (Figure 5.6c). At the beginning of imaging all the plots increase linear by time which is a basic criterion for a random walk model of the particle motion. Thereby, different slopes point to different velocities within the ionic liquids that are ascribed to heterogeneity in the film. The black- and



**Figure 5.6** Analysis of an image sequence of PS<sub>440k</sub>-*b*-P2VP<sub>350k</sub> vesicles in EMIm EtOSO<sub>3</sub> showing different dynamic pathways: a) The initial positions of the encircled vesicles, b) the later position of the encircled vesicles and the related individual trajectories within 24 s and c) the motion analyzed by mean-square-displacement (MSD) calculations [recording duration:  $t = 32$  s with 800 ms/frame (300 ms accumulation, 500 ms read-out); 120 kV TEM voltage, 92 °C holder temperature].

in particularly the red-marked particles perform at some stage a large directed displacement, represented by a characteristic devolution of the slope. The abrupt directed motion is ascribed to long range-attraction by, *e.g.*, charging effects. In contrast, the yellow- and blue-tracked particle resembles more linear relationships suggesting a random walk along the imaging series. Characteristic for all plots is the change in slope for large time intervals which is related to the particle deadlock at the rim of the free-standing film due to attraction to the lacey carbon support. The coexistence of these multidirectional movements in a small sample area and the characteristic of random walk point to individual motion of the nano-objects rather than to a passive motion with the IL film (*e.g.* convective flow). In general, different kinds of motion were observed: i) Convection (Figure S4), (ii) Brownian motion and diffusion (Figure 5.7b) as well as iii) oscillation (Figure S5) and rotation (Figure S6).

As the viscosity decreases by increasing temperature a comparison of the averaged MSD over a number of particles at 25 and 92 °C (Figure 5.7a,b) revealed the temperature dependency of motion represented by a larger slope at 92 °C (Figure 5.7c) and, hence, faster diffusion in the IL. The depletion of the slope of the averaged MSD for 92 °C at large time intervals is characteristic for a confined random walk that is expected for the confined space spanned by the IL film and might be influenced by the film dimensions, adhesion of the particles to the bars of the lacey carbon, additional charging effects, and/or by interactions of the particles. Furthermore, an increase in diffusion by time is observed by the increased slope of the plot for tracking at 25 °C, which might be a result of heating of the IL upon beam irradiation.<sup>44,181</sup>



**Figure 5.7** Temperature-dependent analysis of the motion of PS<sub>440k</sub>-*b*-P2VP<sub>350k</sub> vesicles in EMIm EtOSO<sub>3</sub> by means of the mean-square displacement (MSD): (a) The tracking lines of particle motion at 25 °C, (b) the tracking lines of particle motion at 92 °C and c) the averaged MSD at the different temperatures (25 °C bottom curve, 92 °C top curve), revealing a significant increase in diffusion of the particles at the higher temperature.

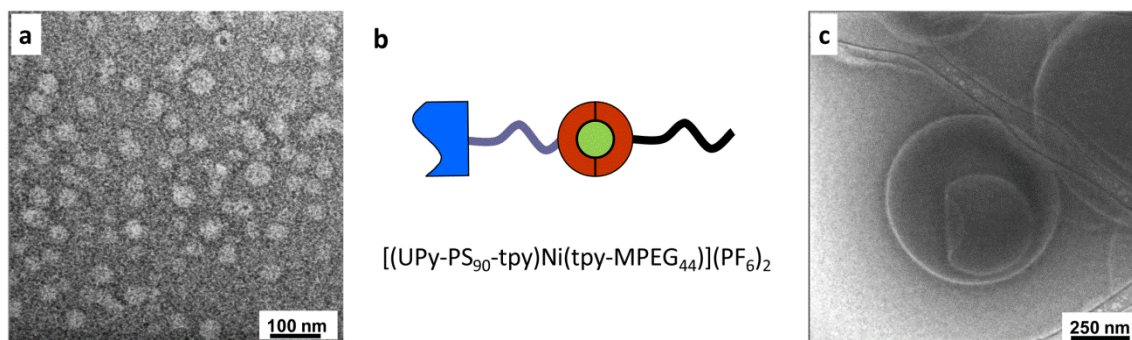
Additionally, a collective movement of individual vesicles of PEG-*b*-PS in BMIm BF<sub>4</sub> was observed (Figure S6) pointing to an entanglement of the corona of the P2VP blocks. It was found that the dimer tends to rotate, while neither separation nor fusion of the vesicles was observed. In general, no deformation of assemblies, *i.e.* no change in shape as well as no fission or fusion processes were observed. This suggests stable aggregates related to the rigid PS block, which is expected to be in a state below the glass transition temperature. In contrast, deformation and transitions of assemblies as dynamic processes should be observed by investigating (i) the present systems at higher temperatures, (ii) block copolymer systems that contain more-flexible insoluble blocks or (iii) LCST/UCST block copolymers showing

assembly/disassembly transitions within the available temperature range between 20 and 90 °C.

Several common polymer classes show temperature-dependent transitions in IL, *i.e.*, certain polyacrylates (LCST), polyamides (UCST) or ethylen oxides (LCST) that were characterized in literature by light scattering methods.<sup>50,153</sup> Relevant examples for the available temperature range between 20 and 90 °C represent PEG derivatives<sup>196-198</sup> and PNiPAm.<sup>197,199</sup> According to this, several diblock systems with short block length to ensure fast transitions were investigated by *in-situ* TEM experiments. Although temperature-dependent assembly were frequently observed for bulk polymer-IL solutions, no correlation to the transition temperature in the film, if present, could be found *via* TEM imaging. This suggests the influence of the film dimensions and beam effects on the assembly transition, which are not understood up to now. However, temperature-dependent transitions in the free-standing films were concluded for (i) PEG-*b*-PNiPAm and PEtOx-*b*-R-PBuEtOx that revealed partially disappearance of assemblies (UCST) and (ii) PEG-*b*-PFGE-*b*-PAGE that showed appearance of assemblies (LCST) by consecutive TEM imaging of the films at 25 and 92 °C, respectively (Table S3, Figure S7). However, the transitions itself could not be visualized or followed by TEM, which is related to interlinked multiple factors, *i.e.* film thickness related diffusion, chain flexibility, transition velocity, interaction of IL and polymer with the beam such as heating, charging, degradation, among others. To minimize the electron dose or irradiation time and, hence the disturbance of the transition by the electron beam, the temperature of transition has to be exactly known within the free-standing film. A crucial, technical problem was the drift of the TEM holder during *in-situ* heating that handicaps the object tracking and imaging.

Assembly/disassembly processes of amphiphilic block copolymers can, beside by temperature changes for LCST/UCST behavior, also be triggered by linking/cleaving of blocks by non-covalent reversible linkages. In accordance to literature examples of the assembly of metal-complex linked block copolymers in water,<sup>200</sup> the prepared metallopolymer [(MPEG<sub>44</sub>-tpy)Ni(tpy-PS<sub>90</sub>-UPy)](PF<sub>6</sub>)<sub>2</sub> (see Chapter 3.3) was assembled in BMIm PF<sub>6</sub> and Bpy Tf<sub>2</sub>N *via* the cosolvent method with dichloromethane. Subsequently the solution was investigated by rtTEM in free-standing films (Figure 5.8).

The assembly proves the stability of the metal complex in the ILs, where the PEG block resembles the soluble block and PS the insoluble block. Thereby, the dimerization of UPy *via*



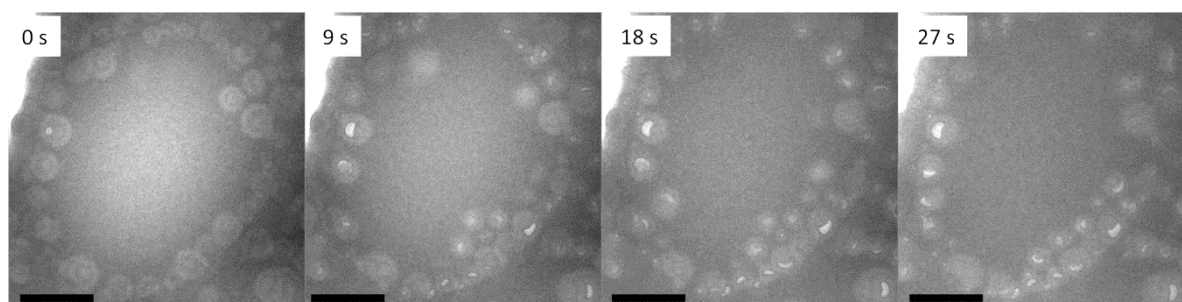
**Figure 5.8** RtTEM images of a 1 wt% solution of [(MPEG<sub>44</sub>-tpy)Ni(6)](PF<sub>6</sub>)<sub>2</sub> (b) in liquid films of Bpy Tf<sub>2</sub>N showing micellar structure (a) and liquid films of BMIm PF<sub>6</sub> showing large vesicular structures (c).



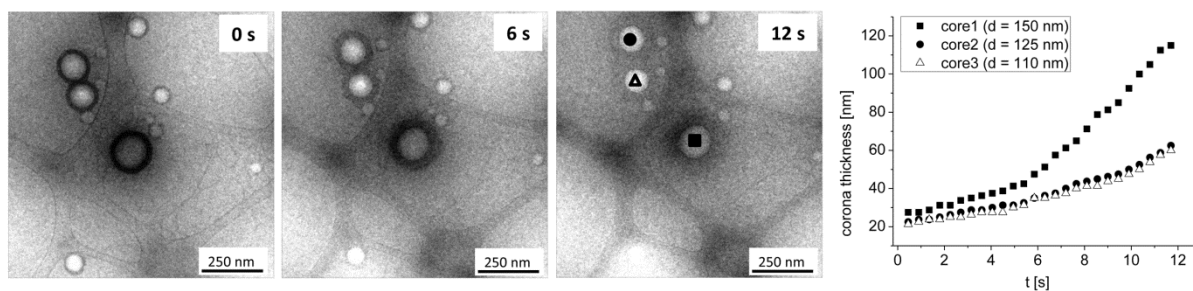
hydrogen bonding is expected to be suppressed by the hydrogen bonding competition with the IL.<sup>153</sup> Large differences in the assembly behavior were observed, since micellar structures with diameters up to 50 nm were found in Bpy Tf<sub>2</sub>N, while large vesicles with diameters up to micrometers were observed in BMIm PF<sub>6</sub> (Figure 5.8). The difference in the assembly behavior is ascribed to either differences in selective solubilities of the IL<sup>201</sup> and/or to electrostatic repulsion of complexes in dependence of the surrounding anions.<sup>202</sup> Up to now, neither motional nor dynamic processes of the nanostructures were observed by rtTEM investigations. However, the diversity in structure by just changing the IL enables investigations of, e.g., micellar or vesicular structures of metallopolymer by using the same polymer system. Moreover, the addressability of the metal complex<sup>203</sup> in combination with the liquid environment offers theoretically the *in-situ* investigations of disassembly processes that are induced by the cleavage of the metal-complex linkages between the blocks.

Since up to now no assembly/disassembly process of the structures could be visualized, the investigations were focussed on the deformation of assemblies as a more basic dynamic process. The deformation in solution is promoted by the flexibility of the blocks. Therefore, low T<sub>g</sub> polymers were chosen as the model system. In the present case, polybutadiene-*block*-poly(*N,N*-dimethylaminoethyl methacrylate) (PB<sub>81</sub>-*b*-PDMAEMA<sub>19</sub>) was investigated (Table S2), where PB represents a prominent example for a low T<sub>g</sub> polymer insoluble in IL.<sup>139</sup> The polymer was assembled in BMIm Tf<sub>2</sub>N (2 wt%) showing vesicles up to 300 nm (Figure 5.9). Motional processes of the objects were already observed at 25 °C in the free-standing IL films, which is caused by the low viscosity of the IL and the short soluble polymer block compared to the PS-*b*-P2VP/EMIm EtOSO<sub>3</sub> system. Although at 92 °C no fusion/fission processes of vesicles could be visualized, characteristic deformations of vesicles were observed upon electron irradiation that could be followed for up to 30 s (Figure 5.9). An explanation for the characteristic deformations can be given by the pronounced evaporation of the cosolvent upon heating caused by irradiation. This leads either to the burst of vesicle as a fission process of the bilayer membrane or to the transition of the cosolvent through the intact membrane causing a suction of the membrane to the inner compartment.<sup>204</sup> In addition, fission of the membranes can be caused by thermal degradation of the polymer blocks as it is known for PDMAEMA at temperatures above 150 °C in water.<sup>205</sup>

Moreover, dynamic processes can be observed by visualization of soluble blocks, which are highly flexible in its dissolved state. In fact, in the course of investigating the intrinsic stained corona of PS-*b*-P2VP in EMIm EtOSO<sub>3</sub> (Chapter 5.1), corona expansions



**Figure 5.9** TEM image series shows the evolution of motion and deformation of vesicular structures of PB<sub>81</sub>-*b*-PDMAEMA<sub>19</sub> in BMIm Tf<sub>2</sub>N [recording duration: t = 30 s with 450 ms/frame (300 ms acquisition, 150 ms read-out); 120 kV TEM voltage, 92 °C holder temperature, scale bar = 400 nm].



**Figure 5.10** TEM images of the dynamic expansion of the P2VP corona of PS<sub>440K</sub>-*b*-P2VP<sub>350K</sub> in EMIm EtOSO<sub>3</sub> upon electron beam irradiation. The corona thickness was analyzed showing non-linear expansions with increased slope by time [recording duration:  $t = 12$  s with 450 ms/frame (300 ms acquisition, 150 ms read-out); 120 kV TEM voltage, 92 °C holder temperature].

were observed upon initial irradiation at 92 °C (Figure 5.10). The expansion is not fully understood and tentatively ascribed to either coulomb repulsion of the charged corona by interaction with the electron beam or to an increased solubility upon heating by the irradiation.<sup>148-150</sup> The diagram in Figure 5.10 shows the dependency of the corona expansion by electron irradiation that increases non-linearly by time. Thereby, steric repulsion of the structures from the bars and each other was observed, while at the same time the contrast of the coronae were faded.

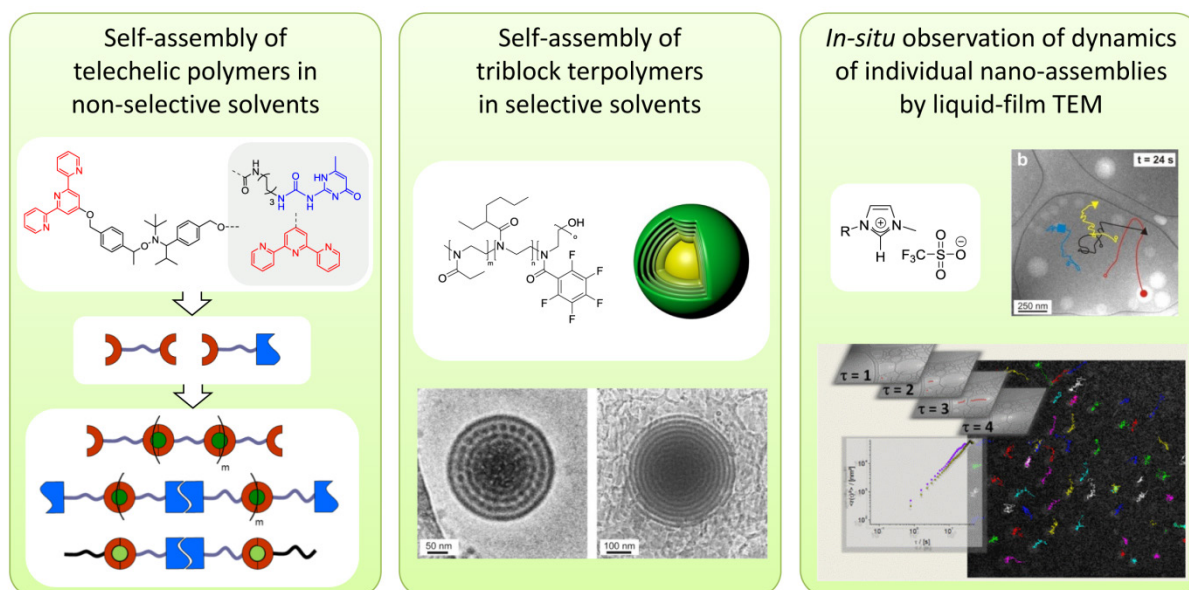
Although the presented initial examples of dynamical processes were affected by irradiation, they allowed for the first time the *in-situ* visualization of individual polymer dynamics at the nanometer scale. The examples illustrate the possibilities of using ionic liquids for time-dependent dynamic investigation of individual supramolecular assemblies or other nano-objects (*e.g.* nanoparticles) in free-standing liquid films by rtTEM. Although the freedom of motion is reduced for particles with dimensions equal to the film thickness, bulk solution-like environment is assumed for motions and dynamics of particles with small dimensions. However, to transfer reliable results to a real liquid environment,<sup>206</sup> intrinsic dynamics of the IL in the films as well as irradiation effects (*e.g.* heating, degradation, charging, solidification; Figure S8) on polymer and the IL have to be understood. In this vein, the use of new radiation-resistant IL<sup>207</sup> offer potentials to minimize beam damage effects.



## Summary

Understanding self-assembly of matter on the nanometer scale is a crucial issue in modern materials' science to increase the control over novel and improved properties such as responsiveness and reversibility for, *e.g.*, sensoric or switchable materials. Such features became accessible by combining non-covalent interactions (*i.e.* metal-to-ligand coordination and hydrogen bonding) with soft matter (*i.e.* organic polymers). This combination was promoted by the vast development of controlled radical polymerizations in the last two decades. Not only the precise control over the polymeric structure is accessible but also the tolerance against a variety of functional groups or even reactive moieties for “click” reactions. Moreover, the placement of the functional groups is well-defined, which is crucial to design the structure of artificial supramolecular assemblies. Thereby, functional groups can be incorporated as end-groups onto the polymer chain by using functional initiators. For the one-step functionalization of both chain ends, nitroxide-mediated polymerization represents a powerful method, since alkoxyamines as initiators can be functionalized on both the initiating and the mediating fragment without disturbing the polymerization.

As previously reported, a heterodifunctional phenylethyl-alkylated 2,2,5-trimethyl-4-phenyl-3-azahexane-3-nitroxide (TIPNO) that was functionalized with 2-ureido-4[1*H*]-pyrimidinone (UPy) on the nitroxide and 2,2':6',2''-terpyridine (tpy) on the initiating fragment, can be used to polymerize styrene (St) in a controlled way. In this work the orthogonal assembly of the heterotelechelic *via* metal-ion complexation of zinc(II) and iron(II) with alternating non-covalent linkages of hydrogen bonding as well as the *in-situ* disassembly of the hydrogen bonding by changing the pH value while the metal complex of iron(II) remained intact is described. In addition, it was shown that the initiator is capable for the bulk polymerization of pentafluorostyrene resulting in telechelic polymers that represents a potential multifunctional scaffold for *para*-fluoro-nucleophile substitution while orthogonal supramolecular bonding *via* metal coordination and the formation of the hydrogen bonding was proven. The heterotelechelic PS were in addition employed for the preparation of metallo-block copolymers. By using a recently introduced protocol for a mild heteroleptic *bis*-terpyridine complexation with nickel(II), tpy-functionalized methoxypoly(ethylene glycol) (MPEG) MPEG-tpy (A) was linked with the heterotelechelic tpy-PS-UPy (B) by complexation towards an AB amphiphilic diblock metallopolymer leading to micellar assembly in DMF/water solution. In addition, the system is capable of forming an orthogonal responsive amphiphilic supramolecular triblock copolymer A(B)<sub>2</sub>A upon dimerization *via* the quadruple hydrogen-bonding motif in aprotic media. The influence of the hydrogen bonding on the phase-separation was also evident in solid films. For comparison, a reference PS-*b*-PEG system was synthesized that bears a hydroxy end-group instead of UPy on the PS starting from the parent hydroxy-functionalized initiator. As a consequence, the reference system represents only an AB diblock upon complexation that is not capable of forming a triblock system. In contrast to the pronounced phase separation of the reference system, only poor phase separation of larger domains was observed for the quasi-triblock polymer that prove the influence of the hydrogen bonding unit in addition to the metal complex. Analogue to the heterofunctionalization, the alkylated TIPNO framework was functionalized on both sites with tpy and used as initiator to control the polymerization of styrene resulting in homo-



**Figure 6.1** Overview over the different kinds of supramolecular assembly and methods to study individual nano-dynamics that were investigated in this thesis.

telechelic tpy-PS-tpy. The homotelechelic PS was self-assembled with iron(II) ions to yield linear metallo-polymers of high molar masses with a theoretically calculated value of  $10^6$  g mol<sup>-1</sup>. The responsiveness was shown by disassembly towards the monomeric telechelic PS using a competitive ligand.

Beside linear supramolecular assembly *via* spatial-defined bonding sites in non-selective solvents, supramolecular assembly can be driven by more general, *i.e.*, attractive or repulsive forces between covalently linked block segments with each other or with a selective solvent. In accordance, the assembly of a series of ABC triblock terpolymers poly[2-ethyl-2-oxazoline-*block*-2-(1-ethylpentyl)-2-oxazoline-*block*-2-(Xfluorophenyl)-2-oxazoline] (PEtOx-*b*-PEPOx-*b*-PXFPPhOx) with varying fluorine content (X = tri, tetra, penta) was investigated by cryoTEM in water. The initial morphology of these systems resembled rod-like micelles, which tends to aggregate hierarchically towards superstructures depending on the length and degree of fluorination of the fluorinated block. Thereby, only the penta-fluorinated terpolymer showed well-defined spherical superstructures representing a unique example of the coexistence of lamellar and bicontinuous phases. This unique structural feature adds the degree of fluorination as an additional parameter to tune the complexity of multi-compartmentalized aggregates in solution. The superstructures were proven to be transient structures as a rod-to-vesicle transition was observed towards thermodynamically favored vesicular assemblies upon elevated temperatures.

However, cryoTEM as a static method only allows the development of tentatively models for dynamic processes, *e.g.* the direction of morphology transitions. Thereon, ionic liquids were investigated as observation matrices due to the negligible vapor pressure in the liquid state that is, in contrast to conventional liquids, compatible with the high vacuum required for TEM. Suitable imidazolium-based ionic liquids were evaluated with respect to their ability to form free-standing liquid films and their durability against electron irradiation, while remaining in the liquid phase. Among those are triflates (TfO<sup>-</sup>) and bis(trifluoromethylsulfonyl)imides (Tf<sub>2</sub>N<sup>-</sup>). Different block copolymers were assembled and their behavior in



liquid films visualized. The motion of PS diblock copolymer assemblies in 1-ethyl-3-methylimidazolium ethyl sulfate (EMIm EtOSO<sub>3</sub>) and 1-butyl-3-methylimidazolium tetrafluoroborate (BMIm BF<sub>4</sub>), respectively, was investigated by *in-situ* TEM up to 92 °C revealing individual motion of particles characterized by single particle tracking and mean-square displacement calculations. To visualize dynamic processes, different block copolymers with lower/upper critical solution temperature (LCST/UCST) transitions were tested by pre-adjusting the temperature of the solution *in situ*. Unfortunately, no assembly/disassembly transition could be visualized up to now, although transitions are present within the free-standing film upon heating in the absence of irradiation for, *e.g.*, poly(ethylene glycol-*block*-*N*-isopropylacrylamide) (PEG-*b*-PNiPAm). On the other hand, by using insoluble blocks with low glass transition temperature, *e.g.* poly(butadiene-*block*-*N,N*-dimethylaminoethyl methacrylate) (PB-*b*-PDMAEMA), deformations of vesicles were observed *in situ* at 92 °C upon irradiation, that is tentatively ascribed to membrane fission.

Ionic liquids were also used as intrinsic staining agents for polymers by negative staining, due to their high electron scattering ability. In the case of poly(styrene-*block*-2-vinylpyridine) (PS-*b*-P2VP) a characteristic positive stained corona was additionally observed that was ascribed to hydrogen bonding interactions between P2VP and the imidazolium cation. As a dynamic feature, upon irradiation an expansion of the flexible stained corona of PS-*b*-P2VP assemblies could be visualized. Furthermore, vitrified IL films revealed a heterogenic melting upon intense irradiation that can be used for visualization of non-contrasted areas of polymer assemblies.

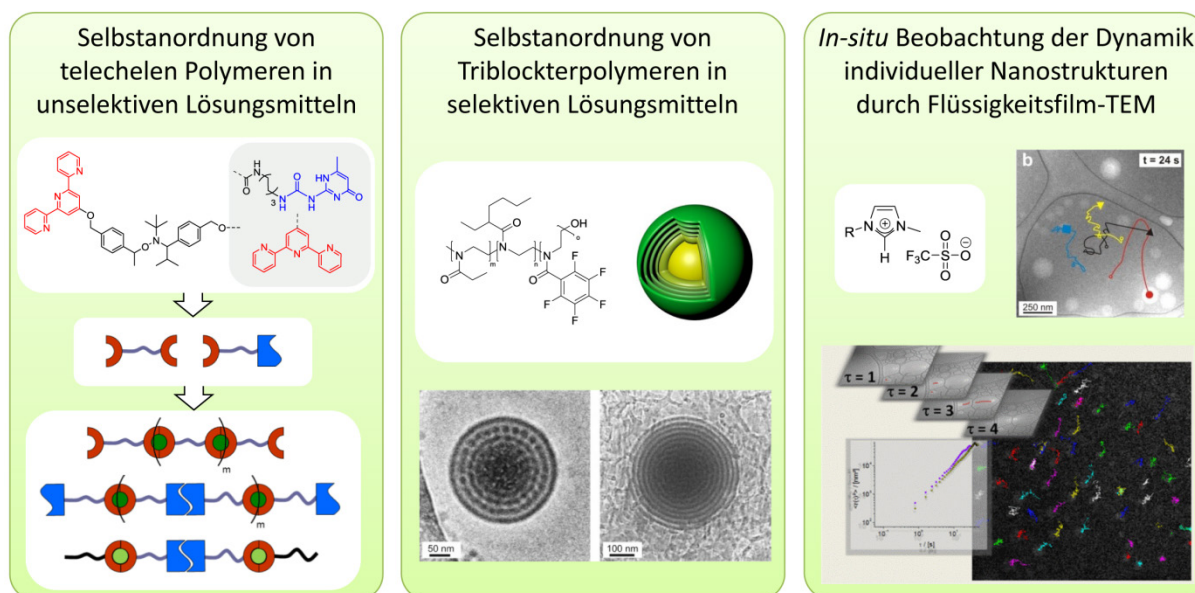
The results shown in this thesis discuss the use of difunctional initiators in NMP for the one-step preparation of telechelic polymers with supramolecular bondings sites and its use for defined self-assembly towards responsive and amphiphilic linear suprapolymers. Since the chain length and composition between the end-groups can be varied in a minimum number of steps, the approach is suitable to adjust the polymeric spacer between the supramolecular binding sites to optimize features such as reversibility for more efficient architectures with potential applications as self-healing or stimuli-responsive materials. Supramolecular assembly can, on the other site, be driven by self-assembly of covalently bonded block copolymers in selective solvent. In particular, by varying the fluorine content in the fluorophilic block of ABC triblock oxazolines unique multicompartement morphology were observed. The fluorine content represents an important parameter to increase the assembly complexity of artificial block copolymers in solution. CryoTEM investigations at different temperatures support furthermore the hierarchical assembly behavior. However, such dynamic processes of supramolecular systems cannot be sufficiently characterized by cryoTEM as a static method. The introduction of ionic liquids as liquid media in TEM enables for the first time with low preparative efforts the possibility to investigate motional and dynamic processes of individual supramolecular assemblies on the nanometer scale, *e.g.* membrane fusion and fission. Moreover, the possibility of adjusting the temperature of the solution *in situ* offers possibilities to adjust the diffusion velocity of the objects and to potentially study temperature-triggered events, *e.g.* phase transitions of thermoresponsive copolymers. However, to transfer reliable results to a real liquid environment, the intrinsic dynamics of the IL in the films as well as irradiation effects on the polymer and the IL have to be understood.



## Zusammenfassung

Die Selbstanordnung von Materie auf der Nanoebene ist heutzutage zu einem nicht mehr wegzudenkenden Bestandteil der Materialforschung geworden. Nicht zuletzt deshalb, um neuartige Eigenschaften wie Ansprechfähigkeit und Reversibilität besser zu kontrollieren, z.B. für sensorische und schaltbare Materialien. Solche Eigenschaften können durch die Zusammenführung von nicht-kovalenten Wechselwirkungen (z.B. Metall-Ligand Koordination oder Wasserstoffbrücken-bindung) mit weicher Materie (z.B. organischen Polymeren) ermöglicht werden. Diese Zusammenführung wurde durch die rasante Entwicklung der kontrollierten, radikalischen Polymerisation in den letzten 20 Jahren maßgeblich vorangetrieben. Nicht nur die Kontrolle über die Synthese vielfältiger Polymerstrukturen konnte erreicht werden, sondern auch die Toleranz gegenüber einer großen Diversität an funktionellen, selbst reaktiver Gruppen z.B. der sogenannten „Click“-Chemie. Hierbei lassen sich die Funktionalitäten im Polymer genau platzieren, was unabdingbar für die Kontrolle über die Selbstanordnung von supramolekularen Systemen ist, welche auf der Wechselwirkung jener Funktionalitäten beruhen. Funktionelle Endgruppen können hierbei durch den Einsatz funktionalisierter Initiatoren eingebaut werden. Für die Ein-Schritt-Funktionalisierung beider Kettenenden hat sich hierbei die Nitroxide-vermittelte Radikalpolymerisation hervorgetan, da die Möglichkeit besteht, difunktionale Alkoxyamine als Initiatoren zu verwenden, die sowohl am initiierenden Fragment als auch am Nitroxid funktionalisierbar sind.

Vor diesem Hintergrund wurde die Selbstanordnung telecheler Polymere mit orthogonalen supramolekularen Endgruppen in Lösung untersucht. Für die Synthese wurde als Initiator für Styrol (St) ein bereits bekanntes heterodifunktionelles Alkoxyamin auf Basis eines azyklischen Nitroxids (TIPNO) verwendet, das mit Terpyridin als tridentaten Metall-Liganden (tpy) und einem Ureidopyrimidin-Derivat als Wasserstoffbrückeneinheit (UPy) funktionalisiert wurde. In der vorliegenden Arbeit konnte die orthogonale Selbstanordnung von tpy-PS-UPy zu hochmolekularen alternierenden Suprapolymeren durch die Komplexierung von Zink(II) oder Eisen(II) bei gleichzeitiger selbstkomplementärer Wasserstoffbrückenbindungen bestätigt werden. Anschließend konnte die Orthogonalität der nichtkovalenten Verknüpfung im Sinne einer selektiven Schaltbarkeit durch das Aufbrechen der H-Brücken – ohne dabei die Metallkomplexe zu beeinflussen – gezeigt werden. Die heterotelechelen Polystyrene konnten darüber hinaus als Bausteine für supramolekulare Blockcopolymere eingesetzt werden. Durch eine milde heteroleptische Komplexierung mit Nickel(II)-Ionen wurde homotelecheles Methoxypoly(ethylenglycol) (MPEG-tpy; A) mittels des *bis*-tpy Komplexes an tpy-PS-UPy (B) angebunden. Die resultierenden amphiphilen Metallopolymere AB zeigten mizellare Anordnungen in selektiven protischen Lösungsmitteln. In aprotischen Lösungsmitteln können sich dagegen über die selbstkomplementäre H-Brückenbindung quasi-Triblockcopolymere AB||BA ausbilden. Der Einfluss der H-Brückenbindung auf die Selbstanordnung konnte an der Phasenseparation in dünnen Filmen nachgewiesen werden. Hierfür wurde ein Diblockcopolymer PS-*b*-PEG (AB) als Referenz synthetisiert, das anstelle des UPy eine Hydroxy-Gruppe trägt und nicht zur Ausbildung von Dimeren (AB||BA) fähig ist. Die signifikante Phasenseparation, die für das



**Figure 7.1** Übersicht über unterschiedliche Arten supramolekularer Selbstanordnung sowie Untersuchung ihrer Struktur und Dynamik, welche in dieser Arbeit diskutiert wurden.

Referenzsystem beobachtet wurde, konnte nicht für das AB||BA bestätigt werden, was auf den Einfluss der Wasserstoffbrücken hinweist.

Analog der Ein-Schritt-Synthese heterotelecheler Polymere konnte das TIPNO-basierte Alkoxyamin auf beiden Seiten mit tpy funktionalisiert und erfolgreich als Initiator in der Polymerisation für homotelechales tpy-PS-tpy eingesetzt werden. Die anschließende Komplexierung mit Eisen(II)-Ionen führte zu hochmolekularen Metallopolymere, die durch kompetitive Liganden *in situ* wieder zur monomeren Form disassemblierten.

Neben der linearen supramolekularen Selbstanordnung, die durch Wechselwirkung räumlich definierter Gruppen in nicht selektiven Lösungsmitteln hervorgerufen wird, kann Selbstanordnung auch durch attraktive und repulsive Kräfte zwischen kovalent verbundenen Blocksegmenten und selektiven Lösungsmitteln entstehen. Hierzu wurden ABC Triblock Terpolymere, d.h. Poly[2-ethyl-2-oxazolin-*block*-2-(1-ethylpentyl)-2-oxazolin-*block*-2-(Xfluorophenyl)-2-oxazolin] (PEtOx-b-PEPOx-b-PXFPhOx) mit variiertem Fluorgehalt (X = tri, tetra, penta) untersucht. Die Ausgangsmorphologie der untersuchten Polymere in Wasser stellen wurmartige Mizellen dar, die hierarchisch abhängig vom Fluorgehalt und der Länge des fluorhaltigen Blocks in komplexere Strukturen übergehen. Hierbei zeigte besonders das penta-fluorinierte Terpolymer wohldefinierte Superstrukturen, die eine neuartige Koexistenz von lamellaren und bikontinuierlichen Phasen aufweisen. Es handelte sich hierbei um transiente Strukturen, die bei höheren Temperaturen der Lösung zu thermodynamisch favorisierten Vesikeln übergehen.

CryoTEM ist wie im genannten Fall zur Aufklärung komplexer Strukturen eine unersetzbare Charakterisierungsmethode. Geht es jedoch um dynamische oder hierarchische Prozesse, wie oft im Falle supramolekularer Systeme, dann ist diese Methode durch den intrinsisch statischen Charakter der festen Matrix eingeschränkt. Um eine für dynamische Prozesse erforderliche flüssige Matrix zu finden, die kompatibel zu den Hochvakuumbedingungen in TEM ist, wurden ionische Flüssigkeiten (IL) als Matrices getestet, da sie als Salze einen großen Temperaturbereich der flüssigen Phase mit vernachlässigbaren

Dampfdruck aufweisen. Hierfür wurden Vertreter der weitverbreiteten Klasse der Imidazolium-basierenden Salze auf ihre Beständigkeit gegen den Elektronenstrahl und ihre Fähigkeit flüssige, freistehende Filme zu bilden untersucht. Als besonders geeignet erwiesen sich hierbei die Triflate ( $\text{TfO}^-$ ) und die Bis(trifluoromethylsulfonyl)imide ( $\text{Tf}_2\text{N}^-$ ) nicht zuletzt wegen ihrer geringen Viskosität. Anschließend wurden diese ILs als selektive Lösungsmittel für die Selbstanordnung verschiedener Blockcopolymerer und deren dynamische Verhalten in den flüssigen Filmen untersucht. Insbesondere die Bewegungen von Nano-Objekten von PS Diblockcopolymeren in 1-Ethyl-3-methylimidazoliumethylsulfat (EMIm EtOSO<sub>3</sub>) und 1-Butyl-3-methylimidazoliumtetrafluoroborat (BMIm BF<sub>4</sub>) wurden durch *in-situ* TEM bei bis zu 92 °C untersucht. Dabei konnte die Partikelbewegung mit Hilfe entsprechender Berechnungen der Brownschen Bewegung zugewiesen und damit eine rein passive Bewegung der Teilchen durch Konvektion der IL ausgeschlossen werden. Um dynamische Prozesse zu beobachten, wurden Aggregate von Blockcopolymeren mit oberer oder unterer kritische Lösungstemperatur (UCST/LCST) durch *in-situ* TEM im Temperaturbereich des Übergangs untersucht. Es konnte bisher jedoch in den freistehenden Filmen keine dynamischen Übergänge direkt beobachtet werden, obwohl Übergänge z.B. für Poly(ethylenglycol-*block-N*-isopropylacrylamid) (PEG-*b*-PNiPAm) bei Temperaturveränderung ohne Elektronenbestrahlung stattfanden. Demgegenüber konnte bei Poly(butadien-*block-N,N*-dimethylaminoethylmethacrylat (PB-*b*-PDMAEMA) bei dem PB den unlöslichen Block mit einer niedrigen Glasübergangstemperatur darstellt, Deformationen bzw. Disassemblierungen von Vesikeln bei 92 °C *in situ* beobachtet werden. Ionische Flüssigkeiten konnten darüber hinaus aufgrund ihrer hohen Elektronenstreuung auch als intrinsische Kontrastmittel verwendet werden. Im Falle von Poly(styrene-*block-2*-vinylpyridine) (PS-*b*-P2VP) wurde zusätzlich in Lösung eine positiv kontrastierte P2VP-Korona beobachtet, die einer Wechselwirkung zwischen P2VP und dem Imidazolium Kation zugeschrieben werden kann. Zusätzlich konnte unter Bestrahlung *in situ* eine Expansion der Korona festgestellt werden.

Die in dieser Arbeit gezeigten Ergebnisse diskutieren difunktionale Initiatoren der Nitroxid-vermittelte Radikalpolymerisation für die Ein-Schritt-Synthese von telechelen Polymeren mit supramolekularen Funktionalitäten und deren definierten Selbstorganisation zu responsiven linearen Suprapolymeren. Da die Kettenlänge zwischen den Endgruppen in einem Minimum an Schritten variiert werden kann, ist diese Präparationsmethode geeignet, um den Abstand zwischen den supramolekularen Verknüpfungen für Eigenschaften wie z.B. die Reversibilität zu optimieren, wodurch sich effizientere Materialien für z.B. Selbstheilung oder Sensoren herstellen lassen. Neben dynamischen Selbstanordnungen, die durch gezielte supramolekulare Wechselwirkungen in nicht selektiven Lösungsmitteln hervorgerufen werden, lassen sich durch selektive Mischbarkeit von Blockcopolymeren und Lösungsmittel dynamische Selbstanordnungen beobachten. Im vorliegenden Fall wurde die Assemblierung von ABC Triblock Oxazolinen mit unterschiedlichem Fluorgehalt des fluorophilen Blocks untersucht. Dieses Beispiel zeigt, dass der Fluorgehalt des fluorophilen Blocks ein wichtiger Parameter ist, um die Komplexität von supramolekularer Anordnung synthetischer Blockcopolymerer in Lösung zu erhöhen. Die cryoTEM Analyse der Lösung bei unterschiedlicher Temperatur unterstützte weiterhin die Annahme der hierarchischen Assemblierung. Solche dynamischen Prozesse supramolekularer Systeme auf der Nanoebene lassen sich mit cryoTEM als statische Methode jedoch nicht hinreichend charakterisieren. Die Einführung von ionischen Flüssigkeiten als flüssiges Medium in Form von freistehenden

Filmen in TEM zeigt erstmalig die Möglichkeit auf, bei minimalem Präparationsaufwand dynamische Prozesse und Bewegungen von individuellen supramolekularen Aggregaten auf der Nanoebene, wie z.B. hierarchische Assemblierung oder Membranfusionsprozesse zeitabhängig zu untersuchen. Zusätzlich ermöglicht die *in-situ* Veränderung der Proben temperatur die Untersuchung temperaturabhängiger Prozesse von individuellen nanoskaligen Strukturen, wie z.B. der Phasenübergänge von thermoresponsiven Copolymeren. Man steht hier aber noch am Anfang der Untersuchungen. Um zuverlässige Ergebnisse auf eine konventionelle flüssige Umgebung übertragen zu können, müssen u.a. die intrinsische Dynamik der ionischen Flüssigkeiten im freistehenden Film sowie die Strahlungseffekte auf das supramolekulare System und die ionische Flüssigkeit verstanden werden.

## References

- [1] J. W. Steed, J. L. Atwood, in *Supramol. Chem.*, John Wiley & Sons, Ltd, **2009**, pp. 591-706.
- [2] R. Dobrawa, F. Würthner, *J. Polym. Sci., Part A: Polym. Chem.* **2005**, *43*, 4981-4995.
- [3] H. Hofmeier, U. S. Schubert, *Chem. Commun.* **2005**, *0*, 2423-2432.
- [4] S. K. Yang, A. V. Ambade, M. Weck, *Chem. Soc. Rev.* **2011**, *40*, 129-137.
- [5] C. J. Hawker, A. W. Bosman, E. Harth, *Chem. Rev.* **2001**, *101*, 3661-3688.
- [6] M. Ouchi, T. Terashima, M. Sawamoto, *Chem. Rev.* **2009**, *109*, 4963-5050.
- [7] M. Szwarc, *Nature* **1956**, *178*, 1168-1169.
- [8] G. Moad, S. H. Thang, *Aust. J. Chem.* **2009**, *62*, 1379-1381.
- [9] R. B. Grubbs, *Polym. Rev.* **2011**, *51*, 104-137.
- [10] H. C. Kolb, M. G. Finn, K. B. Sharpless, *Angew. Chem. Int. Ed.* **2001**, *40*, 2004-2021.
- [11] P. L. Golas, K. Matyjaszewski, *Chem. Soc. Rev.* **2010**, *39*, 1338-1354.
- [12] R. K. Iha, K. L. Wooley, A. M. Nyström, D. J. Burke, M. J. Kade, C. J. Hawker, *Chem. Rev.* **2009**, *109*, 5620-5686.
- [13] A. Winter, M. D. Hager, U. S. Schubert, in *Polymer Science: A Comprehensive Reference, Vol. 5* (Eds.: H.-W. Schmidt, M. Ueda), Elsevier Ltd., Oxford, **2012**.
- [14] T. F. A. De Greef, M. M. J. Smulders, M. Wolfs, A. P. H. J. Schenning, R. P. Sijbesma, E. W. Meijer, *Chem. Rev.* **2009**, *109*, 5687-5754.
- [15] L. Brunsveld, B. J. B. Folmer, E. W. Meijer, R. P. Sijbesma, *Chem. Rev.* **2001**, *101*, 4071-4098.
- [16] W. H. Binder, R. Zirbs, *Adv. Polym. Sci.* **2007**, *207*, 7-78.
- [17] U. S. Schubert, C. Eschbaumer, *Angew. Chem. Int. Ed.* **2002**, *41*, 2892-2926.
- [18] U. S. Schubert, C. Eschbaumer, P. Andres, H. Hofmeier, C. H. Weidl, E. Herdtweck, E. Dulkeith, A. Morteani, N. E. Hecker, J. Feldmann, *Synth. Met.* **2001**, *121*, 1249-1252.
- [19] U. S. Schubert, C. Eschbaumer, G. Hochwimmer, *Synthesis* **1999**, *5*, 779-782.
- [20] F. H. Beijer, R. P. Sijbesma, H. Kooijman, A. L. Spek, E. W. Meijer, *J. Am. Chem. Soc.* **1998**, *120*, 6761-6769.
- [21] G. Gröger, W. Meyer-Zaika, C. Böttcher, F. Gröhn, C. Ruthard, C. Schmuck, *J. Am. Chem. Soc.* **2011**, *133*, 8961-8971.
- [22] T. Aida, E. W. Meijer, S. I. Stupp, *Science* **2012**, *335*, 813-817.
- [23] Y. Mai, A. Eisenberg, *Chem. Soc. Rev.* **2012**, *41*, 5969-5985.
- [24] F. S. Bates, *Science* **1991**, *251*, 898-905.
- [25] F. S. Bates, G. H. Fredrickson, *Phys. Today* **1999**, *52*, 32-38.
- [26] J. N. Israelachvili, D. J. Mitchell, B. W. Ninham, *J. Chem. Soc., Faraday Trans.* **1976**, *72*, 1525-1568.
- [27] P. Alexandridis, B. Lindman, *Amphiphilic Block Copolymers: Self-Assembly and Applications*, Elsevier, Amsterdam, **2000**.
- [28] A. Blanazs, S. P. Armes, A. J. Ryan, *Macromol. Rapid Commun.* **2009**, *30*, 267-277.
- [29] Z. L. Tyrrell, Y. Shen, M. Radosz, *Progr. Polym. Sci.* **2010**, *35*, 1128-1143.
- [30] T. Lohmüller, D. Aydin, M. Schwieder, C. Morhard, I. Louban, C. Pacholski, J. P. Spatz, *Biointerphases* **2011**, *6*, 1-12.



- [31] R. K. O'Reilly, *Phil. Trans. R. Soc. A* **2007**, *35*, 2863-2878.
- [32] J. F. Lutz, A. Laschewsky, *Macromol. Chem. Phys.* **2005**, *206*, 813-817.
- [33] Z. Li, M. A. Hillmyer, T. P. Lodge, *Langmuir* **2006**, *22*, 9409-9417.
- [34] K. Yu, C. Bartels, A. Eisenberg, *Langmuir* **1998**, *31*, 9399-9402.
- [35] A. H. Gröschel, F. H. Schacher, H. Schmalz, O. V. Borisov, E. B. Zhulina, A. Walther, A. H. E. Müller, *Nat. Commun.* **2012**, *3*, 710.
- [36] A. O. Moughton, M. A. Hillmyer, T. P. Lodge, *Macromolecules* **2011**, *45*, 2-19.
- [37] L. Tong, Z. Shen, D. Yang, S. Chen, Y. Li, J. Hu, G. Lu, X. Huang, *Polymer* **2009**, *50*, 2341-2348.
- [38] H. v. Berlepsch, C. Bottcher, K. Skrabania, A. Laschewsky, *Chem. Commun.* **2009**, 2290-2292.
- [39] S. Kubowicz, J.-F. Baussard, J. F. Lutz, A. F. Thünemann, H. v. Berlepsch, A. Laschewsky, *Angew. Chem. Int. Ed.* **2005**, *44*, 5262-5265.
- [40] A. N. Semenov, I. A. Nyrkova, A. R. Khokhlov, *Macromolecules* **1995**, *28*, 7491-7500.
- [41] T. P. Lodge, M. A. Hillmyer, Z. Zhou, Y. Talmon, *Macromolecules* **2004**, *37*, 6680-6682.
- [42] M. A. Hillmyer, T. P. Lodge, *J. Polym. Sci., Part A: Polym. Chem.* **2002**, *40*, 1-8.
- [43] K. Kempe, R. Hoogenboom, S. Hoepfener, C.-A. Fustin, J.-F. Gohy, U. S. Schubert, *Chem. Commun.* **2010**, *46*, 6455-6457.
- [44] L. C. Sawyer, D. T. Grubb, G. F. Meyers, *Polymer Microscopy*, 3rd edition ed., Springer, New York, **2008**.
- [45] G. H. Michler, *Electron Microscopy of Polymers*, Springer, Berlin Heidelberg, **2008**.
- [46] T. Torimoto, T. Tsuda, K. Okazaki, S. Kuwabata, *Adv. Mater.* **2010**, *22*, 1196-1221.
- [47] J. P. Hallett, T. Welton, *Chem. Rev.* **2011**, *111*, 3508-3576.
- [48] H. Weingärtner, *Angew. Chem. Int. Ed.* **2008**, *47*, 654-670.
- [49] S. Kuwabata, T. Tsuda, T. Torimoto, *J. Phys. Chem. Lett.* **2010**, *1*, 3177-3188.
- [50] T. Ueki, M. Watanabe, *Bull. Chem. Soc. Jpn.* **2012**, *85*, 33-50.
- [51] T. L. Greaves, C. J. Drummond, *Chem. Soc. Rev.* **2008**, *37*, 1709-1726.
- [52] C. R. Becer, R. Hoogenboom, U. S. Schubert, *Angew. Chem. Int. Ed.* **2009**, *48*, 4900-4908.
- [53] A. J. Inglis, C. Barner-Kowollik, *Macromol. Rapid Commun.* **2010**, *31*, 1247-1266.
- [54] C. J. Duxbury, D. Cummins, A. Heise, *J. Polym. Sci., Part A: Polym. Chem.* **2009**, *47*, 3795-3802.
- [55] N. V. Tsarevsky, K. V. Bernaerts, B. Dufour, F. E. Du Prez, K. Matyjaszewski, *Macromolecules* **2004**, *37*, 9308-9313.
- [56] C. R. Becer, K. Babiuch, D. Pilz, S. Hornig, T. Heinze, M. Gottschaldt, U. S. Schubert, *Macromolecules* **2009**, *42*, 2387-2394.
- [57] A. Dag, H. Durmaz, V. Kirmizi, G. Hizal, U. Tunca, *Polym. Chem.* **2010**, *1*, 621-623.
- [58] A. A. Kavitha, N. K. Singha, *ACS Appl. Mater. Interfaces* **2009**, *1*, 1427-1436.
- [59] S. Fleischmann, K. Hinrichs, U. Oertel, S. Reichelt, K.-J. Eichhorn, B. Voit, *Macromol. Rapid Commun.* **2008**, *29*, 1177-1185.
- [60] N. J. Agard, J. A. Prescher, C. R. Bertozzi, *J. Am. Chem. Soc.* **2004**, *126*, 15046-15047.
- [61] C. E. Hoyle, C. N. Bowman, *Angew. Chem. Int. Ed.* **2010**, *49*, 1540-1573.

- [62] C. E. Hoyle, A. B. Lowe, C. N. Bowman, *Chem. Soc. Rev.* **2010**, *39*, 1355-1387.
- [63] R. Hoogenboom, *Angew. Chem. Int. Ed.* **2010**, *49*, 3415-3417.
- [64] I. Singh, Z. Zarafshani, J.-F. Lutz, F. Heaney, *Macromolecules* **2009**, *42*, 5411-5413.
- [65] K. L. Heredia, T. H. Nguyen, C.-W. Chang, V. Bulmus, T. P. Davis, H. D. Maynard, *Chem. Commun.* **2008**, 3245-3247.
- [66] J. Sauer, R. Sustmann, *Angew. Chem. Int. Ed.* **1980**, *19*, 779-807.
- [67] V. L. G. Mantovani, L. Tao and D. M. Haddleton, *Chem. Commun.* **2005**, 2089 - 2091.
- [68] M. Rodlert, E. Harth, I. Rees, C. J. Hawker, *J. Polym. Sci., Part A: Polym. Chem.* **2000**, *38*, 4749-4763.
- [69] A. C. Greene, R. B. Grubbs, *J. Polym. Sci., Part A: Polym. Chem.* **2009**, *47*, 6342-6352.
- [70] S. Fleischmann, H. Komber, D. Appelhans, B. I. Voit, *Macromol. Chem. Phys.* **2007**, *208*, 1050-1060.
- [71] A. Hasneen, H. S. Han, H.-J. Paik, *React. Funct. Polym.* **2009**, *69*, 681-687.
- [72] L. B. Sessions, L. A. Miinea, K. D. Ericson, D. S. Glueck, R. B. Grubbs, *Macromolecules* **2005**, *38*, 2116-2121.
- [73] E. Gungor, G. Cote, T. Erdogan, H. Durmaz, A. L. Demirel, G. Hizal, U. Tunca, *J. Polym. Sci., Part A: Polym. Chem.* **2007**, *45*, 1055-1065.
- [74] O. Altintas, B. Yankul, G. Hizal, U. Tunca, *J. Polym. Sci., Part A: Polym. Chem.* **2007**, *45*, 3588-3598.
- [75] W. H. Binder, D. Gloger, H. Weinstabl, G. Allmaier, E. Pittenauer, *Macromolecules* **2007**, *40*, 3097-3107.
- [76] H. Durmaz, F. Karatas, U. Tunca, G. Hizal, *J. Polym. Sci., Part A: Polym. Chem.* **2006**, *44*, 3947-3957.
- [77] R. K. O'Reilly, M. J. Joralemon, C. J. Hawker, K. L. Wooley, *Chem.-Eur. J.* **2006**, *12*, 6776-6786.
- [78] M. Malkoch, R. J. Thibault, E. Drockenmuller, M. Messerschmidt, B. Voit, T. P. Russell, C. J. Hawker, *J. Am. Chem. Soc.* **2005**, *127*, 14942-14949.
- [79] S. Fleischmann, H. Komber, B. Voit, *Macromolecules* **2008**, *41*, 5255-5264.
- [80] D. Gromadzki, J. Lokaj, P. Cernoch, O. Diat, F. Nallet, P. Stepánek, *Eur. Polym. J.* **2008**, *44*, 189-199.
- [81] G. O'Bryan, N. Ningnuek, R. Braslau, *Polymer* **2008**, *49*, 5241-5248.
- [82] E. Harth, C. J. Hawker, W. Fan, R. M. Waymouth, *Macromolecules* **2001**, *34*, 3856-3862.
- [83] S. Pfeifer, J.-F. Lutz, *Chem.-Eur. J.* **2008**, *14*, 10949-10957.
- [84] Y. Guillaneuf, P.-E. Dufils, L. Autissier, M. Rollet, D. Gigmes, D. Bertin, *Macromolecules* **2009**, *43*, 91-100.
- [85] B. Sieczkowska, M. Millaruelo, M. Messerschmidt, B. Voit, *Macromolecules* **2007**, *40*, 2361-2370.
- [86] R. K. O'Reilly, M. J. Joralemon, K. L. Wooley, C. J. Hawker, *Chem. Mater.* **2005**, *17*, 5976-5988.
- [87] G. Temel, B. Aydogan, N. Arsu, Y. Yagci, *Macromolecules* **2009**, *42*, 6098-6106.
- [88] A. Dag, H. Durmaz, E. Demir, G. Hizal, U. Tunca, *J. Polym. Sci., Part A: Polym. Chem.* **2008**, *46*, 6969-6977.
- [89] M. A. Harvison, A. B. Lowe, *Macromol. Rapid Commun.* **2011**, *32*, 779-800.

- [90] D. Benoit, V. Chaplinski, R. Braslau, C. J. Hawker, *J. Am. Chem. Soc.* **1999**, *121*, 3904-3920.
- [91] B. G. G. Lohmeijer, U. S. Schubert, *J. Polym. Sci., Part A: Polym. Chem.* **2004**, *42*, 4016-4027.
- [92] H. Hofmeier, R. Hoogenboom, M. E. L. Wouters, U. S. Schubert, *J. Am. Chem. Soc.* **2005**, *127*, 2913-2921.
- [93] U. Mansfeld, M. D. Hager, R. Hoogenboom, C. Ott, A. Winter, U. S. Schubert, *Chem. Commun.* **2009**, 3386-3388.
- [94] T. Y.-S. But, P. H. Toy, *Chem. Asian J.* **2007**, *2*, 1340-1355.
- [95] J. Hovinen, *Tetrahedron Lett.* **2004**, *45*, 5707-5709.
- [96] U. S. Schubert, A. Winter, G. R. Newkome, *Terpyridine-based Materials*, Wiley-VCH, Weinheim, **2011**.
- [97] R. H. Holyer, C. D. Hubbard, S. F. A. Kettle, R. G. Wilkins, *Inorg. Chem.* **1966**, *5*, 622-625.
- [98] R. Shunmugam, G. J. Gabriel, K. A. Aamer, G. N. Tew, *Macromol. Rapid Commun.* **2010**, *31*, 784-793.
- [99] R. Hogg, R. G. Wilkins, *J. Chem. Soc.* **1962**, 341-350.
- [100] T. Vermonden, J. van der Gucht, P. de Waard, A. T. M. Marcelis, N. A. M. Besseling, E. J. R. Sudhölter, G. J. Fleer, M. A. Cohen Stuart, *Macromolecules* **2003**, *36*, 7035-7044.
- [101] M. Chipper, M. A. R. Meier, D. Wouters, S. Hoepfener, C.-A. Fustin, J.-F. Gohy, U. S. Schubert, *Macromolecules* **2008**, *41*, 2771-2777.
- [102] D. G. Kurth, *Sci. Technol. Adv. Mater.* **2008**, *9*, 014103.
- [103] U. Mansfeld, A. Winter, M. D. Hager, R. Hoogenboom, W. Gunther, U. S. Schubert, *Polym. Chem.* **2013**, *4*, 113-123.
- [104] C. Ott, R. Hoogenboom, U. S. Schubert, *Chem. Commun.* **2008**, 3516-3518.
- [105] C. Ott, C. Ulbricht, R. Hoogenboom, U. S. Schubert, *Macromol. Rapid Commun.* **2012**, *33*, 556-561.
- [106] C. Mugemana, P. Guillet, S. Hoepfener, U. S. Schubert, C.-A. Fustin, J.-F. Gohy, *Chem. Commun.* **2010**, *46*, 1296-1298.
- [107] D. Rablen, G. Gordon, *Inorg. Chem.* **1969**, *8*, 395-397.
- [108] P. A. Cock, C. E. Cottrell, R. K. Boyd, *Can. J. Chem.* **1972**, *50*, 402-411.
- [109] B. G. G. Lohmeijer, U. S. Schubert, *Macromol. Chem. Phys.* **2003**, *204*, 1072-1078.
- [110] B. G. G. Lohmeijer, D. Wouters, Z.-H. Yin, U. S. Schubert, *Chem. Commun.* **2004**, 2886-2887.
- [111] M. Al-Hussein, B. G. G. Lohmeijer, U. S. Schubert, W. H. de Jeu, *Macromolecules* **2003**, *36*, 9281-9284.
- [112] M. Al-Hussein, W. H. de Jeu, B. G. G. Lohmeijer, U. S. Schubert, *Macromolecules* **2005**, *38*, 2832-2836.
- [113] R. Hoogenboom, H. Schlaad, *Polymers* **2011**, *3*, 467-488.
- [114] A. Makino, S. Kobayashi, *J. Polym. Sci., Part A: Polym. Chem.* **2010**, *48*, 1251-1270.
- [115] M. Lobert, H. M. L. Thijs, T. Erdmenger, R. Eckardt, C. Ulbricht, R. Hoogenboom, U. S. Schubert, *Chem. Eur. J.* **2008**, *14*, 10396-10407.
- [116] T. Komenda, R. Jordan, *Abstr. Pap. Am. Chem. Soc.* **2003**, *225*, U573-U573.

- [117] U. Mansfeld, S. Hoepfner, K. Kempe, J.-M. Schumers, J.-F. Gohy, U. S. Schubert, *Soft Matter* **2013**, *9*, 5966-5974.
- [118] M. D. Blanchard, R. P. Hughes, T. E. Concolino, A. L. Rheingold, *Chem. Mat.* **2000**, *12*, 1604-1610.
- [119] L. Chen, H. Shen, A. Eisenberg, *J. Phys. Chem. B* **1999**, *103*, 9488-9497.
- [120] H. Shen, A. Eisenberg, *J. Phys. Chem. B* **1999**, *103*, 9473-9487.
- [121] K. Hales, Z. Chen, K. L. Wooley, D. J. Pochan, *Nano Lett.* **2008**, *8*, 2023-2026.
- [122] A. L. Parry, P. H. H. Bomans, S. J. Holder, N. Sommerdijk, S. C. G. Biagini, *Angew. Chem. Int. Ed.* **2008**, *47*, 8859-8862.
- [123] S. J. Holder, N. Sommerdijk, *Polym. Chem.* **2011**, *2*, 1018-1028.
- [124] J. G. E. M. Fraaije, G. J. A. Sevink, *Macromolecules* **2003**, *36*, 7891-7893.
- [125] S. Qin, W. Z. Yuan, H. Li, Y. Zhang, *Soft Matter* **2012**, *8*, 8405-8412.
- [126] B. E. McKenzie, F. Nudelman, P. H. H. Bomans, S. J. Holder, N. Sommerdijk, *J. Am. Chem. Soc.* **2010**, *132*, 10256-10259.
- [127] X. D. Guo, J. P. K. Tan, L. J. Zhang, M. Khan, S. Q. Liu, Y. Y. Yang, Y. Qian, *Chem. Phys. Lett.* **2009**, *473*, 336-342.
- [128] B. Yu, B. Li, P. Sun, T. Chen, Q. Jin, D. Ding, A.-C. Shi, *J. Chem. Phys.* **2005**, *123*, 234902-234908.
- [129] P. Chen, H. Liang, A.-C. Shi, *Macromolecules* **2008**, *41*, 8938-8943.
- [130] C. E. Conn, O. Ces, X. Mulet, S. Finet, R. Winter, J. M. Seddon, R. H. Templer, *Phys. Rev. Lett.* **2006**, *96*, 108102.
- [131] L. J. Ellison, D. J. Michel, F. Barmes, D. J. Cleaver, *Phys. Rev. Lett.* **2006**, *97*, 237801.
- [132] L. V. Chernomordik, M. M. Kozlov, *Annu. Rev. Biochem.* **2003**, *72*, 175-207.
- [133] L. Yang, H. W. Huang, *Science* **2002**, *297*, 1877-1879.
- [134] V. Percec, D. A. Wilson, P. Leowanawat, C. J. Wilson, A. D. Hughes, M. S. Kaucher, D. A. Hammer, D. H. Levine, A. J. Kim, F. S. Bates, K. P. Davis, T. P. Lodge, M. L. Klein, R. H. DeVane, E. Aqad, B. M. Rosen, A. O. Argintaru, M. J. Sienkowska, K. Rissanen, S. Nummelin, J. Ropponen, *Science* **2010**, *328*, 1009-1014.
- [135] K. Kita-Tokarczyk, J. Grumelard, T. Haefele, W. Meier, *Polymer* **2005**, *46*, 3540-3563.
- [136] M. Almgren, *J. Dispersion Sci. Technol.* **2007**, *28*, 43-54.
- [137] P. Alexandridis, U. Olsson, B. Lindman, *Langmuir* **1998**, *14*, 2627-2638.
- [138] M. Kahlweit, R. Strey, *Angew. Chem. Int. Ed.* **1985**, *24*, 654-668.
- [139] Y. He, Z. Li, P. Simone, T. P. Lodge, *J. Am. Chem. Soc.* **2006**, *128*, 2745-2750.
- [140] P. M. Simone, T. P. Lodge, *Macromol. Chem. Phys.* **2007**, *208*, 339-348.
- [141] K. Skrabania, A. Laschewsky, H. v. Berlepsch, C. Böttcher, *Langmuir* **2009**, *25*, 7594-7601.
- [142] J.-N. I. Marsat, M. Heydenreich, E. Kleinpeter, H. v. Berlepsch, C. Böttcher, A. Laschewsky, *Macromolecules* **2011**, *44*, 2092-2105.
- [143] L. Yin, M. A. Hillmyer, *Macromolecules* **2011**, *44*, 3021-3028.
- [144] C. Tschierske, in *Liq. Cryst., Vol. 318* (Ed.: C. Tschierske), Springer, Berlin, **2012**, pp. 1-108.
- [145] L. Reimer, H. Kohl, *Transmission Electron Microscopy: Physics of Image Formation*, 5 ed., Springer **2008**.

- [146] C. Guerrero-Sanchez, PhD-thesis thesis, Eindhoven University of Technology, Eindhoven, **2007**.
- [147] M. L. Hoarfrost, R. A. Segalman, *Macromolecules* **2011**, *44*, 5281-5288.
- [148] J. M. Virgili, A. Hexemer, J. A. Pople, N. P. Balsara, R. A. Segalman, *Macromolecules* **2009**, *42*, 4604-4613.
- [149] H. Lu, B. Akgun, X. Wei, L. Li, S. K. Satija, T. P. Russell, *Langmuir* **2011**, *27*, 12443-12450.
- [150] H. Lu, D. H. Lee, T. P. Russell, *Langmuir* **2010**, *26*, 17126-17132.
- [151] M. L. Hoarfrost, M. S. Tyagi, R. A. Segalman, J. A. Reimer, *Macromolecules* **2012**, *45*, 3112-3120.
- [152] K. Dong, S. Zhang, D. Wang, X. Yao, *J. Phys. Chem. A* **2006**, *110*, 9775-9782.
- [153] H.-N. Lee, N. Newell, Z. Bai, T. P. Lodge, *Macromolecules* **2012**, *45*, 3627-3633.
- [154] P. A. Hunt, B. Kirchner, T. Welton, *Chem.-Eur. J.* **2006**, *12*, 6762-6775.
- [155] T. Li, P. Zhou, A. Mattei, *CrystEngComm* **2011**, *13*, 6356-6360.
- [156] J. P. M. Lommerse, S. L. Price, R. Taylor, *J. Comput. Chem.* **1997**, *18*, 757-774.
- [157] J. C. Ma, D. A. Dougherty, *Chem. Rev.* **1997**, *97*, 1303-1324.
- [158] T. Ueki, M. Watanabe, *Macromolecules* **2008**, *41*, 3739-3749.
- [159] J. Hou, Z. Zhang, L. A. Madsen, *J. Phys. Chem. B* **2011**, *115*, 4576-4582.
- [160] E. B. Zhulina, O. V. Borisov, *Macromolecules* **2012**, *45*, 4429-4440.
- [161] S. Förster, V. Abetz, A. E. Müller, in *Polyelectrolytes with Defined Molecular Architecture II, Vol. 166* (Ed.: M. Schmidt), Springer Berlin Heidelberg, **2004**, pp. 173-210.
- [162] S. Förster, N. Hermsdorf, C. Böttcher, P. Lindner, *Macromolecules* **2002**, *35*, 4096-4105.
- [163] L. Oss-Ronen, J. Schmidt, V. Abetz, A. Radulescu, Y. Cohen, Y. Talmon, *Macromolecules* **2012**, *45*, 9631-9642.
- [164] I. Goldberg, *Acta Crystallogr., Sect. C* **2009**, *65*, 509-511.
- [165] B. B. Sauer, G. T. Dee, *Macromolecules* **2002**, *35*, 7024-7030.
- [166] N. Nandi, K. Bhattacharyya, B. Bagchi, *Chem. Rev.* **2000**, *100*, 2013-2046.
- [167] C. Eggeling, C. Ringemann, R. Medda, G. Schwarzmann, K. Sandhoff, S. Polyakova, V. N. Belov, B. Hein, C. von Middendorff, A. Schonle, S. W. Hell, *Nature* **2009**, *457*, 1159-1162.
- [168] S. K. Pal, A. H. Zewail, *Chem. Rev.* **2004**, *104*, 2099-2124.
- [169] J. Lippincott-Schwartz, E. Snapp, A. Kenworthy, *Nat. Rev. Mol. Cell Biol.* **2001**, *2*, 444-456.
- [170] P. Mereghetti, D. Kokh, J. A. McCammon, R. Wade, *BMC Biophysics* **2011**, *4*, 2-6.
- [171] K. Sugano, M. Kansy, P. Artursson, A. Avdeef, S. Bendels, L. Di, G. F. Ecker, B. Faller, H. Fischer, G. Gerebtzoff, H. Lennernaes, F. Senner, *Nat. Rev. Drug. Discov.* **2010**, *9*, 597-614.
- [172] C. Bohne, *Langmuir* **2006**, *22*, 9100-9111.
- [173] H. W. Spiess, *Macromolecules* **2010**, *43*, 5479-5491.
- [174] J. R. Bothe, E. N. Nikolova, C. D. Eichhorn, J. Chugh, A. L. Hansen, H. M. Al-Hashimi, *Nat. Methods* **2011**, *8*, 919-931.
- [175] M. Pons, O. Millet, *Prog. Nucl. Magn. Reson. Spectrosc.* **2001**, *38*, 267-324.



- [176] W. Groenewegen, S. U. Egelhaaf, A. Lapp, J. R. C. van der Maarel, *Macromolecules* **2000**, *33*, 3283-3293.
- [177] T. Sato, Y. Matsuda, *Polym. J* **2009**, *41*, 241-251.
- [178] R. J. Roe, *Methods of X-Ray and Neutron Scattering in Polymer Science*, Oxford University Press, New York, **2000**.
- [179] D. E. Discher, A. Eisenberg, *Science* **2002**, *297*, 967-973.
- [180] E. M. Mandelkow, E. Mandelkow, R. A. Milligan, *J. Cell Biol.* **1991**, *114*, 977-991.
- [181] N. de Jonge, F. M. Ross, *Nat. Nanotechnol.* **2011**, *6*, 695-704.
- [182] U. Mirsaidov, C.-D. Ohl, P. Matsudaira, *Soft Matter* **2012**, *8*, 7108-7111.
- [183] E. R. White, S. B. Singer, V. Augustyn, W. A. Hubbard, M. Mecklenburg, B. Dunn, B. C. Regan, *ACS Nano* **2012**, *6*, 6308-6317.
- [184] J. Park, H. Zheng, W. C. Lee, P. L. Geissler, E. Rabani, A. P. Alivisatos, *ACS Nano* **2012**, *6*, 2078-2085.
- [185] J. Y. Huang, L. Zhong, C. M. Wang, J. P. Sullivan, W. Xu, L. Q. Zhang, S. X. Mao, N. S. Hudak, X. H. Liu, A. Subramanian, H. Fan, L. Qi, A. Kushima, J. Li, *Science* **2010**, *330*, 1515-1520.
- [186] S. Chen, K. Kobayashi, R. Kitaura, Y. Miyata, H. Shinohara, *ACS Nano* **2011**, *5*, 4902-4908.
- [187] P. Kim, T. Russell, D. Hoagland, in *APS March Meeting 2013*, American Physical Society, **2013**, p. abstract #Q1.169.
- [188] P. Kim, T. Russell, D. Hoagland, in *APS March Meeting 2012*, American Physical Society, **2012**, p. abstract #C1.109.
- [189] I. A. Shkrob, S. D. Chemerisov, J. F. Wishart, *J. Phys. Chem. B* **2007**, *111*, 11786-11793.
- [190] I. A. Shkrob, T. W. Marin, S. D. Chemerisov, J. F. Wishart, *J. Phys. Chem. B* **2011**, *115*, 3872-3888.
- [191] I. A. Shkrob, T. W. Marin, S. D. Chemerisov, J. L. Hatcher, J. F. Wishart, *J. Phys. Chem. B* **2011**, *115*, 3889-3902.
- [192] I. A. Shkrob, *J. Phys. Chem. B* **2009**, *114*, 368-375.
- [193] J. Apgar, Y. Tseng, E. Fedorov, M. B. Herwig, S. C. Almo, D. Wirtz, *Biophys. J.* **2000**, *79*, 1095-1106.
- [194] D. Nykypanchuk, H. H. Strey, D. A. Hoagland, *Science* **2002**, *297*, 987-990.
- [195] K. Jaqaman, D. Loerke, M. Mettlen, H. Kuwata, S. Grinstein, S. L. Schmid, G. Danuser, *Nat. Methods* **2008**, *5*, 695-702.
- [196] R. Tsuda, K. Kodama, T. Ueki, H. Kokubo, S.-i. Imabayashi, M. Watanabe, *Chem. Commun.* **2008**, 4939-4941.
- [197] H.-N. Lee, Z. Bai, N. Newell, T. P. Lodge, *Macromolecules* **2010**, *43*, 9522-9528.
- [198] H.-N. Lee, T. P. Lodge, *J. Phys. Chem. Lett.* **2010**, *1*, 1962-1966.
- [199] T. Ueki, M. Watanabe, T. P. Lodge, *Macromolecules* **2009**, *42*, 1315-1320.
- [200] J.-F. Gohy, *Coord. Chem. Rev.* **2009**, *253*, 2214-2225.
- [201] P. M. Simone, T. P. Lodge, *Macromolecules* **2008**, *41*, 1753-1759.
- [202] J.-F. Gohy, B. G. G. Lohmeijer, S. K. Varshney, U. S. Schubert, *Macromolecules* **2002**, *35*, 7427-7435.
- [203] C. Mugemana, P. Guillet, C.-A. Fustin, J.-F. Gohy, *Soft Matter* **2011**, *7*, 3673-3678.

- 
- [204] K. T. Kim, J. Zhu, S. A. Meeuwissen, J. J. L. M. Cornelissen, D. J. Pochan, R. J. M. Nolte, J. C. M. van Hest, *J. Am. Chem. Soc.* **2010**, *132*, 12522-12524.
- [205] S. G. Roy, K. Bauri, S. Pal, A. Goswami, G. Madras, P. De, *Polym. Int.* **2013**, *62*, 463-473.
- [206] M. Doi, S. F. Edwards, *The Theory of Polymer Dynamics, Vol. 1*, Oxford University Press New York, **1986**.
- [207] I. A. Shkrob, T. W. Marin, S. D. Chemerisov, J. Hatcher, J. F. Wishart, *J. Phys. Chem. B* **2012**, *116*, 9043-9055.
- [208] R. Hoogenboom, S. Rogers, A. Can, C. R. Becer, C. Guerrero-Sanchez, D. Wouters, S. Hoepfener, U. S. Schubert, *Chem. Commun.* **2009**, 5582-5584.
- [209] K. Kempe, PhD-thesis, Friedrich-Schiller-Universität, Jena, **2012**.
- [210] F. Schacher, M. Müllner, H. Schmalz, A. H. E. Müller, *Macromol. Chem. Phys.* **2009**, *210*, 256-262.
- [211] H. Wei, S. Perrier, S. Dehn, R. Ravarian, F. Dehghani, *Soft Matter* **2012**, *8*, 9526-9528.
- [212] M. M. Bloksma, S. Hoepfener, C. D'Haese, K. Kempe, U. Mansfeld, R. M. Paulus, J.-F. Gohy, U. S. Schubert, R. Hoogenboom, *Soft Matter* **2012**, *8*, 165-172.
- [213] M. J. Barthel, T. Rudolph, S. Crotty, F. H. Schacher, U. S. Schubert, *J. Polym. Sci., Part A: Polym. Chem.* **2012**, *50*, 4958-4965.



## Supplementary information

### Experimental section of Chapter 4

#### Materials

The IIs depicted in Table S1 were purchased from Iolitec and were used as supplied. Lacey carbon-coated TEM copper grids (Mesh 400) were purchased from Agar Scientific and were plasma-cleaned prior to use, for 1 minute.

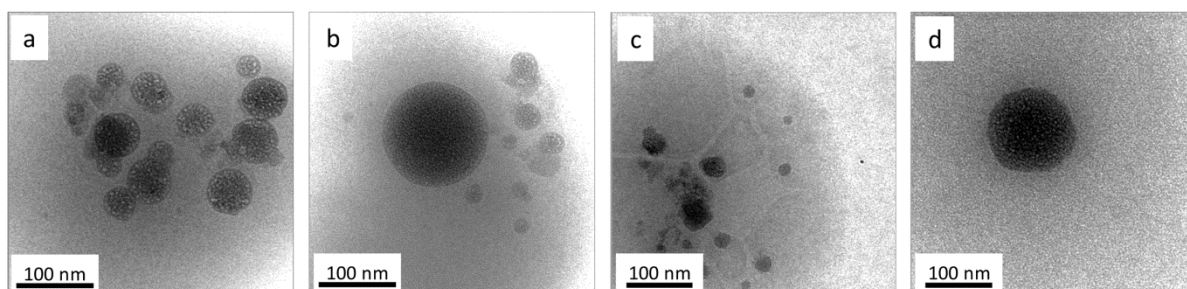
#### Instrumentation

For dryTEM the solution was dropped onto a carbon-supported copper grid (Mesh 400), was dried and subsequently measured at room temperature. For cryoTEM, the solution was dropped onto lacey carbon-coated grids and for cryoTEM, the blotted specimens were blotted and were rapidly plunged into a cryogen reservoir containing liquid ethane using an in-housebuilt controlled environment vitrification system (CEVS). After preparation the sample were stored and measured using a sample holder (Gatan 626-DH) at a temperature of approximately  $-180$  °C. The images were recorded with a bottom-mounted  $1k \times 1k$  pixel charge-coupled-device (CCD) camera from TVIPS. In the case of toluene, liquid nitrogen was used to vitrify the sample.

#### *Assembly of supramolecular block copolymers in aprotic solvents*

For the investigation of orthogonal supramolecular block copolymer  $[(\text{MPEG})\text{Ni}(\mathbf{6})]_2(\text{PF}_6)_4$  allowing beside metal-ion complexation also for quadruple hydrogen bonding, the assembly and measurement capability by either cryoTEM or dryTEM was tested in less protic/unpolar solvents, *i.e.* toluol, phenyl-decane, decaline, xylol, toluol, diethyl ether. As a reference system that is not capable of quadruple hydrogen bonding  $[(\text{MPEG})\text{Ni}(\mathbf{8})](\text{PF}_6)_2$  was used.

For this purpose, a  $1 \text{ g L}^{-1}$  solution was prepared using the cosolvent method with dichlormethane. Only in phenyl-decane, characteristic multicompartments assemblies were found for both systems that are different from the micellar assembly in DMF/water (Figure 3.3). In the unpolar solvent the PS block is soluble, while the PEG block represents the non-soluble block. However no significant difference between  $[(\text{MPEG})\text{Ni}(\mathbf{6})]_2(\text{PF}_6)_4$  and  $[(\text{MPEG})\text{Ni}(\mathbf{8})](\text{PF}_6)_2$  was found suggesting a minor influence of the quadruple hydrogen-bonding on the assembly in solution in the present case.



**Figure S 1** DryTEM images of assembly of  $[(\text{MPEG})\text{Ni}(\mathbf{6})]_2(\text{PF}_6)_4$  (a,b) and  $[(\text{MPEG})\text{Ni}(\mathbf{8})](\text{PF}_6)_2$  (c,d) in phenyl-decane.

## Experimental section of Chapter 5

### Materials

The IIs depicted in Table S1 were purchased from Iolitec and were used as supplied. Lacey carbon-coated TEM copper grids (Mesh 400) were purchased from Agar Scientific and were plasma-cleaned prior to use, for 1 minute.

### Instrumentation

The TEM samples were examined using a Phillips CM-120 transmission electron microscope, operated at 80 and 120 kV. For rtTEM, specimens were investigated using a sample holder (Gatan 626-DH) at 20 up to 92 °C. For cryoTEM, the blotted specimens were rapidly plunged into a cryogen reservoir containing liquid ethane using an in-housebuilt controlled environment vitrification system (CEVS). After preparation the sample were stored and measured using a sample holder (Gatan 626-DH) at a temperature of approximately –180 °C. The images were recorded with a bottom-mounted 1k×1k pixel charge-coupled-device (CCD) camera from TVIPS.

### *Preparation of the free-standing liquid films*

A small droplet of IL solution was dropped onto the lacey carbon grids at ambient conditions and blotted manually for 5 up to 15 s between filter paper, whereby the blotting times strongly depends on the viscosity of the IL. The remaining traces of the co-solvent were removed during the sample-transfer process to the TEM in the prevacuum pumping cycle. The liquid film formation as well as their durability against the electron beam was tested:

**Table S1** Overview of the used IL, their abbreviations and qualitative validation for free-standing liquid film investigation by TEM.

Ionic liquid	Abbreviation	Film formation	Beam durability
1-Ethyl-3-methylimidazolium bis(trifluoromethylsulfonyl)imide	EMIm Tf <sub>2</sub> N	+	++
1-Ethyl-3-methylimidazolium dicyanamide	EMIm N(CN) <sub>2</sub>	+	+
1-Ethyl-3-methylimidazolium ethyl sulfate	EMIm EtOSO <sub>3</sub>	+	+
1-Ethyl-3-methylimidazolium diethyl phosphate	EMIm DEP	+	-
1-Ethyl-3-methylimidazolium tetrafluoroborate	EMIm BF <sub>4</sub>	+	+
1-Ethyl-3-methylimidazolium triflate	EMIm TfO	+	++
1-Butyl-3-methylimidazolium hexafluorophosphate	BMIm PF <sub>6</sub>	+	+
1-Butyl-3-methylimidazolium tetrafluoroborate	BMIm BF <sub>4</sub>	+	+
1-Butyl-3-methylimidazolium triflate	BMIm TfO	+	++
1-Butyl-3-methylimidazolium bis(trifluoromethylsulfonyl)imide	BMIm Tf <sub>2</sub> N	+	++
1-Butyl-3-methylimidazolium iodide	BMIm I	-	-
1-Butylpyridinium bis(trifluoromethylsulfonyl)imide	BPy Tf <sub>2</sub> N	+	+
1-Butyl-1-methylpyrrolidinium bis(trifluoromethylsulfonyl)imide	BMpyrol Tf <sub>2</sub> N	+	-
Methyl octyl imidazolium tetrafluoroborate	MOIm BF <sub>4</sub>	+	-
Methyltriocylammonium bis(trifluoromethylsulfonyl)imide	MO <sub>3</sub> N Tf <sub>2</sub> N	-	-
Triethylsulfonium bis(trifluoromethylsulfonyl)imide	Et <sub>3</sub> S Tf <sub>2</sub> N	-	-

<sup>+</sup> remains liquid after irradiation/ good film formation; <sup>++</sup> remains liquid for long irradiation periods; <sup>-</sup> bad film formation, not stable upon irradiation (*i.e.* bursting, solidification, flowing).

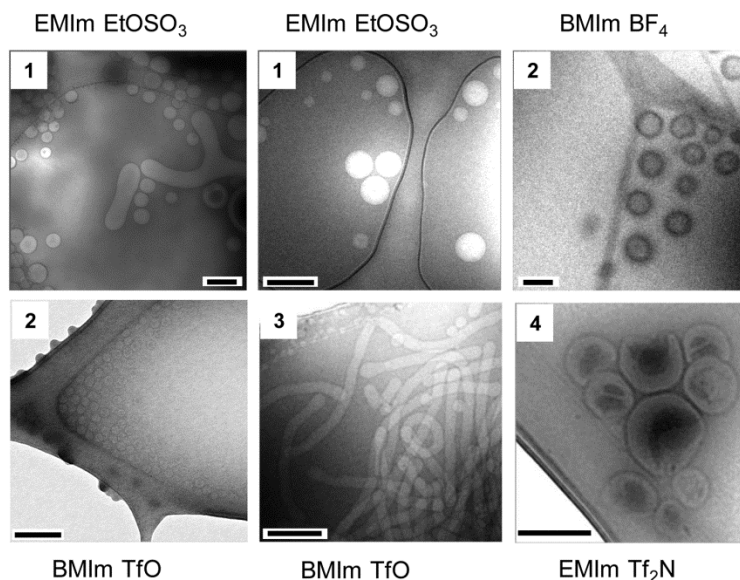
### General preparation of polymeric assemblies in ionic liquids

If not otherwise stated, to prepare a stock solution, the polymer (10 mg) was dissolved in dichloromethane (400  $\mu\text{L}$ ). The ionic liquid (40  $\mu\text{L}$ ) was slowly added into the diluted solution (20  $\mu\text{L}$  of polymer solution and 100  $\mu\text{L}$  dichloromethane) and the dichloromethane was subsequently evaporated at 60 to 80  $^{\circ}\text{C}$ .

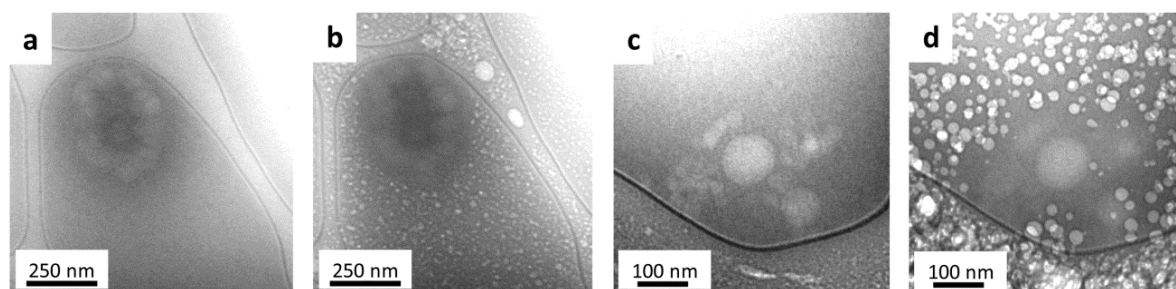
**Table S 2** Selection of investigated diblock polymers that show various assemblies in IL.

No.	Polymer	$M_n$ [kg/mol]	PDI
1	PS- <i>b</i> -P2VP <sup>a</sup>	440- <i>b</i> -350	1.19
2	PS- <i>b</i> -PEG <sup>a</sup>	100- <i>b</i> -34	--
3	PS- <i>b</i> -PMMA <sup>b</sup>	28- <i>b</i> -10	1.5
4	PS- <i>b</i> -PEtOx <sup>b</sup>	13- <i>b</i> -2	--
5	PB- <i>b</i> -PDMAEMA <sup>c</sup>	4.5- <i>b</i> -3.5	--

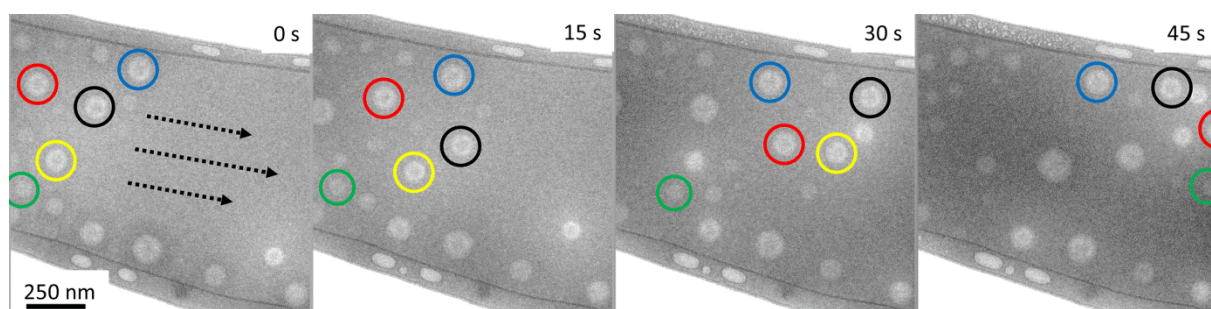
<sup>a</sup> The polymer was purchased from Polymer Source<sup>TM</sup>; <sup>b</sup> the polymers were provided and synthesized by the group of Prof. U. S. Schubert: 3,<sup>[208]</sup> 4;<sup>[209]</sup> <sup>c</sup> the polymer was provided and synthesized by the group of Prof. F. H. Schacher.<sup>[210]</sup>



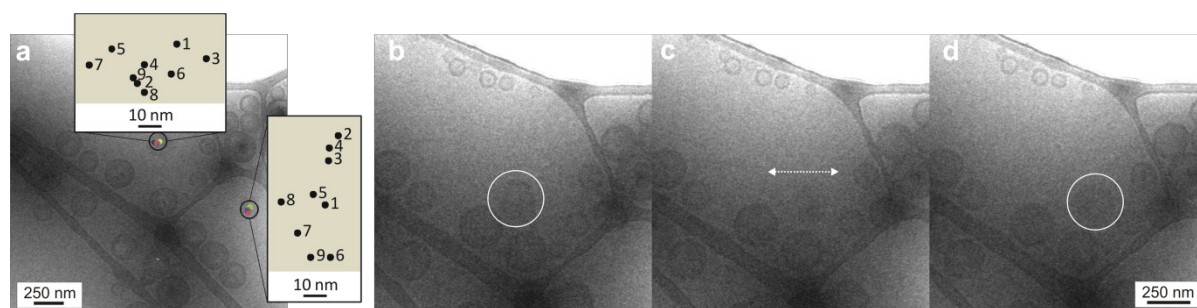
**Figure S 2** Overview of rtTEM images of selected polymers (Table S2) as 1 wt% solution in suitable IL for free-standing liquid film formation (scale bar = 500 nm).



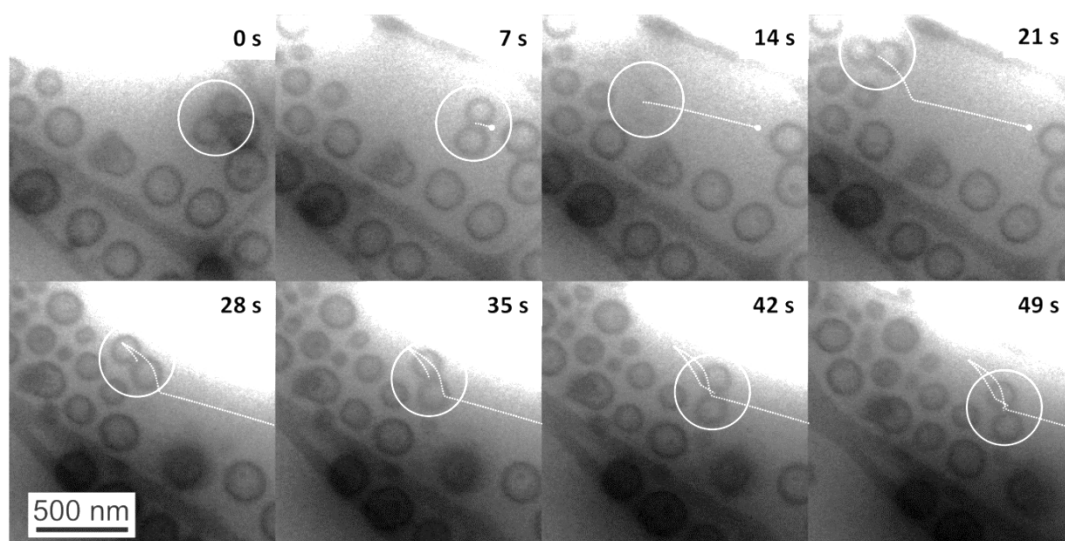
**Figure S 3** CryoTEM images of the assembly of PS<sub>440k</sub>-*b*-P2VP<sub>350k</sub> in solution (1 wt%) of EMIm Tf<sub>2</sub>N before (a) and after irradiation (b) as well as of Bpy Tf<sub>2</sub>N before (c) and after irradiation (d).



**Figure S 4** Convection driven movement of micelles by the IL for PS<sub>440K</sub>-*b*-P2VP<sub>350K</sub> in EMIm EtOSO<sub>3</sub> [recording duration:  $t = 51$  s with 800 ms/frame (300 ms accumulation, 500 ms read-out); 120 kV TEM voltage, 92 °C specimen temperature].



**Figure S 5** Images of a vesicle of PS<sub>100K</sub>-*b*-PEO<sub>34K</sub> in BMIm BF<sub>4</sub> at 92 °C. a) Analysis of the lateral movement of an individual vesicle over nine subsequently recorded images within 8 s. A detailed schematic representation of the particle positions provides the trajectory of the vesicle movement. b-d) Image sequence of an oscillation cycle of an individual vesicle between two distinct positions. The oscillation was observed over a time scale of 29 s [recording duration:  $t = 51$  s with 800 ms/frame (300 ms accumulation, 500 ms read-out); 80 kV TEM voltage, 92 °C specimen temperature].



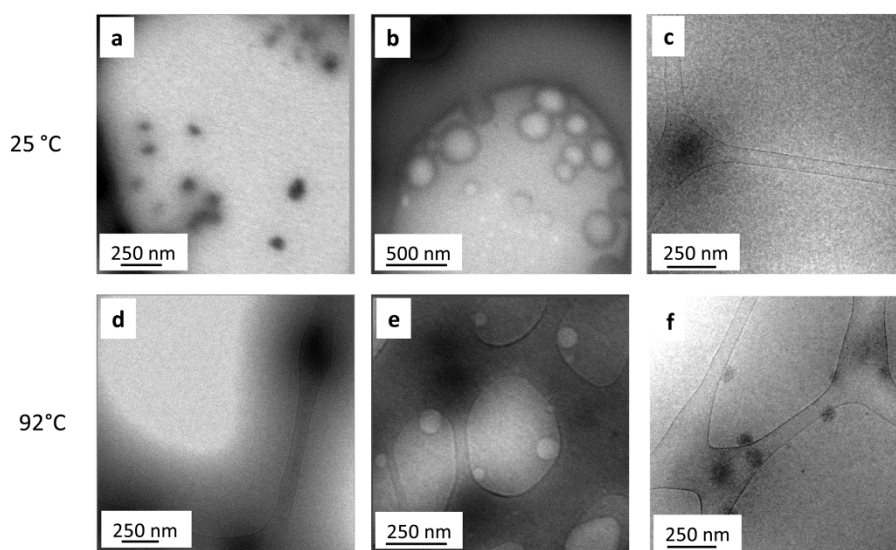
**Figure S 6** Image sequence of the collective movement of vesicles (encircled) of PS<sub>100K</sub>-*b*-PEO<sub>34K</sub> in BMIm BF<sub>4</sub> at 92 °C. The vesicle dimer is apparently free to rotate along its axis. The dimer is stable due to the entanglement of the polymeric coronas [recording duration:  $t = 51$  s with 800 ms/frame (300 ms accumulation, 500 ms read-out); 80 kV TEM voltage, 92 °C specimen temperature].



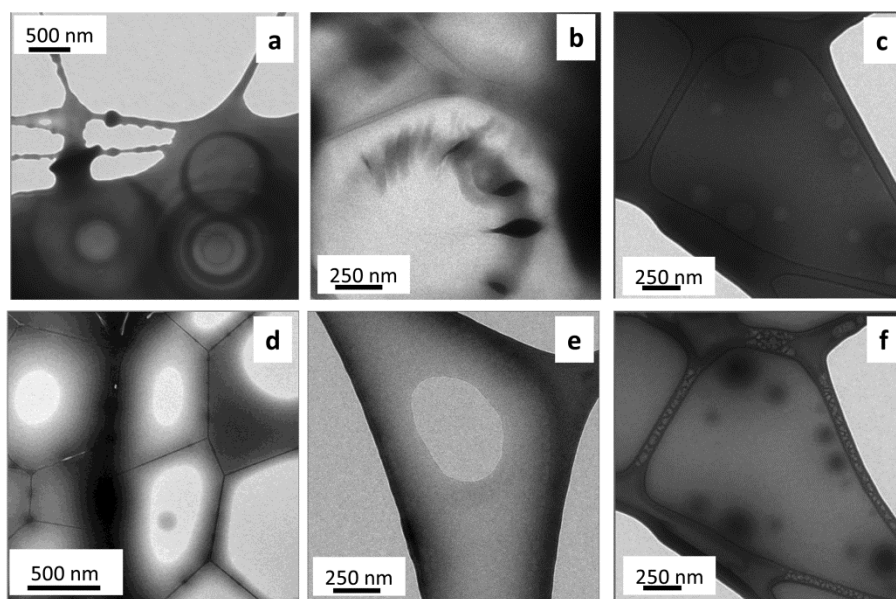
**Table S 3** Overview of the block copolymers that show temperature-dependent assembly within the free-standing liquid films.

Polymer	$M_n$ [g mol <sup>-1</sup> ]	IL	c [wt%]	Cloud point
PEG <sub>17,5k</sub> - <i>b</i> -PNiPAm <sub>5,5k</sub> <sup>a</sup>	23,000	BMIIm BF <sub>4</sub>	2	~70 °C (UT)
PEtOx <sub>67</sub> - <i>b</i> -R-PBuEtOx <sub>12</sub> <sup>a</sup>	10,000	EMIIm BF <sub>4</sub>	0.1	~70 °C (UT)
PEG <sub>334</sub> - <i>b</i> -PFGE <sub>20</sub> - <i>b</i> -PAGE <sub>20</sub> <sup>a</sup>	17,000	EMIIm BF <sub>4</sub>	3	~80 °C (LT)

<sup>a</sup> The polymers were kindly provided and synthesized by the group of Prof. U S. Schubert: PEG<sub>17,5k</sub>-*b*-PNiPAm<sub>5,5k</sub>,<sup>[211]</sup> PEtOx<sub>67</sub>-*b*-R-PBuEtOx<sub>12</sub>,<sup>[212]</sup> PEG<sub>334</sub>-*b*-PFGE<sub>20</sub>-*b*-PAGE<sub>20</sub> according to literature<sup>[213]</sup> with additional polymerization of PAGE as the third block.



**Figure S 7** TEM images of the temperature-dependent assembly upon heating of PEG<sub>17,5k</sub>-*b*-PNiPAm<sub>5,5k</sub> (a, d) showing disappearance of structures, PEtOx<sub>67</sub>-*b*-R-PBuEtOx<sub>12</sub> (b, e) showing partially disappearance of vesicles and PEG<sub>334</sub>-*b*-PFGE<sub>20</sub>-*b*-PAGE<sub>20</sub> (c, f) showing appearance of assemblies.



**Figure S 8** Room-temperature TEM images of various irradiation effects: a, b) Beam interaction as flowing of the IL, c, f) polymer film showing negative contrast of the charging and upon radiation contrast inversion caused by decomposition of polymer and IL as well as d, e) solidification of free-standing films.





## List of abbreviations

AAC	alkyne-alkyne homocoupling
AFM	atomic force microscopy
ATRP	atom transfer radical polymerization
BMI <sub>m</sub>	1-butyl-3-methylimidazolium
CH <sub>2</sub> Cl <sub>2</sub>	dichloromethane
CHCl <sub>3</sub>	chloroform
CRP	controlled radical polymerization
cryoTEM	cryogenic transmission electron microscopy
CuAAC	azide-alkyne 1,3-dipolar cycloaddition
DA	diels-alder
DIAD	diisopropyl azodicarboxylate
DMAc	dimethylacetamide
DMF	dimethylformamide
DOSY	difusion-ordered spectroscopy
EMIm	1-ethyl-3-methylimidazolium
EtOSO <sub>3</sub>	ethyl sulfate
GC	gas chromatography
HEEDTA	<i>N</i> -(2-hydroxyethyl)ethylenediaminetriacetic acid
HR-ESI MS	high resolution electrospray ionization mass spectrometry
IL	ionic liquid
$K_1, K_2$	stability constants
LCST	lower critical solution temperature
[M]	monomer concentration
[M <sub>0</sub> ]	monomer concentration at the beginning
MALDI-TOF MS	matrix-assisted laser desorption ionization time-of-flight mass spectrometry
MeOH	methanol
$M_n$	molar mass
MSD	mean-square displacement
NMP	nitroxide-mediated polymerization
NMR	proton nuclear magnetic resonance
P( <i>n</i> -BA)	poly( <i>n</i> -butyl acrylate)
P2VP	poly(2-vinylpyridine)
PAGE	poly(allyl glycidyl ether)
PB	poly(butadiene)
PBuEtOx	poly(butylethyl oxazoline)
PDI	polydispersity index
PDiFPhOx	poly(2-(2,6-difluorophenyl)-2-oxazoline)
PDMAEMA	poly( <i>N,N</i> -dimethylaminoethyl methacrylate)

## List of abbreviations

---

MPEG	methoxypoly(ethylene glycol)
PEPOx	poly(2-(1-ethylpentyl)-2-oxazoline)
PEtOx	poly(2-ethyl-2-oxazoline)
PFGE	poly(furfuryl glycidyl ether)
PFPhOx	poly(2-(pentafluorophenyl)-2-oxazoline)
PFSt	pentafluorostyrene
Ph <sub>3</sub> P	triphenylphosphane
PMMA	poly(methyl methacrylate)
PNiPAm	poly( <i>N</i> -isopropylacrylamide)
PNonOx	poly(2-nonyl-2-oxazoline)
poC	post-click
PPFS	poly(pentafluorostyrene)
prC	pre-click
PS	polystyrene
PTetFPhOx	poly(2-(tetrafluorophenyl)-2-oxazoline)
PTriFPhOx	poly(2-(trifluorophenyl)-2-oxazoline)
RAFT	reversible addition fragmentation chain transfer polymerization
RI	refractive index
rtTEM	room-temperature transmission electron microscopy
SEC	size-exclusion chromatography
St	styrene
TEM	transmission electron microscopy
TEMPO	tetramethylpiperidinyloxy
Tf <sub>2</sub> N	bis(trifluoromethylsulfonyl)imide
TFA	trifluoroacetic acid
TfO	triflate
TIPNO	2,2,5-trimethyl-4-phenyl-3-azahexane-3-nitroxide
TMS	trimethyl silyl
tpy	2,2':6',2''-terpyridine
UCST	upper critical solution temperature
UPy	2-ureido-4[1 <i>H</i> ]-pyrimidinone
UV-vis	ultraviolet-visible
ZnANC	nitrile-azide cycloaddition

# Publication list

## Refereed publications in scientific journals

1. U. Mansfeld, M. D. Hager, R. Hoogenboom, C. Ott, A. Winter, U. S. Schubert, “Advanced supramolecular initiator for nitroxide-mediated polymerizations containing both metal-ion coordination and hydrogen-bonding sites”, *Chem. Commun.* **2009**, 3386-3388.
2. U. Mansfeld, C. Pietsch, R. Hoogenboom, C. R. Becer, U.S. Schubert, “Clickable initiators, monomers and polymers in controlled radical polymerizations – a prospective combination in polymer science”, *Polym. Chem.* **2010**, *1*, 1560-1598.
3. M. M. Bloksma, S. Hoepfener, C. D'Haese, K. Kempe, U. Mansfeld, R. M. Paulus, J.-F. Gohy, U. S. Schubert, R. Hoogenboom, “Self-assembly of chiral block and gradient copolymers”, *Soft Matter* **2012**, *8*, 165-172.
4. C. Pietsch, U. Mansfeld, C. Guerrero-Sanchez, S. Hoepfener, A. Vollrath, M. Wagner, R. Hoogenboom, S. Saubern, S. H. Thang, C. R. Becer, J. Chiefari, U. S. Schubert, “Thermo-induced self-assembly of responsive poly(DMAEMA-*b*-DEGMA) block copolymers into multi- and unilamellar vesicles”, *Macromolecules* **2012**, *45*, 9292-9302.
5. U. Mansfeld, A. Winter, M. D. Hager, R. Hoogenboom, W. Günther, U. S. Schubert, “Orthogonal self-assembly of stimuli-responsive supramolecular polymers using one-step prepared heterotelechelic building blocks”, *Polym. Chem.* **2013**, *4*, 113-123.
6. U. Mansfeld, A. Winter, M. D. Hager, W. Günther, E. Altuntas, U. S. Schubert, “A homotelechelic bis-terpyridine macroligand: One-step synthesis and its metallo-supramolecular self-assembly” *J. Polym. Sci., Part A: Polym. Chem.* **2013**, *51*, 2006-2015.
7. U. Mansfeld, A. Winter, M. D. Hager, G. Festag, S. Hoepfener, U. S. Schubert, „Amphiphilic supramolecular A(B)<sub>2</sub>A quasi-triblock copolymers”, *Polym. Chem.* **2013**, *4*, 3177-3181.
8. U. Mansfeld, S. Hoepfener, K. Kempe, J.-M. Schumers, J.-F. Gohy, U. S. Schubert, “Tuning the morphology of triblock terpoly(2-oxazoline)s containing a 2-phenyl-2-oxazoline block with varying fluorine content”, *Soft Matter* **2013**, *9*, 5966-5974.

9. U. Mansfeld, S. Hoepfener, U. S. Schubert, "Investigating the motion of diblock copolymer assemblies in ionic liquids by *in-situ* electron microscopy", *Adv. Mater.* **2013**, *25*, 761-765.
10. M. J. Barthel, U. Mansfeld, S. Hoepfener, J. A. Czaplewska, F. H. Schacher, U. S. Schubert, "Understanding and tuning the self-assembly of polyether-based triblock terpolymers in aqueous solution", *Soft Matter* **2013**, *9*, 3509-3520.
11. F. Kretschmer, U. Mansfeld, S. Hoepfener, M. D. Hager, U. S. Schubert, "Tunable synthesis of poly(ethylene imine)-gold nanoparticle clusters", *Chem. Comm.* **2013**, DOI: 10.1039/C3CC45090B.

## Patent

1. U. Mansfeld, S. Hoepfener, U. S. Schubert, "*Observation method by TEM or SEM and specimen for use therein*", **2012**, Dutch Polymer Institute, WO2013135876 A1.

## Posters

1. *Synthesis of a new bifunctional initiator for NMRP: Towards tailor-made telechelic supramolecular polymers*, GDCh Conference ORCHEM, Weimar, Germany, 01.-03.09.2008, U. Mansfeld, M. D. Hager, R. Hoogenboom, A. Winter, U. S. Schubert.
2. *A new supramolecular initiator for NMRP containing metal-ion coordination and hydrogen-bonding sites*, Microstructural Control in Free-Radical Polymerization, Clausthal, Germany, 05.-08.10.2008, U. Mansfeld, M. D. Hager, R. Hoogenboom, A. Winter, U. S. Schubert.
3. *One-step preparation of telechelic polymers towards supramolecular architectures*, DPI Annual Meeting, Eindhoven, The Netherlands, 17.-18.11.2009, U. Mansfeld, M. D. Hager, R. Hoogenboom, A. Winter, U. S. Schubert.
4. *Ionic Liquids as alternative imaging media for self-assembled nanostructures by cryo-TEM*, CeNS Workshop, Venice, Italy, 19.-23.09.2011, U. Mansfeld, S. Hoepfener, U. S. Schubert.
5. *Investigating the motion of copolymer assemblies in ionic liquids by in-situ electron microscopy*, DPI Annual Meeting, Zeist, The Netherlands, 13.-14.09.2012, U. Mansfeld, S. Hoepfener, U. S. Schubert.

## Oral Presentations

1. *One-step preparation of supramolecular telechelics using advanced initiators for nitroxide-mediated polymerization*, CRP-meeting, Houffalize, Belgium, 17.-18.09.2009.





# Curriculum Vitae



- 07.08.1982 Born in Lutherstadt Eisleben, Germany
- 06/1993 – 06/2002 Acquirement of University-Entrance Diploma, Martin-Luther-Gymnasium, Lutherstadt Eisleben, Germany
- 07/2002 – 06/2003 Civilian service at “Burg und Schloß Allstedt”, Allstedt, Germany
- 10/2003 – 12/2008 Studies of Chemistry, Friedrich-Schiller-University, Jena, Germany
- 09/2006 Vordiplom (equivalent to B. Sc. honors)
- 11/2007 – 07/2008 Diploma thesis was performed at the Eindhoven University of Technology in the group of Prof. Dr. Ulrich S. Schubert, Eindhoven, The Netherlands
- 12/2008 Diplom (equivalent to M.Sc.honors)
- Since 04/2009 PhD student at the Laboratory of Organic and Macromolecular Chemistry at the Friedrich-Schiller-University Jena in the group of Prof. Dr. Ulrich S. Schubert, Jena, Germany

Jena, den \_\_\_\_\_

\_\_\_\_\_



## Acknowledgment

At this point, I would like to express my gratitude to all the persons that supported me during my PhD time. This thesis would have not been possible without their help, advices and encouragement.

First of all, I would like to thank Prof. Dr. Ulrich S. Schubert for the opportunity to perform my PhD work in his multilateral and pleasant group. Thank you for the continuous support and for giving me the freedom to do research and the room to grow ideas. Furthermore, I would like to acknowledge the Dutch Polymer Institute for the continuous financial support.

I want to express gratitude to Dr. Stephanie Höppener for the scientific mentoring. Thank you a lot for the continuous encouragement and scientific input throughout the research time and, of course, for the splendid espresso. I would like to thank Dr. Martin Hager and Dr. Andreas Winter for their striking support in tuning the manuscripts while having always an sympathetic ear for versatile questions. Thank you Martin for helping me to find the adequate research focus. Many thanks additionally to Prof. Richard Hoogenboom for fruitful discussions and notable advices to enrich some manuscripts. I want to kindly acknowledge Prof. Dr. Felix H. Schacher for helpful discussions, for triggering new ideas and for the scientific input.

Of course, there were a lot of more people I have benefited from over the years but it would be difficult to name them all. Nonetheless, I would like to give special gratitude to the following persons: I want to acknowledge Frank Steiniger for the help and the technical as well as scientific advices at the transmission electron microscope. Hereon, I want to thank the whole team of the electron microscopy center of the university of Jena for the kind atmosphere. I would like to thank Dr. Wolfgang Günther and his team for NMR experiments, also because the experiments were sometimes time-consuming. Dr. Grit Festag and Nicole Fritz are cordially acknowledged for many SEC measurements and related analysis. I'm obliged to Dr. Esra Altuntas for ESI-MS measurements and to Dr. Anja Baumgärtel for MALDI-MS measurements. In addition, I want to thank Sandra Köhn and Beate Lentvogt for elemental analysis. Also, I would like to thank Dr. Stephanie Höppener for AFM measurements. Furthermore, I want to thank the people that provided me with samples for the dynamic TEM studies: Prof. Dr. J.-F. Gohy, Prof. Dr. Felix H. Schacher, Dr. Christine Weber, Dr. Kristian Kempe, Dr. Christian Pietsch, Aydin Can, Markus Barthel, Christian von der Ehe, Andreas Krieg, Florian Kretschmer and Dr. Meta Bloksma.

Of course there are persons that are not directly related with the results of this thesis, but without their commitment and organisation the research would have not been possible in this way. Thereon, I want to acknowledge Dr. Jürgen Vitz and Renzo Paulus for taking care of the technical administration and keeping a lot of facilities and devices running, so that we can use them as convenient as possible. Furthermore, I want to express my gratitude to Dr. Uwe Köhn, Sylvia Braunsdorf, Anja Helbig, Tanja Wagner, Simone Burchardt and Doreen Kuchler for their organisational and administrative help.

## Acknowledgment

---

I want to thank the people that worked with me in the lab for the cooperative and friendly atmosphere: Julia Kötteritzsch, Dr. Andreas Wild, Florian Schlütter and Florian Kretschmer. I'm grateful to my office mates Grit, Sandra, Almut, Steffi, Stephanie, He, Erik and Benjamin for the enjoyable discussions, the cakes and laughter. In a broader sense, I'm grateful to all the members of the Schubert group for the versatile cooperation, pleasant time, and nice get-togethers. The research day would not have been the same without the lunch breaks that I had, in particular, with Michael, Benjamin and Christian, the one who held them all together: I want to thank you not only for the funny as well as serious debates we had, but also for having a sympathetic ear and good words on decisions.

I would like to express my deepest gratitude to my parents, who supported me over all the years and being always there for help and advices, while giving me the freedom to find my own way. On this note, I also want to thank my brother Johannes for being a true companion in my life, in particular over the last years in Jena.

Lastly, I would like to thank Juliane for the belief in me, for keeping me grounded and balanced while making this time so much more valuable.

## **Declaration of Authorship/Selbstständigkeitserklärung**

Ich erkläre, dass ich die vorliegende Arbeit selbständig und unter Verwendung der angegebenen Hilfsmittel, persönlichen Mitteilungen und Quellen angefertigt habe.

I certify that the work presented here is, to the best of my knowledge and belief, original and the result of my own investigations, except as acknowledged, and has not been submitted, either in part or whole, for a degree at this or any other university.

Jena, den \_\_\_\_\_

\_\_\_\_\_





## **Publications P1– P7**

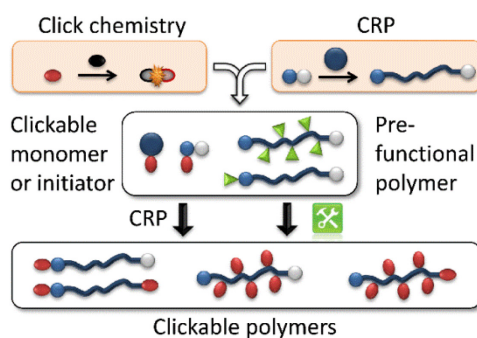


## Publication P1:

### *Clickable initiators, monomers and polymers in controlled radical polymerizations – a prospective combination in polymer science*

U. Mansfeld, C. Pietsch, R. Hoogenboom, C. R. Becer, U. S. Schubert,

*Polym. Chem.* **2010**, *1*, 1560-1598



Reproduced by permission of The Royal Society of Chemistry

<http://dx.doi.org/10.1039/C0PY00168F>



# Clickable initiators, monomers and polymers in controlled radical polymerizations – a prospective combination in polymer science

Ulrich Mansfeld,<sup>abc</sup> Christian Pietsch,<sup>abc</sup> Richard Hoogenboom,<sup>b</sup> C. Remzi Becer<sup>\*ab</sup> and Ulrich S. Schubert<sup>\*abc</sup>

Received 30th May 2010, Accepted 2nd July 2010

DOI: 10.1039/c0py00168f

Preparation of multifunctional and well-defined macromolecules requires a smart selection of the most suitable controlled polymerization technique in combination with appropriate click reactions. In this review, we provide an overview on the use of various “clickable” initiators and monomers as well as on the postpolymerization modifications that have been widely used to construct clickable macromolecules. As such, this contribution will aid polymer chemists to select a suitable combination of CRP and click methodologies to design the target structures.

## 1. Introduction

The synthesis of well-defined polymers has been the ultimate challenge of polymer chemists in the last decades. The development of anionic polymerization by Szwarc *et al.* opened new avenues and a new field of materials research.<sup>1,2</sup> Besides, polymeric materials have improved the quality of our lives in all areas from engineering to electronics and medical applications.<sup>3–5</sup> Following the invention of anionic polymerization, other possible types of living and/or controlled polymerizations, cationic and radical, have been widely studied.<sup>6–9</sup> The most significant controlled radical polymerization (CRP) techniques to date could be listed as atom transfer radical polymerization (ATRP),<sup>6–8</sup> nitroxide-mediated radical polymerization (NMP)<sup>9,10</sup>

and reversible addition-fragmentation chain transfer polymerization (RAFT).<sup>11,12</sup> Each of these techniques requires the use of a dedicated metal/ligand complex, chain transfer agent (CTA) or nitroxide mediator to gain control over the polymerization of various monomeric structures. All these parameters have been extensively investigated in detail and reported by numerous research groups. Consequently, nowadays well-defined polymers can be successfully synthesized and characterized by performing these techniques under specific conditions.

After significant advances in the controlled/“living” radical polymerization techniques over the last years, functionalization of the macromolecules has been the following challenge for polymer chemists. Synthesis of end- or side-functional macromolecules has been achieved by using functional initiators, monomers or end capping techniques. However, these specific functional groups might have enormous effects on the polymerization rate, control over the polydispersity index and the composition of the polymers. Fortunately, a decade ago, the click chemistry concept was introduced by Sharpless *et al.* that enables nowadays the preparation of not only telechelic polymers but also side-group functionalized polymers using clickable initiators, monomers or polymers.<sup>13–21</sup> Sharpless and coworkers

<sup>a</sup>Laboratory of Organic and Macromolecular Chemistry, Friedrich-Schiller-University Jena, Humboldtstr. 10, 07743 Jena, Germany. E-mail: ulrich.schubert@uni-jena.de; c.r.becer@warwick.ac.uk

<sup>b</sup>Laboratory of Macromolecular Chemistry and Nanoscience, Eindhoven University of Technology, P. O. Box 513, 5600 MB Eindhoven, The Netherlands

<sup>c</sup>Dutch Polymer Institute (DPI), P. O. Box 902, 5600 AX Eindhoven, The Netherlands



Ulrich Mansfeld

Ulrich Mansfeld studied chemistry at the Friedrich-Schiller-University Jena (Germany; 2003–2008) and accomplished the master thesis at the Eindhoven University of Technology (Netherlands) under the supervision of Prof. Ulrich S. Schubert. In 2009, he began his PhD studies working in the fields of controlled radical polymerizations and supramolecular chemistry.



Christian Pietsch

Christian Pietsch studied chemistry at the Friedrich-Schiller-University Jena (Germany). He completed his MSc in 2008 at the University of Technology in Eindhoven (Netherlands), where he worked on the synthesis of stimuli-responsive copolymers under the supervision of Prof. Ulrich S. Schubert. He continued as a PhD student in Jena working on responsive copolymers as well as living radical polymerization and dye-labeled polymers. Recently, he spent two months at CSIRO (Melbourne, Australia), where he carried out research on RAFT polymerizations.

drew attention to several highly efficient organic reactions, such as the copper-catalyzed [3 + 2] Huisgen cycloaddition reaction (CuAAC), which has developed into the most widely employed click reaction.<sup>22,23</sup> This reaction requires a copper salt and a ligand as catalysts but proceeds very rapidly and selectively at room temperature.<sup>24</sup> Several other efficient organic reactions have been claimed to be “click” reactions since they fulfilled all or some of the click chemistry criteria, which can be listed as modular and wide in scope, high efficiency and high yields, no or inoffensive byproducts, stereospecific, readily available starting materials and reagents, no solvent or a benign solvent, and simple purification techniques.<sup>17</sup>

Metal-free click reactions have attracted the greatest attention in recent years since they eliminate the main disadvantage of CuAAC click reactions: the use of a copper catalyst.<sup>17,25</sup> This opens new avenues to rapid and efficient reactions that can be

employed in, *e.g.*, living organisms.<sup>26</sup> Several types of metal-free click-like reactions have been developed and the most prominent ones are thiol-ene,<sup>19,27,28</sup> thiol-yne,<sup>29,30</sup> thiol-*para*-fluoro,<sup>31,32</sup> nitrile oxide-alkyne cycloaddition,<sup>33</sup> pyridyl disulfide exchange,<sup>34–36</sup> and Diels–Alder reactions.<sup>37–39</sup> These reactions have pros and cons in comparison to each other. Each of them can be used for certain monomers, initiators or polymerization techniques. Therefore, one should carefully design the synthetic route to prepare the desired functional polymer.

The aim of this review is to provide an insight on the selection of the most suitable CRP technique and click reaction for the synthesis of the desired tailor-made macromolecule. The range of functional initiators and monomers are listed in tables for each CRP technique. Hereby, click reactions performed before (“preclick”) and after (“postclick”) the polymerization initiated by a functional initiator or propagated with a functional monomer are discussed. The special focus will be on the combinations of CRP and click chemistry techniques rather than discussing each of them in details.

## 2. Overview on click reactions used in combination with controlled radical polymerization techniques

In the following section the click reactions that have been used in combination with CRP are briefly summarized while referring to the original literature (Scheme 1).

The most widely applied click reaction has been the copper-catalyzed azide-alkyne 1,3-dipolar cycloaddition (CuAAC) as shown in Scheme 1.<sup>40</sup> Sharpless *et al.* defined this type of cycloaddition as the ideal click reaction and the reaction principle has been employed in various fields of synthetic chemistry, *i.e.* medicinal chemistry, polymer chemistry, material chemistry, inorganic chemistry and, in particular, organic chemistry.<sup>13</sup> This reaction proceeds very rapidly in aqueous medium and even under ambient conditions. The major drawback of this reaction



**Richard Hoogenboom**

*Richard Hoogenboom was born in 1978 in Rotterdam (Netherlands) and studied chemical engineering at the Eindhoven University of Technology (TU/e; Netherlands). In 2005, he obtained his PhD under the supervision of Ulrich S. Schubert (TU/e) and continued working as project leader for the Dutch Polymer Institute. After postdoctoral training with Martin Möller at the RWTH Aachen (Humboldt fellowship) and Roeland J. M. Nolte at the Radboud University Nijmegen (NWO veni-grant), he was appointed as associate professor at Ghent University from July 2010. His research interests include stimuli-responsive polymers, supramolecular polymers, and poly(2-oxazoline)s.*



**C. Remzi Becer**

*C. Remzi Becer was born in 1980 in Izmir, Turkey. He received his BSc degree in 2003 at the Chemistry Department of the Istanbul Technical University (ITU). In 2005, he received his MSc degree in Polymer Science and Technology at the ITU. He completed his PhD study titled as “Controlling Polymer Architectures” in 2009 under the supervision of Ulrich S. Schubert at the Eindhoven University of Technology (Netherlands) and the Friedrich-Schiller-University Jena (Germany). Since late 2009, he has been a Marie Curie Research Fellow in the University of Warwick (United Kingdom). His research interests include controlled living polymerization techniques, click reactions and glycopolymers.*



**Ulrich S. Schubert**

*Ulrich S. Schubert was born in Tübingen in 1969. He studied chemistry at the Universities of Frankfurt and Bayreuth (both Germany) and the Virginia Commonwealth University, Richmond (USA). His PhD thesis was executed at the University of Bayreuth and the University of South Florida Tampa. After postdoctoral training with Professor Lehn at the Université Strasbourg (France) he moved to the Technische Universität München (Germany) to obtain his Habilitation in 1999. From 1999 to 2000 he held a temporal position as professor at the Center for NanoScience, Universität München (Germany). From 2000 to 2007 he was Full-Professor at the Eindhoven University of Technology. Currently he holds a chair at the Friedrich-Schiller-University Jena.*

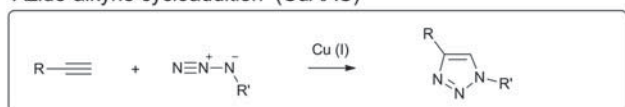
is the necessity of using a copper salt, which requires a purification step following the click reaction.<sup>41</sup>

Nevertheless, this drawback can be overcome by choosing alkynes with higher reactivity. For instance, cyclooctyne derivatives can undergo strain-promoted azide-alkyne click reactions in biological environments.<sup>42</sup> Similarly, electron-deficient alkynes and activated alkynes also provide highly efficient reactions.<sup>43</sup> Apparently, alkyne compounds play a crucial role in many different click-like reactions. As an example, Tunca and Hizal *et al.* demonstrated the synthesis of A<sub>2</sub>-B<sub>2</sub> 4-miktoarm star copolymers using the Glaser coupling as an alkyne-alkyne homocoupling reaction (AAC),<sup>44</sup> which is a copper-catalyzed reaction that reaches completion at room temperature in three

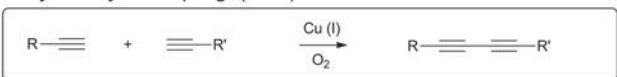
days.<sup>45</sup> Recently, Lutz and Heaney *et al.* reported the cycloaddition of alkynes with nitrile oxides (NOAC)<sup>46</sup> in combination with CRP as a potential click reaction.<sup>33</sup> This reaction proceeds at room temperature, in polar medium, in the absence of transition metal catalyst, in high yields and is highly regioselective. Besides alkynes, also nitriles can react with azides in a zinc-catalyzed cycloaddition<sup>47</sup> and can be used in combination with CRP.<sup>48</sup>

Alkynes do not only react with azides<sup>49</sup> or its own kind but also react with thiols, known as thiol-yne click reaction.<sup>29,30</sup> This represents a very efficient reaction and results in addition of two thiol compounds per alkyne molecule, which can be either added by a base-catalyzed Michael addition or by a photo-initiated

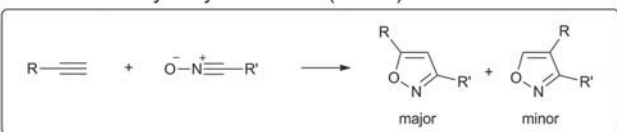
#### Azide-alkyne cycloaddition (CuAAC)



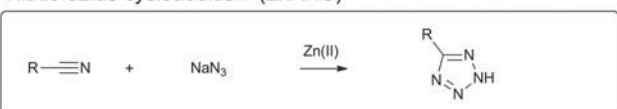
#### Alkyne-alkyne coupling (AAC)



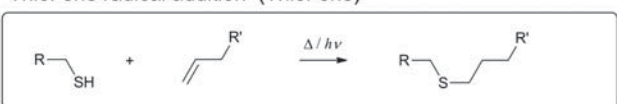
#### Nitrile oxide-alkyne cycloaddition (NOAC)



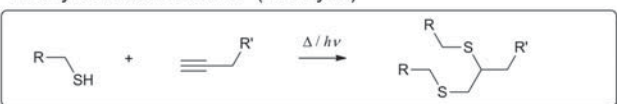
#### Nitrile-azide cycloaddition (ZnANC)



#### Thiol-ene radical addition (Thiol-ene)



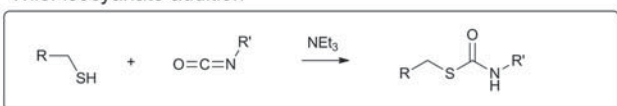
#### Thiol-yne radical addition (Thiol-yne)



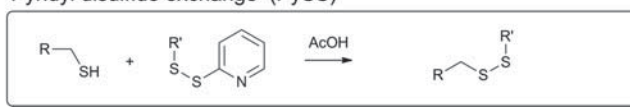
#### Michael addition (MAdd)



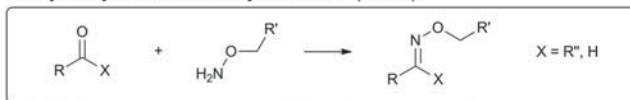
#### Thiol-isocyanate addition



#### Pyridyl disulfide exchange (PySS)



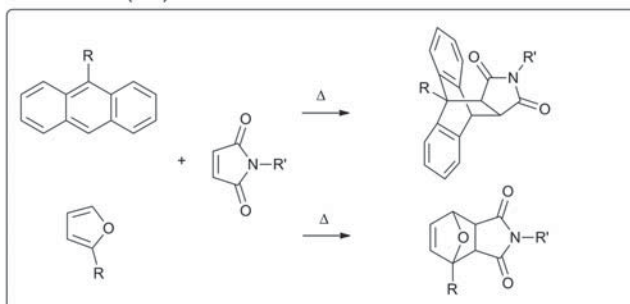
#### O-Hydroxylamine-carbonyl addition (Oxim)



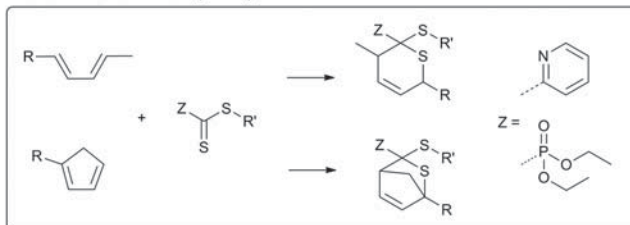
#### Ring-opening reaction of epoxides (RO)



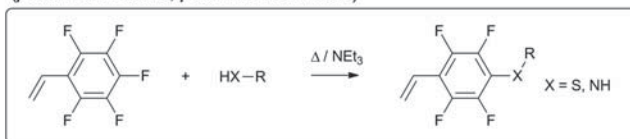
#### Diels Alder (DA)



#### Hetero Diels Alder (HDA)



#### *para*-Fluoro-nucleophile substitution (*para*-fluoro-thiol, *para*-fluoro-amine)



**Scheme 1** Schematic representation of the click reactions that have been used in combination with controlled radical polymerization techniques.



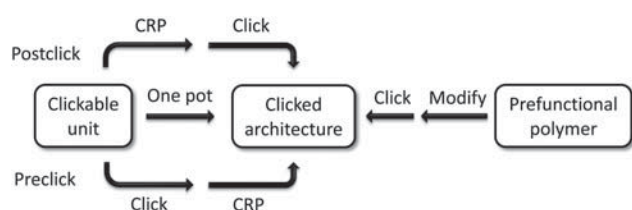
Anti-Markovnikov-addition.<sup>29,50</sup> Thiol compounds have been in the focus of click reactions in the last couple of years due to their high reactivity towards common functional groups, *i.e.* alkene, alkyne, isocyanate and pentafluorophenyl.<sup>51</sup> The thiol-ene click reaction has been utilized by several groups for the synthesis of dendrimers, the side-chain functionalization of well-defined backbones and for the synthesis of block copolymers.<sup>19,28,52</sup> Advantages and disadvantages of this type of click reaction have been discussed in several review articles.<sup>10,53</sup> Other thiol-based click reactions can be counted as thiol-maleimide addition (MAdd),<sup>28</sup> thiol-isocyanate addition<sup>54</sup> and pyridyl disulfide exchange (PySS).<sup>36</sup> Thiol-terminated polymers can be easily obtained by RAFT polymerization of a wide range of monomers and a subsequent cleavage of the chain transfer agent. However, hetero Diels–Alder (HDA) reaction using a dedicated chain transfer agent can be employed without a transformation of the RAFT agent to prepare AB block copolymers.<sup>55</sup> Commonly, the Diels–Alder reaction (DA) has been employed to construct miktoarm star polymers<sup>56</sup> or to engineer self-healing polymers by reversible crosslinking.<sup>57</sup>

A frequently used reaction for bioconjugation is the oxime formation (Oxim) that has been applied in the conjunction of carbonyl-functionalized proteins and aminoxy-functionalized polymers.<sup>58</sup> Furthermore, the ring-opening reaction of epoxides as a well-known spring-loaded reaction<sup>13</sup> is used in combination with the CRP of glycidyl methacrylate mostly to introduce other clickable functionalities<sup>59</sup> or for attachment on surfaces.<sup>60</sup>

In practice, some combinations of click reactions and CRP techniques are most commonly applied which will be discussed in detail in the following sections.

### 3. Strategies towards clicked polymer architectures

There are at least four common ways to combine controlled radical polymerization techniques and click chemistry to construct various clicked polymeric architectures. Thereby, each approach has its inherent drawbacks and amenities. The strategies are summarized in Scheme 2 and will be discussed in a general way in the following.



**Scheme 2** Schematic representation of the strategies towards clicked architectures.

#### 3.1 Postclick strategy

By using functional initiators or monomers with clickable moieties for controlled radical polymerizations, clickable polymers can be achieved to construct various architectures by clicking post to the polymerization.

As a limitation, the clickable functionality must not interfere with the polymerization process or has to be protected to gain

control over the polymerization and, thus, yielding well-defined polymers with high functional group fidelity up to sufficient monomer conversions. Moreover, most functional monomers or initiators are not commercially available and have to be synthesized prior to the polymerization.

The clickable polymer represents a platform for versatile click functionalization, while retaining the polymer characteristics *i.e.* chain length, monomer composition and molar mass dispersity. Herein, the approach has a wide scope by means of construction flexibility, in contrast to the preclick approach (see below), since different functional polymers can be prepared from a single batch of a clickable macromolecule. Furthermore, the same molar mass and its distribution allow for a better comparison of changes related to the functionality.

The postclick approach offers high functional group fidelity compared to the postmodification approach. In particular, for the polymerization of clickable monomers each repeating unit of the resultant polymer bears the clickable unit in contrast to a prefunctional homopolymer that have to be modified with the clickable moiety after polymerization. Accordingly, using  $\alpha$ -functionalized initiators each chain is monoterminally functionalized, while end-group functionalization *via* the postmodification are limited by the yield of the final modification step.

#### 3.2 Preclick strategy

Clicked polymeric architectures can be also obtained by using functional initiators or monomers with clickable moieties that are clicked prior to the polymerization in a so-called “preclick” route. This method is predominantly used if the clickable units interfere with the radical process or the temperature of the polymerization and can not be sufficiently protected.

As a limitation, the clicked moiety must be stable under the applied polymerization conditions. It should be mentioned that Diels–Alder adducts tend to undergo retro Diels–Alder reactions at elevated temperatures and, hence, are not in principle amenable for this strategy. However, the stability range of the Diels–Alder adducts is strongly system dependent.<sup>61,62</sup> Recently, some literature examples discussed the polymerizability and stability of related clicked initiators and monomers. Maleimide functionalities are often protected by the reversible Diels–Alder reaction with furan to make it more compatible with radical polymerization processes, which was demonstrated by Sanyal and coworkers using a furan-maleimide methacrylate. This monomer was polymerized by a free radical polymerization procedure at 65 °C and deprotected *via* retro-DA at 125 °C.<sup>63</sup> Syrett *et al.* reported an ATRP reaction with a clicked initiator linked *via* the maleimide-furan adduct, where the polymerization was successfully performed at 50–60 °C and the retro Diels–Alder reaction occurred at 120 °C.<sup>64</sup> By using a clicked initiator with the maleimide-anthracene adduct significantly higher thermal stability was observed upon the retro Diels–Alder reaction. In addition, Barner-Kowollik *et al.* investigated a hetero Diels–Alder cycloadduct of a dithioester and cyclopentadiene that was rapidly formed at room temperature and cleaved above 80 °C.<sup>65</sup> By contrast, the Huisgen 1,3-dipolar cycloaddition of alkynes with azides represents a prominent reaction for this strategy, since the triazole ring is stable under the typically applied polymerization conditions. Furthermore, the bulkiness of the clicked unit should

not disturb the polymerization process by causing slow propagation or deactivating of the catalytic system.

In case the clicked monomers can be successfully polymerized *via* CRP, this procedure provides the highest control over the incorporation of the clicked functionality into polymeric architectures, while having the lowest scope by means of construction flexibility:

On the one hand, the click reaction has been performed with small molecules (monomers or initiators) that can be easily purified and analyzed. Hereon, subsequent polymerization is carried out with less reactive material leading to high functional-group fidelity, whereby no further functionalization is required. However, in order to obtain clicked architectures with different clicked functionalities, the click reaction as well as the polymerization has to be carried out for each clicked architecture. This method has been successfully employed for the preparation of comb-shaped polymers with almost quantitative functionalization of each repeating unit.<sup>66,67</sup>

### 3.3 Simultaneous/one pot strategy

In many cases the catalyst used in the ATRP polymerization, *i.e.* CuBr/PMDETA (*N,N,N',N'',N'''* pentamethyldiethylene triamine), is the same as for the click reaction that allows a simultaneous/one-pot process of polymerization and click reaction. The combination of the Cu(I)-catalyzed Huisgen cycloaddition and a CRP process allows the one-pot synthesis of a wide range of products, *i.e.*  $\alpha$ -functional- (clickable initiator), grafted- (clickable monomer), star-shaped polymers and polymeric networks, respectively. The simultaneous process means that CRP and click reaction occur at the same time during the polymer synthesis. In contrast to a one-pot process, whereas at first the polymerization and then the click reaction are performed or *vice versa* (subsequent addition of the second compound). The advantage of this strategy in contrast to the “preclick” or “postclick” way is that for clicked polymeric architectures only one synthesis step and one purification step is required. However, it should be noted that the click reaction generally proceeds much faster than the ATRP and, thus, most click coupling reactions will occur during the initial stages of the polymerization.

The first example of this combined route was demonstrated by Haddleton *et al.* in 2005 using an azide-functionalized ATRP initiator for the polymerization of methyl methacrylate as indicated by a linear relationship of the first order kinetic plot. The efficiency of the click reaction was investigated in the presence of alkyne-functional dyes.<sup>68</sup> Another example of simultaneous click and CRP with an unprotected propargyl methacrylate was also reported by Haddleton *et al.* It was shown that the copper-catalyzed azide-alkyne click reaction proceeds much faster compared to the ATRP.<sup>69</sup> The authors could also show that the ratio of rate constants for the polymerization and the click process can be controlled by varying the solvent, the temperature or the concentration of the catalyst. Thus, it was demonstrated that the rate of CuAAC in DMSO is slower than the polymerization, whereas in DMF or toluene the click reaction is faster than the polymerization. The measured PDI values of the synthesized copolymers were found to be below 1.3.<sup>69</sup> As a limitation, the clickable functionality must be used without a protection group to allow the Huisgen cycloaddition and, hence, side reactions can occur.

Also the one-pot/tandem process is often used for the preparation of clicked polymeric architectures by using ATRP polymerization and CuAAC. This approach uses the same catalytic system for both the click reaction as well as ATRP, but sequentially. Thereby, both ways are possible: At first the click reaction followed by the polymerization or *vice versa* (in the manner that the second compound was added later). In contrast, if all components are added at once, the click reaction can be performed at room temperature, while after full conversion, the temperature was raised to initiate the polymerization.<sup>70</sup> In all cases well-defined copolymers were obtained. Dubois *et al.* discussed these different routes and showed that both the preclick as well as the one-pot route give similar results in molar mass and PDI values, whereby the postclick route leads to an increase of the polydispersity index from 1.3 to 1.5.<sup>70</sup>

### 3.4 Postmodification strategy

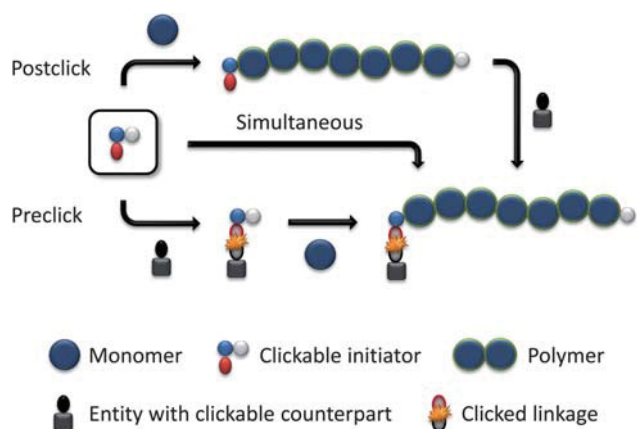
Prefunctional polymers with latent groups prepared by CRP can be modified with clickable moieties to obtain clickable polymers. The modification reaction must be efficient, since it correlates to the fidelity of functional groups in the modified polymer. Mostly, purification steps are necessary, since even efficient modification reactions are not quantitative. In this case, modification as well as clicking are carried out at the polymer, which might complicate in principle the purification and analysis. In particular, incomplete modification is critical for pendant functional polymers, since the unreacted functionalities are attached to the same polymer backbone as the converted ones and, thus, can not be separated as it can be done for endgroup-modified polymers.

As an advantage, the starting materials by means of initiators and monomers are in most cases commercially available or can be easily synthesized allowing for large scale experiments. This approach can be used for terminal and pendant functionalized polymers, except for comb-shaped polymers, since electronic and steric effects may hinder full transformation. This method is in particular suitable for clicked architectures where the clickable as well as the clicked moiety interfere with the polymerization process.

It should be noted that in a narrower sense the described reactions are defined as click reactions for the conjunction of small molecules, since they feature among other characteristics a high efficiency and selectivity allowing for the equimolar usage of the click counterparts. However, the conjunction of polymers using these reactions leads not always to full conversion probably due to sterical hindrance or affected diffusion of the polymer chains.<sup>53</sup> To drive the reaction to completion, an excess of one clickable polymer can be used. If the click reaction is completed, the typical problems of purification due to the equal solubility behavior of both product and educt polymer can be overcome by adding a click-functionalized resin containing the click counterpart related to the excess one.<sup>71,72</sup> The subsequent purification of the desired clicked architecture can be then easily performed by filtration of the clicked resin.

## 4. Clickable initiators

The use of functional initiators in controlled radical polymerization processes lead to terminal-functionalized polymers in one



**Scheme 3** Schematic representation of the strategies using clickable initiators.

step. Thereby, two possible routes can be employed using clickable initiators. As illustrated in Scheme 3, click reactions can be performed either after the polymerization (postclick) or prior to the polymerization (preclick). For ATRP initiators only  $\alpha$ -clickable polymers are inherently possible in one step. With the ability of the synthesis of initiators/transfer agents for NMP and RAFT with functional groups on both the initiating as well as on the mediating fragment the toolbox expands and  $\omega$ -clickable polymers as well as  $\alpha,\omega$ -clickable polymers are accessible in a one step procedure. The advantage of the clickable initiator approach compared to the clickable monomer route is the lower concentration of the clickable unit. Hence, side reactions are reduced and protection is not strictly necessary while leading to a controlled polymerization with a high degree of functionalization of the clickable moiety. In the following, an overview of potential clickable initiators is given and is summarized in Tables 1 to 7. Possible combinations and the restrictions of CRP and click reactions are discussed. Unless otherwise noted, all selected initiators belong to the postclick approach.

#### 4.1 Atom transfer radical polymerization (ATRP)

ATRP is the most widely employed CRP technique using the clickable initiator approach because of the easy preparation of functional initiators. Different types of initiators are discussed in the following subsections (Tables 1–3).

**Alkyne-functionalized initiators.** The first report on the combination of click chemistry and a controlled radical polymerization technique was published by van Hest *et al.* in 2005 showing the facile approach towards block copolymers *via* the azide-alkyne cycloaddition.<sup>73</sup> By using propargyl 2-bromoisobutyrate (Entry 1) as clickable initiator terminal alkyne-functionalized polystyrenes and polyacrylates were synthesized. The initiator is based on a common ATRP initiator group, which is an  $\alpha$ -halo ester. The terminal alkyne was protected with a trimethylsilyl group (TMS) to prevent possible side reactions under the polymerization conditions: (i) Complexation with the copper catalyst,<sup>73–75</sup> (ii) subsequent homocoupling of alkynes,<sup>44</sup> (iii) chain transfer by hydrogen abstraction from the alkyne<sup>76</sup> and interference with propagating radicals leading to crosslinking.<sup>77</sup>

Nevertheless, the TMS group was found to be instable under the polymerization conditions using CuBr/PMDETA as catalyst that leads to a loss of protecting group up to 70%.<sup>78</sup> The loss was ascribed to a nucleophilic attack to the TMS group by one of the nitrogen atoms of PMDETA. As a consequence, the less nucleophilic ligand bipyridine (bpy) was chosen to reduce the deprotection although it is not the optimum catalyst for ATRP reactions and does not avoid the decomposition completely.<sup>78</sup> Another strategy uses the more stable triisopropylsilyl group (TIPS) instead of TMS revealing no loss during the polymerization.<sup>78</sup> This might be due to the bulky character of the protecting group that hinders the nucleophilic attack of the metal/ligand complex. The alkyne-functionalized initiators bearing either a chlorine or a bromine atom as an initiating moiety were frequently reported for the polymerization of styrene, acrylates, methacrylates and *N*-isopropylacrylamide, whereby in some cases the terminal alkyne was protected with TMS<sup>33,44,76,79,80</sup> or not protected.<sup>81–86</sup> Haddleton and coworkers used the unprotected alkyne initiator depicted in Entry 1 for the random copolymerization of methyl methacrylate (MMA) and hostasol methacrylate (HMA) ( $M_n = 15\,000\text{ g mol}^{-1}$ , PDI = 1.2–1.3).<sup>82</sup> The  $\alpha$ -functionalized fluorescent copolymer was clicked onto cotton and both Wang and Merrifield resins using the Huisgen [2 + 3] cycloaddition. Recently, Tunca and coworkers used the protected initiator (Entry 1) for the preparation of block copolymers of styrene and divinylbenzene to form multiarm star polymers with terminal alkyne groups.<sup>87–89</sup> At first, styrene was polymerized to obtain linear alkyne-functional PS (up to  $M_n = 6\,000\text{ g mol}^{-1}$ , PDI = 1.1). Subsequently, the prepared PS was used as macroinitiator in the polymerization of divinylbenzene leading to a crosslinked second block that form the core of the multiarm star polymer (up to  $M_w = 250\,000\text{ g mol}^{-1}$ , PDI = 1.2). Besides the initiator depicted in Entry 1, its analogue propargyl 2-halopropionate (Entry 2) was also used as clickable initiator for the polymerization of acrylates and NIPAM without any protection.<sup>90,91</sup>

In most cases of the unprotected initiators, good control over the polymerization was achieved yielding alkyne-functional polymers with low PDI values. In these cases, the undesired chain transfer and termination reactions are suppressed to a negligible amount by decreasing the reaction time<sup>84</sup> and keeping the polymerization at low conversions to reduce the termination reactions at the  $\omega$ -end of the chain. The bromine atom is often substituted in a postmodification reaction with sodium azide to yield heterotelechelic polymers bearing an alkyne and an azide end group, respectively. Furthermore, side reactions involving the alkyne functionality were suppressed by using low alkyne concentrations according to a high monomer-to-initiator ratio<sup>92</sup> or by using relatively low temperatures,<sup>85,91</sup> *i.e.* 40 °C for the polymerization of *t*BMA<sup>85</sup> or NIPAM.<sup>91</sup> In contrast, the polymerization of styrene was conducted for 6 h at 90 °C with the initiator depicted in Entry 1 as nonprotected alkyne initiator revealing significant termination reactions as indicated by SEC measurements.<sup>86</sup> It should be noted that direct polymerization throughout the triple bond is hindered, because radical transfer reactions from the styrene or methacrylate radical are suppressed by their low reactivity (Q-values, r-values).

Most of the alkyne-functionalized ATRP initiators are based on the  $\alpha$ -halo isobutyrate group. This class of alkyl halides possesses high activation rates due to the suitable radical-stabilization

**Table 1** Alkyne-containing initiators for ATRP (poC = postclick, prC = preclick, simult = simultaneous)

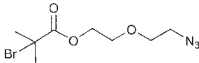
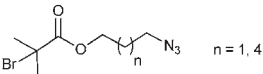
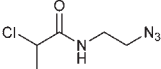
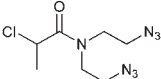
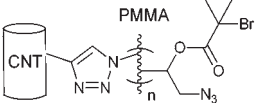
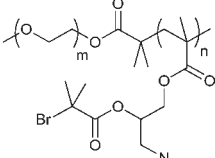
Entry	Structure	Click	CRP	Monomer (Abbr./Entry)	Strategy	Ref
1		CuAAC	ATRP	St, MA, OEGA <i>t</i> BA, NIPAM, <i>t</i> BMA, DEAEMA, HMA	poC	73,76,78–81, 83–89,103,104
		AAC NOAC	ATRP ATRP	St St	poC poC	44 33
2		CuAAC	ATRP	NIPAM, EEA	poC	90,91
3		CuAAC	ATRP	NIPAM, <b>46</b> , <b>53</b>	prC	95
4		CuAAC	ATRP	St, <i>t</i> BA, MMA	simult	96
5		CuAAC	ATREP	St, VBA, <b>50</b>	simult	83
6		CuAAC	ATRP	St	poC	97
7		CuAAC	ATRP	St	poC	98
8		CuAAC	ATRP	MMA	prC	99
9		CuAAC	ATRP ROP	St, MMA, <i>t</i> BA DMAEMA, NIPAM	poC	71,94,100
			ATRP ROP	St	prC	101
10		CuAAC	ATRP	<i>t</i> BA	poC	102

effects of the tertiary carbon and the vicinal ester group resulting in a high initiation efficiency, which is required to control molar masses and molar mass distributions.<sup>93</sup> In most of the present cases, this type of initiator is used for ATRP regardless of the

polymerized monomer class, *e.g.* styrenes, acrylates or methacrylates. However, normally the initiator structure is carefully chosen for each given monomer and its reactivity.<sup>6,93</sup> Therefore, special focus appear not to be on the optimal initiator structure for



**Table 2** Azide-containing initiators for ATRP (poC = postclick, prC = preclick, simult = simultaneous)

Entry	Structure	Click	CRP	Monomer	Strategy	Ref
11		CuAAC	ATRP	DMAEMA, St	poC	92,106,107
12		CuAAC	ATRP	MMA, DEAEMA, HEMA, KSPMA, HMA, NIPAM, DMAEMA, DEAM, St	poC, simult	68,82,94,109–112
13		CuAAC	ATRP	NIPAM	poC	113
14		CuAAC	ATRP	NIPAM	poC	110
15		CuAAC	ATRP	St, <i>n</i> BMA	poC, prC	114
16		CuAAC	ATRP	DEGMA	poC	104

control, but on the accessibility of an alkyne-functionalized one. Practically,  $\alpha$ -bromoisobutyryl bromide is commercial available and is mostly functionalized *via* esterification reaction with propargyl alcohol.

The most widely employed catalytic system is CuBr and PMDETA again regardless of the initiator or monomer type. Besides, other catalytic systems, *e.g.* CuCl/tris(2-(dimethylamino)-ethyl)amine (Me<sub>6</sub>TREN) for the polymerization of NIPAM<sup>91,94</sup> or 1,1,4,7,10,10-hexamethyltriethylenetetramine (HMTETA),<sup>44</sup> could provide better control over the polymerizations. The catalytic activity of the metal complex and, hence, the ability to control the polymerization can be correlated to the ability to stabilize the Cu(II) oxidation state, thus forming a reducing Cu(I) complex.<sup>93</sup> The polymerization can proceed relatively fast even at low temperatures when a catalyst with a high activity is used.<sup>6</sup> PMDETA is a good ligand for Cu(I) with moderate activity between the less active bpy (two magnitudes lower in activation rate) and the more active Me<sub>6</sub>TREN (two magnitudes higher in activation rate) and, therefore, can be used for a wide range of monomers.<sup>93</sup>

Besides the attachment of propargyl alcohol, the alkyne moiety can also be incorporated onto an ATRP initiator by the

reaction of propargyl amine with  $\alpha$ -haloisobutyryl halides. An example is shown in Entry 3.<sup>95</sup> Hereby, a combination of the pre- and the postclick approach was utilized. The initiator was clicked prior to the polymerization with azide-functionalized dansyl as a fluorescent label. By using this compound as initiator in ATRP different random copolymers of alkyne- or azide-functionalized acrylamides were obtained: Poly(NIPAM-*r*-propargylacrylamide) ( $M_n = 20\,000\text{ g mol}^{-1}$ , PDI = 1.3) and poly[NIPAM-*r*-(3-azidopropylacrylamide)] ( $M_n = 10\,000\text{ g mol}^{-1}$ , PDI = 1.2). The pendant clickable polymers were attached onto an azide-functionalized silica particle in an elegant layer-by-layer click approach to yield thermoresponsive microcapsules after removal of the silica template.<sup>95</sup>

In Entry 4 an initiator is shown where the alkyne is linked to the mediating bromide *via* an *o*-nitrobenzyl ester as a photo-cleavable group.<sup>96</sup> The initiator was used in a one-pot click-CRP reaction for the polymerization of either St, *t*BA or MMA in the presence of azide-functionalized PEO or PS to prepare photo-cleavable block copolymers as clicked structures with the labile group between the polymer blocks: PEO-*b*-PS ( $M_n = 38\,000\text{ g mol}^{-1}$ , PDI = 1.2), PEO-*b*-*t*BA ( $M_n = 63\,000\text{ g mol}^{-1}$ , PDI = 1.2), PS-*b*-PMMA ( $M_n = 38\,000\text{ g mol}^{-1}$ , PDI = 1.2–1.3).

The initiator can bear more than one alkyne functionality. Multifunctional initiators can be used to create two or three dimensional architectures such as star polymers or networks. The initiator depicted in Entry 5 contains two bromoisobutyrate groups as well as two propargyl groups (unprotected alkynes) and is used in atom transfer radical emulsion polymerization in water to synthesize crosslinked nanoparticles of styrene and vinylbenzyl azide.<sup>83</sup> An example that can be better analyzed by means of molar mass and its polydispersity index is described for the initiator depicted in Entry 6 bearing both two alkyne and two bromoisobutyrate groups. The polymerization of styrene was carried out for 2 h at 110 °C without the protection of the terminal alkyne groups ( $M_n = 4\,000\text{ g mol}^{-1}$ , PDI = 1.1–1.2), while the subsequent alkyne-azide cycloaddition leads to figure-of-eight-shaped polymers.<sup>97</sup>

Another alkyne-functionalized initiator (Entry 7) is functionalized with one bromoisobutyrate as well as two propargyl groups.<sup>98</sup> Thereby, one alkyne moiety was clicked with an azide-functionalized poly(ethyleneglycol) (PEG) and was subsequently utilized in the polymerization of styrene without protecting the second alkyne moiety that resulted in a “tadpole-shaped” architecture after the second click reaction.<sup>98</sup>

In addition, a trialkyne-functionalized initiator (Entry 8) was synthesized by the substitution reaction of propargyl

bromide with pentaerythritol followed by the attachment of  $\alpha$ -bromoisobutyryl bromide on the remaining alcohol groups.<sup>99</sup> The initiator was used in a preclick approach: First, azido-PS prepared by RAFT ( $M_n = 2\,500\text{ g mol}^{-1}$ , PDI = 1.1) was clicked onto the initiator. Thereby, the molar mass distribution increased to 1.2 due to the presence of small amounts of macroinitiator, where only two PS-chains were attached. Subsequently, the PS-macroinitiator was used in the polymerization of MMA to yield 4-arm stars ( $M_n = 34\,000\text{ g mol}^{-1}$ , PDI = 1.3–1.4). The high polydispersity was assigned to a lack of control in the initial stages of the polymerization.

Furthermore, alkyne-functionalized initiators were combined with other polymerization techniques or methods by incorporating, *e.g.*, alcohol groups for ring-opening polymerization (ROP) (Entry 9), whereby the polymerization techniques do not interfere with each other and can be applied simultaneously<sup>100</sup> or subsequently.<sup>101</sup> Besides the incorporation of  $\alpha$ -haloisobutanoyl halides (halide = Cl, Br) into small molecules they can also be incorporated into alcohol-functionalized polymers to form ATRP macroinitiators as shown in Entry 10.<sup>102</sup> In this example, polystyrene was synthesized *via* anionic polymerization and functionalized with propargyl bromide and  $\alpha$ -bromoisobutanoyl bromide to provide an alkyne-functionalized ATRP macroinitiator. Polymerization of *t*BA yielded mid-chain alkyne-

**Table 3** Other click-functionalized initiators for ATRP (poC = postclick, prC = preclick)

Entry	Structure	Click	CRP	Monomer (Abbr./Entry)	Strategy	Ref
17		DA MAdd	ATRP ATRP	<i>t</i> BA, MMA OEGMA, 45, SMA	poC prC poC	115,117,120,121,125 64 66,122,123
18		MAdd	ATRP	NIPAM	prC	35,58
19		DA	ATRP	St, MMA	poC	87,89,121,124,125
20		DA	ATRP	St	–	126
21		Thiol-ene	ATRP	St, MMA	poC	127
22		PySS	ATRP	St, <i>t</i> BMA, MMA	poC prC	34,128,129 35,58
23		Oxim	ATRP	NIPAM, HEMA, OEGMA	poC	131,132

functionalized PS-*b*-PtBA block copolymers ( $M_n = 15\,000\text{ g mol}^{-1}$ , PDI = 1.2–1.3).

**Azide-functionalized initiators.** The cycloaddition counterparts to the alkyne-functionalized initiators are azide-functionalized ones. The common procedure for their syntheses is the functionalization of a basic framework with (i) an azide *via* substitution reaction of an alkyl halide with sodium azide and (ii) with  $\alpha$ -haloisobutyrate as the ATRP initiating fragment *via* esterification of an amine or alcohol function.

One can mistrust the requirement of azide-functionalized initiators, since the azide functionality can be easily and efficiently introduced by substitution of the mediating halide with sodium azide. However, the degree of azide functionalization that can be reached with the initiator approach is higher compared to the postmodification route. The reason lies in the nature of controlled radical polymerizations: Termination reactions always occur and, hence, not all polymer chains retain the halide at the  $\omega$ -terminus which is the bottleneck for the degree of functionalization that can be reached *via* postmodification. In contrast, using functional initiators, every chain that is initiated by the initiator bears the azide moiety at the  $\alpha$ -terminus independently from termination reactions.

The azide moiety is used without protection during polymerization, although some side reactions were described: (i) Cyclization reactions between the azide and the propagating radical that causes low initiator efficiency,<sup>68,92</sup> (ii) 1,3-cycloaddition of azides with the double bond of the monomer occurs in the absence of a catalyst at high temperatures and long reaction times, at which the amount decreases in the order of acrylates > acrylamides >> methacrylates > styrenes.<sup>105</sup>

To reduce the side reactions to a negligible amount, short reaction times<sup>92,106</sup> and low temperatures<sup>92,107</sup> are preferably used. It was shown that the polymerization at room temperature completely suppressed side reactions involving the azide.<sup>108</sup> Hence, monomer classes are favored that can be polymerized at moderate temperatures.

In contrast, it was shown that the azide group does not act as an initiating species itself as indicated by controlled polymerizations with an azide-containing initiator.<sup>92</sup>

The initiator structure depicted in Entry 11 (top) was used for the polymerization of *N,N*-dimethylamino-2-ethyl methacrylate (DMAEMA)<sup>92,106</sup> in THF with CuBr/HMTETA at 60 °C in a controlled way (PDI = 1.1–1.3). However, the initiator efficiency was low ( $f = 0.4$ ) due to intramolecular cyclization at the early stages of the polymerization involving the azide and the propagating radical.<sup>92</sup> Therefore, the “pre-click” method was utilized to circumvent these side reactions as the azide-functionalized initiator was “clicked” onto an alkyne-functionalized poly( $\epsilon$ -caprolactone) (PCL). As expected, an increase in the initiation efficiency to  $f = 0.85$  could be observed when using the “clicked” PCL macroinitiator.<sup>92</sup> This is a good example where the preclick method is used since the postclick route failed in parts due to side reactions involving the clickable unit.

The initiator structure depicted in Entry 11 (bottom) containing a cleavable *p*-alkoxybenzyl ester was used in bulk polymerization of styrene at 90 °C, whereby no termination reactions were observed ( $M_n = 4\,000\text{ g mol}^{-1}$ , PDI = 1.1–1.2).<sup>107</sup>

The spacer between the initiating fragment and the azide function seems to have a significant influence on the initiation efficiency in terms of intramolecular cyclization: The initiator depicted in Entry 12 shows, despite a controlled polymerization of MMA ( $M_n = 6\,000\text{ g mol}^{-1}$ , PDI = 1.2–1.3), a reduced initiation efficiency for the hexyl spacer (70 to 80%) compared to the propyl spacer (100%).<sup>68</sup> Hence, the initiator efficiency can be optimized by choosing an initiator structure by means of a spacer that prevents cyclization in the early stages of the polymerization.

In Table 2, 3-azidopropyl 2-bromoisobutyrate (APBIB) has been the most widely used azide-functionalized initiator (Entry 12,  $n = 1$ ). Controlled polymerization of St ( $M_n = 4\,500\text{ g mol}^{-1}$ , PDI = 1.3),<sup>109</sup> NIPAM ( $M_n = 10\,000\text{ g mol}^{-1}$ , PDI = 1.1–1.2),<sup>110</sup> and DMAEMA ( $M_n = 10\,000\text{ g mol}^{-1}$ , PDI = 1.1–1.2) have been reported.<sup>111</sup>

Moreover, Haddleton and coworkers used the azide-functionalized initiator depicted in Entry 12 for the random copolymerization of MMA and hostasol methacrylate (HMA) ( $M_n = 8\,000\text{ g mol}^{-1}$ , PDI = 1.2).<sup>82</sup> The  $\alpha$ -functionalized fluorescent copolymer was clicked onto cotton and both Wang and Merrifield resins using Huisgen [2 + 3] cycloaddition.

In addition, Topham and coworkers have polymerized a number of acrylates and methacrylates (MA) in a controlled way using APBIB as initiator:<sup>112</sup> 2-Aminoethyl methacrylate hydrochloride ( $M_n = 7\,000\text{ g mol}^{-1}$ , PDI = 1.1–1.2), 2-(diethylamino)ethyl methacrylate (DEAEMA) ( $M_n = 21\,000\text{ g mol}^{-1}$ , PDI = 1.3), DMAEMA ( $M_n = 7\,000\text{ g mol}^{-1}$ , PDI = 1.3), 2-hydroxyethyl methacrylate (HEMA) ( $M_n = 7\,000\text{ g mol}^{-1}$ , PDI = 1.3), 2-hydroxypropyl methacrylate (HPMA) ( $M_n = 5\,000\text{ g mol}^{-1}$ , PDI = 1.2), 2-(methacryloyloxy)ethyl phosphorylcholine ( $M_n = 15\,000\text{ g mol}^{-1}$ , PDI = 1.2), glycerol monomethacrylate ( $M_n = 11\,000\text{ g mol}^{-1}$ , PDI = 1.2), potassium 3-sulfopropyl methacrylate (KSPMA) ( $M_n = 20\,000\text{ g mol}^{-1}$ , PDI = 1.2), and methyl chloride-quaternized 2-(dimethylamino)-ethyl methacrylate ( $M_n = 5\,000\text{ g mol}^{-1}$ , PDI = 1.2).

Furthermore, 2-chloropropionamide linked with an ethyl spacer to the azide moiety (Entry 13) was utilized in the controlled polymerization of NIPAM ( $M_n = 12\,000\text{ g mol}^{-1}$ , PDI = 1.3).<sup>113</sup> The *N,N*-diazido-2-chloropropionamide (Entry 14) was used in the polymerization of NIPAM to incorporate two azide functionalities on the same chain end ( $M_n = 10\,000\text{ g mol}^{-1}$ , PDI = 1.1)<sup>110</sup> In this way, 3-arm star polymers can be prepared.

Besides the initiators discussed above, there are also azide-functionalized macroinitiators available. An elegant example of a multi-clickable initiator that is attached to a carbon nanotube (CNT) is shown in Entry 15.<sup>114</sup> Poly(glycidyl methacrylate) (PGMA) is functionalized in a ring-opening reaction with sodium azide and subsequently reacted with 2-bromoisobutryl bromide to yield a multi-clickable polymeric macroinitiator. This multiazide-functionalized polymer was clicked onto a multialkyne-functionalized CNT, whereby the excess of azide functions over the alkyne ones preserve free azides on the surface of the carbon nanotube. This coated CNT was used to click PEG in a grafting-onto approach as well as to polymerize St or *n*BMA in a grafting-from approach to yield amphiphilic polymer brushes on carbon nanotubes.



A similar macroinitiator was prepared from a copolymer (PEG-*b*-PGMA), whereby the poly(glycidyl methacrylate) was functionalized in a ring-opening reaction with sodium azide and subsequently reacted with 2-bromoisobutryl bromide to yield a multi-clickable polymeric macroinitiator (Entry 16).<sup>104</sup> Polymerization of DEGMA yielded azide-functionalized PEO-*b*-[PGMA-*g*-(N<sub>3</sub>)(PDEGMA)] ( $M_n = 52\,000\text{ g mol}^{-1}$ , PDI = 1.2). In a grafting-onto approach alkyne-functionalized PDEAEMA was attached *via* click reaction to obtain coil-rod double hydrophilic diblock copolymers.

**Maleimide-functionalized initiators.** Another frequently used click reaction is the Diels–Alder reaction that becomes more and more prominent in combination with controlled radical polymerizations in the field of material science.<sup>57,115–121</sup>

A widely used example is the [4 + 2] cycloaddition of maleimide and anthracene, whereby both moieties can be used as clickable functions attached to common ATRP initiators. The maleimide function must be protected, since it can act as a polymerizable monomer leading to crosslinking and a significant decrease of clickable fidelity after polymerization.<sup>122</sup> Therefore, the maleimide is protected prior to the polymerization *via* Diels–Alder reaction with furan that can be easily cleaved after the polymerization in a retro Diels–Alder reaction by heating the protected polymer. Besides, the maleimide can also undergo Michael addition with thiols as a Michael acceptor (Entry 17, 18).<sup>35,58,66,122,123</sup>

An often used maleimido initiator is depicted in Entry 17. In general, the maleimide was attached to 2-bromoisobutyrate in a stepwise fashion. At first, maleic anhydride reacts with furan to protect the double bond. Subsequently, the imide was formed with ethanolamine under reflux and as the last step commercially available 2-bromoisobutryl bromide was reacted.<sup>122</sup> This protected initiator was utilized *via* the postclick approach in the homopolymerization of MMA<sup>115,117,120,121</sup> (up to  $M_n = 3\,000\text{ g mol}^{-1}$ , PDI = 1.1–1.2), OEGMA (up to  $M_n = 32\,000\text{ g mol}^{-1}$ , PDI = 1.2),<sup>122</sup> (2,2-dimethyl-1,3-dioxolan-4-yl)methyl methacrylate (up to  $M_n = 35\,000\text{ g mol}^{-1}$ , PDI = 1.2),<sup>122</sup> *t*-butyl acrylate (*t*BA)<sup>115</sup> (up to  $M_n = 3\,000\text{ g mol}^{-1}$ , PDI = 1.2) and the random copolymerization of different methacrylates<sup>66,123</sup> containing protected alkyne, ketosol and hostasol or rhodamine B as fluorescent dyes ( $M_n = 10\,000\text{ g mol}^{-1}$ , PDI = 1.2). In none of these cases, side reactions were observed or discussed. Furthermore, this initiator was used in preclick approaches by Haddleton and coworkers for the polymerization of MMA at 50 °C (up to  $55\,000\text{ g mol}^{-1}$ , PDI < 1.2).<sup>64</sup> Thereby, the alcohol-functionalized maleimide was clicked *via* DA reaction with an alcohol-functionalized furan or anthracene moiety and was subsequently reacted with 2-bromoisobutryl bromide to obtain clicked dual-initiators with ATRP-mediating moieties on both click counterparts.

The anthracene-functionalized initiator depicted in Entry 19 was synthesized from commercially available 9-anthracenemethanol and 2-bromoisobutryl bromide<sup>124</sup> and was utilized in the homopolymerization of MMA<sup>87,124</sup> (up to  $M_n = 30\,000\text{ g mol}^{-1}$ , PDI = 1.1) and styrene<sup>121</sup> ( $M_n = 5\,000\text{ g mol}^{-1}$ , PDI = 1.1).

Tunca and coworkers used the initiator shown in Entry 19 for the preparation of block copolymers of styrene and divinylbenzene to form multiarm star polymers with terminal anthracene

groups.<sup>125</sup> At first, styrene was polymerized to obtain linear anthracene-functional PS (up to  $M_n = 6\,000\text{ g mol}^{-1}$ , PDI = 1.1). Subsequently, the prepared PS was used as macroinitiator in the polymerization of divinylbenzene leading to a crosslinked second block that form the core of the multiarm star polymer (up to  $M_w = 75\,000\text{ g mol}^{-1}$ , PDI = 1.5). Furthermore, anthracene functional PS (prepared with the initiator shown in Entry 19) as well as alkyne functional PS (prepared with the initiator shown in Entry 1) were used as macroinitiators for the ATRP of divinylbenzene yielding multiarm star polymers with terminal alkyne and anthracene groups ( $M_w = 250\,000\text{ g mol}^{-1}$ ).<sup>89</sup> The orthogonality of the two clickable groups were utilized in a sequential double click reaction to selectively attach azide-functionalized P*t*BA and maleimide-functionalized PMMA.

In addition, commercially available 9-chloromethylanthracene was applied as initiator in the polymerization of styrene ( $M_n = 4\,500\text{ g mol}^{-1}$ , PDI = 1.2) using CuCl/bpy as catalytic system in THF (Entry 20).<sup>126</sup> Although the prepared polymers were not yet applied in a Diels–Alder reaction, the terminal anthracene moiety represents a potential group for this click reaction.

**Ene-functionalized initiators.** Since the thiol-ene reaction is a rather new type of click reaction, only one example of an ATRP initiator was published so far to the best of our knowledge (Entry 21).<sup>127</sup> Hawker and coworkers reported an alkene-containing  $\alpha$ -bromoisobutyrate type of initiator. The polymerization of St and MMA was carried out yielding terminal alkene-functionalized polymers. In a postmodification reaction with sodium azide, the  $\omega$ -bromide could be easily exchanged with an azide moiety to form a heterotelechelic clickable polymer. The orthogonality of the subsequent thiol-ene and CuAAC click reaction was proven by stepwise “clicking”, whereby the thermal thiol-ene reaction was preferred due to possible side reactions of the alkyne during UV-light exposure.

**Pyridyl-disulfide-functionalized initiators.** Another click-like reaction that is used in combination with ATRP is the pyridyl disulfide exchange which is important in particular in bioconjugation.<sup>128,129</sup> It is a metal-free reaction and can be considered as a click reaction in a broader sense. The reaction is not an oxidative radical coupling reaction of thiols but a nucleophilic exchange reaction, whereby the formed thiolate must be a good leaving group. It is reported that pyridyl disulfides are known to undergo direct coupling with free thiols under ambient conditions in bioconjugation, whereby 2-pyridinethione is released as a good leaving group.<sup>34</sup> The pyridyl disulfide moiety can be considered as a protected thiol and can be used in radical polymerizations. However, side reactions in terms of chain coupling and transfer involving the disulfide were observed at high conversions and at high amounts of catalyst (catalyst to initiator ratio of 1 : 1). Side reactions could be reduced by using less catalyst<sup>130</sup> (catalyst to initiator ratio of 1 : 0.2) or by changing the catalytic system from CuBr/bpy to CuCl/bpy<sup>34</sup> which decreases the amount of free radicals.

An ATRP initiator with a pyridyl disulfide moiety is depicted in Entry 22 and was introduced by Maynard and coworkers.<sup>34</sup> It was used for the homopolymerization of MMA ( $M_n =$

10 000 g mol<sup>-1</sup>, PDI = 1.2), *N*-acetyl-*D*-glucosamine-functionalized methacrylate<sup>128</sup> ( $M_n = 13\,000$  g mol<sup>-1</sup>, PDI = 1.1), *N*-hydroxysuccinimidyl methacrylate<sup>129</sup> ( $M_n = 10\,000$  g mol<sup>-1</sup>, PDI = 1.3), 2-THP-protected HEMA<sup>129</sup> ( $M_n = 10\,000$  g mol<sup>-1</sup>, PDI = 1.3), *t*-butyl methacrylate (*t*BMA)<sup>129</sup> ( $M_n = 5\,000$  g mol<sup>-1</sup>, PDI = 1.5), HEMA<sup>34</sup> ( $M_n = 16\,000$  g mol<sup>-1</sup>, PDI = 1.2–1.3), and St<sup>129</sup> ( $M_n = 13\,000$  g mol<sup>-1</sup>, PDI = 1.2).

In contrast to these postclick approaches for bioconjugation also the preclick approaches are conducted with retention of the bioactivity.<sup>35</sup> As advantages of the grafting-from approach the following issues can be pointed out: (i) The purification of the bioconjugate from catalyst and monomer is simplified compared to the purification from the polymer in the grafting-onto approach and (ii) the placement of the polymer is predetermined facilitating the synthesis and characterization.<sup>58</sup> Herein, 2-bromoisobutyrate as an ATRP initiator functionalized with either pyridyl disulfide (Entry 22) or maleimide (Entry 18) was clicked prior to the polymerization onto the free cysteine of a protein (Bovine Serum Albumin or T4 lysozyme). Using these protein macroinitiators NIPAM could be polymerized *in situ* (PDI = 1.3).<sup>35,58</sup>

**Initiators for oxime formation.** A well-known reaction in bioconjugation is the oxime formation of aminoxy-functionalized compounds with carbonyl-containing proteins. Due to the tolerance of functional groups in controlled radical polymerizations,  $\alpha$ -functionalized polymers could be synthesized using *t*-butoxycarbonyl-protected (Boc) aminoxy-initiators for ATRP as shown by Maynard and coworkers.<sup>131,132</sup> Thereby, no termination reactions occurred during the polymerization induced by the protected aminoxy functionalization. After polymerization the aminoxy group can be easily deprotected with trifluoroacetic acid. As depicted in Entry 23, the aminoxy moiety was linked *via* a tetra(ethylene glycol) spacer to either 2-bromoisobutyrate for the polymerization of methacrylates or 2-chloropropionate for the polymerization of acrylamides. In this way,  $\alpha$ -functionalized polymers were obtained with NIPAM ( $M_n = 16\,000$  g mol<sup>-1</sup>, PDI = 1.1), HEMA ( $M_n = 40\,000$  g mol<sup>-1</sup>, PDI = 1.2), and oligo(ethylene

glycol) methacrylate (OEGMA) ( $M_n = 23\,000$  g mol<sup>-1</sup>, PDI = 1.2–1.3).<sup>131,132</sup>

#### 4.2 Reversible addition fragmentation chain transfer (RAFT)

In principle, all types of monomers which can be polymerized by free radical polymerization can also be polymerized by RAFT using the appropriate type of RAFT agents, *i.e.* dithiobenzoates, trithiocarbonates and xanthates.<sup>11,12</sup> AIBN has been the most widely used initiator for RAFT polymerization. In general, clickable moieties are attached to the initiating fragment (R group) of the chain transfer agents. The advantage of the R group compared to the mediating group (Z group) is the high end-group fidelity of the resulting polymer. The related clickable CTAs are depicted in Tables 4 to 6.

**Alkyne-functionalized CTAs.** Alkyne-containing CTAs are mostly prepared by an esterification of propargyl alcohol with an activated acid on the RAFT agent. The alternative route is using a halogen alkyne compound and the potassium salt of the dithioester or trithiocarbonate *via* a nucleophilic substitution.

The first report on click chemistry and the RAFT process for the preparation of diblock copolymers of styrene and vinyl acetate *via* polymer-polymer conjugation was provided by Barner-Kowollik and coworkers ( $M_n = 12\,100$  g mol<sup>-1</sup>, PDI = 1.1–1.2).<sup>133</sup>

Another combination of click chemistry and the RAFT process was published by Hawker *et al.* in 2006 showing the facile formation of clickable micelles from block copolymers of protected acrylic acid and styrene polymerized with an alkyne-functionalized RAFT agent (Entry 24). Azide-alkyne cycloaddition is possible with the terminal alkyne-functionalized block copolymers. Protection of the terminal alkyne with the trimethylsilyl group was not necessary in this case.<sup>134</sup>

Furthermore, a similar approach to well-defined block copolymers was reported using a TMS-protected alkyne dithiobenzoate as shown in Entry 24. Terminal alkyne-functionalized

**Table 4** Alkyne-containing chain transfer agents for RAFT (poC = postclick, prC = preclick)

Entry	Structure	Click	CRP	Monomer	Strategy	Ref
24		CuAAC	RAFT	MA, THPA, St, NIPAM	poC	133–136,143,144
25		CuAAC	RAFT	AM, St, MA, 4VP, NIPAM, MMA	poC prC	137–140,145,146 147
26		CuAAC	RAFT	St, <i>n</i> BA	prC	142
27		Thiol-yne RAFT	RAFT	NIPAM	poC	141
27		CuAAC	RAFT	VAc, NVP, St, <i>n</i> BA	prC	142

**Table 5** Azide-containing chain transfer agents for RAFT (poC = postclick, prC = preclick)

Entry	Structure	Click	CRP	Monomer	Strategy	Ref
28		CuAAC	RAFT	St, VAc, DMA	poC	99,133,148
29		CuAAC	RAFT	St, DMA, NIPAM, nBA, OEGA	poC	148–152,156
30		CuAAC	RAFT	NIPAM, DMA	poC	105,157,158
31		CuAAC	RAFT	VAc	poC, prC	135,144,153–155

poly(styrene) was synthesized at 60 °C in a controlled way ( $M_n = 8\,200\text{ g mol}^{-1}$ , PDI = 1.1) and it was shown that the molar mass linearly increased with monomer conversion.<sup>133</sup> The same RAFT agent was used for the polymerization of an *O*-methacryloyl

mannose monomer resulting in an alkyne-functionalized glyco-polymer ( $M_n = 4\,300\text{ g mol}^{-1}$  and PDI = 1.1–1.2).<sup>135</sup> Similarly, an alkyne-functionalized RAFT agent bearing an unprotected alkyne group was used for the polymerization of styrene and

**Table 6** Other click-functionalized chain transfer agents for RAFT (poC = postclick, prC = preclick)

Entry	Structure	Click	CRP	Monomer	Strategy	Ref
32		CuAAC	RAFT	HPMAM, MMA, St, OEGA, NIPAM	poC	159
33		PySS	RAFT	nBA, OEGA, NIPAM	poC, prC	162,36,163, 160,161
34		PySS	RAFT	OEGA, St	poC	164
35		HDA	RAFT	St, <i>i</i> BoA	poC	38,39,55,165–170
36		MAdd	RAFT	NIPAM	prC	171

NIPAM at 70 to 80 °C. Different homopolymers were synthesized in a molar mass range between 2 700 to 3 700 g mol<sup>-1</sup> for poly(styrene) and 4 900 to 11 000 g mol<sup>-1</sup> for poly(NIPAM).<sup>136</sup>

Also a terminal alkyne-functionalized trithiocarbonate (Entry 25) has been used for the RAFT polymerization of different monomers by Brittain.<sup>137,138</sup> For example, surface-mediated RAFT polymerization of styrene and methyl acrylate resulted in poly(St-*b*-MA) with a molar mass of  $M_n = 34\,000$  g mol<sup>-1</sup>.<sup>137</sup> Furthermore, the same group reported on the modification of silica nanoparticles using the tandem approach of RAFT polymerization of styrene and click chemistry.<sup>138</sup>

The chain transfer agent as shown in Entry 25 was clicked to azido end-functionalized poly(isobutylene) and was subsequently used as a clicked macro-RAFT agent for the polymerization of NIPAM ( $M_n = 24\,800$ – $53\,200$  g mol<sup>-1</sup>, PDI < 1.1). First order kinetic plots for the polymerization of NIPAM were obtained and revealed that this monomer polymerizes in a controlled way.<sup>139</sup>

The alkyne-functionalized chain transfer agent depicted in Entry 25 was reported by another research group for the polymerization of 4-vinylpyridine (NVP) initiated with AIBN at 80 °C resulting in a polymer with a molar mass of 13 600 g mol<sup>-1</sup> with a PDI value of 1.4.<sup>140</sup>

Hyperbranched polymers were prepared by thiol-yne click chemistry by Perrier *et al.* using the alkyne-terminated transfer agent shown in Entry 26. After a postmodification step to cleave the RAFT agent into a thiol it was clicked (by UV light at room temperature with yields over 95%) to form a styrene hyperbranched polymer.<sup>141</sup> Furthermore, a xanthate type of RAFT agent (Entry 27) containing an alkyne group has been used for the polymerization of VAc and NVP by Klumperman.<sup>142</sup> In all cases, xanthates were first clicked and then used as functionalized RAFT agents in the polymerization of VAc ( $M_n = 3\,900$  g mol<sup>-1</sup>, PDI = 1.2–1.3), NVP ( $M_n = 5\,400$  g mol<sup>-1</sup>, PDI = 1.1–1.2), St ( $M_n = 7\,500$  g mol<sup>-1</sup>, PDI = 1.1–1.2) and *n*BA ( $M_n = 10\,000$  g mol<sup>-1</sup>, PDI = 1.1).<sup>142</sup> Semi-logarithmic kinetic plots indicated controlled polymerizations using these RAFT agents.

It seems that the protection of the alkyne group is not strictly necessary. As shown above, there are examples for both protected and unprotected CTAs demonstrating that polymers with high end-group fidelity (> 90%) can be prepared. The temperature and the ratio between the alkyne terminated RAFT agent and the monomer play an important role to achieve a sufficient control over the polymerization.

**Azide-functionalized CTAs.** The common procedure for the synthesis of azide-containing CTAs is the esterification of 2-azidoethanol and an activated acid of the RAFT agent. The two largest classes of RAFT agents (dithiobenzoates and trithiocarbonates) have been mostly used as azido-functionalized chain transfer agents.

The azide moiety is used without protection during the polymerization, although some side reactions were described. To decrease the amount of side reactions, low temperatures and/or low conversions are favored that will be discussed in the following.

The dithiobenzoate RAFT agents depicted in Entry 28 were used for the bulk polymerization of styrene at 60 °C and provide a good control over the polymerization ( $M_n = 1\,900$  to  $5\,300$  g mol<sup>-1</sup>, PDI = 1.1<sup>143</sup> and  $M_n = 3\,200$  to  $11\,000$  g mol<sup>-1</sup>,

PDI = 1.1<sup>133</sup>). Moreover, Sumerlin *et al.* using the initiator listed in Entry 28 for the polymerization of St and DMA resulting in azido functional PS ( $M_n = 5\,500$  to  $12\,000$  g mol<sup>-1</sup>, PDI = 1.1–1.3) and poly(DMA) ( $M_n = 10\,800$  to  $21\,800$  g mol<sup>-1</sup>, PDI = 1.30).<sup>148</sup> A thionaphthoyl RAFT agent containing the azide functionality (Entry 28) was also used for the polymerization of styrene in bulk at 80 °C ( $M_n = 2\,400$  g mol<sup>-1</sup>, PDI = 1.1). A linear relationship in the semi-logarithmic kinetic plot was reported indicating that the concentration of propagating chains are almost constant throughout the reaction.<sup>99</sup>

Among the azide-functionalized RAFT agents belonging to the class of the trithiocarbonates, the CTA with a C<sub>12</sub>-side chain is frequently used for the RAFT polymerization of acrylamides (Entry 29): First order kinetic plots for this CTA indicate a constant concentration of propagating chains.<sup>148,149</sup> In addition, Gondi *et al.* used the initiator depicted in Entry 29 with AIBN for the controlled polymerization of styrene ( $M_n = 5\,100$ – $8\,600$  g mol<sup>-1</sup>, PDI = 1.1–1.2) and DMA ( $M_n = 5\,000$ – $10\,000$  g mol<sup>-1</sup>, PDI = 1.1–1.2).<sup>148</sup> Furthermore, the same group reported on the synthesis of poly(DMA-*b*-NIPAM) using this azido-RAFT agent. In this way, telechelic polymers were synthesized: PNIPAM ( $M_n = 2\,700$  g mol<sup>-1</sup>, PDI = 1.1–1.2), PDMA ( $M_n = 4\,200$  g mol<sup>-1</sup>, PDI = 1.1) and poly(DMA-*b*-NIPAM) ( $M_n = 6\,000$  g mol<sup>-1</sup>, PDI = 1.15).<sup>149</sup> In addition, NIPAM was polymerized with the initiator shown in Entry 29 at 60 °C in a controlled way resulting in azido end-functionalized polymers ( $M_n = 16\,300$  g mol<sup>-1</sup>, PDI = 1.1), which were further used for protein coupling by the copper-catalyzed azide-alkyne cycloaddition.<sup>150</sup> The RAFT agent depicted in Entry 29 was also applied for the preparation of 3-miktoarm star polymers by using a combination of RAFT, ring-opening polymerization and click chemistry. After the polymerization at 70 °C of *n*BA ( $M_n = 3\,500$  g mol<sup>-1</sup>, PDI = 1.1), OEGA ( $M_n = 4\,800$  g mol<sup>-1</sup>, PDI = 1.1) or NIPAM ( $M_n = 4\,600$  g mol<sup>-1</sup>, PDI = 1.1) propargyl diol was clicked to the azide.<sup>151</sup> Furthermore, an azide-functionalized CTA (Entry 29) was used for the preparation of hyperbranched polymers. For this purpose, a propargyl acrylate was clicked onto the CTA and subsequently copolymerized with St or NIPAM.<sup>152</sup> Perrier *et al.* used a trithiocarbonate (Entry 30) for the RAFT polymerization of NIPAM ( $M_n = 2\,600$ – $10\,600$  g mol<sup>-1</sup>, PDI = 1.1), but side reactions involving the azido moiety occurred such as 1,3-dipolar cycloaddition with electron-deficient olefins, *i.e.* NIPAM.<sup>105</sup> The cycloadditions to the triazoline or to the pyrazoline (by a second addition of NIPAM) were confirmed by high resolution mass spectrometry.<sup>105</sup>

As depicted in Entry 31, an azide-functionalized xanthate has been used for the polymerization of VAc ( $M_n = 6\,800$  g mol<sup>-1</sup>, PDI = 1.15)<sup>135</sup> as well as for grafting to an alkyne side-chain functional copolymer.<sup>153</sup> A xanthate-terminated dextran was prepared by using click chemistry of an azido RAFT agent shown in Entry 31. The resulting macro-CTA was used for the bulk polymerization of VAc resulting in a block copolymer. The molar mass linearly increased by conversion, although the polydispersity index was increasing.<sup>154</sup> A similar xanthate was used for the bulk polymerization of VAc at 80 °C resulting in a broader molar mass distribution at higher monomer conversion (PDI > 1.4).<sup>155</sup>

**Heterodifunctional CTAs for orthogonal click chemistry.** A difunctional CTA with clickable moieties on both the initiating



as well as on the mediating side was described by Stenzel and Barner-Kowollik *et al.* using a RAFT agent that combines clickable units for dipolar cycloaddition and pyridyl disulfide exchange as two orthogonal click reactions (Entry 32). The reported RAFT agent bears an azide and a dithiopyridine group at the R and Z fragments, respectively. St, NIPAM, and OEGA were polymerized in a controlled way as indicated by kinetic investigations. In contrast, the polymerizations of HPMAM and MMA could not be performed in a controlled manner, since the trithiocarbonate CTA is less suitable for methacrylates. Well-defined heterotelechelic polymers were observed for St ( $M_n = 5\,000\text{--}14\,000\text{ g mol}^{-1}$ , PDI = 1.1), NIPAM ( $M_n = 3\,200\text{--}16\,200\text{ g mol}^{-1}$ , PDI = 1.12 to 1.14) and OEGA ( $M_n = 7\,500\text{--}12\,500\text{ g mol}^{-1}$ , PDI = 1.1).<sup>159</sup>

**Pyridyl-disulfide-containing CTAs.** The chain transfer agent depicted in Entry 33 (top) was used by Davis and coworkers for the homopolymerization of OEGA.<sup>36</sup> The PDI values of the OEGA homopolymers ( $M_n = 12\,000\text{--}34\,000\text{ g mol}^{-1}$ ) were smaller than 1.20 for all samples and for one sample of the block copolymerization with *n*BA (by increasing the conversion the molar mass distribution broadened). The high end-group fidelity of the pyridyl disulfide groups was indicated by <sup>1</sup>H NMR spectroscopy. Furthermore, the same RAFT agent (Entry 33) was used by Davis *et al.* for the polymerization of NIPAM and OEGA resulting in different molar masses and polydispersity indices:<sup>160–163</sup> POEGA ( $M_n = 15\,500\text{--}23\,000\text{ g mol}^{-1}$ , PDI = 1.2–1.3) and PNIPAM ( $M_n = 5\,100\text{--}18\,000\text{ g mol}^{-1}$ , PDI = 1.2–1.5).<sup>163</sup> The PySS end group is often used for the preparation of polymer bioconjugates, *e.g.* with BSA *via* the free thiol group. Semilogarithmic kinetic plots are reported for the RAFT polymerization of OEGA and NIPAM with the CTA pictured in Entry 33 (top) by Bulmus and Davis showing a linear relationship between  $\ln\left(\frac{[M]_0}{[M]}\right)$  and reaction time, which indicates a constant level of radical concentration during the polymerization.<sup>163</sup> The symmetric trithiocarbonate RAFT agents depicted in Entry 34 were used for the polymerization of OEGA at 70 °C and provide a good control over the polymerization ( $M_n = 4\,600\text{--}23\,400\text{ g mol}^{-1}$ , PDI = 1.2–1.3). With these homopolymers a chain extension using styrene was performed resulting in block copolymers of type ABA ( $M_n = 19\,100\text{--}37\,900\text{ g mol}^{-1}$ , PDI = 1.2–1.3).<sup>164</sup>

**Functional CTAs for hetero Diels–Alder reactions.** Besides an alkyne or an azide moiety on the RAFT agent, the C=S double bond (dienophile) was directly used as a clickable group for hetero Diels–Alder reactions with dienes (Scheme 1, HDA). This approach represents a straightforward pathway to block copolymers without an additional synthesis step for a postmodification or any other preparation step. The first study on this approach was reported by Barner-Kowollik, Stenzel and coworkers in 2008. The authors prepared polymer conjugates of PS polymerized by RAFT and a diene-terminated poly( $\epsilon$ -caprolactone). The use of these electron-deficient dithioesters (Entry 35) allow the polymerization of styrene in a controlled manner ( $M_n = 2\,200\text{--}2\,800\text{ g mol}^{-1}$ , PDI = 1.1).<sup>38</sup> This class of RAFT agents was also used for the polymerizations of St and isobornyl acrylate (*i*BoA) with different molar masses (stopped at low monomer conversion to ensure high end-group fidelity). All obtained polymers were well-defined and have low polydispersity indices. The prepared polymers were clicked *via* the HDA with cyclopentadienyl- or 2,4-hexadiene-ended polymers.<sup>38,39,55,165–170</sup>

**Functional CTAs for Michael addition.** A functional CTA for Michael addition was described by Sumerlin *et al.* using a RAFT agent with a maleimide end group (Entry 36). After the modification with BSA the RAFT polymerization of NIPAM was performed resulting in polymer-protein conjugation with a molar mass of  $240\,000\text{ g mol}^{-1}$ .<sup>171</sup>

### 4.3 Nitroxide-mediated radical polymerization (NMP)

For nitroxide-mediated polymerizations very few examples of clickable initiators were described up to now. In comparison to ATRP and RAFT polymerizations, usually higher reaction temperatures are necessary for NMP. This decreases the number of suitable click functionalities that can be used during the polymerization without exceeding acceptable amounts of side reactions.

It was shown that unimolecular initiators such as phenylethyl-alkylated 2,2,6,6-tetramethylpiperidinylnitroxide (TEMPO) and 2,2,5-trimethyl-4-phenyl-3-azahexane-3-nitroxide (TIPNO) can be functionalized without influencing the control over the polymerization.<sup>172–174</sup> Thereby, the functionalization can be performed in principle at the initiating as well as at the mediating fragment of the alkoxyamine. Until now, clickable moieties are only attached to the initiating fragment. The advantage of this side compared to the mediating side is the high end-group fidelity of the resulting polymer. This is caused by the nature of the NMP process: The incorporation of a functional group at the initiating chain end is done in one step, whereas the incorporation of a certain functionality at the mediating chain end contains many reaction steps until the final polymer is formed, which increases the probability of side reactions.

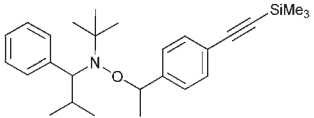
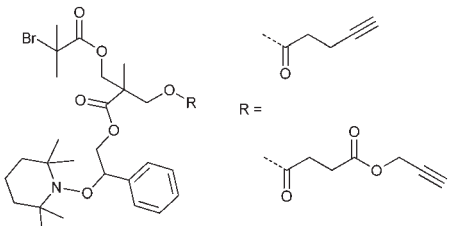
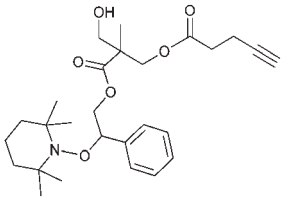
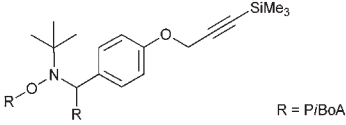
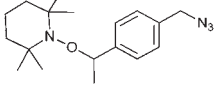
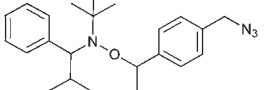
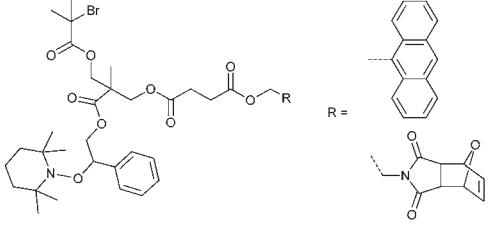
The general synthetic strategy towards a functional unimolecular initiator is the radical coupling reaction of TIPNO or of the commercially available TEMPO with a functionalized vinyl compound activated by a manganese(III) salen complex (Jacobsen's reagent).<sup>175</sup> The related clickable initiators for NMP are shown in Table 7.

**Alkyne-functionalized initiators.** In Entry 37 an alkyne-functionalized alkoxyamine based on PhEt-TIPNO is shown that was synthesized according to the general radical coupling of TIPNO and 4-(trimethylsilylethynyl)styrene that was obtained by Sonogashira reaction of 2-bromostyrene and trimethylsilyl acetylene.<sup>176</sup>

The alkyne was protected with the TMS group to reduce the possible side reactions under polymerization conditions: (*i*) chain transfer by hydrogen abstraction from the alkyne as well as polymerization along the triple bond leading to cross-linking<sup>76,77,176,177</sup> and (*ii*) addition of nitroxide radicals to the triple bond.<sup>178</sup> It can be noted that even a small loss of nitroxide during polymerization has a large impact on the controlled character of the polymerization, since it shifts the equilibrium towards the free propagating radical resulting in a significant increase in termination and transfer reactions in particular at higher conversions.

The protected initiator (Entry 37) was used in the homopolymerization of styrene resulting in  $\alpha$ -functionalized clickable PS ( $M_n = 24\,000\text{ g mol}^{-1}$ , PDI = 1.1) after deprotection with tetrabutylammonium fluoride (TBAF). In contrast to ATRP, no uncontrolled deprotection of the TMS-alkyne was noticed

**Table 7** Clickable initiators for NMP (poC = postclick, prC = preclick)

Entry	Structure	Click	CRP	Monomer (Abbr./Entry)	Strategy	Ref
37		CuAAC	NMP	St	poC	176
38		CuAAC	NMP	St	poC	179–181
		AAC	ATRP	MMA	poC	45
39		CuAAC	NMP	St	poC	182–184
		AAC	ROP	ε-CL	poC	45
40		CuAAC	NMP	–	–	185
41		CuAAC	NMP	–	–	175
42		CuAAC	NMP	St, <i>t</i> BA St, NIPAM, <i>n</i> BA	poC prC	174 176,188
43		DA	NMP	St	poC	118
			ATRP	<i>t</i> BA	prC	119,190

during the polymerization. Furthermore, a combination of ATRP and NMP with the same initiator is possible as demonstrated by Tunca and Hizal *et al.*<sup>45,179–181</sup> Although both techniques are radical polymerizations and, hence, might interfere with each other, they can be applied subsequently: (i) NMP of styrene can be conducted without affecting the ATRP initiator in the absence of any metal catalyst<sup>45,180,181</sup> and (ii) ATRP of methacrylate can be conducted at lower temperature (60 °C) at which the nitroxide is still inactive and not able to mediate radical propagation.<sup>179</sup> Entry 38 shows such an alkyne-functionalized multifunctional initiator for ATRP and NMP.<sup>45,179–181</sup> The structure contains (i) 2-bromoisobutyrate as mediator for the ATRP polymerization of MMA, (ii) TEMPO as mediator for

NMP polymerization of styrene and an unprotected alkyne, whereas the fragments are linked *via* ester groups.

The unprotected alkyne is thermally stable up to 125 °C and the TEMPO-mediated polymerization of styrene seems not to interfere with the unprotected alkyne. Apparently, even after 17 h at 125 °C the polymerization was controlled and no significant loss of alkyne was observed for the resulting PS-macroinitiator ( $M_n = 10\,000\text{ g mol}^{-1}$ , PDI = 1.2) as judged by <sup>1</sup>H NMR spectroscopy and SEC measurements of the subsequent clicked structure.<sup>181</sup> By contrast, the ATRP of MMA was kept short in every case (30 min at 60 °C) to prevent significant amounts of side reaction with the catalytic system resulting in PMMA macroinitiator ( $M_n = 6\,000\text{ g mol}^{-1}$ , PDI = 1.2).<sup>179</sup>

However, the amount of side reactions is negligible in most cases due to the low concentration of alkyne-containing initiator.

Furthermore, alkyne-functionalized NMP initiators are combined with other controlled polymerization techniques by the incorporation of, e.g., alcohol groups for the ring-opening polymerization of  $\epsilon$ -caprolactone (Entry 39). These polymerization techniques do not interfere with each other and can be applied simultaneously<sup>182,183</sup> or subsequently.<sup>45,184</sup> For the consecutive procedure, first the ROP of  $\epsilon$ -CL with the initiator depicted in Entry 39 was conducted at 110 °C for 2 h using Sn(Oct)<sub>2</sub> as catalyst ( $M_n = 4\,000\text{ g mol}^{-1}$ , PDI = 1.1) followed by NMP of styrene at 125 °C for 15 h ( $M_n = 19\,000\text{ g mol}^{-1}$ , PDI = 1.3).<sup>45,184</sup> On the other hand, in a simultaneous one-pot approach St and  $\epsilon$ -CL were heated with Sn(Oct)<sub>2</sub> for 22 h at 120 °C ( $M_n = 12\,000\text{ g mol}^{-1}$ , PDI = 1.1).<sup>182</sup> For all examples, copolymers of PCL-*b*-PS with an alkyne as clickable function at the junction point were achieved, whereby the alkyne was not protected even in the polymerization at 120 °C for 22 h. Hence, the alkyne must be stable under the applied polymerization conditions of NMP and ROP.

In addition, since both polymerization techniques do not interfere with the azide-alkyne cycloaddition, 3-miktoarm star terpolymers can be constructed by conducting ROP of  $\epsilon$ -CL (with Sn(Oct)<sub>2</sub>), NMP of St (with initiator shown in Entry 39) and either simultaneously (one-pot/one-step) or subsequently (one-pot/two-step) clicking an azide-functionalized polymer with CuBr/PMDETA as catalyst.<sup>183</sup> Thereby, 3-arm stars of PEG-PCL-PS ( $M_n = 14\,000\text{ g mol}^{-1}$ , PDI = 1.3) and PMMA-PCL-PS ( $M_n = 14\,500\text{ g mol}^{-1}$ , PDI = 1.2) with the one-pot/one-step technique and stars of PtBA-PCL-PS ( $M_n = 16\,000\text{ g mol}^{-1}$ , PDI = 1.1) and PEG-PCL-PS ( $M_n = 15\,000\text{ g mol}^{-1}$ , PDI = 1.1) in the one pot/two step approach could be synthesized, respectively.<sup>183</sup>

Another type of an alkyne-functionalized macroinitiator ( $M_n = 7\,700\text{ g mol}^{-1}$ , PDI = 1.1–1.2) is depicted in Entry 40, whereas PtBoA is attached on both the initiating and the mediating fragment of the alkoxyamine.<sup>185</sup> The macroinitiator was obtained by a nitrene-mediated radical coupling reaction of activated ATRP-made PtBoA ( $M_n = 4\,300\text{ g mol}^{-1}$ , PDI = 1.2) in the presence of an alkyne-functionalized nitrene. To the best of our knowledge, this macroalkoxyamine had not yet been used as initiator in NMP. Nevertheless, it seems to be a potential candidate, since in a similar approach polystyrene midchain-functionalized with a parent alkoxyamine (not including the alkyne moiety) was used as initiator in NMP of St, *n*-BA and NIPAM for the chain extension towards ABA triblock copolymers.<sup>186,187</sup>

**Azide-functionalized initiators.** One of the first azide-functionalized structures that is capable for a controlled radical polymerization was published in 1998 by Hawker and coworkers.<sup>175</sup> In the common procedure (manganese-catalyzed radical coupling of nitroxides with styrenics for the synthesis of alkoxyamines) *p*-chloromethyl styrene was trapped with the commercial available TEMPO radical after radical activation and was subsequently reacted with sodium azide to yield an azide-functionalized initiator (Entry 41). However, this initiator was up to now to the best of our knowledge neither used in polymerizations nor used in combination with alkyne-azide cycloadditions. In this particular case, the azide was used to gain

an amino-functionalization by reduction with lithium aluminium hydride.

In a similar approach the *p*-(azidomethyl)phenylethyl-TIPNO was synthesized, whereby the *p*-chloromethyl styrene was functionalized with the azide prior to the radical coupling with TIPNO (Entry 42). The initiator was used in the polymerization of styrene ( $M_n = 9\,000\text{ g mol}^{-1}$ , PDI = 1.1 after 3 h, 120 °C) and *n*-butylacrylate ( $M_n = 6\,500\text{ g mol}^{-1}$ , PDI = 1.2–1.3 after 13 h at 120 °C), whereby the polymerization was controlled and no side reactions of the azide were discussed.<sup>174</sup>

In contrast, Voit *et al.* discussed that the polymerization of styrene with the azido-functionalized initiator depicted in Entry 42 failed due to the side reactions that were assigned to the cyclization of the azide with the vinylic double bond of the monomer.<sup>176</sup> Since the azide group is not thermally stable,<sup>49</sup> either postmodification or preclick approaches could be successfully utilized to prepare the  $\alpha$ -functionalized polymers. In the postmodification, *p*-(chloromethyl)phenylethyl-TIPNO was used in the polymerization of styrene and the chloro group was subsequently converted with sodium azide into azide (N<sub>3</sub>-PS:  $M_n = 8\,000\text{ g mol}^{-1}$ , PDI = 1.2). Following the preclick approach, an alkyne-functionalized moiety (Cbz-protected adenine derivative) was clicked onto the azide prior to the polymerization of styrene resulting in  $\alpha$ -functionalized PS ( $M_n = 52\,000\text{ g mol}^{-1}$ , PDI = 1.2).<sup>176</sup>

To study the steric and electronic influence of the triazole moiety for the initiation quality of the alkoxyamine shown in Entry 42, two different alkoxyamines were synthesized starting from 4-(chloromethyl)phenylethyl-TIPNO, whereby the chloro group was substituted either by azide or by 4-azidobenzoate to vary the distance of the azide to the alkoxyamine skeleton.<sup>188</sup> Polymerization of NIPAM using these azido-functionalized alkoxyamines as initiators failed in both cases. Therefore, the azido group was functionalized *via* 1,3 dipolar cycloaddition with either a 1,2-dihydroxyalkyl moiety, a barbituric acid moiety or a phenyl moiety. The initiators where the triazole was directly bound to the alkoxyamine group showed poor initiation. In contrast, the alkoxyamine with a rigid spacer revealed good control over the polymerization of NIPAM ( $M_n = 5\,000\text{ g mol}^{-1}$ , PDI = 1.2) and *n*-BA ( $M_n = 6\,000\text{ g mol}^{-1}$ , PDI = 1.2). The poor initiation efficiency in the first case was partly ascribed to an electronic influence but mostly to intramolecular hydrogen bonding between the propagating radical and the barbituric acid that hindered propagation. This was sterically prevented with the rigid spacer in the second case. In these preclick cases the azide moiety of the initiator described in Entry 42 opens the field towards versatile functionalized initiators *via* the facile incorporation of functional groups.

**Functional initiators for Diels–Alder reactions.** Besides an alkyne moiety also anthracene or furan-protected maleimide were attached to ATRP-NMP initiators as clickable groups for Diels–Alder reactions (Entry 43). The synthesis of these mikto-functional initiator starts from 2,2-bis(hydroxymethyl)propionic acid as the basic framework,<sup>189</sup> where the ATRP-initiating fragment (2-bromoisobutyrate), the NMP fragment (TEMPO) and the clickable moiety (protected maleimide or anthracene) were incorporated by esterification reactions.<sup>118,119,190</sup>



The anthracene-functionalized mikto-initiator depicted in Entry 43 was only used in the preclick approach, whereby the Diels–Alder reaction was conducted prior to the NMP of styrene followed by ATRP of *t*BA. With this strategy, different block copolymers were obtained: (i) H-shaped terpolymers<sup>119</sup> (PS)(*Pt*BA)-PEO-(*Pt*BA)(PS) ( $M_n = 18\,000\text{ g mol}^{-1}$ , PDI = 1.3) and (PS)(*Pt*BA)-PPO-(*Pt*BA)(PS) ( $M_n = 31\,000\text{ g mol}^{-1}$ , PDI = 1.3) and (ii) 3-miktoarm star polymer<sup>190</sup> PEG-PS-*Pt*BA ( $M_n = 18\,000\text{ g mol}^{-1}$ , PDI = 1.3). The protected maleimide-functionalized miktoinitiator described in Entry 43 was initially used in the ATRP of *t*BA ( $M_n = 4\,000\text{ g mol}^{-1}$ , PDI = 1.3) and subsequently “clicked” with anthracene-functionalized PCL prior to the NMP of styrene to obtain a 3-miktoarm terpolymer (PCL-*Pt*BA-PS) ( $M_n = 40\,000\text{ g mol}^{-1}$ , PDI = 1.7).<sup>118</sup> The high polydispersity index was ascribed to a loss of TEMPO during the Diels–Alder reaction at 100 °C, indicated by a shoulder in the SEC trace at lower molar masses.

The preclick approach for the anthracene or maleimide moiety in combination with NMP should be used, since the maleimide and anthracene moieties cause side reactions under the polymerization conditions of NMP. Hence, to the best of our knowledge no example for the postclick approach is yet reported.

## 5. Clickable monomers

Clickable monomers can be used to synthesize pendant functionalized polymers (Scheme 4) that can be easily modified in a grafting-onto approach *via* click chemistry. Thereby, the clickable monomer can be homopolymerized or copolymerized to obtain versatile random-, block- or comb polymers. Most widely used in controlled radical polymerization processes are MMA and St derivatives.

The polymerization of these click-functionalized monomers represents often a synthetic challenge, because the clickable unit as a reactive group is frequently in conflict with the radical polymerization conditions. In contrast to the initiator approach a higher amount of side reactions involving the clickable functionality is expected, which is caused by the higher concentration of the monomer used during the polymerization process compared to the initiator. This fact is in particularly pronounced for bulk polymerizations or for side reactions involving besides

the clickable unit other parts of the monomer, *e.g.* the vinyl group of azide-containing monomers, where cycloaddition between the double bond and the azide can occur. To circumvent such side reactions, either the clickable unit has to be protected, or polymerization time or temperature have to be reduced.

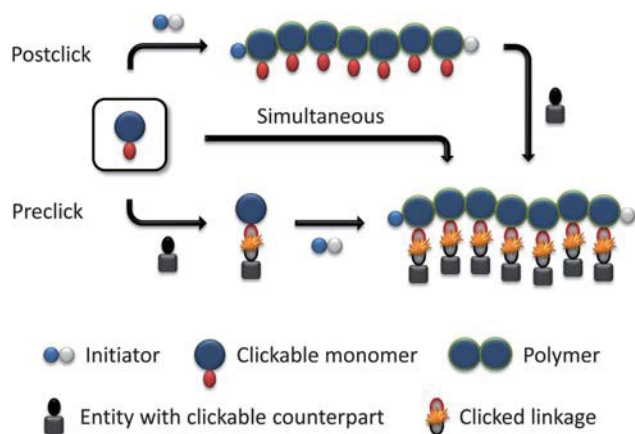
However, the degree of functionalization is much higher in this approach compared to the initiator one. Clickable initiators would provide polymers only with terminal functionalities, which would be one or two for linear polymers and equal the number of arms for star-shaped polymers. In contrast, homopolymerization of a clickable monomer would yield a polymer with functionalities as many as the number of repeating units. The degree of functionality can be decreased by copolymerization, which also decreases possible side reactions that are caused by the clickable monomers. In this section we discuss clickable monomers according to the functional groups, *i.e.* alkyne, azide, diene, thiol, para-fluoro and others. An overview over the clickable and clicked monomers is given in Tables 8–10.

### 5.1 Alkyne-containing monomers

The synthesis of alkyne-functionalized monomers is straightforward, whereby most synthetic routes involve the esterification of (meth)acryloyl chloride with propargyl alcohol or propargyl amine for (meth)acrylates<sup>3,66,153,191,192</sup> and acrylamides,<sup>95,193</sup> respectively. The propargyl derivatives can be protected by the reaction with trimethylsilyl chloride and 1,8-diazabicyclo[5.4.0]undec-7-ene catalyzed by silver chloride. The synthesis of alkyne-functionalized styrene is often accomplished *via* the Sonogashira reaction of 4-bromostyrene with (trimethylsilyl)acetylene.<sup>60,193–195</sup>

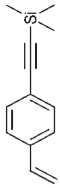
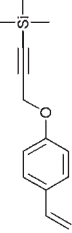



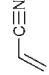

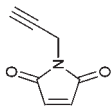
The protection of acetylene-functionalized monomers by the alkylsilyl group is of prime importance, because the terminal alkyne is known to be chemically<sup>196</sup> and thermally<sup>197</sup> not stable under the polymerization conditions required for the CRP techniques.<sup>194</sup> However, some researchers have used unprotected alkynes and indeed demonstrated that the terminal alkyne undergoes side reactions such as (i) radical addition to the triple bond,<sup>193</sup> (ii) chain transfer,<sup>198</sup> (iii) complexation of the terminal triple bond to copper-based ATRP catalysts and insertion reactions leading to insoluble crosslinked networks.<sup>77,193,199,200</sup> In one of these reports, Matyjaszewski and coworkers reported that the ATRP of unprotected propargyl methacrylate was hardly controllable (PDI values > 3), due to the involvement of the acetylene moiety during the catalyzed radical process.<sup>77</sup>

**Styrenes.** The first report on alkyne-functionalized styrene was reported in 2005 by Hawker and coworkers using protected 4-(trimethylsilylethynyl)styrene (St-C≡C-TMS) (Entry 44) in nitroxide-mediated polymerizations for the preparation of co- and terpolymers.<sup>193</sup> By utilizing the PhEt-TIPNO alkoxyamine as unimolecular initiator, poly(St-*co*-St-C≡CH) ( $M_n = 47\,000\text{ g mol}^{-1}$ , PDI = 1.2), poly(St-C≡CH-*co*-DMAM) ( $M_n = 40\,000\text{ g mol}^{-1}$ , PDI = 1.2) and poly(St-*r*-St-C≡CH-*r*-HEMA) ( $M_n = 32\,000\text{ g mol}^{-1}$ , PDI = 1.2) could be prepared in a controlled manner, whereby the alkyne monomer was incorporated into the polymers up to 10%. Without TMS-protection, significant amounts of crosslinked polymers at a higher content of alkyne-functionalized monomer or at high conversion were



**Scheme 4** Schematic representation of the strategies *via* clickable monomers.

**Table 8** Alkyne-containing monomers (poC = postclick, prC = preclick, simult = simultaneous)

Entry	Structure	Click	Strategy	CRP	Initiator/CTA (Abbr./Entry)	Comonomers	Ref
44		CuAAC	poC	RAFT NMP	MCPMDB PhEt-TIPNO	THPA, St St, DMAM, HEMA, GMA, rBOST, rBA, THPA	194,203 60,193-195
45		CuAAC	poC	NMP RAFT	PhEt-TIPNO DDAT	St, rBOST, AcOSi St	195,201 201
46		CuAAC	poC	NMP RAFT RAFT	PhEt-TIPNO BPIT 28	rBA AA NIPAM	193 205,206 156
47		CuAAC	poC	ATRP RAFT	15, TosCl, BMP CPDB, CPADB, CDB, CBDB, DDAT, MCPMDB	<i>ε</i> -CL, MMA, SMA, mPEG OEGMA, MMA, GMA	3,123,192,209 153,191,199,200,207,208
48		CuAAC	poC	ATRP NMP RAFT	BMPABE CPDB 17	- MMA -	69 214 66
49		ZnANC	poC	ATRP NMP	BPN, PEB BPO, TEMPO	St St	48 210
50		CuAAC	poC prC	ATRP RAFT	EBiB MPPCTTA	MMA St	213 67
51		CuAAC	poC	ATRP	PEB	St	216

observed. The efficiency and the orthogonality of the alkyne-azide click reaction were proven by one-pot functionalization either in a cascade or in a simultaneous approach. In related work, Voit *et al.* synthesized poly(*St-r-St-C≡CH-r-GMA*) ( $M_n = 30\,000\text{ g mol}^{-1}$ , PDI = 1.3) random terpolymers *via* NMP using the TMS-protected alkyne monomer. The deprotection with TBAF was performed without affecting the glycidyl moiety resulting in a pendant functionalized terpolymer bearing two orthogonal clickable moieties.<sup>60</sup>

Furthermore, *St-C≡CH* was used for the preparation of poly(*tBOSSt-b-[St-co-St-C≡CH]*) ( $M_n = 60\,000\text{ g mol}^{-1}$ , PDI = 1.3–1.4) and poly(*pHSt-b-[St-co-St-C≡CH]*) ( $M_n = 26\,000\text{ g mol}^{-1}$ , PDI = 1.2) diblock terpolymers which were applied in block copolymer lithography.<sup>195,201</sup>

In addition, *St-C≡C-TMS* was used in the synthesis of amphiphilic diblock terpolymers consisting of a hydrophilic poly(acrylic acid) block and a hydrophobic copolymer poly(*St-co-St-C≡CH*).<sup>194</sup> Since acrylic acid can not be directly polymerized in a sufficiently controlled way with NMP<sup>202</sup> – due to decomposition of the nitroxide under acidic condition – one can use the protection/deprotection strategy. First, a *PtBA*-macroinitiator was applied in the nitroxide-mediated polymerization of *St* and *St-C≡C-TMS* leading to poly(*tBA-b-[St-co-St-C≡CTMS]*) ( $M_n = 32\,000\text{ g mol}^{-1}$ , PDI = 1.2–1.3). However, deprotection of the *PtBA* block to *PAA* leads to a significant loss of alkyne functionality even of the protected one. Therefore, tetrahydropyran acrylate (THPA) was used which can be deprotected under milder conditions, but this compound was not stable under the temperature required for NMP. The *P(THPA)* macroinitiator could be polymerized *via* RAFT at 70 °C and was used in the copolymerization of styrene and 4-(trimethylsilylethynyl)styrene. Following the deprotection amphiphilic block copolymers *PAA-b-[PS-co-PSC≡CH]* ( $M_n = 16\,000\text{ g mol}^{-1}$ , PDI = 1.2) were obtained that are capable to form micelles with a clickable hydrophobic core.<sup>194,203</sup>

In the discussed cases protected *St-C≡CH* was incorporated up to 20% in a statistical copolymerization with styrene. This might be sufficient for the specific attachment of functional groups by clicking, but for the tailoring of macroscopic properties homopolymers with pendant alkyne groups seem to be more promising. Voit and coworkers showed that by increasing the amount of protected 4-ethynylstyrene the control of nitroxide-mediated polymerization with *PhEt-TIPNO* as unimolecular initiator is lost indicated by polydispersity indices around 1.9 and large differences of the calculated molar masses to the observed ones for the homopolymer of poly(*St-C≡C-TMS*).<sup>195</sup> The authors assigned the loss of control to a shift of the active-dormant species equilibrium towards the active side caused by sterical hindrance and also to the recombination of the nitroxide and the TMS group of the propagating 4-(trimethylsilylethynyl) styrene radical. This assumption is supported by the fact that a controlled polymerization is obtained if an excess of free nitroxide is added to the polymerization medium. This shifts the equilibrium back to the dormant side and results in the synthesis of well-defined poly(*St-C≡C-TMS*) ( $M_n = 3\,500\text{ g mol}^{-1}$ , PDI = 1.2).<sup>195</sup>

To circumvent the sterical hindrance during the polymerization as well as to provide enhanced accessibility to the alkyne for the postmodification, 4-(3'-trimethylsilyl-ethynylmethoxy)styrene (*St-OMe-C≡CTMS*) containing a methoxy group as a flexible spacer

was investigated (Entry 45). The synthesis of the monomer was performed by a substitution reaction of 4-hydroxystyrene with propargyl bromide and subsequent protection with TMS. The homopolymerization proceeded in a controlled manner without the necessity of any free nitroxide (poly(*St-OMe-C≡CTMS*):  $M_n = 6\,000\text{ g mol}^{-1}$ , PDI = 1.2–1.3). Besides, the TMS group is labile under basic and acidic conditions prohibiting the use of acetic acid as a polymerization enhancer. Moreover, the TMS group is thermally labile and a partial loss of the protecting group was observed for the reaction at 120 °C. Unfortunately, the more stable *t*-butyldimethyl-silyl (TBDMS) or triisopropylsilyl (TIPS) protected monomers could not be synthesized. With *St-OMe-C≡CTMS* as monomer in hand the following diblock copolymers were synthesized: poly(*tBOSSt-b-St-OMe-C≡CH*) ( $M_n = 52\,000\text{ g mol}^{-1}$ , PDI = 1.2), poly(*AcOSSt-b-St-OMe-C≡CH*) ( $M_n = 21\,000\text{ g mol}^{-1}$ , PDI = 1.4) as well as poly(*pHSt-b-St-OMe-C≡CH*) ( $M_n = 16\,000\text{ g mol}^{-1}$ , PDI = 1.2).<sup>195,201</sup>

Not only nitroxide-mediated polymerization but also the RAFT polymerization technique was used for the preparation of diblock copolymers poly(*St-b-St-OMe-C≡CH*) with a trithiocarbonate RAFT agent.<sup>201</sup> Although alkyne-functionalized ATRP initiators are widely used for the polymerization of styrene, no alkyne-functionalized styrene derivative was polymerized *via* ATRP so far. A reason for that might be the higher polymerization temperature for the ATRP of styrene compared to other monomer classes promoting side reactions. It can be noted that the partial loss of the trimethylsilyl-protecting group at elevated temperatures leads to a higher amount of terminal acetylene compared to the initiator approach, which might cause a significant loss of control due to interference with the copper catalyst.

**Acrylates.** There are only a few examples using propargyl acrylates in CRP. A possible reason for that is the less controllable polymerization of acrylate monomers which can undergo some side reactions due to the formation of mid-chain radicals in poly(acrylates) (intermolecular transfer of radicals) resulting in branching and scission.<sup>204</sup> The triple bond at the monomer makes it even more difficult to gain control over the molecular structure.

The unprotected propargyl acrylate depicted in Entry 46 was copolymerized with acrylic acid at 60 °C by Caruso *et al.* using the RAFT method with a trithiocarbonate CTA resulting in a broad molar mass distribution ( $M_w = 86\,000\text{ g mol}^{-1}$  and a PDI value of 2.2).<sup>205</sup> In addition, a similar copolymer was prepared using a trithiocarbonate CTA yielding a copolymer with a molar mass of  $M_n = 53\,000\text{ g mol}^{-1}$  and a polydispersity index of 1.9. The broad mass distribution is attributed to branching of the unprotected alkyne-functionalized monomer.<sup>206</sup>

Furthermore, TMS-protected propargyl acrylate was randomly copolymerized with *tBA* using *PhEt-TIPNO* as initiator for NMP by Malkoch and coworkers, but no detailed discussion was provided regarding the obtained molar masses and polydispersity of the isolated polymers.<sup>193</sup>

**Methacrylates.** The TMS-protected propargyl methacrylate (Entry 47) can be polymerized under usual polymerization conditions for CRP (60–85 °C).<sup>3,153,191,192,207,208</sup> This type of monomer was mostly polymerized by ATRP or RAFT. In the case of RAFT polymerization a dithiobenzoate as chain transfer agent and AIBN as radical source was used. It is reported that for

the homopolymers molar masses up to 10 000 g mol<sup>-1</sup> are achievable.<sup>153</sup> The polymerizations were carried out for 3 to 16 h with protection of the terminal alkyne group resulting in well-defined polymers (PDI < 1.3). Also some block and random copolymers were prepared with different comonomers (MMA, OEGMA).<sup>208</sup> A kinetic study for propargyl methacrylate (Entry 47), including semilogarithmic kinetic plots of the RAFT polymerization of the propargyl methacrylate and the silyl-protected monomer was reported by Barner-Kowollik and coworkers. The authors demonstrated that the protected monomer polymerizes at a much lower rate than the nonprotected monomer.<sup>153,191</sup> Another RAFT copolymerization of the unprotected methacrylate (Entry 47) and MMA or GMA showed that the PDI values increase (PDI = 1.6–2.0,  $M_n$  = 15 000–25 000 g mol<sup>-1</sup>) and that under these polymerization conditions side reactions such as transfer and insertion reactions occur.<sup>199</sup>

TMS-protected propargyl methacrylate was also polymerized by ATRP. The first contribution was reported by Haddleton and coworkers using CuBr/*N*-ethyl-2-pyridylmethanimine as catalytic system. Kinetic studies indicated a living process and SEC measurements of the resulting polymers revealed a good control over the polymerization (PDI < 1.3).<sup>3</sup> This monomer is also used for the synthesis of block copolymers with poly( $\epsilon$ -caprolactone) as macroinitiator. A block copolymer ( $M_n$  = 14 100 g mol<sup>-1</sup>, PDI = 1.2) was obtained after the deprotection with TBAF and followed by the alkyne-azide cycloaddition leading to a functional graft copolymer.<sup>192</sup>

Drockenmuller *et al.* reported an *in situ* approach of ATRP polymerization and copper-catalyzed azide-alkyne click reaction using propargyl methacrylate as clickable monomer. The resulting functionalized copolymers revealed a broader molar mass distribution (PDI = 1.3–2.1) due to the use of unprotected alkyne.<sup>209</sup>

**Acrylamides.** The protected alkyne-functionalized acrylamide shown in Entry 48 is polymerized by ATRP using CuBr/Me<sub>6</sub>TREN as catalytic system and dansyl-bromide as initiator at 0 °C with NIPAM as comonomer ( $M_n$  = 13 900–19 600 g mol<sup>-1</sup>, PDI = 1.2–1.3).<sup>95</sup>

Additionally, the protected acrylamide was copolymerized with (*N,N*-dimethyl)acrylamide and TMS-protected 2-(hydroxyethyl)methacrylate *via* NMP using PhEt-TIPNO as initiator to prepare water-soluble random terpolymers.<sup>193</sup>

**Acrylonitrile.** The acrylonitrile monomer (AN) can be used without further functionalization for click reactions (Entry 49) since it contains nitrile groups which can be used for 1,3 dipolar cycloadditions with azides. Since this cycloaddition belongs to the list of reactions defined as click reaction by Sharpless and coworkers,<sup>13</sup> acrylonitrile can be in principle considered as a clickable monomer.

Acrylonitrile was polymerized *via* ATRP using 2-bromopropionitrile as initiator and CuBr/bpy as catalytic system by Du Prez and Matyjaszewski. The initiator contains the monomer group as initiating fragment that poses equal radical reactivity as the monomer itself providing fast initiation.<sup>48</sup> Thereby, poly(acrylonitrile) PAN ( $M_n$  = 40 000 g mol<sup>-1</sup>, PDI = 1.1) as well

as poly(AN-*b*-St) (PDI = 1.1) and poly(AN-*r*-St) ( $M_n$  = 8 500 g mol<sup>-1</sup>, PDI = 1.1) were prepared. For the block copolymer, first a PAN-macroinitiator was prepared followed by the polymerization of styrene as the second block to ensure high initiating rates and, hence, a narrow molar mass distribution.<sup>48</sup> In addition, acrylonitrile was polymerized *via* NMP using TEMPO/dibenzoylperoxide (BPO) as bimolecular initiator for the polymerization of the random copolymer poly(St-*r*-AN) ( $M_n$  = 10 000 g mol<sup>-1</sup>, PDI = 1.3–1.4) and the diblock polymer poly(St-*b*-[St-*r*-AN]) ( $M_n$  = 87 000 g mol<sup>-1</sup>, PDI = 1.2) that was initiated with a PS-macroinitiator.<sup>210</sup> Thereby the control increases with the content of acrylonitrile in the acrylonitrile/styrene feed.

Regarding possible postmodifications, it should be noted that the pendant nitrile group in polymeric materials is up to now efficiently modified only to the corresponding tetrazole ring using the reaction with sodium azide and zinc chloride as catalyst in DMF 120 °C for 40–50 h.<sup>48,210</sup> Herewith, the nitrile-azide cycloaddition is used to modify macroscopic properties rather than to place functional groups or to attach polymeric side chains.

The reason for this limitation lies within the nature of the ring formation of the tetrazoles: To allow an efficient ring formation under mild conditions, the azide should not be sterically hindered (which limits the use of polymeric azides), while the nitrile group has to be electron-poor (*e.g.* tosyl nitrile), which is not sufficiently fulfilled for the nitrile group along the backbone of (poly-)acrylonitrile.<sup>49,211,212</sup>

However, with the efficient modification to the corresponding tetrazole ring the macroscopic properties of the prepared diblock copolymers changes: (*i*) solubility and swellability in protic solvents increase, (*ii*) the morphology changes, since the tetrazole formation increases the incompatibility between the blocks<sup>210</sup> and (*iii*) the temperature stability for the tetrazole-modified material significantly decreases (by 60–120 °C) compared to the nitrile-based polymer.<sup>48</sup>

**Vinylacetylene.** The TMS-protected vinylacetylene (Entry 50) was polymerized using the ATRP process by Matyjaszewski.<sup>213</sup> This monomer was copolymerized with MMA using CuBr/2,2'-bipyridine catalyst and ethyl 2-bromoisobutyrate as initiator in anisole. Different environmental parameters such as temperature, time or ratio of copper to ligand to initiator were varied resulting in different polymers ( $M_n$  = 5 000–12 000 g mol<sup>-1</sup>, PDI = 1.1–1.5).<sup>213</sup>

Alkyne-functionalized maleimide (Entry 51) will be discussed in Section 6.1.2.7.

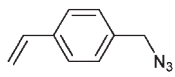
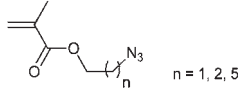
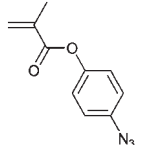
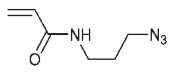
## 5.2 Azide-containing monomers

Azide-containing monomers based on (meth)acrylates or (meth)acrylamides are prepared by an esterification of 2-azidoethanol or 3-azidopropylamine with a (meth)acryloyl chloride or an activated acid of (meth)acrylic acid.<sup>77,90,108,217–220</sup> In addition, the route starting from the 2-hydroxyethyl methacrylate to the corresponding azide *via* the Mitsunobu reaction is described.<sup>221</sup> In the case of azide-functionalized styrene, the alkyne functionality is incorporated *via* substitution reaction of 4-vinylbenzyl chloride with sodium azide.<sup>83</sup>

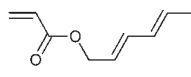
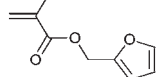
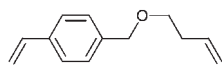
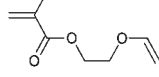
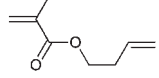
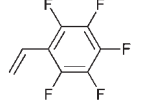
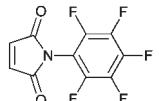
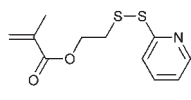
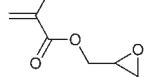
The used temperature represents an important criterion for the controlled polymerization of these monomers. The instability of the azide group at elevated temperatures is described, resulting in (i) the decomposition with evolution of nitrogen to form reactive

nitrenes that undergo insertion reactions<sup>49,217,222–225</sup> or (ii) cycloaddition with the monomer to form triazolines.<sup>49,105,108,226,227</sup> Both side reactions result in the formation of a crosslinked polymer. The higher concentration of azide groups in the

**Table 9** Azide-containing clickable monomers (poC = postclick, simult = simultaneous)

Entry	Structure	Click	Strategy	CRP	Initiator/CTA (Abbr./Entry)	Comonomers	Ref
52		CuAAC	simult	ATREP	5	St	83
53		CuAAC	poC	ATRP RAFT	EBiB, TosCl, CDB, CBDN, CPADB	MMA, DMAEMA, <i>t</i> BMA MMA	77,90,209,220,221 108,207,219,221
54		CuAAC	poC	RAFT	BICDT, CPDB	MMA, MA, St	217
55		CuAAC	poC	ATRP RAFT	3 CPADB	NIPAM NIPAM, DMA	95 218

**Table 10** Other click-functionalized monomers (poC = postclick)

Entry	Structure	Click	Strategy	CRP	Initiator/CTA	Comonomers	Ref
56		DA	poC	RAFT	BDAT	St	228
57		DA	poC	ATRP	EBiB, BBiBE	MMA, EHA	57,229–232
58		Thiol ene	poC	RAFT	MCPMDB	St	127
59		Thiol ene	poC	RAFT	CPADB	–	234
60		Thiol ene	poC	ATRP	EBiB	MMA	127
61		Thiol para-fluoro, Amine para-fluoro	poC	NMP	Blocbuilder®, PhEt-TIPNO	St	31,32
62		Thiol para-fluoro	poC	ATRP	PEB	St	216
63		PySS	poC	RAFT	CPADB TIPNO	HPMAM	235,236
64		RO RO	poC poC	NMP ATRP	EBiB	St, MA <i>t</i> BMA, MMA	9,60 59,114,244



polymerization solution (1–2 M or bulk) compared to the initiator approach constrains the polymerization conditions of CRP to lower temperatures to gain sufficient control over the polymerization.<sup>77,90,95,108,217,219,220</sup> Nonetheless, there are also two reports published using normal ATRP conditions (65–70 °C) claiming that the polymerization proceeded in a controlled manner.<sup>207,218</sup> Regarding the orthogonality of ATRP and azide-containing monomers, it is known for azides to undergo the Staudinger reaction, *i.e.* reduction to amines, in the presence of phosphines that are typically used as ligand for iron complexes as the “new generation” catalytic systems in ATRP.<sup>6,15,49</sup>

**Styrenes.** One example for the simultaneous click chemistry and atom transfer radical emulsion polymerization (ATREP) is known for 4-vinylbenzyl azide (Entry 52).<sup>83</sup> This method allows the preparation of crosslinked PS nanoparticles by copolymerization of 4-vinylbenzyl azide and styrene and an alkyne-containing ATRP initiator with CuBr/PMDETA as the catalytic system.

**Methacrylates.** A kinetic study, including semi-logarithmic kinetic plots of the RAFT polymerization of an azide methacrylate derivative (Entry 53) is reported by Benicewicz at different temperatures and at different monomer conversions. The pseudo-first-order kinetic plots are reported for 40 °C as well as 30 °C showing a linear relationship between  $\ln([M]_0/[M]_t)$  and time, which indicates a constant level of radical concentration during the polymerization. At higher temperature (50 °C) a shoulder at higher molar masses could be observed which was caused by coupling or branching of the polymer chains. At 30 °C it was shown that the azide monomer can be polymerized by RAFT with a dithionaphthalate RAFT agent ( $M_n = 21\,500\text{ g mol}^{-1}$ , PDI = 1.1).<sup>108</sup> Benicewicz and coworkers also reported that the RAFT polymerization of 6-azidoethyl methacrylate showed a linear pseudo-first-order kinetic plot at 30 °C. It was noted that with higher monomer conversion (25%) a high molar mass shoulder was observed by SEC measurements.<sup>219</sup> 2-Azidoethyl methacrylate (Entry 53) was used for the copolymerization with MMA *via* ATRP or RAFT. The copolymer prepared by ATRP had a molar mass of  $M_n = 5\,400\text{ g mol}^{-1}$  and a PDI value of 1.2, whereas the copolymer prepared by RAFT had a molar mass of  $M_n = 7\,100\text{ g mol}^{-1}$  and a PDI value of 1.4. These copolymers were used for further functionalization with cyclooctyne derivatives (copper-free clicking).<sup>221</sup> The 4-azidophenyl methacrylate (Entry 54) can be copolymerized with different monomers in a controlled manner at room temperature by using a carbodithioate or a dithiobenzoate as initiator. Methyl acrylate, methyl methacrylate and styrene have been used as comonomers. The resulting copolymers were well-defined (PDI < 1.3) and in a molar mass ( $M_n$ ) range between 3 000 and 16 000  $\text{g mol}^{-1}$ .<sup>217</sup>

With the azide-functionalized monomer depicted in Entry 53 also a tandem click chemistry/ATRP procedure was applied by Drockenmuller *et al.* using CuBr/bpy as the catalytic system and TosCl as the initiator. Different copolymers with MMA were prepared ( $M_n < 22\,400\text{ g mol}^{-1}$ , PDI = 1.5).<sup>209</sup>

**Acrylamides.** There have been two reports published on the controlled radical polymerization of azido acrylamides (Entry 55). The first one is reported by Chang *et al.* for ATRP with a dansyl-

labeled initiator and CuBr/Me<sub>6</sub>TREN as catalyst. The polymerization was performed with NIPAM as comonomer at 0 °C to avoid side reactions ( $M_n = 9\,500\text{--}13\,300\text{ g mol}^{-1}$ , PDI = 1.2).<sup>95</sup> In another study, the authors polymerized 3-azidopropylacrylamide by RAFT with DMAM and NIPAM, where 4-cyanopentanoic acid dithiobenzoate was used as CTA and 4,4'-azobis(4-cyanopentanoic acid) as initiator to yield random copolymers ( $M_n = 14\,700\text{ g mol}^{-1}$ , PDI = 1.2).<sup>218</sup>

### 5.3 Monomers for Diels–Alder reactions

There are only a few examples for clickable monomers (dienophile or diene containing ones) that are suitable for Diels–Alder reactions. The furfuryl methacrylate is commercially available and therefore accessible for the controlled polymerization without further functionalization.

**Acrylates.** One report was published by Barner-Kowollik and Stenzel *et al.* using a hexa-2,4-dienyl acrylate (Entry 56), which was polymerized by RAFT using a trithiocarbonate chain transfer agent and styrene as comonomer ( $M_n = 5\,000\text{--}6\,000\text{ g mol}^{-1}$ , PDI = 1.2–1.4).<sup>228</sup>

**Methacrylates.** Singha *et al.* polymerized furfuryl methacrylate (FMA) (Entry 57) by ATRP (catalyst: CuCl/HMTETA, initiator: EBiB) at 90 °C. Moderate levels of monomer conversions (~60%) could be achieved during the homopolymerization of this type of monomer. Surprisingly, the polymers did not gel and preserved their low PDI values, which indicated no or negligible amounts of side reactions involving the addition of radicals to the furfuryl functionality. Semi-logarithmic kinetic plots revealed that the polydispersity decreased by increasing conversion.<sup>229</sup> Nonetheless, well-defined homopolymers ( $M_n = 6\,500\text{ g mol}^{-1}$ , PDI = 1.3) and copolymers with MMA ( $M_n = 10\,000\text{ g mol}^{-1}$ , PDI = 1.3) were obtained.<sup>57,229–231</sup> Furthermore, FMA was successfully used in the preparation of block copolymers with 2-ethylhexyl acrylate (EHA) and 1,2-bis(bromoisobutyryloxy)ethane (BBiBE) as initiator.<sup>232</sup> The ATRP reaction was conducted at 90 °C using CuCl/HMTETA as catalytic system. The obtained PFMA-*b*-PEHA-*b*-PFMA (up to  $M_n = 51\,000\text{ g mol}^{-1}$ , PDI = 1.3) was crosslinked with a bismaleimide to yield materials with self-healing properties.

### 5.4 Monomers for thiol-ene clicking

In the last years, the thiol-ene click reaction has attracted significant attention in the field of polymer science. These robust and efficient reactions have enormous advantages for the construction of polymeric structures. Recently, several reviews summarized the power of thiol-ene chemistry.<sup>19,28,53,233</sup>

Since thiol groups readily undergo side reactions under radical polymerization conditions, preferably ene-functionalized monomers were synthesized and used as clickable monomers. (Meth)acrylates containing a terminal double bond are prepared by an esterification of an alcohol (*e.g.* ethylene glycol vinyl ether or 3-butene-1-ol) with an acid chloride or an anhydride of (meth)acrylate acid.<sup>127,234</sup> Styrenes containing a terminal double bond are synthesized by substitution of a chloride group (*e.g.* from 4-vinylbenzyl chloride, using 3-butene-1-ol).<sup>127</sup> The controlled polymerization of this class of monomers is easily possible due to

the rather low reactivity of the unconjugated alkene group. Thus, no or less crosslinking occurs during the polymerization.<sup>127</sup>

**Styrenes.** There is only one report published for the polymerization of the ene-functionalized styrene derivative depicted in Entry 58. Hawker *et al.* reported a RAFT copolymerization to obtain alkene backbone-functionalized copolymers. The polymerization was performed with a dithiobenzoate as CTA at 75 °C resulting in a copolymer with St of a molar mass of  $M_n = 14\,000\text{ g mol}^{-1}$  and a PDI value of 1.1.<sup>127</sup>

**Methacrylates.** Vinyloxyethyl methacrylate (Entry 59) was polymerized by the RAFT process using a photoinitiator and a dithiobenzoate RAFT agent reported by Bulmus and coworkers.<sup>234</sup> Monomodal molar mass distributions were obtained at low monomer conversions (~25%) that broadened by increasing the polymerization time resulting in a hyperbranched polymer due to the incorporation of the vinyl ether group (PDI = 1.3–2.0).<sup>234</sup> Controlled polymerization of another alkene methacrylate (Entry 60) was described by Hawker and coworkers. The authors reported on the ATRP of but-3-enyl methacrylate. The copolymerization with MMA was initiated by ethyl 2-bromoisobutyrate and catalyzed by CuBr/PMDETA ( $M_n = 17\,000\text{ g mol}^{-1}$ , PDI = 1.2).<sup>127</sup>

### 5.5 Monomers for *para*-fluoro substitution

**Styrenes.** The commercially available pentafluorostyrene (Entry 61) can be used as a clickable monomer as recently shown by Schubert and coworkers. Thereby, the *para*-fluoro atom can be substituted in a postmodification by functionalized amines or thiols under mild conditions (see Section 2).<sup>31,32</sup> Pentafluorostyrene (PFS) was polymerized using the commercial available  $\beta$ -phosphonylated alkoxyamine (MMA-SG1: “BlocBuilder”) as unimolecular initiator for NMP polymerization at 110 °C. Thereby, homopolymer poly(PFS) ( $M_n = 3\,500\text{ g mol}^{-1}$ , PDI = 1.1), random copolymer poly(PFS-*r*-PS) ( $M_n = 9\,000\text{ g mol}^{-1}$ , PDI = 1.1) and diblock copolymers poly(PFS-*b*-PS) ( $M_n = 17\,000\text{ g mol}^{-1}$ , PDI = 1.2) could be prepared, where either a PFS- or a PS-macroinitiator was used.<sup>32</sup> Terpyridine-functionalized PhEt-TIPNO alkoxyamine as unimolecular initiator was also used for the NMP of PFS at 120 °C to yield poly(PFS) ( $M_n = 4\,500\text{ g mol}^{-1}$ , PDI = 1.1) and poly(PFS-*b*-PS) ( $M_n = 10\,000\text{ g mol}^{-1}$ , PDI = 1.2).<sup>31</sup>

The pentafluorophenyl-functionalized maleimide (Entry 62) will be discussed in Section 6.1.2.7.

### 5.6 Monomers for pyridyl disulfide exchange

In entry 63 a monomer is shown, where the pyridyl disulfide moiety is linked to methacrylate. The PySS group can be exchanged in a postmodification or premodification step by thiol functional compounds under mild reaction conditions, because of the facile leaving character of the 2-pyridinethione. The release of 2-pyridinethione allows the monitoring of the PySS exchange by UV/vis spectroscopy. This procedure is often used for the preparation of polymer bioconjugates (*e.g.* with oligopeptide) or for anticancer drugs, such as doxorubicin linked *via* the free thiol group.<sup>235,236</sup>

The monomer was used in RAFT polymerization with CPADB as CTA. These polymers were used as macro CTAs for the preparation of block copolymer of HPMAM resulting in different block segments with different molar mass ( $M_n = 13\,400\text{--}49\,000\text{ g mol}^{-1}$ , PDI = 1.2–1.3). These block copolymers were further crosslinked as micelles.<sup>235</sup>

Moreover, homopolymers of the PySS monomer were prepared by using the RAFT method by Bulmus *et al.* Different semilogarithmic plots are examined for this monomer indicating the controlled character of the polymerization. Numerous homopolymers were synthesized as basis for further bio-functionalization ( $M_n = 8\,000\text{--}12\,600\text{ g mol}^{-1}$ , PDI = 1.1–1.4).<sup>236</sup>

### 5.7 Monomers for ring-opening reactions

Ring-opening reaction of strained heterocycles are considered as a click reaction based on the spring-loaded character towards nucleophiles by Sharpless and coworkers.<sup>13</sup> For this purpose, glycidyl methacrylate (GMA) is a commercially available monomer, and thus can be used as a clickable monomer without further modification (Entry 64). CRP of GMA has been well studied by NMP,<sup>9</sup> RAFT<sup>237</sup> and ATRP.<sup>238–243</sup> For ATRP of GMA it is important to note that the epoxide might react with free ligand, which leads to unwanted branching. Thus, the catalyst has to be preformed before the addition of the monomer.<sup>59</sup> Moreover, any strong nucleophile should be avoided during polymerization. Apart from that, the epoxide is stable under the polymerization conditions even at elevated temperatures typically required for NMP.

With the “boom” of click chemistry in polymer science, the ring opening of epoxides with nucleophiles as a click-type reaction experienced also a revival in the last few years, but rather to introduce azides or alkynes than as a click reaction itself (Scheme 1, Entry 89). Why modifying towards another clickable functionality although the ring-opening reaction is an efficient click reaction itself? This is caused by the poor selectivity of epoxides. In contrast, the orthogonality is strongly increased for, *e.g.*, the azide-alkyne click reaction allowing the orthogonal functionalization in one-pot, simultaneous or cascade reactions.<sup>193</sup>

Various polymers containing glycidyl methacrylate were synthesized as basis for further click reactions: Poly(St-*r*-(C≡C-CH<sub>2</sub>-St)-*r*-GMA) was prepared *via* NMP with TIPNO as mediating nitroxide ( $M_n = 30\,000\text{ g mol}^{-1}$ , PDI = 1.3).<sup>60</sup> By ATRP the homopolymer as well as the random copolymers were synthesized (Entry 64): poly(GMA) with  $M_n = 27\,000\text{ g mol}^{-1}$  and PDI = 1.3,<sup>114</sup> poly(GMA-*r*-*t*BMA) with  $M_n = 8\,000\text{ g mol}^{-1}$  and PDI = 1.2<sup>244</sup> as well as poly(GMA-*r*-MMA) with  $M_n = 20\,000\text{ g mol}^{-1}$  and PDI = 1.2 to 1.5,<sup>59</sup> whereby the polydispersity index for the latter increases by increasing the fraction of GMA used in the feed.

### 5.8 Clicked monomers

Clicked monomers are formed by the azide-alkyne 1,3-dipolar cycloaddition and contain the triazole ring which is linked to the polymerizable vinyl group. There are only few examples of clicked monomers. Hawker *et al.* have described the RAFT polymerization of a series of 4-vinyl-1,2,3-triazoles (Entry 50). Different (co)polymers were prepared in a controlled manner using a dithioester.<sup>67</sup> Sumerlin *et al.* used propargyl acrylate



(Entry 46) that was clicked onto an azide-containing trithiocarbonate (Entry 29) for the RAFT polymerization of branched poly(*N*-isopropylacrylamide) (PDI = 1.5–2.1).<sup>156</sup> Also the chain extension of this macro-CTA with DMA was performed. 1-(3'-Aminopropyl)-4-acrylamido-1,2,3-triazole hydrochloride (Entry 48) was polymerized by the RAFT using a poly(NIPAM) macro-RAFT agent resulting in block copolymers ( $M_n = 19\,600\text{ g mol}^{-1}$ , PDI = 1.2).<sup>215</sup> Propargyl methacrylate (Entry 47) was clicked by a Cu-catalyzed 1,3-dipolar cycloaddition with 3-azido-7-diethylaminochromen-2-one and subsequently copolymerized with MMA by RAFT using 2-cyanoprop-2-yl dithiobenzoate (CPDB) as chain transfer agent ( $M_n = 10\,200\text{ g mol}^{-1}$ , PDI = 1.2).<sup>214</sup>

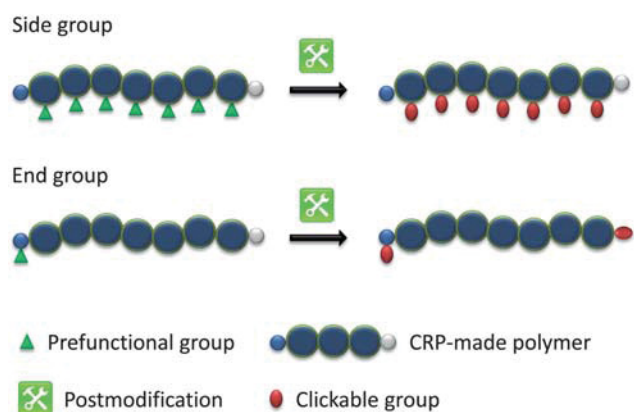
## 6. Postmodification

Postmodification reactions are used to transform latent functional groups into clickable units, whereby the polymer can be modified either at pendant or at terminal positions (Scheme 5). For the terminal modification the initiating side, the mediating side or both can be modified. An overview of the end-group modification approaches are depicted in Tables 11 and 12 and the side-group modifications are shown in Table 13, which will be discussed in the following.

### 6.1 End-group modification

Linear polymers prepared by controlled radical processes contain two functional end groups, one on the initiating end and the other one on the mediating end. Therefore, a polymer can be further functionalized on the  $\alpha$ - and/or the  $\omega$ -terminus. In particular for the  $\omega$ -terminus, unavoidable radical termination reactions during the polymerization such as recombination as well as disproportionation occur and, thus, parts of its functionality are lost to a certain amount. Assuming an efficient postmodification reaction, these side reactions for the prefunctional polymer can be considered as the bottleneck for the degree of functionalization that can be reached for  $\omega$ -functionalized polymers *via* the postmodification strategy.

**6.1.1 Modification on the  $\alpha$ -terminus.** The  $\alpha$ -terminus of the polymer is more preferred for modification in comparison to the  $\omega$ -terminus due to a higher end-group fidelity.



**Scheme 5** Schematic representation of the postmodification strategies.

**6.1.1.1 RAFT – Modification towards alkyne functionality.** An  $\alpha$ -endgroup modification of the initiating group was reported by Bertozzi *et al.*, where a pentafluorophenyl ester as a labile ester group (Entry 75) was attached to the initiating fragment. After polymerization the labile ester was cleaved with diisopropylethylamine in the presence of propargyl amine resulting in an  $\alpha$ -terminated alkyne polymer. Apparently, the trithiocarbonate was not attacked by the amine and, therefore, a defined polymer could be obtained.<sup>245</sup>

**6.1.1.2 NMP – Modification towards azide functionality.** Despite the versatility of functional groups that can be introduced as an initiating fragment on the  $\alpha$ -functionalized polymers prepared by NMP with functional alkoxyamines,<sup>175</sup> there is only one synthetic route reported for the transformation into a clickable moiety: The modification of the benzylic chloro group into an azide *via* a nucleophilic substitution with sodium azide (Entry 78, 79).

Initially, Hawker *et al.* described the postmodification from chloride into azide  $\alpha$ -functionalized polystyrene in 2004.<sup>246</sup> Thereby, the sodium azide was activated by the addition of catalytic amounts of 18-crown-6 ether while an excess of sodium azide was used. This postmodification was also utilized by Voit *et al.* using acetone as solvent and three equivalence of sodium azide at room temperature to achieve full conversion after several hours.<sup>176</sup> In 2008, Braslau *et al.* obtained azide-functionalized polystyrene by the reaction of the chloride counterpart in DMF with sodium azide (3 eq.) at 50 °C in the absence of crown ethers to almost full conversion.<sup>247</sup> Furthermore, the transformation was applied by O'Reilly *et al.* for the preparation of azido-functionalized poly(acrylic acid-*b*-styrene) ( $N_3CH_2$ -PhEt-PAA-*b*-PS) as clickable amphiphilic diblock copolymers. The postmodification of the benzylic chloro group attached to the PAA block was conducted in water at room temperature using a 5-fold excess of sodium azide to yield clickable micelles in water with azide groups on the outer shell.<sup>134</sup>

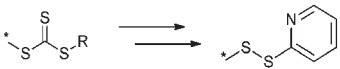
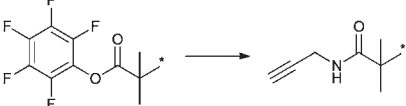
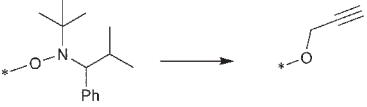
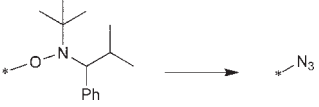
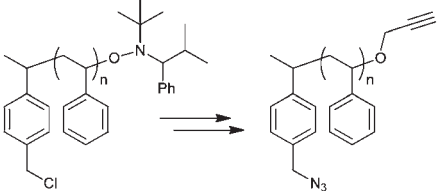
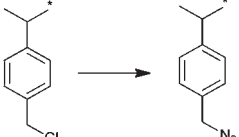
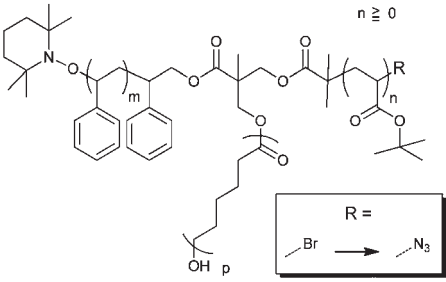
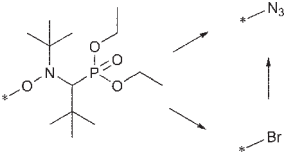
**6.1.2 Modification on the  $\omega$ -terminus.** The efficiency of the  $\omega$ -terminal modification depends on the stability of the mediating fragment of the polymer chain that is affected through side reactions inherent for controlled radical polymerization processes. In general, polymerizations intended for  $\omega$ -postmodification were kept at low conversions in order to avoid a significant loss of functionality.

**6.1.2.1 ATRP – Modification towards azide functionality.** The most prominent postmodification reaction towards a clickable functionality of ATRP-prepared polymers is the substitution of halides such as bromide against azide, since the halide is inherently present at the  $\omega$ -chain end after the ATRP process (Entry 65). The reaction is very efficient with sodium azide in DMF at room temperature, allowing for a specific transformation in the presence of distinct labile groups. In this context, it is important to note that Matyjaszewski and coworkers developed the method for this nucleophilic substitution in 1997/1998 for polystyrenes and polyacrylates to allow an easy access to amines over the azide *via* a reduction<sup>248</sup> or *via* the Staudinger process.<sup>249</sup> The authors also studied the rate constant for the substitution of selected model halogen compounds with sodium azide.<sup>250</sup>

Table 11 Postmodification – end group

Entry	Modification	Click	CRP	Type	Monomer	Ref
65		CuAAC	ATRP	Nucleophilic substitution	St, <i>t</i> BA, MA, OEGA, <i>t</i> BoA, MMA, GMA, OEGMA	59, 78–80, 90, 97, 98, 102, 114, 251–261
66		CuAAC	ATRP	Nitroxide radical coupling	St <i>t</i> BoA	263
67		CuAAC	ATRP	Nitroxide-mediated radical coupling		185
68		DA	ATRP	Nucleophilic substitution	St, MMA, MA, <i>t</i> BoA	39, 266
69		Thiol-ene Thiol-yne MAdd	RAFT RAFT RAFT	Aminolysis Aminolysis Aminolysis	NIPAM, OPA, EA, HEA St NIPAM	116, 245, 267, 270, 275–278 141 116, 273
70		Thiol-ene Thiol-yne Thiol-isocyanate MAdd	RAFT RAFT RAFT RAFT	Aminolysis Aminolysis Aminolysis Aminolysis	DEAEMA, BA, NIPAM, MMA, HPMAM, OEGA NIPAM DEAEMA DEAEMA, NIPAM, MMA	50, 267–271 50 54 50, 233, 271, 272, 274
71		CuAAC	RAFT	Aminolysis, Substitution	MMA, DEGMA, LMA, St, NIPAM	280
72		CuAAC	RAFT	Radical exchange	St	143
73		CuAAC	RAFT	Radical insertion	St, MA	281

**Table 12** Postmodification – end group (continued)

Entry	Modification	Click	CRP	Type	Monomer	Ref
74		PySS	RAFT	Aminolysis, Substitution	NIPAM	267
75		CuAAC	RAFT	Ester cleavage	OPA	245
76		CuAAC	NMP	Oxidative cleavage	St	284
77		CuAAC	NMP	Radical exchange	St	247
78		CuAAC	NMP	i) Substitution ii) Oxidative cleavage	St	247
79		CuAAC	NMP	Substitution	St, <i>t</i> BA	134,176,247
80		CuAAC	NMP ROP ATRP	Substitution	St $\epsilon$ -CL <i>t</i> BA	71,72
81		CuAAC	NMP	Radical exchange, Substitution		285

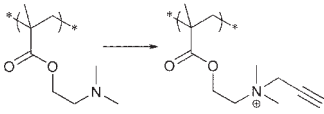
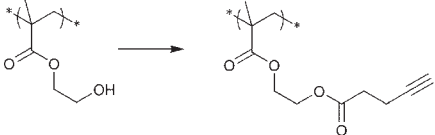
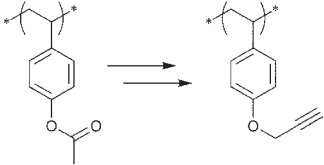
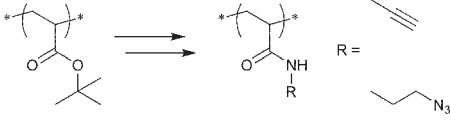
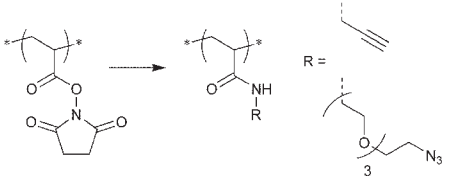
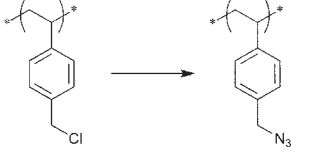
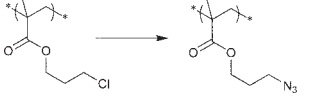
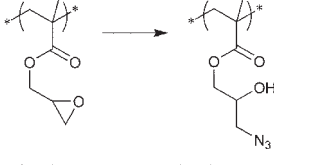
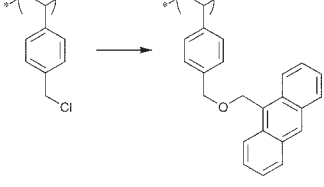
Up to now a lot of different polymers were postmodified *via* this azidation method. Poly(styrenes), poly(acrylates), poly(methacrylates) and their copolymers at different molar masses have been reported.<sup>59,78–80,90,97,98,102,114,251–261</sup> It should be noted that the azidation of poly(methacrylates) is significantly slower compared to poly(acrylates) and poly(styrenes) due to the tertiary bromine.<sup>262</sup> The modification can be used, *e.g.*, in combination with multifunctional initiators bearing functional termini for NMP or ROP (Entry **80**). The multifunctional initiator was used in NMP of styrene, ROP of  $\epsilon$ -caprolactone as well as ATRP of *t*BA followed by the quantitative substitution of the

bromine against azide, while the molar masses and the polydispersity indices retained.<sup>71,72</sup>

**6.1.2.2 ATRP – Modification towards alkyne functionality.** Only a few examples are described for polymers prepared by ATRP dealing with the exchange of the bromine end group against alkyne-functionalized groups.<sup>185,263</sup> Low molar masses and conversions are targeted by preparing the polymers to assure a high end-group fidelity of the  $\omega$ -terminating bromide.

Monteiro and coworkers used the high reactivity of PS towards cleavage of the bromine end group in the presence of

**Table 13** Postmodification – side group

Entry	Modification	Click	CRP	Type	Comonomers	Initiator	Ref
82		CuAAC	ATRP	Quaternization	DMAEMA, DEGMA, DEAEMA	EBiB	288
83		CuAAC	ATRP	Esterification	—	EBiB	289
84		CuAAC	NMP	i) Hydrolysis ii) Substitution	St	PhEt-TIPNO	291
85		CuAAC	NMP	i) Acidolysis ii) Amidation	St	PhEt-TIPNO	292,295
86		CuAAC	NMP	Amidation	St, <i>t</i> BA, AM	PhEt-TIPNO	193
87		CuAAC	NMP	Substitution	St, <i>t</i> BA	PhEt-TEMPO	117,292–294
88		CuAAC	RAFT	Substitution	AA	BPIT, PEDT	205,206
89		CuAAC	ATRP	Ring opening	MMA, <i>t</i> BMA	EBiB	59,104,114,244,290
90		DA	NMP	Etherification	St	PhEt-TEMPO	117,120

Cu(I)Br, Me<sub>6</sub>TREN and DMSO promoting a single electron transfer (SET) *via* the formation of nascent Cu(0).<sup>263</sup> The emerging carbon-centered radical was trapped by an alkyne-functionalized nitroxide (2,2,6,6-tetramethyl-4-(prop-2-ynoxy)piperidin-1-lyoxy)<sup>264</sup> to result in alkyne-terminated PS with near quantitative yields within 10 min at room temperature (Entry 66). A unique

feature of the nitroxide radical coupling (NRC) as a selective and highly efficient reaction is the reversible formation of the C–O bond of the alkoxyamine that undergoes homolytical cleavage upon heating. In this fashion, the coupled nitroxide can be substituted by an excess of other functional nitroxides (10-fold excess) at elevated temperatures.

Recently, Barner-Kowollik and coworkers established a new approach towards midchain-functionalized polymers by using nitrones in a dual radical capturing process.<sup>185,265</sup> Nitrones can rapidly react with carbon-centered radicals to form nitroxides that further trap radicals to form alkoxyamines. As such, nitrones can be used for efficient polymer conjugation by mediating the radical coupling reactions of macroradicals. The authors activated ATRP-made PiBoA with Cu(0)/PMDETA in toluene at 60 °C in the presence of an alkyne-functionalized nitron (2-fold excess), while the alkyne was protected with TMS.<sup>185</sup> In this vein, midchain alkyne-functionalized polymers as depicted in Entry 67 can be prepared in high yields as indicated by <sup>1</sup>H NMR spectroscopy (~90%). The midchain functional PiBoA was clicked after deprotection with either PS-N<sub>3</sub> or PiBoA-N<sub>3</sub> to form 3-arm star polymers.

As an additional feature, the prepared polymers bear an alkoxyamine functionality in the backbone that could in principle be used as a macroinitiator in a nitroxide-mediated polymerization for the insertion of another polymer block towards triblock copolymers. Hence, the present approach can also be considered as a preparation of clickable or clicked macroinitiators for NMP (Entry 40; Section 4.3).

**6.1.2.3 ATRP – Modification toward diene functionality for Diels–Alder reactions.** In Entry 68 a nucleophilic substitution of a bromo-terminated polymer with cyclopentadienyl as reported by Barner-Kowollik is described. This strategy allows the direct access to dienes which can be used for catalyst-free click reactions, *i.e.* Diels–Alder reaction. The reaction was performed with sodium cyclopentadienide (NaCp) or nickelocene (NiCp<sub>2</sub>) as the substituting agent at ambient temperature. It should be mentioned that side reactions can occur during the substitution with the more reactive NaCp, in particular for PMMA-Br, PiBoA-Br and PMA-Br, but not for PS-Br. It could be shown that the use of NiCp<sub>2</sub> using tributylphosphine and sodium iodide as promoters eliminates these side reactions. In this manner, cyclopentadienyl-functionalized polymers of PMMA, PiBoA, PMA and PS are reported (PDI < 1.3).<sup>39,266</sup>

**6.1.2.4 RAFT – Modification towards thiol functionality.** In recent years, an alternative click strategy has been established in polymer research for the design of complex macromolecular architectures. This strategy is based on the special chemical nature of thiol compounds that can be used for radical coupling processes in thiol-ene and thiol-yne reactions, as well as for nucleophilic addition reactions such as thiol-isocyanate addition or Michael addition. The radical-mediated addition of a thiol to an yne is a “sister” reaction to the radical thiol-ene reaction, whereby two thiols can be added (two-step process). All these reactions can be performed under mild conditions.

The ω-end of the polymer chains prepared by the RAFT polymerization can be easily modified to generate a reactive thiol group. In most of the reports a trithiocarbonate (Entry 69) or a dithiobenzoate (Entry 70) have been used as chain transfer agents for RAFT. These group can be easily modified into thiol groups. There are two synthetic pathways towards thiols: (i) Aminolysis with a primary amine<sup>50,54,141,245,267–275</sup> and (ii) reduction with NaBH<sub>4</sub>.<sup>276–278</sup> Care should be taken in this post-modification to prevent the coupling of two chains to form

a disulfide bridge, which are often visible by a shoulder at lower elution volumes in the SEC measurements. However, coupling of thiols can be easily reversed by addition of a reducing agent, *e.g.* phosphine derivatives.<sup>50,54,116,268,271,273,276</sup> Limitations of the thiol-ene reaction for polymer-polymer conjugation were recently described by Du Prez *et al.*<sup>53</sup>

In some cases, further purification of the ω-thiol functional polymers is necessary and dialysis or precipitation are the preferred techniques. A calorimetric method for the determination of the free thiol concentration was developed by Ellman.<sup>279</sup> Ellman’s reagent converts a thiol into a 5,5’-dithiobis(2-nitrobenzoic acid) derivative, which has a strong absorption and therefore the degree of functionalization can be determined.<sup>267,269,270,273,275</sup> Alternatively, this can be indirectly estimated by clicking a fluorescence dye (*e.g.* pyrene).<sup>274,276</sup> The degree of functionalization can be varied from 60% up to 99.5%. Often short polymer chains are used for the modification to provide high end-group fidelity on the mediating side ( $M_n < 10\,000\text{ g mol}^{-1}$ ). Different polymers were used for the modification towards thiols, *i.e.* acrylate-, methacrylate- and acrylamide derivatives.

An elegant example for the orthogonality of the Michael addition as nucleophilic thiol-ene reaction to the radical thiol-ene was recently described by Lowe *et al.*<sup>50</sup> By using the fact that the nucleophilic reaction of the thiols is selective for double bonds conjugated with electron-withdrawing groups (*e.g.* α,β-unsaturated carbonyl compounds), a consecutive reaction of a heterofunctional polymer with different thiols, first reacted *via* Michael addition and followed by the radical thiol-ene or thiol-yne reaction could be shown. The reverse case leads to the loss of orthogonality due to the unselective nature of the radical coupling.

**6.1.2.5 RAFT – Modification towards alkyne functionality.** An elegant approach to generate ω-end group functionalized triple bonds, which can be used for the Cu(I)-catalyzed cycloaddition, was reported by Theato and coworkers using butynyl methane thiosulfonate (Entry 71). Five different acetylene-terminated polymers (MMA, DEGMA, LMA, St, NIPAM) could be clicked to an azide.<sup>280</sup> Another approach towards alkyne-terminated polymer chains is the cleavage of the RAFT agent by a radical process (Entry 72).<sup>143</sup> Thereby, an excess of alkyne-modified initiator is used, which decomposes while generating radicals that react with the C = S of the thio-carbonylthio moiety in the polymer chain. Higher temperatures (80 °C) and a large excess of the initiator are necessary and it should be taken into account that side reactions during end-group modification can occur by means of recombination during insertion.<sup>143</sup> ABCD 4-miktoarm star polymers could be prepared by RAFT polymerization of styrene followed by an insertion reaction applying a large excess of 2-hydroxyethyl-3-(4-(prop-2-ynyloxy)phenyl) acrylate to stop the polymerization at 110 °C. Hence, a unprotected triple bond attached at the end of the polymer chain could be obtained (Entry 73). The reaction is not very efficient, because a large amount of unreacted macroinitiator is present after the diblock copolymerization.<sup>281</sup>

**6.1.2.6 RAFT – Modification towards pyridyl disulfide functionality.** Chemical modification of the ω-endgroup by aminolysis in the presence of 2,2’-dithiodipyridine was reported to generate a pyridyl-disulfide-terminated polymer chain (Entry



74). The pyridyl disulfide end groups allowed straightforward conjugation with oligonucleotides and peptides.<sup>267</sup>

#### 6.1.2.7 NMP – Conventional modification and possibilities.

Only a few examples are described dealing with the exchange of the nitroxide moiety on the polymer. The first study was conducted by Rizzardo, reducing the TEMPO to a hydroxy group with a mixture of zinc/acetic acid.<sup>282</sup> A radical-cleavage approach towards more versatile functional end groups was presented by Hawker and coworkers. Thereby, the propagating radical was trapped at the polymerization temperature by *N*-functionalized maleimides as non-self-polymerizing monomers, while the TIPNO nitroxide decomposed at elevated temperatures resulting in the maleimide-functionalized polymer.<sup>283</sup> The transformation yield for polystyrene, polyisoprene and poly(*n*-butylacrylate) was typically 90 to 95%, while no changes in molar masses and the polydispersity indices were observed.

This approach offers the possibility to introduce clickable units at the  $\omega$ -terminus by using functionalized maleimides. Following this strategy, Lutz and coworkers synthesized a library of functional maleimides and used them in the copolymerization with styrene *via* ATRP, while the maleimide was incorporated at a specific place in the polymer chain.<sup>216</sup> Among those, *N*-pentafluorophenyl maleimide or *N*-propargyl maleimide could be incorporated into the polymer, while the latter one had to be protected due to pronounced side reactions (Entry 51, 62). In principle, clickable  $\omega$ -functionalized polymers should be accessible using these monomers in the radical-cleavage procedure by Hawker as well.

6.1.2.8 NMP – Modification towards alkyne functionality. In contrast to the thermal cleavage of the alkoxyamine-terminated polymer, oxidative cleavage under much milder thermal conditions can be achieved by single electron oxidation with ceric ammonium nitrate (CAN).<sup>247,284</sup> After the oxidation the alkoxyamine cleaves heterolytically into a nitroxide and the cation-terminated polymer that can be trapped by nucleophiles. Braslau and coworkers treated TIPNO-terminated polystyrene with CAN and propargyl alcohol as nucleophile at room temperature under anhydrous conditions to obtain alkyne-functionalized PS (Entry 76) with an end-group fidelity of 65% as determined by UV-vis experiments.<sup>247</sup> Investigating PhEt-TEMPO as a model compound for TEMPO-terminated polymers, a heterolytic cleavage similar to the TIPNO counterpart was obtained. It could be shown that this method can also be used for TEMPO-terminated polymers. In contrast, polyacrylates terminated with TIPNO or TEMPO also undergo oxidative cleavage, but the cation-terminated polymer interferes with CAN by forming nitrate ester and prohibit further attachment of functional groups *via* the addition of nucleophiles.<sup>284</sup>

The modification of polystyrene that was prepared by NMP with commercially available  $\beta$ -phosphonylated alkoxyamine BlocBuilder<sup>®</sup> cannot be performed *via* the described oxidative cleavage with CAN due to the electronic and steric nature of SG1.<sup>285</sup>

#### 6.1.2.9 NMP – Modification towards azide functionality.

Terminal azide-functionalized polystyrene could be obtained starting from the nitroxide-terminated polymer through the

reaction with ethanesulfonyl azide (EtSO<sub>2</sub>N<sub>3</sub>) that was introduced by Renaud and Ollivier<sup>286</sup> as an azidation method for carbon radicals. Braslau and coworkers showed that polystyrene prepared by NMP reacts in the presence of an excess of EtSO<sub>2</sub>N<sub>3</sub> in *N*-methyl-2-pyrrolidinone at 120 °C to the azido-functionalized PS (Entry 77), although the azidation was incomplete as judged by labelling experiments with an alkyne-functionalized dye analyzed *via* UV-vis experiments.<sup>247</sup> Using PhEt-TIPNO as a model compound, the treatment with EtSO<sub>2</sub>N<sub>3</sub> led to less than 30% of the desired transformation.<sup>247</sup> This was explained by the weak electrophilic character of the styryl radical, since only electron-rich radicals can efficiently add onto EtSO<sub>2</sub>N<sub>3</sub>.<sup>287</sup> This also explains why polyacrylates could not be modified with this method.

The azidation reaction of nitroxide-terminated polystyrene was further studied by Bertin and coworkers for polystyrenes prepared with the commercial available BlocBuilder<sup>®</sup>.<sup>285</sup> Thereby, a one-step as well as a two-step approach towards the terminal azido-functionalized polymer were performed (Entry 81). In the one-step approach EtSO<sub>2</sub>N<sub>3</sub> was used under optimized reaction conditions using a large excess (50 eq.) at 90 °C. In the two-step approach the alkoxyamine was reacted at 75 °C in a radical exchange reaction with 2-bromoisobutyrate as solvent as well as the bromination agent to obtain the exchange of the nitroxide by bromine. Furthermore, this bromo-functionalized polymer was reacted with sodium azide following the well-known ATRP postmodification procedure at room temperature in DMF. For both approaches the azide-functionalization degree was around 70%.

### 6.1.3 Heteromodification on both termini

6.1.3.1 NMP. Since the azide group is stable against the mild conditions of the oxidative exchange of the nitroxide against propargyl alcohol by ceric ammonium nitrate (Section 4.1.1), alkyne-azide-functionalized heterotelechelic polystyrene could be efficiently synthesized in a two step synthesis as demonstrated by Braslau *et al.* (Entry 78).<sup>247</sup> At first the chloro group of the  $\alpha$ -functionalized polystyrene prepared by NMP was transformed into the azide followed by the oxidative cleavage reaction with CAN at room temperature and the *in situ* nucleophilic addition of propargyl alcohol.

## 6.2 Side-group modification

In contrast to the terminal functionalization, the modification of pendant groups is more influenced by steric or electronic effects, in particular for homopolymers, where every repeating unit has to be modified. Nonetheless, this method represents a convenient alternative route to multiple click-functionalized polymers, if the direct polymerization of these monomers is relatively more difficult and/or side reactions occur during the polymerization.

### 6.2.1 ATRP

Modification towards alkyne functionality. In Entry 82 the alkyne moiety could be selectively introduced by quaternization of the amine of 2-(dimethylamino)ethyl methacrylate (DMAEMA) with propargyl bromide at room temperature (Menschutkin reaction).<sup>288</sup> Due to sterical hindrance, the DMAEMA is more reactive towards quaternization than DEAEMA allowing for the selective modification of a terpolymer containing DEGMA,



DMAEMA and DEAEMA.<sup>288</sup> The purification of the quaternized copolymer was achieved simply by precipitation. The extent of quaternization of the DMAEMA units was evaluated by <sup>1</sup>H NMR spectroscopy to be 35%.

Alkynyl side groups were introduced into polymeric backbones of a linear poly(2-hydroxyethyl methacrylate) by an esterification reaction between the hydroxyl groups and 4-pentynoic acid that was activated by *N,N'*-dicyclohexylcarbodiimide (Entry **83**). The degree of functionalization was estimated by <sup>1</sup>H NMR spectroscopy to be close to 100%. No change of the apparent molar masses and PDI values occurred.<sup>289</sup>

**Modification towards azide functionality.** An efficient and convenient synthesis route to azides is the ring-opening reaction of epoxides as shown in Entry **89**. The oxirane ring is often opened with sodium azide in the presence of ammonium chloride to yield the corresponding 1-hydroxy-2-azido compounds. The reactions can be followed by IR spectroscopy of the characteristic vibration bands of the azide (2104 cm<sup>-1</sup>) and the epoxide ring (909 cm<sup>-1</sup>). This click reaction was applied for the preparation of copolymers with multiple azide groups, whereby different methacrylates are used, resulting in defined copolymers.<sup>59,104,114,244,290</sup>

### 6.2.2 RAFT

**Modification towards azide functionality.** In Entry **88**, a nucleophilic substitution of a pendant chloro group against azide was performed for a poly(3-chloropropyl acrylate-*co*-acrylic acid). The reaction was conducted with sodium azide at 80 °C and the final product was subsequently dialyzed. High molar mass copolymers were obtained:  $M_n = 86\,000$  and  $135\,000\text{ g mol}^{-1}$  with polydispersity indices of 2.2 and 1.4, respectively.<sup>205,206</sup>

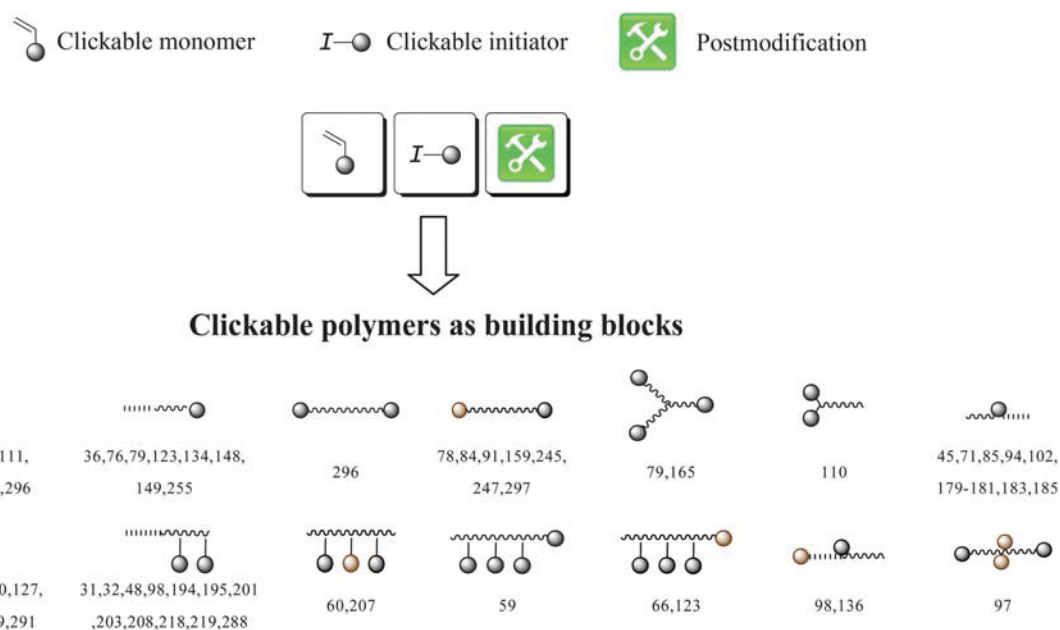
### 6.2.3 NMP

**Modification towards either alkyne or azide functionality.** A substitution reaction was carried out as pendant postmodification

for the random copolymer poly[styrene-*r*-(4-acetoxystyrene)] (Entry **84**).<sup>291</sup> The acetyl group was used as a protection for the phenolic hydroxy group that cannot be polymerized directly, since it acts as a radical scavenger. Deprotection was accomplished by using hydrazine monohydrate as a base for hydrolysis at room temperature to yield poly[styrene-*r*-(4-hydroxystyrene)]. The hydroxy group was further reacted with propargyl bromide under basic conditions in a Williamson ether synthesis to yield the clickable styrenic copolymer while retaining molar mass and polydispersity indices of the protected copolymer.<sup>291</sup>

Another postmodification strategy towards clickable side groups is the carbodiimide-mediated condensation which was demonstrated for the block copolymer poly(*t*BA-*b*-St) by Woolley and Hawker (Entry **85**).<sup>292</sup> First, the *t*-butyl group, acting as a protecting group, was cleaved using trifluoroacetic acid at room temperature. The resulting amphiphilic diblock polymer poly(acrylic acid-*b*-styrene) was assembled into micelles in water and partly functionalized with either 3-azidopropylamine or propargyl amine in a condensation reaction at room temperature using 1-[3'-(dimethylamino)propyl]-3-ethylcarbodiimide methiodide to activate the acid. The residual acid groups were crosslinked to obtain nanoparticles with azides or alkyne moieties on the outer shell.

Another postmodification strategy uses succinimide-functionalized acrylates as active ester for the condensation with amines under mild conditions.<sup>193</sup> The active ester is stable under the applied polymerization conditions and can be polymerized in a controlled way, while in contrast to alkyl acrylates no deprotection for further modification is required. Hereon, Malkoch *et al.* showed the preparation of random copolymers of *N*-(acryloyloxy)succinimide with either styrene, *t*-butylacrylate or acrylamide followed by a successful condensation reaction with propargyl amine or 1-amino-11-azido-3,6,9-trioxoundecane at 50 °C (Entry **86**). In addition, the amidation reaction does not interfere with the click reaction and can be used in a one-pot cascade reaction or simultaneously.<sup>193</sup>



**Scheme 6** Schematic representation of clickable polymers: wavy = polymer chain; ○, ● = orthogonal click functionalities, ■■■■ = block segments.



A facile approach towards pendant azide-functionalized polymers *via* postmodification is the reaction of benzylic chloride with sodium azide in a nucleophilic substitution reaction (Entry 87). The reaction is efficient at room temperature in DMF. Following this procedure, a random copolymer consisting of 4-(chloromethyl)styrene and styrene was transformed with sodium azide.<sup>293</sup> Furthermore, a random terpolymer consisting of 4-(chloromethyl)styrene, styrene as well as 4'-(anthracene-methyloxymethyl)styrene was efficiently modified to the pendant azido- and anthracene-containing derivative.<sup>117</sup> O'Reilly *et al.* modified the amphiphilic diblock copolymer poly[(acrylic acid)-*b*-styrene-*r*-4-chloromethylstyrene] *via* the described procedure to obtain, after crosslinking, nanoparticles with azide-functionalized cores.<sup>292</sup> In 2009, Ting *et al.* transformed homopolymers of 4-(chloromethyl)styrene as well as random and block copolymers with styrene at 60 °C in a mixture of DMSO/THF to the pendant azide-functionalized polymers.<sup>294</sup>

*Modification towards diene functionality for Diels–Alder reaction.* The pendant benzylic chloro group in 4-(chloromethyl)styrene containing polymers were also modified by the etherification reaction with 9-(oxymethyl)anthracene (Entry 90). Thereby, an excess of 9-(oxymethyl)anthracene was activated with sodium hydride to react with poly(styrene-*r*-4-chloromethylstyrene) to the anthracene-functionalized polymer at room temperature,<sup>117</sup> although the conversion only went to completion by using higher temperatures.<sup>120</sup>

## 7. Applications of clickable polymers

The concept of click chemistry combined with the concept of controlled radical polymerizations represent an ideal pair for the preparation of tailor-made macromolecular architectures.

The striking advantage of this combination can be clearly seen by the variety of clicked architectures that become possible by using clickable polymers as building blocks (Schemes 6 and 7). The schemes should provide an overview over the clickable and clicked architectures, while assigning assorted references. The origin for the large variety of architectures is the overcoming of limitations inherent for other techniques, which allows the design of new architectures prepared in high yields and with a wide range of accessible molar masses and constitutions. In this way, some block combinations become possible, which were not directly polymerizable due to disparate reactivities. An example for such an architecture is the block copolymer of styrene and ethylene glycol (EG) using the 1,3-dipolar cycloaddition of azides and acetylene of the respective end groups.

Utilizing the different approaches (clickable initiator, clickable monomer and postmodification) different types of highly functional polymers are accessible and can act as building blocks for the preparation of more complex structures. Several clickable polymers can be prepared: (i) End functional polymers on one or on both sites, (ii) mid-chain functional polymers, (iii) side-chain functional polymers and (iv) combinations of them (Scheme 6). These clickable polymers act as basic modules for further functionalization reactions to engineer more complex architectures (Scheme 7). Hereon, different linear block copolymers such as di-, ter- or quarterpolymers were prepared. The synthesis of different cyclic polymers such as eight-shaped or tadpole

polymers, which are limited for other non-click methods, has been realized using the click concept. These building blocks were also often used for the preparation of star-shaped polymers with 3 up to 12 arms as well as H-shaped or miktoarm star polymers. In this respect, two strategies arise for the synthesis of star-like polymers by clicking: (i) Using mid-chain functional polymers or (ii) end functional polymers onto a multifunctional core. Furthermore, several dendrimers and hyperbranched architectures were also realized by combining CRP and click chemistry. An elegant example represents the thiol-yne reaction for the preparation of hyperbranched polymers.

Another focus of polymer research is the grafting approach of side-chain functional polymers, which can be prepared by using the clickable monomer approach or the postmodification approach of pendant groups. The main advantage for this strategy is the facile tuning of polymer properties for a specific application. One clickable polymer backbone can act as building block for a variety of functionalization reactions (Scheme 6). Moreover, surface patterning is also of interest in material science. Polymers were clicked *via* CuAAC to different surfaces such as carbon nanotubes or nanoparticles (Si, Au). Also the construction of multilayer systems (layer-by-layer approach) are possible by using the 1,3-dipolar cycloaddition and CRP.

The interest in polymer-functionalized biomaterials strongly increased in the last years due to the facile access by using click chemistry for efficient conjugation and CRPs for tailoring the polymeric architectures. In this vein, different functional polymers were coupled with several proteins and siRNA.

## 8. Conclusion and outlook

In summary, it is clearly demonstrated in recent years that the combination of controlled/“living” radical polymerization (CRP) techniques and click reactions has become an inevitable route for preparing highly functional tailor-made macromolecules. This combination has been tremendously advanced since the introduction of the concept of click chemistry in 2001 by the cumulative efforts of a large number of research groups all over the globe. These developments on the preparation of new well-defined clickable polymers enabled straightforward access to demanding polymer structures such as cyclic and miktoarm star polymers.

Two combinations of CRP with click chemistry seem to be the perfect match: ATRP in combination with azide cycloaddition and RAFT with thio-click chemistry. Halogen-terminated polymers are directly obtained by ATRP and can be transformed to azide-terminated polymers using a simple azidation procedure. As a limitation, this combination may not be suitable for the preparation of clickable polymers of high molar masses, since a high end-group fidelity of the halogen-terminated polymers is only assured for low molar masses and low conversions. Even the most efficient postmodification reaction will not overcome this inherent problem. Nevertheless, ATRP and azide-alkyne click reactions are one of the most prominent combinations to prepare functional materials. Alternatively, thiol-terminated polymers are easily accessible from polymers prepared using the RAFT technique by reduction of the CTA end group. It has been demonstrated that these thiol-terminated polymers can be clicked not only to unsaturated double bonds but also to alkynes,

bromo, and *para*-fluoro groups making the combination of RAFT polymerizations with thio-click chemistry a powerful method. It should be noted that certain kinds of radical thiol-ene reactions do not fulfill the click criterion of a high reaction efficiency if they are applied for polymer-polymer conjugation.

We are confident that the combination of CRP and click chemistry methods will continue flourishing in the near future leading to new functional polymeric materials. Eventually, this will lead to a further establishment of CRP in combination with click chemistry as a scientific tool rather than being a separate research topic. Furthermore, it is evident that new trends in click chemistry, *e.g.* the development of advanced metal-free click reactions employing more reactive clickable units such as cyclooctynes as click counterparts to nitrones or nitrile oxides, will be combined with CRP methods in the near future, which will further expand the potential field of applications.

## Abbreviations

AcOSt	4-acetoxystyrene	DDAT	<i>S</i> -1-dodecyl- <i>S'</i> -( $\alpha,\alpha'$ -dimethyl- $\alpha''$ -acetic acid) trithiocarbonate
AA	acrylic acid	DDET	<i>S</i> -1-dodecyl- <i>S'</i> -( $\alpha,\alpha'$ -dimethyl- $\alpha''$ -ethyl acetate) trithiocarbonate
AIBN	azoisobutyronitrile	DEGMA	di(ethylene glycol) methylether methacrylate
AM	acrylamide	DIPEA	<i>S</i> -dodecyl- <i>S'</i> -( $\alpha,\alpha'$ -dimethylpentafluorophenyl acetate) trithiocarbonate
AN	acrylonitrile	DMAM	<i>N,N</i> -dimethylacrylamide
APBIB	3-azidopropyl 2-bromoisobutyrate	DEAM	<i>N,N</i> -diethylacrylamide
ATRP	atom transfer radical polymerization	DEAEMA	2-(diethylamino) ethyl methacrylate
ATREP	atom transfer radical emulsion polymerization	DMAEMA	2-(dimethylamino) ethyl methacrylate
BBiBE	1,2-bis(bromoisobutyryloxy)ethane	EBiB	ethyl 2-bromoisobutyrate
BDAT	<i>S,S'</i> -bis( $\alpha,\alpha'$ -dimethyl- $\alpha''$ -acetic acid) trithiocarbonate	EA	ethyl acrylate
BDB	benzyl dithiobenzoate	EEA	1-ethoxyethyl acrylate
BETP	benzyl 2-(ethylthiocarbonothioylthio) propanoate	EHA	2-ethylhexyl acrylate
BICDT	benzyl 1 <i>H</i> -imidazole-1-carbodithioate	EtSO <sub>2</sub> N <sub>3</sub>	ethanesulfonyl azide
bpy	2,2'-bipyridine	FMA	furfuryl methacrylate
BlocBuilder®	<i>N</i> -(2-methylpropyl)- <i>N</i> -(1-diethylphosphono-2,2-dimethylpropyl)- <i>O</i> -(2-carboxylprop-2-yl) hydroxylamine	GMA	glycidyl methacrylate
BMP	2-bromo-2-methyl-propionate	HEA	2-hydroxyethyl acrylate
BMPA	2-bromo-2-methyl-propionamide	HEMA	2-hydroxyethyl methacrylate
BMPABE	2-bromo-2-methyl-propionic acid benzyl ester	HMA	hostasol methacrylate
BPIT	butyl phthalimidomethyl trithiocarbonate	HMTETA	1,1,4,7,10,10-hexamethyl triethylenetetramine
BPN	2-bromopropionitrile	HPMA	2-hydroxypropyl methacrylate
BPO	dibenzoylperoxide	HPMAM	2-hydroxypropyl methacrylamide
BSPA	3-benzylsulfanyl-thiocarbonylsulfanyl propionic acid	<i>i</i> BoA	<i>i</i> -bornyl acrylate
CAN	ceric ammonium nitrate	<i>p</i> HSt	4-hydroxystyrene
CBDB	2-cyano-2-butyl dithiobenzoate	KSPMA	potassium 3-sulfopropyl methacrylate
CBDN	$\alpha$ -cyanobenzyl dithionaphthalate	LMA	lauryl methacrylate
CDB	2-phenylpropan-2-yl dithiobenzoate (cumyl dithiobenzoate)	MA	methyl acrylate
CNT	carbon nanotube	MAA	methacrylic acid
$\epsilon$ -CL	$\epsilon$ -caprolactone	MCPMDB	( <i>S</i> )-methoxycarbonylphenylmethyl dithiobenzoate
CPADB	(4-cyanopentanoic acid) dithiobenzoate	Me <sub>6</sub> TREN	tris(2-(dimethylamino)-ethyl) amine
CPDB	(2-(2-cyano-propyl)) dithiobenzoate	MMA	methyl methacrylate
CTA	chain transfer agent	mPEG	linear methoxy poly(ethylene glycol)
CRP	controlled radical polymerization	MPPCTTA	methyl 2-phenyl-2-(phenylcarbonothioylthio) acetate
		NaCp	cyclopentadienide
		<i>n</i> BA	<i>n</i> -butyl acrylate
		<i>n</i> BMA	<i>n</i> -butyl methacrylate
		NIPAM	<i>N</i> -isopropylacrylamide
		NiCp <sub>2</sub>	nickelocene
		NMP	nitroxide-mediated radical polymerization
		NP	nanoparticle
		NVP	<i>N</i> -vinylpyrrolidone
		OEGA	oligo(ethylene glycol) methylether acrylate
		OEGMA	oligo(ethylene glycol) methylether methacrylate
		OPA	(2-oxopropyl)acrylate
		PBP	propargyl 2-bromopropionate
		PDB	1-phenylethyl dithiobenzoate
		PEB	1-phenylethylbromide
		PEDT	<i>S</i> -1-phenylethyl- <i>S'</i> -dodecyl-trithiocarbonate
		PFPPCV	pentafluorophenyl-(4-phenylthiocarbonylthio-4-cyanovalerate)
		PFS	pentafluorostyrene
		PMDETA	<i>N,N,N',N',N''</i> -pentamethyldiethylene-triamine



poC	postclick
prC	preclick
RAFT	reversible addition-fragmentation chain transfer polymerization
ROP	ring-opening polymerization
SGI	<i>N</i> -(2-methylpropyl)- <i>N</i> -(1-diethylphosphono-2,2-dimethylpropyl)- <i>N</i> -oxyl
SMA	solketal methacrylate
St	styrene
<i>t</i> BA	<i>t</i> -butyl acrylate
<i>t</i> BMA	<i>t</i> -butyl methacrylate
TBAF	tetrabutylammonium fluoride
<i>t</i> BOS	4- <i>t</i> -butyloxystyrene
TBDMS	<i>t</i> -butyldimethyl-silyl
TEMPO	2,2,6,6-tetramethylpiperidinylnitroxide
THPA	tetrahydropyran acrylate
TIPNO	2,2,5-trimethyl-4-phenyl-3-aza-hexane-3-nitroxide
TIPS	triisopropylsilyl
TMS	trimethylsilyl
TosCl	<i>p</i> -toluenesulfonyl chloride
VAc	vinylacetate
VBA	vinylbenzyl azide
4VP	4-vinylpyridine.

Polymer abbreviations are formed by adding the suffix 'P' or 'poly' to the corresponding monomer abbreviation. The only exception is styrene, where the monomer is represented by St and the polymer by PS.

## Acknowledgements

Financial support of the Dutch Polymer Institute (DPI) and of the Thuringian Ministry for Education, Science and Culture (grant #B514-09051, NanoConSens) is gratefully acknowledged.

## Notes and references

- M. Szwarc, *Nature*, 1956, **178**, 1168–1169.
- M. Szwarc, M. Levy and R. Milkovich, *J. Am. Chem. Soc.*, 1956, **78**, 2656–2657.
- V. Ladmiral, G. Mantovani, G. J. Clarkson, S. Cauet, J. L. Irwin and D. M. Haddleton, *J. Am. Chem. Soc.*, 2006, **128**, 4823–4830.
- E. R. Gillies and J. M. J. Fréchet, *Drug Discovery Today*, 2005, **10**, 35–43.
- K. Matyjaszewski, *Prog. Polym. Sci.*, 2005, **30**, 858–875.
- M. Ouchi, T. Terashima and M. Sawamoto, *Chem. Rev.*, 2009, **109**, 4963–5050.
- K. Matyjaszewski and J. Xia, *Chem. Rev.*, 2001, **101**, 2921–2990.
- M. Kamigaito, T. Ando and M. Sawamoto, *Chem. Rev.*, 2001, **101**, 3689–3746.
- C. J. Hawker, A. W. Bosman and E. Harth, *Chem. Rev.*, 2001, **101**, 3661–3688.
- R. K. Iha, K. L. Wooley, A. M. Nyström, D. J. Burke, M. J. Kade and C. J. Hawker, *Chem. Rev.*, 2009, **109**, 5620–5686.
- G. Moad, E. Rizzardo and S. H. Thang, *Aust. J. Chem.*, 2006, **59**, 669–692.
- G. Moad, E. Rizzardo and S. H. Thang, *Aust. J. Chem.*, 2009, **62**, 1402–1472.
- H. C. Kolb, M. G. Finn and K. B. Sharpless, *Angew. Chem., Int. Ed.*, 2001, **40**, 2004–2021.
- D. Fournier, R. Hoogenboom and U. S. Schubert, *Chem. Soc. Rev.*, 2007, **36**, 1369–1380.
- W. H. Binder and R. Sachsenhofer, *Macromol. Rapid Commun.*, 2007, **28**, 15–54.
- Wolfgang H. Binder and Robert Sachsenhofer, *Macromol. Rapid Commun.*, 2008, **29**, 952–981.
- C. R. Becer, R. Hoogenboom and U. S. Schubert, *Angew. Chem., Int. Ed.*, 2009, **48**, 4900–4908.
- J.-F. Lutz, *Angew. Chem., Int. Ed.*, 2007, **46**, 1018–1025.
- A. B. Lowe, *Polym. Chem.*, 2010, **1**, 17–36.
- P. L. Golas and K. Matyjaszewski, *Chem. Soc. Rev.*, 2010, **39**, 1338–1354.
- C. Barner-Kowollik and A. J. Inglis, *Macromol. Chem. Phys.*, 2009, **210**, 987–992.
- D. D. Diaz, S. Punna, P. Holzer, A. K. McPherson, K. B. Sharpless, V. V. Fokin and M. G. Finn, *J. Polym. Sci., Part A: Polym. Chem.*, 2004, **42**, 4392–4403.
- P. Wu, A. K. Feldman, A. K. Nugent, C. J. Hawker, A. Scheel, B. Voit, J. Pyun, J. M. J. Fréchet, K. B. Sharpless and V. V. Fokin, *Angew. Chem., Int. Ed.*, 2004, **43**, 3928–3932.
- W. D. Sharpless, P. Wu, T. V. Hansen and J. G. Lindberg, *J. Chem. Educ.*, 2005, **82**, 1833–1836.
- J.-F. Lutz, *Angew. Chem., Int. Ed.*, 2008, **47**, 2182–2184.
- A. J. Inglis and C. Barner-Kowollik, *Macromol. Rapid Commun.*, 2010, **31**, 1247–1266.
- C. E. Hoyle, T. Y. Lee and T. Roper, *J. Polym. Sci., Part A: Polym. Chem.*, 2004, **42**, 5301–5338.
- C. E. Hoyle and C. N. Bowman, *Angew. Chem., Int. Ed.*, 2010, **49**, 1540–1573.
- A. B. Lowe, C. E. Hoyle and C. N. Bowman, *J. Mater. Chem.*, 2010, **20**, 4745–4750.
- R. Hoogenboom, *Angew. Chem., Int. Ed.*, 2010, **49**, 3415–3417.
- C. Ott, R. Hoogenboom and U. S. Schubert, *Chem. Commun.*, 2008, 3516–3518.
- C. R. Becer, K. Babiuch, D. Pilz, S. Hornig, T. Heinze, M. Gottschaldt and U. S. Schubert, *Macromolecules*, 2009, **42**, 2387–2394.
- I. Singh, Z. Zarafshani, J.-F. Lutz and F. Heaney, *Macromolecules*, 2009, **42**, 5411–5413.
- D. Bontempo, K. L. Heredia, B. A. Fish and H. D. Maynard, *J. Am. Chem. Soc.*, 2004, **126**, 15372–15373.
- K. L. Heredia, D. Bontempo, T. Ly, J. T. Byers, S. Halstenberg and H. D. Maynard, *J. Am. Chem. Soc.*, 2005, **127**, 16955–16960.
- J. Liu, V. Bulmus, C. Barner-Kowollik, M. H. Stenzel and T. P. Davis, *Macromol. Rapid Commun.*, 2007, **28**, 305–314.
- H. Durmaz, A. Dag, O. Altintas, T. Erdogan, G. Hizal and U. Tunca, *Macromolecules*, 2007, **40**, 191–198.
- S. Sinnwell, A. J. Inglis, T. P. Davis, M. H. Stenzel and C. Barner-Kowollik, *Chem. Commun.*, 2008, 2052–2054.
- A. J. Inglis, S. Sinnwell, M. H. Stenzel and C. Barner-Kowollik, *Angew. Chem. Int. Ed.*, 2009, **48**, 2411–2414.
- R. Huisgen, *Angew. Chem., Int. Ed. Engl.*, 1963, **2**, 565–598.
- P. Cintas, A. Barge, S. Tagliapietra, L. Boffa and G. Cravotto, *Nat. Protoc.*, 2010, **5**, 607–616.
- N. J. Agard, J. A. Prescher and C. R. Bertozzi, *J. Am. Chem. Soc.*, 2004, **126**, 15046–15047.
- S. S. v. Berkel, A. J. Dirks, S. A. Meeuwissen, D. L. L. Pingen, O. C. Boerman, P. Laverman, F. L. v. Delft, J. J. L. M. Cornelissen and F. P. J. T. Rutjes, *ChemBioChem*, 2008, **9**, 1805–1815.
- C. J. Duxbury, D. Cummins and A. Heise, *J. Polym. Sci., Part A: Polym. Chem.*, 2009, **47**, 3795–3802.
- E. Gungor, G. Hizal and U. Tunca, *J. Polym. Sci., Part A: Polym. Chem.*, 2008, **46**, 6703–6711.
- F. Himo, T. Lovell, R. Hilgraf, V. V. Rostovtsev, L. Noodleman, K. B. Sharpless and V. V. Fokin, *J. Am. Chem. Soc.*, 2005, **127**, 210–216.
- Z. P. Demko and K. B. Sharpless, *J. Org. Chem.*, 2001, **66**, 7945–7950.
- N. V. Tsarevsky, K. V. Bernaerts, B. Dufour, F. E. Du Prez and K. Matyjaszewski, *Macromolecules*, 2004, **37**, 9308–9313.
- S. Bräse, C. Gil, K. Knepper and V. Zimmermann, *Angew. Chem., Int. Ed.*, 2005, **44**, 5188–5240.
- B. Yu, J. W. Chan, C. E. Hoyle and A. B. Lowe, *J. Polym. Sci., Part A: Polym. Chem.*, 2009, **47**, 3544–3557.
- C. E. Hoyle, A. B. Lowe and C. N. Bowman, *Chem. Soc. Rev.*, 2010, **39**, 1355–1387.

- 52 K. L. Killops, L. M. Campos and C. J. Hawker, *J. Am. Chem. Soc.*, 2008, **130**, 5062–5064.
- 53 S. P. S. Koo, M. M. Stamenovic, R. A. Prasath, A. J. Inglis, F. E. Du Prez, C. Barner-Kowollik, W. V. Camp and T. Junkers, *J. Polym. Sci., Part A: Polym. Chem.*, 2010, **48**, 1699–1713.
- 54 H. Li, B. Yu, H. Matsushima, C. E. Hoyle and A. B. Lowe, *Macromolecules*, 2009, **42**, 6537–6542.
- 55 A. J. Inglis, M. H. Stenzel and C. Barner-Kowollik, *Macromol. Rapid Commun.*, 2009, **30**, 1792–1798.
- 56 A. Dag, H. Durmaz, V. Kirmizi, G. Hizal and U. Tunca, *Polym. Chem.*, 2010, **1**, 621–623.
- 57 A. A. Kavitha and N. K. Singha, *ACS Appl. Mater. Interfaces*, 2009, **1**, 1427–1436.
- 58 K. L. Heredia and H. D. Maynard, *Org. Biomol. Chem.*, 2007, **5**, 45–53.
- 59 N. V. Tsarevsky, S. A. Bencherif and K. Matyjaszewski, *Macromolecules*, 2007, **40**, 4439–4445.
- 60 S. Fleischmann, K. Hinrichs, U. Oertel, S. Reichelt, K.-J. Eichhorn and B. Voit, *Macromol. Rapid Commun.*, 2008, **29**, 1177–1185.
- 61 H. Kwart and K. King, *Chem. Rev.*, 1968, **68**, 415–447.
- 62 J. Sauer and R. Sustmann, *Angew. Chem., Int. Ed. Engl.*, 1980, **19**, 779–807.
- 63 T. Dispinar, R. Sanyal and A. Sanyal, *J. Polym. Sci., Part A: Polym. Chem.*, 2007, **45**, 4545–4551.
- 64 J. A. Syrett, G. Mantovani, W. R. S. Barton, D. Price and D. M. Haddleton, *Polym. Chem.*, 2010, **1**, 102–106.
- 65 A. J. Inglis, L. Nebhani, O. Altintas, F. G. Schmidt and C. Barner-Kowollik, *Macromolecules*, 2010, **43**, 5515–5520.
- 66 J. Geng, G. Mantovani, L. Tao, J. Nicolas, G. Chen, R. Wallis, D. A. Mitchell, B. R. G. Johnson, S. D. Evans and D. M. Haddleton, *J. Am. Chem. Soc.*, 2007, **129**, 15156–15163.
- 67 R. J. Thibault, K. Takizawa, P. Lowenheim, B. Helms, J. L. Mynar, J. M. J. Frechet and C. J. Hawker, *J. Am. Chem. Soc.*, 2006, **128**, 12084–12085.
- 68 V. L. G. Mantovani, L. Tao and D. M. Haddleton, *Chem. Commun.*, 2005, 2089–2091.
- 69 J. Geng, J. Lindqvist, G. Mantovani and D. M. Haddleton, *Angew. Chem., Int. Ed.*, 2008, **47**, 4180–4183.
- 70 L. Mespouille, M. Vachaudez, F. Suriano, P. Gerbaux, O. Coulembier, P. Degee, R. Flammang and P. Dubois, *Macromol. Rapid Commun.*, 2007, **28**, 2151–2158.
- 71 O. Altintas, G. Hizal and U. Tunca, *J. Polym. Sci., Part A: Polym. Chem.*, 2008, **46**, 1218–1228.
- 72 E. Gungor, H. Durmaz, G. Hizal and U. Tunca, *J. Polym. Sci., Part A: Polym. Chem.*, 2008, **46**, 4459–4468.
- 73 J. A. Opsteen and J. C. M. van Hest, *Chem. Commun.*, 2005, 57–59.
- 74 M. A. Bennett, *Chem. Rev.*, 1962, **62**, 611–652.
- 75 R. Nast, *Coord. Chem. Rev.*, 1982, **47**, 89–124.
- 76 A. Hasneen, H. S. Han and H.-J. Paik, *React. Funct. Polym.*, 2009, **69**, 681–687.
- 77 B. S. Sumerlin, N. V. Tsarevsky, G. Louche, R. Y. Lee and K. Matyjaszewski, *Macromolecules*, 2005, **38**, 7540–7545.
- 78 J. A. Opsteen and J. C. M. Van Hest, *J. Polym. Sci., Part A: Polym. Chem.*, 2007, **45**, 2913–2924.
- 79 Z. Zarafshani, O. Akdemir and J.-F. Lutz, *Macromol. Rapid Commun.*, 2008, **29**, 1161–1166.
- 80 C. N. Urbani, C. A. Bell, D. Lonsdale, M. R. Whittaker and M. J. Monteiro, *Macromolecules*, 2008, **41**, 76–86.
- 81 G. D. Fu, L. Q. Xu, F. Yao, K. Zhang, X. F. Wang, M. F. Zhu and S. Z. Nie, *ACS Appl. Mater. Interfaces*, 2009, **1**, 239–243.
- 82 G. J. Chen, L. Tao, G. Mantovani, V. Ladmiral, D. P. Burt, J. V. Macpherson and D. M. Haddleton, *Soft Matter*, 2007, **3**, 732–739.
- 83 L. Q. Xu, F. Yao, G. D. Fu and L. Shen, *Macromolecules*, 2009, **42**, 6385–6392.
- 84 N. V. Tsarevsky, B. S. Sumerlin and K. Matyjaszewski, *Macromolecules*, 2005, **38**, 3558–3561.
- 85 C. H. Li, Z. S. Ge, H. W. Liu and S. Y. Liu, *J. Polym. Sci., Part A: Polym. Chem.*, 2009, **47**, 4001–4013.
- 86 W. Lin, Q. Fu, Y. Zhang and J. Huang, *Macromolecules*, 2008, **41**, 4127–4135.
- 87 H. Durmaz, A. Dag, D. Gursoy, A. L. Demirel, G. Hizal and U. Tunca, *J. Polym. Sci., Part A: Polym. Chem.*, 2010, **48**, 1557–1564.
- 88 H. Durmaz, A. Dag, E. Erdogan, A. L. Demirel, G. Hizal and U. Tunca, *J. Polym. Sci., Part A: Polym. Chem.*, 2010, **48**, 99–108.
- 89 A. Dag, H. Durmaz, V. Kirmizi, G. Hizal and U. Tunca, *Polym. Chem.*, 2010, **1**, 621–623.
- 90 W. Van Camp, V. Germonpre, L. Mespouille, P. Dubois, E. J. Goethals and F. E. Du Prez, *React. Funct. Polym.*, 2007, **67**, 1168–1180.
- 91 J. Xu, J. Ye and S. Y. Liu, *Macromolecules*, 2007, **40**, 9103–9110.
- 92 L. Mespouille, M. Vachaudez, F. Suriano, P. Gerbaux, W. Van Camp, O. Coulembier, P. Degee, R. Flammang, F. Du Prez and P. Dubois, *React. Funct. Polym.*, 2008, **68**, 990–1003.
- 93 W. A. Braunecker and K. Matyjaszewski, *Prog. Polym. Sci.*, 2007, **32**, 93–146.
- 94 Y. F. Zhang, L. Hao, J. M. Hu, C. H. Li and S. Y. Liu, *Macromol. Rapid Commun.*, 2009, **30**, 941–947.
- 95 C. J. Huang and F. C. Chang, *Macromolecules*, 2009, **42**, 5155–5166.
- 96 J.-M. Schumers, J.-F. Gohy and C.-A. Fustin, *Polym. Chem.*, 2010, **1**, 161–163.
- 97 G. Y. Shi and C. Y. Pan, *Macromol. Rapid Commun.*, 2008, **29**, 1672–1678.
- 98 Y. Q. Dong, Y. Y. Tong, B. T. Dong, F. S. Du and Z. C. Li, *Macromolecules*, 2009, **42**, 2940–2948.
- 99 J. Zhu, X. L. Zhu, E. T. Kang and K. G. Neoh, *Polymer*, 2007, **48**, 6992–6999.
- 100 Y. F. Zhang, C. H. Li and S. Y. Liu, *J. Polym. Sci., Part A: Polym. Chem.*, 2009, **47**, 3066–3077.
- 101 G. H. Deng, D. Y. Ma and Z. Z. Xu, *Eur. Polym. J.*, 2007, **43**, 1179–1187.
- 102 G. W. Wang, X. L. Luo, C. Liu and J. L. Huang, *J. Polym. Sci., Part A: Polym. Chem.*, 2008, **46**, 2154–2166.
- 103 B. A. Laurent and S. M. Grayson, *J. Am. Chem. Soc.*, 2006, **128**, 4238–4239.
- 104 C. H. Li, Z. S. Ge, J. Fang and S. Y. Liu, *Macromolecules*, 2009, **42**, 2916–2924.
- 105 V. Ladmiral, T. M. Legge, Y. L. Zhao and S. Perrier, *Macromolecules*, 2008, **41**, 6728–6732.
- 106 W. Agut, D. Taton and S. Lecommandoux, *Macromolecules*, 2007, **40**, 5653–5661.
- 107 S. Pfeifer, Z. Zarafshani, N. Badi and J.-F. Lutz, *J. Am. Chem. Soc.*, 2009, **131**, 9195–9197.
- 108 Y. Li, J. W. Yang and B. C. Benicewicz, *J. Polym. Sci., Part A: Polym. Chem.*, 2007, **45**, 4300–4308.
- 109 M. Urien, H. Erothu, E. Cloutet, R. C. Hiorns, L. Vignau and H. Cramail, *Macromolecules*, 2008, **41**, 7033–7040.
- 110 C. H. Li, J. M. Hu, J. Yin and S. Y. Liu, *Macromolecules*, 2009, **42**, 5007–5016.
- 111 X. Jiang, M. C. Lok and W. E. Hennink, *Bioconjugate Chem.*, 2007, **18**, 2077–2084.
- 112 P. D. Topham, N. Sandon, E. S. Read, J. Madsen, A. J. Ryan and S. P. Armes, *Macromolecules*, 2008, **41**, 9542–9547.
- 113 A. Narumi, K. Fuchise, R. Kakuchi, A. Toda, T. Satoh, S. Kawaguchi, K. Sugiyama, A. Hirao and T. Kakuchi, *Macromol. Rapid Commun.*, 2008, **29**, 1126–1133.
- 114 Y. Zhang, H. K. He and C. Gao, *Macromolecules*, 2008, **41**, 9581–9594.
- 115 A. Dag, H. Durmaz, G. Hizal and U. Tunca, *J. Polym. Sci., Part A: Polym. Chem.*, 2008, **46**, 302–313.
- 116 M. Li, P. De, S. R. Gondi and B. S. Sumerlin, *J. Polym. Sci., Part A: Polym. Chem.*, 2008, **46**, 5093–5100.
- 117 A. Dag, H. Durmaz, E. Demir, G. Hizal and U. Tunca, *J. Polym. Sci., Part A: Polym. Chem.*, 2008, **46**, 6969–6977.
- 118 O. Altintas, G. Hizal and U. Tunca, *Des. Monomers Polym.*, 2009, **12**, 83–98.
- 119 H. Durmaz, F. Karatas, U. Tunca and G. Hizal, *J. Polym. Sci., Part A: Polym. Chem.*, 2006, **44**, 3947–3957.
- 120 B. Gacal, H. Durmaz, M. A. Tasdelen, G. Hizal, U. Tunca, Y. Yagci and A. L. Demirel, *Macromolecules*, 2006, **39**, 5330–5336.
- 121 H. Durmaz, A. Dag, A. Hizal, G. Hizal and U. Tunca, *J. Polym. Sci., Part A: Polym. Chem.*, 2008, **46**, 7091–7100.
- 122 G. Mantovani, F. Lecolley, L. Tao, D. M. Haddleton, J. Clerx, J. J. L. M. Cornelissen and K. Velonia, *J. Am. Chem. Soc.*, 2005, **127**, 2966–2973.
- 123 B. Le Droumaguet, G. Mantovani, D. M. Haddleton and K. Velonia, *J. Mater. Chem.*, 2007, **17**, 1916–1922.



- 124 M. Erdogan, G. Hizal, Ü. Tunca, D. Hayrabetyan and Ö. Pekcan, *Polymer*, 2002, **43**, 1925–1931.
- 125 A. Dag, H. Durmaz, U. Tunca and G. Hizal, *J. Polym. Sci., Part A: Polym. Chem.*, 2009, **47**, 178–187.
- 126 W. Zhang, W. Zhang, Z. Zhang, J. Zhu, Q. Pan and X. Zhu, *Polym. Bull.*, 2009, **63**, 467–483.
- 127 L. M. Campos, K. L. Killops, R. Sakai, J. M. J. Paulusse, D. Damiron, E. Drockenmüller, B. W. Messmore and C. J. Hawker, *Macromolecules*, 2008, **41**, 7063–7070.
- 128 V. Vázquez-Dorbatt, Z. P. Tolstyka, C.-W. Chang and H. D. Maynard, *Biomacromolecules*, 2009, **10**, 2207–2212.
- 129 A. Klaiherd, S. Ghosh and S. Thayumanavan, *Macromolecules*, 2007, **40**, 8518–8520.
- 130 N. V. Tsarevsky and K. Matyjaszewski, *Macromolecules*, 2002, **35**, 9009–9014.
- 131 H. D. Maynard, K. L. Heredia, R. C. Li, D. P. Parra and V. Vázquez-Dorbatt, *J. Mater. Chem.*, 2007, **17**, 4015–4017.
- 132 K. L. Heredia, Z. P. Tolstyka and H. D. Maynard, *Macromolecules*, 2007, **40**, 4772–4779.
- 133 D. Quemener, T. P. Davis, C. Barner-Kowollik and M. H. Stenzel, *Chem. Commun.*, 2006, 5051–5053.
- 134 R. K. O'Reilly, M. J. Joralemon, C. J. Hawker and K. L. Wooley, *J. Polym. Sci., Part A: Polym. Chem.*, 2006, **44**, 5203–5217.
- 135 S. R. S. Ting, A. M. Granville, D. Quemener, T. P. Davis, M. H. Stenzel and C. Barner-Kowollik, *Aust. J. Chem.*, 2007, **60**, 405–409.
- 136 G. Y. Shi, X. Z. Tang and C. Y. Pan, *J. Polym. Sci., Part A: Polym. Chem.*, 2008, **46**, 2390–2401.
- 137 R. Ranjan and W. J. Brittain, *Macromol. Rapid Commun.*, 2008, **29**, 1104–1110.
- 138 R. Ranjan and W. J. Brittain, *Macromol. Rapid Commun.*, 2007, **28**, 2084–2089.
- 139 A. J. D. Magenau, N. Martinez-Castro, D. A. Savin and R. F. Storey, *Macromolecules*, 2009, **42**, 8044–8051.
- 140 T. Zhang, Y. P. Wu, X. M. Pan, Z. H. Zheng, X. B. Ding and Y. X. Peng, *Eur. Polym. J.*, 2009, **45**, 1625–1633.
- 141 D. Konkolewicz, A. Gray-Weale and S. Perrier, *J. Am. Chem. Soc.*, 2009, **131**, 18075–18077.
- 142 N. Akeroyd, R. Pfukwa and B. Klumperman, *Macromolecules*, 2009, **42**, 3014–3018.
- 143 A. S. Goldmann, D. Quemener, P. E. Millard, T. P. Davis, M. H. Stenzel, C. Barner-Kowollik and A. H. E. Mueller, *Polymer*, 2008, **49**, 2274–2281.
- 144 L. Barner, T. P. Davis, M. H. Stenzel and C. Barner-Kowollik, *Macromol. Rapid Commun.*, 2007, **28**, 539–559.
- 145 R. Ranjan and W. J. Brittain, *Macromolecules*, 2007, **40**, 6217–6223.
- 146 T. Zhang, Z. H. Zheng, X. B. Ding and Y. X. Peng, *Macromol. Rapid Commun.*, 2008, **29**, 1716–1720.
- 147 S. Puttick, D. J. Irvine, P. Licence and K. J. Thurecht, *J. Mater. Chem.*, 2009, **19**, 2679–2682.
- 148 S. R. Gondi, A. P. Vogt and B. S. Sumerlin, *Macromolecules*, 2007, **40**, 474–481.
- 149 P. De, S. R. Gondi and B. S. Sumerlin, *Biomacromolecules*, 2008, **9**, 1064–1070.
- 150 M. Li, P. De, S. R. Gondi and B. S. Sumerlin, *Macromol. Rapid Commun.*, 2008, **29**, 1172–1176.
- 151 A. Vora, K. Singh and D. C. Webster, *Polymer*, 2009, **50**, 2768–2774.
- 152 A. P. Vogt, S. R. Gondi and B. S. Sumerlin, *Aust. J. Chem.*, 2007, **60**, 396–399.
- 153 D. Quemener, M. Le Hellaye, C. Bissett, T. P. Davis, C. Barner-Kowollik and M. H. Stenzel, *J. Polym. Sci., Part A: Polym. Chem.*, 2008, **46**, 155–173.
- 154 J. Bernard, M. Save, B. Arathoon and B. Charleux, *J. Polym. Sci., Part A: Polym. Chem.*, 2008, **46**, 2845–2857.
- 155 F. Chen, Z. P. Cheng, J. Zhu, W. Zhang and X. L. Zhu, *Eur. Polym. J.*, 2008, **44**, 1789–1795.
- 156 A. P. Vogt and B. S. Sumerlin, *Macromolecules*, 2008, **41**, 7368–7373.
- 157 Z. S. An, W. Tang, M. H. Wu, Z. Jiao and G. D. Stucky, *Chem. Commun.*, 2008, 6501–6503.
- 158 X. P. Qiu, F. Tanaka and F. M. Winnik, *Macromolecules*, 2007, **40**, 7069–7071.
- 159 C. Boyer, J. Liu, V. Bulmus, T. P. Davis, C. Barner-Kowollik and M. H. Stenzel, *Macromolecules*, 2008, **41**, 5641–5650.
- 160 J. Liu, V. Bulmus, D. L. Herlambang, C. Barner-Kowollik, M. H. Stenzel and T. P. Davis, *Angew. Chem., Int. Ed.*, 2007, **46**, 3099–3103.
- 161 K. L. Heredia, T. H. Nguyen, C.-W. Chang, V. Bulmus, T. P. Davis and H. D. Maynard, *Chem. Commun.*, 2008, 3245–3247.
- 162 C. Boyer, V. Bulmus, J. Liu, T. P. Davis, M. H. Stenzel and C. Barner-Kowollik, *J. Am. Chem. Soc.*, 2007, **129**, 7145–7154.
- 163 C. Boyer, J. Liu, L. Wong, M. Tippett, V. Bulmus and T. P. Davis, *J. Polym. Sci., Part A: Polym. Chem.*, 2008, **46**, 7207–7224.
- 164 J. Liu, H. Liu, C. Boyer, V. Bulmus and T. P. Davis, *J. Polym. Sci., Part A: Polym. Chem.*, 2009, **47**, 899–912.
- 165 S. Sinnwell, A. J. Inglis, M. H. Stenzel and C. Barner-Kowollik, *Macromol. Rapid Commun.*, 2008, **29**, 1090–1096.
- 166 L. Nebhani, P. Gerstel, P. Atanasova, M. Bruns and C. Barner-Kowollik, *J. Polym. Sci., Part A: Polym. Chem.*, 2009, **47**, 7090–7095.
- 167 L. Nebhani, S. Sinnwell, C. Y. Lin, M. L. Coote, M. H. Stenzel and C. Barner-Kowollik, *J. Polym. Sci., Part A: Polym. Chem.*, 2009, **47**, 6053–6071.
- 168 S. Sinnwell, M. Lammens, M. H. Stenzel, F. E. Du Prez and C. Barner-Kowollik, *J. Polym. Sci., Part A: Polym. Chem.*, 2009, **47**, 2207–2213.
- 169 A. J. Inglis, S. Sinnwell, T. P. Davis, C. Barner-Kowollik and M. H. Stenzel, *Macromolecules*, 2008, **41**, 4120–4126.
- 170 S. Sinnwell, C. V. Synatschke, T. Junkers, M. H. Stenzel and C. Barner-Kowollik, *Macromolecules*, 2008, **41**, 7904–7912.
- 171 P. De, M. Li, S. R. Gondi and B. S. Sumerlin, *J. Am. Chem. Soc.*, 2008, **130**, 11288–11289.
- 172 S. Marque, H. Fischer, E. Baier and A. Studer, *J. Org. Chem.*, 2001, **66**, 1146–1156.
- 173 M. Rodlert, E. Harth, I. Rees and C. J. Hawker, *J. Polym. Sci., Part A: Polym. Chem.*, 2000, **38**, 4749–4763.
- 174 Nicole L. Hill and Rebecca Braslau, *J. Polym. Sci., Part A: Polym. Chem.*, 2007, **45**, 2341–2349.
- 175 J. Dao, D. Benoit and C. J. Hawker, *J. Polym. Sci., Part A: Polym. Chem.*, 1998, **36**, 2161–2167.
- 176 S. Fleischmann, H. Komber, D. Appelhans and B. I. Voit, *Macromol. Chem. Phys.*, 2007, **208**, 1050–1060.
- 177 G. F. D'Alelio and R. C. Evers, *J. Polym. Sci., Part A-1*, 1967, **5**, 999–1014.
- 178 L. B. Sessions, L. A. Miinea, K. D. Ericson, D. S. Glueck and R. B. Grubbs, *Macromolecules*, 2005, **38**, 2116–2121.
- 179 O. Altintas, G. Hizal and U. Tunca, *J. Polym. Sci., Part A: Polym. Chem.*, 2006, **44**, 5699–5707.
- 180 A. Gozgen, A. Dag, H. Durmaz, O. Sirkecioglu, G. Hizal and U. Tunca, *J. Polym. Sci., Part A: Polym. Chem.*, 2009, **47**, 497–504.
- 181 E. Gungor, G. Cote, T. Erdogan, H. Durmaz, A. L. Demirel, G. Hizal and U. Tunca, *J. Polym. Sci., Part A: Polym. Chem.*, 2007, **45**, 1055–1065.
- 182 O. Altintas, A. L. Demirel, G. Hizal and U. Tunca, *J. Polym. Sci., Part A: Polym. Chem.*, 2008, **46**, 5916–5928.
- 183 O. Altintas, B. Yankul, G. Hizal and U. Tunca, *J. Polym. Sci., Part A: Polym. Chem.*, 2007, **45**, 3588–3598.
- 184 E. Gungor, G. Hizal and U. Tunca, *J. Polym. Sci., Part A: Polym. Chem.*, 2009, **47**, 3409–3418.
- 185 E. H. H. Wong, M. H. Stenzel, T. Junkers and C. Barner-Kowollik, *Macromolecules*, 2010, **43**, 3785–3793.
- 186 T. Junkers, E. H. H. Wong, M. H. Stenzel and C. Barner-Kowollik, *Macromolecules*, 2009, **42**, 5027–5035.
- 187 E. H. H. Wong, T. Junkers and C. Barner-Kowollik, *J. Polym. Sci., Part A: Polym. Chem.*, 2008, **46**, 7273–7279.
- 188 W. H. Binder, D. Gloger, H. Weinstabl, G. Allmaier and E. Pittenauer, *Macromolecules*, 2007, **40**, 3097–3107.
- 189 U. Tunca, Z. Ozyurek, T. Erdogan and G. Hizal, *J. Polym. Sci., Part A: Polym. Chem.*, 2004, **42**, 4228–4236.
- 190 H. Durmaz, F. Karatas, U. Tunca and G. Hizal, *J. Polym. Sci., Part A: Polym. Chem.*, 2006, **44**, 499–509.
- 191 A. Krieg, C. R. Becer, R. Hoogenboom and U. S. Schubert, *Macromol. Symp.*, 2009, **275–276**, 73–81.
- 192 J. T. Wiltshire and G. G. Qiao, *J. Polym. Sci., Part A: Polym. Chem.*, 2009, **47**, 1485–1498.
- 193 M. Malkoch, R. J. Thibault, E. Drockenmüller, M. Messerschmidt, B. Voit, T. P. Russell and C. J. Hawker, *J. Am. Chem. Soc.*, 2005, **127**, 14942–14949.

- 194 R. K. O'Reilly, M. J. Joralemon, C. J. Hawker and K. L. Wooley, *Chem.-Eur. J.*, 2006, **12**, 6776–6786.
- 195 S. Fleischmann, H. Komber and B. Voit, *Macromolecules*, 2008, **41**, 5255–5264.
- 196 T. Ishizone, G. Uehara, A. Hirao, S. Nakahama and K. Tsuda, *Macromolecules*, 1998, **31**, 3764–3774.
- 197 F. Bertini, G. Audisio, J. Kiji and M. Fujita, *J. Anal. Appl. Pyrolysis*, 2003, **68–69**, 61–81.
- 198 M. M. Martin and E. B. Sanders, *J. Am. Chem. Soc.*, 1967, **89**, 3777–3782.
- 199 R.-V. Ostaci, D. Damiron, Y. Grohens, L. Léger and E. Drockenmüller, *Langmuir*, 2010, **26**, 1304–1310.
- 200 Y. Zhang, H. He, C. Gao and J. Y. Wu, *Langmuir*, 2009, **25**, 5814–5824.
- 201 J. Stadermann, S. Fleischmann, M. Messerschmidt, H. Komber and B. Voit, *Macromol. Symp.*, 2009, **275–276**, 35–42.
- 202 C. Ladaviere, N. Dorr and J. P. Claverie, *Macromolecules*, 2001, **34**, 5370–5372.
- 203 R. K. O'Reilly, M. J. Joralemon, C. J. Hawker and K. L. Wooley, *New J. Chem.*, 2007, **31**, 718–724.
- 204 T. Junkers and C. Barner-Kowollik, *J. Polym. Sci., Part A: Polym. Chem.*, 2008, **46**, 7585–7605.
- 205 G. K. Such, J. F. Quinn, A. Quinn, E. Tjijto and F. Caruso, *J. Am. Chem. Soc.*, 2006, **128**, 9318–9319.
- 206 G. K. Such, E. Tjijto, A. Postma, A. P. R. Johnston and F. Caruso, *Nano Lett.*, 2007, **7**, 1706–1710.
- 207 A. R. de Luzuriaga, N. Ormategui, H. J. Grande, I. Odriozola, J. A. Pornposo and I. Loinaz, *Macromol. Rapid Commun.*, 2008, **29**, 1156–1160.
- 208 X. W. Zhang, X. M. Lian, L. Liu, J. Zhang and H. Y. Zhao, *Macromolecules*, 2008, **41**, 7863–7869.
- 209 D. Damiron, M. Desorme, R. V. Ostaci, S. Al Akhrass, T. Hamaide and E. Drockenmüller, *J. Polym. Sci., Part A: Polym. Chem.*, 2009, **47**, 3803–3813.
- 210 D. Gromadzki, J. Lokaj, P. Cernoch, O. Diat, F. Nallet and P. Štěpánek, *Eur. Polym. J.*, 2008, **44**, 189–199.
- 211 M. Aldhoun, A. Massi and A. Dondoni, *J. Org. Chem.*, 2008, **73**, 9565–9575.
- 212 V. Aureggi and G. Sedelmeier, *Angew. Chem., Int. Ed.*, 2007, **46**, 8440–8444.
- 213 J. Aimi, L. A. McCullough and K. Matyjaszewski, *Macromolecules*, 2008, **41**, 9522–9524.
- 214 D. G. Li, J. Zhu, Z. P. Cheng, W. Zhang and X. L. Zhu, *React. Funct. Polym.*, 2009, **69**, 240–245.
- 215 Y. M. Zhou, K. Q. Jiang, Y. Q. Chen and S. Y. Liu, *J. Polym. Sci., Part A: Polym. Chem.*, 2008, **46**, 6518–6531.
- 216 S. Pfeifer and J.-F. Lutz, *Chem.-Eur. J.*, 2008, **14**, 10949–10957.
- 217 G. Li, H. T. Zheng and R. K. Bai, *Macromol. Rapid Commun.*, 2009, **30**, 442–447.
- 218 X. Z. Jiang, J. Y. Zhang, Y. M. Zhou, J. Xu and S. Y. Liu, *J. Polym. Sci., Part A: Polym. Chem.*, 2008, **46**, 860–871.
- 219 Y. Li and B. C. Benicewicz, *Macromolecules*, 2008, **41**, 7986–7992.
- 220 J. Y. Zhang, Y. M. Zhou, Z. Y. Zhu, Z. S. Ge and S. Y. Liu, *Macromolecules*, 2008, **41**, 1444–1454.
- 221 L. A. Canalle, S. S. v. Berkel, L. T. d. Haan and J. C. M. v. Hest, *Adv. Funct. Mater.*, 2009, **19**, 3464–3470.
- 222 L. González, A. Rodríguez, J. L. d. Benito and A. Marcos-Fernández, *J. Appl. Polym. Sci.*, 1997, **63**, 1353–1359.
- 223 J. E. Leffler and H. H. Gibson, *J. Am. Chem. Soc.*, 1968, **90**, 4117–4121.
- 224 C. J. Ruud, J. Jia and G. L. Baker, *Macromolecules*, 2000, **33**, 8184–8191.
- 225 C. K. Govindan, *Org. Process Res. Dev.*, 2002, **6**, 74–77.
- 226 G. T. Anderson, J. R. Henry and S. M. Weinreb, *J. Org. Chem.*, 1991, **56**, 6946–6948.
- 227 W. Broeckx, N. Overbergh, C. Samyn, G. Smets and G. L'abbé, *Tetrahedron*, 1971, **27**, 3527–3534.
- 228 A. Bousquet, C. Barner-Kowollik and M. H. Stenzel, *J. Polym. Sci., Part A: Polym. Chem.*, 2010, **48**, 1773–1781.
- 229 A. A. Kavitha and N. K. Singha, *Macromol. Chem. Phys.*, 2007, **208**, 2569–2577.
- 230 A. A. Kavitha and N. K. Singha, *J. Polym. Sci., Part A: Polym. Chem.*, 2007, **45**, 4441–4449.
- 231 A. A. Kavitha, A. Choudhury and N. K. Singha, *Macromol. Symp.*, 2006, **240**, 232–237.
- 232 A. A. Kavitha and N. K. Singha, *Macromolecules*, 2010, **43**, 3193–3205.
- 233 M. J. Kade, D. J. Burke and C. J. Hawker, *J. Polym. Sci., Part A: Polym. Chem.*, 2010, **48**, 743–750.
- 234 Z. Jia, J. Liu, T. P. Davis and V. Bulmus, *Polymer*, 2009, **50**, 5928–5932.
- 235 Z. Jia, L. Wong, T. P. Davis and V. Bulmus, *Biomacromolecules*, 2008, **9**, 3106–3113.
- 236 L. Wong, C. Boyer, Z. Jia, H. M. Zareie, T. P. Davis and V. Bulmus, *Biomacromolecules*, 2008, **9**, 1934–1944.
- 237 J. Zhu, Z. Di, X. Zhu and G. Chen, *J. Polym. Sci., Part A: Polym. Chem.*, 2004, **42**, 2558–2565.
- 238 K. Dayananda and R. Dhamodharan, *J. Polym. Sci., Part A: Polym. Chem.*, 2004, **42**, 902–915.
- 239 R. Krishnan and K. S. V. Srinivasan, *Macromolecules*, 2003, **36**, 1769–1771.
- 240 J. L. De La Fuente, P. F. Canamero and M. Fernandez-Garcia, *J. Polym. Sci., Part A: Polym. Chem.*, 2006, **44**, 1807–1816.
- 241 P. F. Cañamero, J. L. de la Fuente, E. L. Madruga and M. Fernández-García, *Macromol. Chem. Phys.*, 2004, **205**, 2221–2228.
- 242 R. Krishnan and K. S. V. Srinivasan, *Macromolecules*, 2004, **37**, 3614–3622.
- 243 G. Li, X. Zhu, J. Zhu, Z. Cheng and W. Zhang, *Polymer*, 2005, **46**, 12716–12721.
- 244 Y.-Y. Yuan, Q. Du, Y.-C. Wang and J. Wang, *Macromolecules*, 2010, **43**, 1739–1746.
- 245 K. Godula, D. Rabuka, K. T. Nam and C. R. Bertozzi, *Angew. Chem., Int. Ed.*, 2009, **48**, 4973–4976.
- 246 R. K. O'Reilly, C. J. Hawker and K. L. Wooley, *Polym. Prepr. (Am. Chem. Soc., Div. Polym. Chem.)*, 2004, **45**, 780.
- 247 G. O'Bryan, N. Ningnuek and R. Braslau, *Polymer*, 2008, **49**, 5241–5248.
- 248 K. Matyjaszewski, Y. Nakagawa and S. G. Gaynor, *Macromol. Rapid Commun.*, 1997, **18**, 1057–1066.
- 249 V. Coessens, Y. Nakagawa and K. Matyjaszewski, *Polym. Bull.*, 1998, **40**, 135–142.
- 250 V. Coessens and K. Matyjaszewski, *J. Macromol. Sci., Part A: Pure Appl. Chem.*, 1999, **36**, 667–679.
- 251 S. O. Kyeremateng, E. Amado, A. Blume and J. Kressler, *Macromol. Rapid Commun.*, 2008, **29**, 1140–1146.
- 252 A. Sinaga, P. Ravi, T. A. Hatton and K. C. Tam, *J. Polym. Sci., Part A: Polym. Chem.*, 2007, **45**, 2646–2656.
- 253 J.-F. Lutz, H. G. Borner and K. Weichenhan, *Macromol. Rapid Commun.*, 2005, **26**, 514–518.
- 254 J.-F. Lutz, H. G. Borner and K. Weichenhan, *Macromolecules*, 2006, **39**, 6376–6383.
- 255 Q. C. Liu and Y. M. Chen, *J. Polym. Sci., Part A: Polym. Chem.*, 2006, **44**, 6103–6113.
- 256 A. P. Vogt and B. S. Sumerlin, *Macromolecules*, 2006, **39**, 5286–5292.
- 257 H. F. Gao and K. Matyjaszewski, *Macromolecules*, 2006, **39**, 4960–4965.
- 258 O. Altintas, B. Yankul, G. Hizal and U. Tunca, *J. Polym. Sci., Part A: Polym. Chem.*, 2006, **44**, 6458–6465.
- 259 B. S. Lee, J. K. Lee, W. J. Kim, Y. H. Jung, S. J. Sim, J. Lee and I. S. Choi, *Biomacromolecules*, 2007, **8**, 744–749.
- 260 M. Degirmenci and N. Genli, *Macromol. Chem. Phys.*, 2009, **210**, 1617–1623.
- 261 Q. Liu, P. Zhao and Y. Chen, *J. Polym. Sci., Part A: Polym. Chem.*, 2007, **45**, 3330–3341.
- 262 P. L. Golas, N. V. Tsarevsky and K. Matyjaszewski, *Macromol. Rapid Commun.*, 2008, **29**, 1167–1171.
- 263 J. Kulis, C. A. Bell, A. S. Micallef, Z. Jia and M. J. Monteiro, *Macromolecules*, 2009, **42**, 8218–8227.
- 264 A. Gheorghe, A. Matsuno and O. Reiser, *Adv. Synth. Catal.*, 2006, **348**, 1016–1020.
- 265 E. H. H. Wong, C. Boyer, M. H. Stenzel, C. Barner-Kowollik and T. Junkers, *Chem. Commun.*, 2010, **46**, 1959–1961.
- 266 A. J. Inglis, T. Paulöhr and C. Barner-Kowollik, *Macromolecules*, 2010, **43**, 33–36.
- 267 C. Boyer, V. Bulmus and T. P. Davis, *Macromol. Rapid Commun.*, 2009, **30**, 493–497.
- 268 J. W. Chan, B. Yu, C. E. Hoyle and A. B. Lowe, *Polymer*, 2009, **50**, 3158–3168.

- 269 C. W. Chang, E. Bays, L. Tao, S. N. S. Alconcel and H. D. Maynard, *Chem. Commun.*, 2009, 3580–3582.
- 270 C. Boyer, A. Granville, T. P. Davis and V. Bulmus, *J. Polym. Sci., Part A: Polym. Chem.*, 2009, **47**, 3773–3794.
- 271 J. W. Chan, B. Yu, C. E. Hoyle and A. B. Lowe, *Chem. Commun.*, 2008, 4959–4961.
- 272 V. Lima, X. Jiang, J. Brokken-Zijp, P. J. Schoenmakers, B. Klumperman and R. V. D. Linde, *J. Polym. Sci., Part A: Polym. Chem.*, 2005, **43**, 959–973.
- 273 X.-P. Qiu and F. M. Winnik, *Macromol. Rapid Commun.*, 2006, **27**, 1648–1653.
- 274 M. Nakayama and T. Okano, *Biomacromolecules*, 2005, **6**, 2320–2327.
- 275 F. Segui, X.-P. Qiu and F. M. Winnik, *J. Polym. Sci., Part A: Polym. Chem.*, 2008, **46**, 314–326.
- 276 C. W. Scales, A. J. Convertine and C. L. McCormick, *Biomacromolecules*, 2006, **7**, 1389–1392.
- 277 H. Kakwere and S. Perrier, *J. Am. Chem. Soc.*, 2009, **131**, 1889–1895.
- 278 A. S. Goldmann, A. Walther, L. Nebhani, R. Joso, D. Ernst, K. Loos, C. Barner-Kowollik, L. Barner and A. H. E. Mueller, *Macromolecules*, 2009, **42**, 3707–3714.
- 279 G. L. Ellman, *Arch. Biochem. Biophys.*, 1958, **74**, 443–450.
- 280 P. J. Roth, D. Kessler, R. Zentel and P. Theato, *J. Polym. Sci., Part A: Polym. Chem.*, 2009, **47**, 3118–3130.
- 281 L. P. Yang, H. X. Zhou, G. Y. Shi, Y. Wang and C. Y. Pan, *J. Polym. Sci., Part A: Polym. Chem.*, 2008, **46**, 6641–6653.
- 282 D. H. Solomon, E. Rizzardo and P. Cacioli, US Patent, 4581 429, 1985.
- 283 E. Harth, C. J. Hawker, W. Fan and R. M. Waymouth, *Macromolecules*, 2001, **34**, 3856–3862.
- 284 G. O'Bryan and R. Braslau, *Macromolecules*, 2006, **39**, 9010–9017.
- 285 Y. Guillaeneuf, P.-E. Dufils, L. Autissier, M. Rollet, D. Gigmes and D. Bertin, *Macromolecules*, 2010, **43**, 91–100.
- 286 C. Ollivier and P. Renaud, *J. Am. Chem. Soc.*, 2001, **123**, 4717–4727.
- 287 P. Panchaud and P. Renaud, *J. Org. Chem.*, 2004, **69**, 3205–3207.
- 288 X. Z. Jiang, G. Y. Zhang, R. Narain and S. Y. Liu, *Langmuir*, 2009, **25**, 2046–2054.
- 289 H. Gao and K. Matyjaszewski, *J. Am. Chem. Soc.*, 2007, **129**, 6633–6639.
- 290 D. Cummins, C. J. Duxbury, P. Quaedflieg, P. Magusin, C. E. Koning and A. Heise, *Soft Matter*, 2009, **5**, 804–811.
- 291 B. Sieczkowska, M. Millaruelo, M. Messerschmidt and B. Voit, *Macromolecules*, 2007, **40**, 2361–2370.
- 292 R. K. O'Reilly, M. J. Joralemon, K. L. Wooley and C. J. Hawker, *Chem. Mater.*, 2005, **17**, 5976–5988.
- 293 G. Temel, B. Aydogan, N. Arsu and Y. Yagci, *Macromolecules*, 2009, **42**, 6098–6106.
- 294 W.-H. Ting, S. A. Dai, Y.-F. Shih, I.-K. Yang, W.-C. Su and R.-J. Jeng, *Polymer*, 2008, **49**, 1497–1505.
- 295 M. J. Joralemon, R. K. O'Reilly, C. J. Hawker and K. L. Wooley, *J. Am. Chem. Soc.*, 2005, **127**, 16892–16899.
- 296 P. L. Golas, N. V. Tsarevsky, B. S. Sumerlin and K. Matyjaszewski, *Macromolecules*, 2006, **39**, 6451–6457.
- 297 M.-A. Berthet, Z. Zarafshani, S. Pfeifer and J.-F. Lutz, *Macromolecules*, 2010, **43**, 44–50.

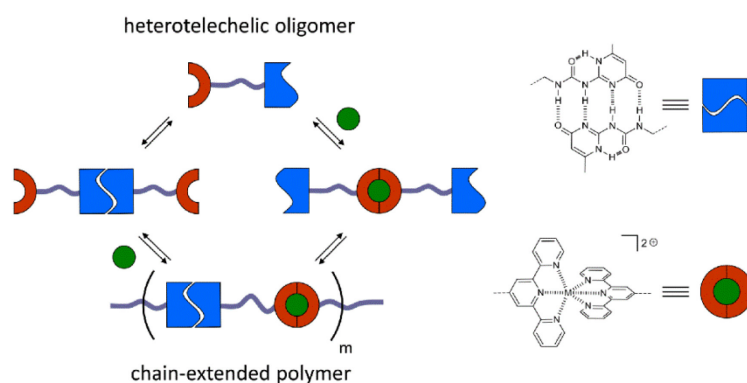


## Publication P2:

### *Orthogonal self-assembly of stimuli-responsive supramolecular polymers using one-step prepared heterotelechelic building blocks*

U. Mansfeld, A. Winter, M. D. Hager, R. Hoogenboom, W. Günther, U. S. Schubert

*Polym. Chem.* **2013**, *4*, 113-123



Reproduced by permission of The Royal Society of Chemistry

<http://dx.doi.org/10.1039/C2PY20559A>





## Orthogonal self-assembly of stimuli-responsive supramolecular polymers using one-step prepared heterotelechelic building blockst

Cite this: *Polym. Chem.*, 2013, 4, 113

Ulrich Mansfeld,<sup>abc</sup> Andreas Winter,<sup>abc</sup> Martin D. Hager,<sup>abc</sup> Richard Hoogenboom,<sup>d</sup> Wolfgang Günther<sup>a</sup> and Ulrich S. Schubert<sup>\*abc</sup>

The one-step preparation of heterodifunctional telechelic polymers containing 2,2':6',2''-terpyridine (tpy) and 2-ureido-4[1*H*]-pyrimidinone (UPy) end-groups, as orthogonal supramolecular moieties, is reported. The utilization of an appropriately functionalized alkoxyamine, as an initiator for the nitroxide-mediated radical polymerization (NMP), directly constitutes the end-groups of the resultant polymers. The targeted alkoxyamines are based on the nitroxide structure of 2,2,5-trimethyl-3-(1-phenylethoxy)-4-phenyl-3-azahexane (TIPNO) and were obtained *via* stepwise functionalization of a heterodifunctional alkoxyamine skeleton. Controlled radical polymerization of styrenics using the alkoxyamine tpy-TIPNO-UPy, as an initiator, is demonstrated to generate well-defined telechelic polymers in one step. These telechelics represent promising building blocks for supramolecular architectures *via* self-assembly processes, yielding linear chain-extended polymers of high molar masses. Due to the orthogonality of the metal ion complexation and hydrogen bonding, the system can be addressed selectively by external stimuli. Besides for various applications, *e.g.* as self-healing materials, the strategy is highly attractive for tailoring the material's properties of supramolecular polymers, since the nature and the length of the polymer chain between the terminal supramolecular motifs can be controlled in a facile way.

Received 24th July 2012  
Accepted 18th August 2012

DOI: 10.1039/c2py20559a

[www.rsc.org/polymers](http://www.rsc.org/polymers)

### Introduction

The preparation of well-defined adaptive macromolecular architectures is one of the main challenges in today's polymer science. Nowadays, the fast progress in living and controlled polymerization techniques provides straightforward access to advanced macromolecules, for instance, (multi)block copolymers, star-shaped (co)polymers as well as graft and comb-like (co)polymers.<sup>1–3</sup> Although excellent control over the molecular structure is generally assured, these systems suffer from poor control over the structures of higher order and adaptivity when compared to natural macromolecules. In particular, the spontaneous assembly/disassembly of natural systems driven by the surrounding environmental conditions has to be named in this context. Nature utilizes a combination of tailor-made

macromolecular structures and non-covalent interactions to create responsive systems that adapt to changes in the environment. Thereby, solvophobic and ionic interactions as well as hydrogen bonding and metal-to-ligand coordination serve as non-covalent, *i.e.* supramolecular, interactions. Inspired by these natural systems, polymer chemists have investigated the usage of non-covalent interactions for the design of supramolecular polymers featuring responsive behavior, *i.e.* their properties can be changed by varying the environmental conditions.<sup>4–14</sup> If reversibility of the change in properties is guaranteed, the material can be switched between a self-assembled and a disassembled state by simply applying an external stimuli: *e.g.* a change in temperature, pH value, redox potential and concentration. Any change between the two different states will also be accomplished by changes in the polymer's macroscopic properties, thus enabling the application in property changing, *e.g.* for self-healing materials.<sup>15</sup> From the range of non-covalent interactions, in particular metal-to-ligand coordination and hydrogen bonding can offer both complementarity and directionality – essential features for the formation of complex supramolecular polymers, including block and graft copolymers.<sup>8,16–18</sup>

The combination of different non-covalent interactions in one supramacromolecular ensemble provides the opportunity to selectively address one of them *via* an external stimulus, if they are orthogonal to each other, thus expanding the range of

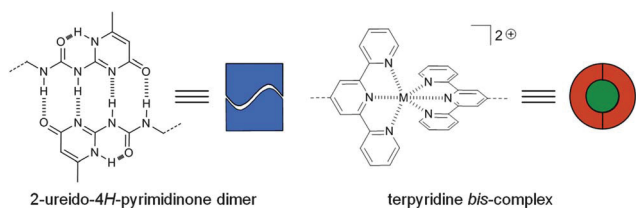
<sup>a</sup>Laboratory of Organic and Macromolecular Chemistry (IOMC), Friedrich-Schiller-University Jena, Humboldtstr. 10, 07743 Jena, Germany. E-mail: [ulrich.schubert@uni-jena.de](mailto:ulrich.schubert@uni-jena.de); Web: [www.schubert-group.de](http://www.schubert-group.de); Fax: +49 (0)3641 948202; Tel: +49 (0)3641 948200

<sup>b</sup>Jena Center for Soft Matter (JCSM), Friedrich-Schiller-University Jena, Philosophenweg 7, 07743 Jena, Germany

<sup>c</sup>Dutch Polymer Institute (DPI), P.O. Box 902, 5600 AX Eindhoven, The Netherlands

<sup>d</sup>Supramolecular Chemistry Group, Department of Organic Chemistry, Ghent University, Krijgslaan 281 S4, 9000 Ghent, Belgium

† Electronic supplementary information (ESI) available. See DOI: 10.1039/c2py20559a



**Scheme 1** Schematic representation of the chemical structure of the 2-ureido-4H-pyrimidinone quadruple hydrogen bonding array (left) and the terpyridine metal ion complexes (right).

responsiveness of the system. The concept of orthogonal supramolecular interactions in the field of polymer science has been evaluated in several review articles.<sup>18–23</sup> As a key example, Weck and co-workers were able to synthesize supramolecular ABC triblock copolymers utilizing orthogonal binding units, namely a hydrogen bonding unit (Hamilton wedge) and pyridine, which can coordinate to a Pd pincer.<sup>24</sup> Recently, the authors showed the versatility of the combination of metal–ligand interactions with hydrogen bonding units: a multi-responsive reversible polymer network was synthesized using the same binding units.<sup>25</sup>

Moreover, we have shown that the incorporation of a terpyridine (tpy)<sup>26–28</sup> and a 2-ureido-4H-pyrimidinone (UPy) moiety, as a metal-binding site and quadruple hydrogen bonding entity (Scheme 1), into polymers gives rise to the formation of chain-extended supramolecular polymers in the presence of divalent transition metal ions.<sup>29–32</sup> In these materials, the polymeric building blocks were held together by *bis*-terpyridine complexes and UPy dimers in an alternating fashion. The initial synthetic strategies towards the heterotelechelic building blocks were based on a monofunctionalized initiator<sup>29,30</sup> with a postmodification to attach the second moiety. More recently, we reported a heterodifunctional alkoxyamine initiator<sup>29,30</sup> for the nitroxide-mediated radical polymerization (NMP) bearing already both end-groups of the resultant polymer. This latter approach provides a significantly higher versatility since the chain length and composition between the supramolecular binding sites can be varied without compromising the end-group fidelity and simple purification by precipitation, which is less straightforward for the post-modification procedure.

In a continuation of this previous work,<sup>30</sup> the ability of the heterodifunctional initiator tpy-TIPNO-UPy (TIPNO: 2,2,5-trimethyl-4-phenyl-3-azahexane-3-nitroxide), bearing both UPy and tpy supramolecular binding sites, in NMP is further explored in the current work. The orthogonality of the two non-covalent interactions within the supramolecular polymer is also evaluated by addressing the selective responsivity to external stimuli. Functionalized TIPNO derivatives were initially reported by Hawker and co-workers as universal initiators in NMP featuring a high end-group fidelity and a high tolerance towards a broad range of functional groups.<sup>33</sup> Lohmeijer and Schubert expanded the scope of functional TIPNOs to the field of terpyridine chemistry by using tpy-TIPNO, as an initiator, for the synthesis of terpyridine-functionalized block copolymers *via* NMP.<sup>34</sup>

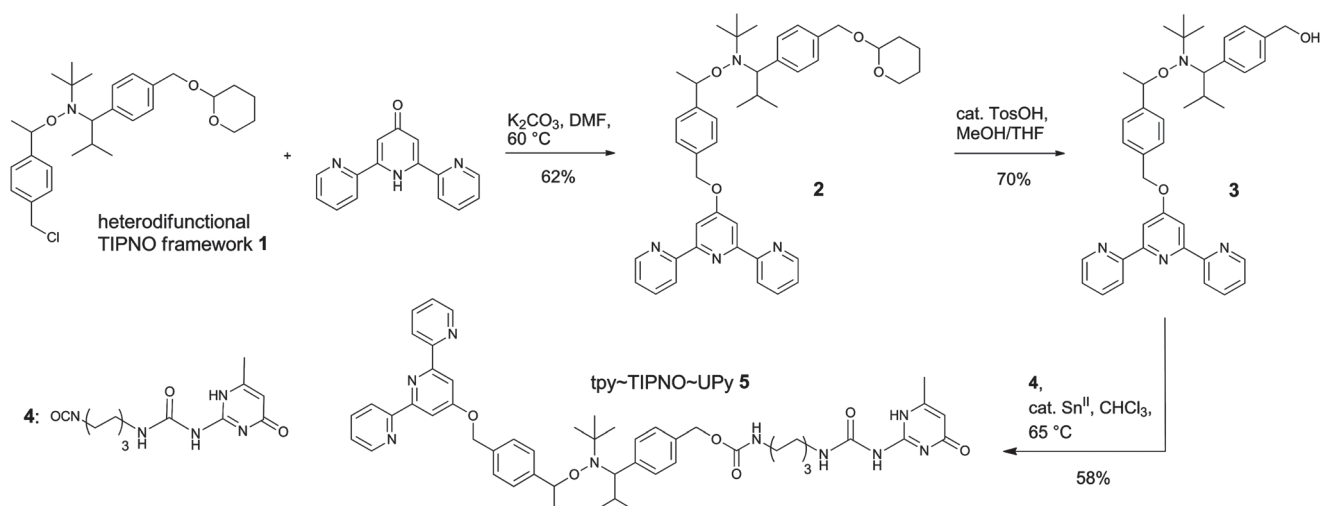
## Results and discussion

### Synthesis and characterization of the TIPNO-based initiator

The synthesis of the heterodifunctional initiator tpy-TIPNO-UPy (**5**) *via* stepwise functionalization of the nitroxide building block **1** has already been published elsewhere.<sup>30</sup> As outlined in Scheme 2, the terpyridine-containing initiator **3**, as a key building block, was obtained by a nucleophilic substitution reaction of **1** with 2,2':6',2''-terpyridin-4'(1'*H*)-one<sup>35</sup> and subsequent cleavage of the tetrahydropyran (THP) protecting group of the intermediate **2**. The heterodifunctional alkoxyamine system **5** was then prepared in good yields from **3** by isocyanate-coupling with the UPy derivative **4**. Due to the presence of two stereogenic centers within the central TIPNO unit, **5** was obtained as a mixture of two diastereomers. Consequently, two main sets of signals (in an almost 1 : 1 ratio) could be observed in the <sup>1</sup>H and (partially) also the <sup>13</sup>C NMR spectra.<sup>30</sup> Full unambiguous assignment of the spectra was achieved by 2D NMR experiments. It should be noted that additional signals were observed in the <sup>1</sup>H NMR spectra arising from the presence of the analogous *meta*-substituted isomer of **5** since commercial 4-chloromethylstyrene was used for the synthesis of **1**, which consists of a mixture of *para*- and *meta*-isomers in a *ca.* 9 : 1 ratio. The presence of this second isomer is not expected to interfere or moderate the polymerization behavior of this alkoxyamine initiator. The MALDI-TOF mass spectrometric analysis of **5** showed the expected [M + H]<sup>+</sup> adduct at *m/z* = 910.64; also the experimental isotopic pattern was in good agreement with the one for calculated *m/z* = 910.49.<sup>30</sup>

### Polymerization of styrenes using the TIPNO-based initiator

**SYNTHESIS OF THE POLYMERS.** For the successful utilization of alkoxyamine **5** as an initiator for NMP to obtain telechelic polymers some criteria have to be met: in particular, the polymerization has to be highly controlled leading to a high end-group fidelity, *i.e.* the functional groups at both chain ends must not be lost in the course of the polymerization due to extensive chain transfer or termination reactions. To evaluate the control over the polymerization, the NMP of styrene initiated by alkoxyamine **5** was investigated (Fig. 1a). Polymerizations with different monomer-to-initiator (M/I) ratios and different polymerization times were performed; the results are summarized in Table 1. With increasing polymerization time, the SEC traces of tpy-PS<sub>*m*</sub>-UPy (**6c–g**) were shifted to shorter elution times corresponding to an increase of the molar mass; all polymers revealed symmetrical curves with a minor tailing to lower molar masses, indicating good control over the polymerization (Fig. 1b). However, low polydispersity index (PDI) values do not provide unambiguous evidence for a controlled polymerization and, thus, a kinetic study was also performed. For this purpose, a stock solution with the telechelic initiator and styrene (solvent: anisole) was divided over different reaction vessels; after the removal of oxygen, the vessels were heated in an oil bath and the reactions were stopped after different polymerization times. The resulting tpy-PS-UPy (**6c–g**) *M<sub>n</sub>* values (PDI < 1.2) were in good agreement with the theoretical



**Scheme 2** Schematic representation of the synthesis of the hetero- and homodifunctional initiators via sequential functionalization of the heterodifunctional alkoxyamine **1**.

values (Table 1). However, the first order kinetic plot of  $\ln([M_0]/[M])$  as a function of time revealed a non-linear time dependency, indicating a variation in radical concentration during the polymerization (Fig. 2). The obtained data could be satisfactorily fitted to a time dependency of  $t^{2/3}$ , which evidences the persistent radical effect (PRE):<sup>36,37</sup> the radical initiation rate of another species, *e.g.* the monomer itself, is much lower than the dissociation rate of the alkoxyamine.<sup>36</sup> This is pronounced, since the autoinitiation of the monomer was tremendously reduced due to the dilution with an inert solvent and provided the excess of persistent radicals within the non-steady-state polymerization. Under these conditions, the rate of self-termination of the propagating radical is much lower than the cross-reaction to the dormant species. The decomposition rate of the nitroxide is negligible, since this would hinder the certain build-up of the persistent radical with respect to the  $t^{2/3}$ -dependency. Finally, the controlled character of the polymerization is evident from the linear increase of the number average molar mass plotted against the conversion (Fig. 3).

Similarly, pentafluorostyrene (PFS) was utilized as a monomer in the NMP, yielding tpy-PPFS-UPy (**7**) (Fig. 1a, 1c and Table 1). As for the non-fluorinated styrene monomer good

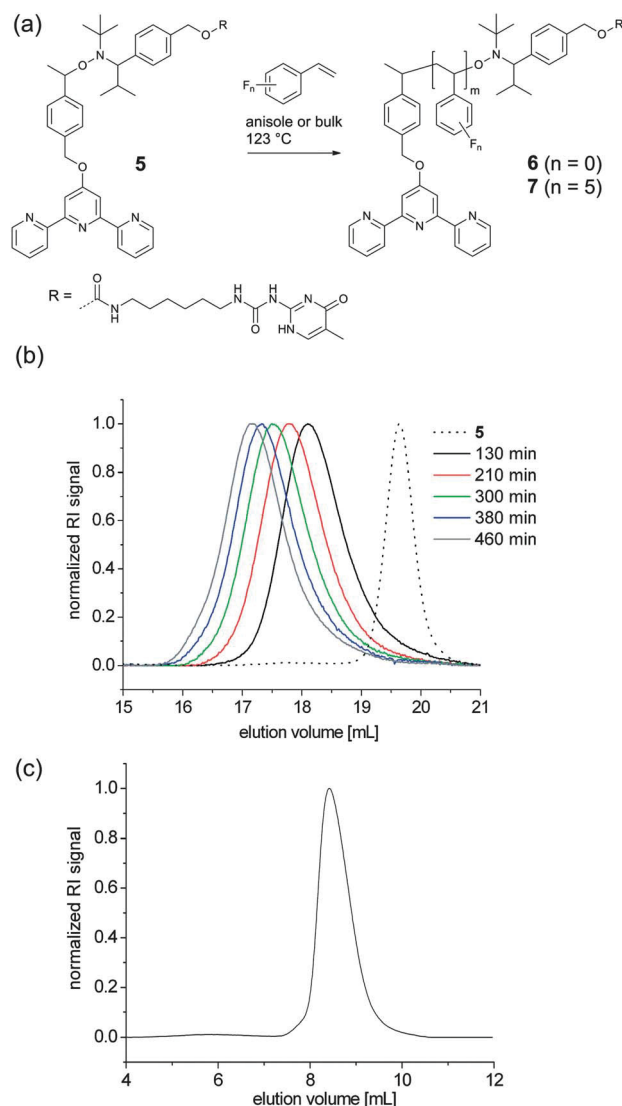
control over the polymerization, in bulk, was observed after 5 h with a  $M_n$  value of  $10\,500\text{ g mol}^{-1}$  and a PDI value of 1.13. Since PPFS **7** was not soluble in DMA, a linear polystyrene calibration with chloroform as an eluent was used. Pentafluorostyrene was polymerized to show that the use of this initiator is not limited to styrene. An additional value relies on the potential of a click-like side-chain modification via the *para*-fluoro position.<sup>38–40</sup>

**NMR SPECTROSCOPIC ANALYSIS.** Polystyrenes **6** and **7** were investigated by  $^1\text{H}$  NMR spectroscopy in order to confirm the incorporation of the telechelic functional groups into the polymeric material. The  $^1\text{H}$  NMR spectra of **6** and **7** revealed signals for both end-groups where the characteristic terpyridine signals (7.2 to 8.8 ppm) as well as the hydrogen bonding signals for the UPy unit (10 to 13 ppm) were clearly present (Fig. S1 and S2†). According to  $^1\text{H}$  NMR spectroscopy, the alkoxyamine initiator **5** as well as the polymers appeared exclusively as the dimeric species (**5**)<sub>2</sub>, (**6**)<sub>2</sub>, and (**7**)<sub>2</sub>, respectively, in non-polar solvents, *i.e.* dichloromethane and chloroform. Temperature-dependent NMR experiments (in *d*<sub>4</sub>-*ortho*-dichlorobenzene) revealed that these dimers were stable up to at least 75 °C. According to diffusion-ordered-spectroscopy (DOSY) measurements, a second signal at  $\delta = 1.7$  ppm, with almost the same

**Table 1** Details for nitroxide-mediated polymerizations using alkoxyamine **5** as the initiator

	Time [min]	Monomer	M/I	Conv. [%] (GC)	$M_n$ [g mol <sup>-1</sup> ] theor. <sup>a</sup>	$M_n$ [g mol <sup>-1</sup> ] (SEC) <sup>b,c</sup>	PDI (SEC)
<b>6a</b>	400	St	35	50	2700	6800	1.07
<b>6b</b>	360	St	200	35	8000	11 400	1.16
<b>6c</b>	130	St	200	21	5700	5900	1.18
<b>6d</b>	210	St	200	29	7400	7600	1.18
<b>6e</b>	300	St	200	35	8700	9000	1.17
<b>6f</b>	380	St	200	39	9800	10 400	1.18
<b>6g</b>	460	St	200	44	10 800	11 500	1.19
<b>7</b>	300	PFS	200	— <sup>d</sup>	— <sup>d</sup>	10 500 <sup>e</sup>	1.11

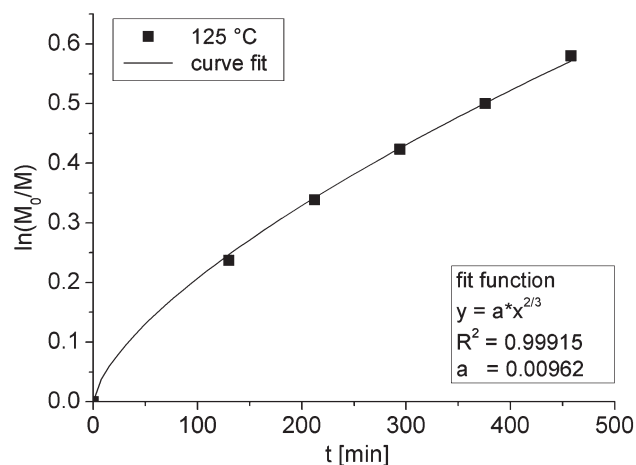
<sup>a</sup>  $M_n$  (theor.) represents the targeted  $M_n$  with respect to the conversion (GC). <sup>b</sup> After precipitation of the polymer into methanol. <sup>c</sup> A linear polystyrene calibration with DMA as eluent was used. <sup>d</sup> Bulk polymerization lacks a reference signal for GC measurements. <sup>e</sup> A linear polystyrene calibration with chloroform as eluent was used.



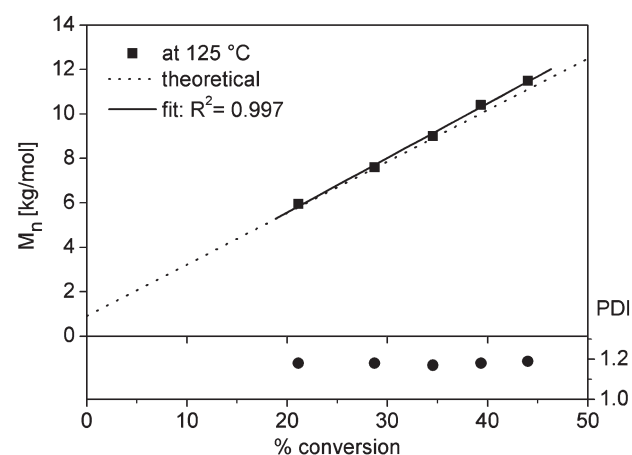
**Fig. 1** Schematic representation of the polymerization of styrenic monomers using **5** as an initiator (a) and SEC traces of polystyrenes **6c-g** with increasing polymerization time (b) and of poly(pentafluorostyrene) **7** (c). Eluent: *N,N*-dimethyl acetamide for polystyrene and chloroform for poly(pentafluorostyrene).

diffusion behavior as for dichloromethane, was present in (5)<sub>2</sub> (Fig. 4, left). Moreover, an exchange between *one* of the hydrogen bonding protons and this signal could be observed. Most likely this second signal can thus be ascribed to residual water: apparently, the proton-exchange process hindered the removal of water from the product by drying. In addition, the 2D DOSY spectrum confirmed that all signals (apart from the solvents) belonged to the same compound due to the same range of the relative diffusion coefficient, thereby proving that both UPy and tpy are attached to the TIPNO.

In this vein, the 2D DOSY spectrum of the resultant telechelic polystyrene (6<sub>2</sub>) also shows the same relative diffusion coefficient for the signals of both end-groups and the polymer backbone proving that UPy and tpy are attached to the polystyrene (Fig. 4, right). The addition of trifluoroacetic acid (TFA), as a strong competitor for hydrogen bonding, led to significant changes in the NMR spectrum.

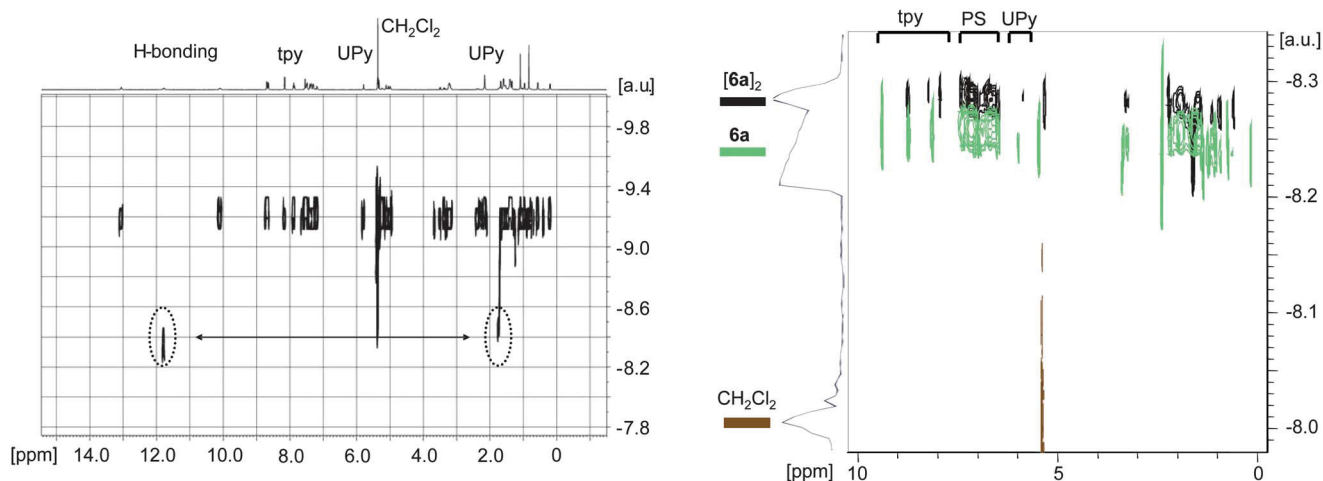


**Fig. 2** Kinetic plot for the polymerization of styrene **6c-g** as an initiator with the semilogarithmic monomer conversion plotted against the polymerization time.

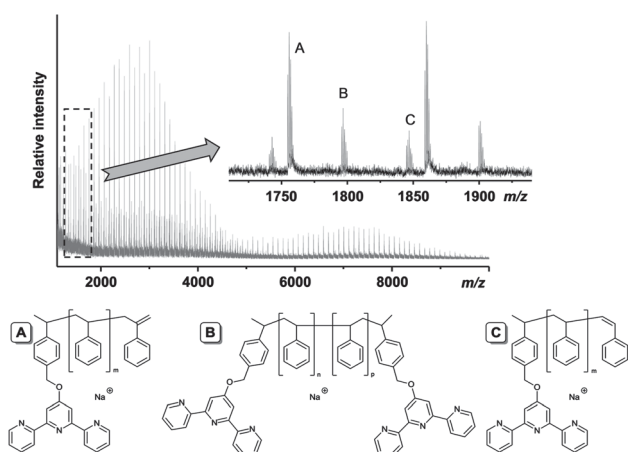


**Fig. 3** Kinetic plot for the polymerization of styrene **6c-g** with the molar mass plotted against the conversion showing a linear increase of the number average molar mass with the conversion.

As expected, the quantitative disappearance of the signals arising from hydrogen bonding as well as a high-field shift of the terpyridine signals, due to protonation, could be observed in the <sup>1</sup>H NMR spectrum (Fig. S3†). It was concluded that predominantly the monomeric form of **6** was present under these conditions. Subsequent DOSY measurements revealed a significant shift for the diffusion coefficients of *all* signals of the tpy and UPy moieties as well as the polystyrene with respect to the diffusion coefficient in dichloromethane (Fig. 4, right). Thus, the change in molar mass related to the monomeric and dimeric forms of **6** can be probed by the relative diffusion coefficients. It can be concluded within the sensitivity limits of NMR spectroscopy that both end-groups are attached to the polymer chain and the presence of auto-polymerized non-functionalized polystyrene or monofunctional tpy-PS could be excluded, as they would reveal a different diffusion coefficient range for the terpyridine and polystyrene signals.

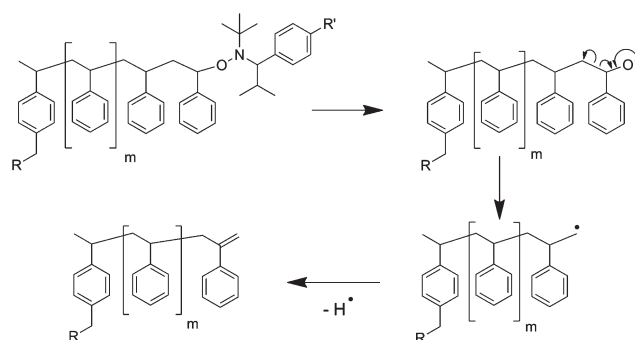


**Fig. 4** Left: 2D DOSY spectrum of  $(5)_2$  revealing the exchange of water with a hydrogen bonding proton of the UPy moiety (400 MHz,  $CD_2Cl_2$ , 298 K). Right: comparison of the 2D DOSY spectra for **6a** (green,  $CD_2Cl_2$  and TFA) and  $(6a)_2$  (black,  $CD_2Cl_2$ ) demonstrating the same significant change of the diffusion coefficients for signals of tpy, UPy and polystyrene (for both spectra: 400 MHz, 298 K).



**Fig. 5** MALDI-TOF mass spectrum of polystyrene **6a**. The inset shows the three observed modes of fragmentation (A–C). The proposed corresponding structures are shown on the bottom.

**MASS SPECTROMETRIC ANALYSIS.** The polymers were also investigated by mass spectrometry. The MALDI-TOF MS of **6** revealed three distributions that could all be correlated to polystyrenes (*i.e.* in all cases  $m/z$ -differences of 104 amu between two signals, Fig. 5). No distribution could be directly related to the heterodifunctional telechelic polymer **6**, thus fragmentation by abstraction of the nitroxide residue has to be assumed (the proposed fragmentation products are shown in Fig. 5). Nitroxide-functionalized polymers are well-known to be prone to fragmentation during the MALDI process;<sup>41</sup> however, the characteristic fragmentation due to loss of the *tert*-butyl group of the TIPNO moiety could not be observed. The observed fragmentations for series B and C could also be characteristic products of termination reactions during the polymerization. On this note, it is not fully clear if these fragments were formed during the MALDI process or during the polymerization—the latter possibility can only be neglected within the limits of  $^1H$  NMR

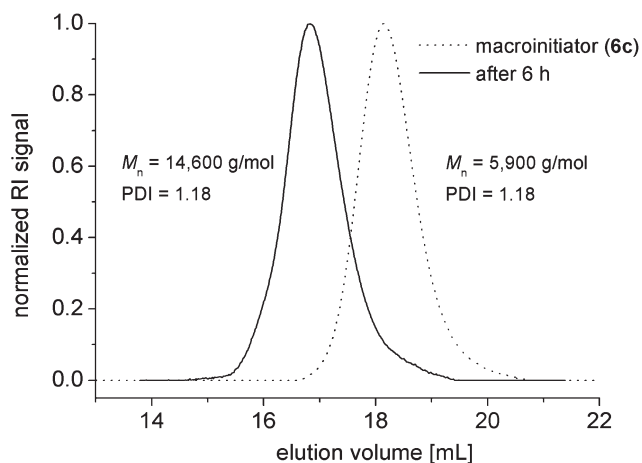


**Fig. 6** Schematic representation of the proposed mechanism for the chain-end degradation of the polymer (formation of series C).

spectroscopy and SEC. The proposed mechanism for the chain-end degradation for **6a** during the MALDI process according to Schulte *et al.* is shown in Fig. 6.<sup>42</sup> The distribution at higher molar mass up to  $m/z = 10\,000$  could be assigned to the recombination product of two polystyrene chains (B). Taking the slight tailing of the SEC traces of **6a** to higher molar masses into account, a small degree of recombination during the NMP appears to be plausible, which, however, will not strongly interfere with the formation of supramolecular polymer.

**CHAIN EXTENSION VIA NMP.** The control and end-group fidelity of the telechelic polymers was further confirmed by using them as macroinitiators for a chain-extension experiment. More specifically, the heterodifunctional polystyrene **6c** was applied as a macroinitiator for chain extension with styrene. The polymerization was conducted in anisole, as a solvent, in order to allow a correlation to the NMP performance of the heterodifunctional alkoxyamine initiator **5**. As shown in Fig. 7, a complete shift of the  $M_n$  value from  $6000\text{ g mol}^{-1}$  to  $14\,600\text{ g mol}^{-1}$  was observed while retaining the narrow polydispersity index ( $PDI < 1.2$ ), demonstrating the controlled character of the NMP initiated by **6c** and, thus, proving that





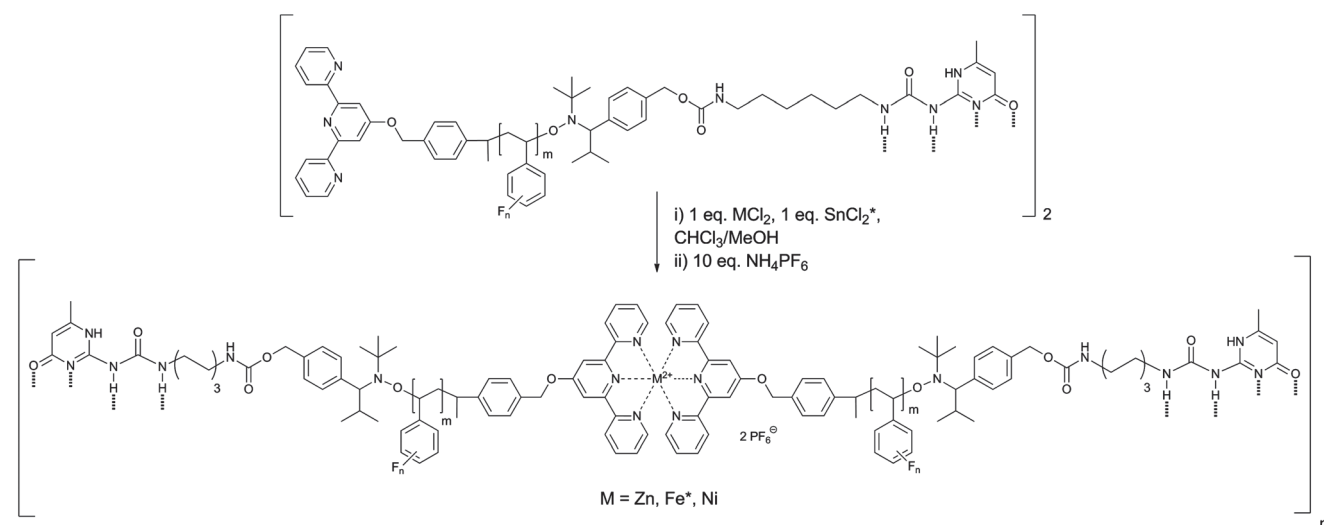
**Fig. 7** SEC traces of macroinitiator tpy-PS<sub>m</sub>-UPy (**6c**) and the chain-extended polymer tpy-PS-*b*-PS-UPy (**8**). Eluent: *N,N*-dimethyl acetamide (DMA) with LiCl (2.1 g L<sup>-1</sup>).

almost all of the polymer chains of **6c** still bear the UPy-functionalized nitroxide as an end-group. Thus, the telechelic polymers represent suitable building blocks for the preparation of block copolymers containing two orthogonal supramolecular end-groups *via* CRP.

### Chain extension *via* metal ion complexation

The combination of hydrogen bonding and metal-to-ligand coordination was applied by Hofmeier *et al.* for the preparation of supramolecular chain-extended poly( $\epsilon$ -caprolactone) of high molar masses.<sup>20,29</sup> In particular, the divalent cations of the first row transition metals are suited for this purpose, since the formation of octahedral *bis*-complexes with terpyridine ligands is highly preferred.<sup>43</sup> However, the low kinetic stability of some *bis*-terpyridine complexes (according to the Irving-Williams series) on the one hand and the paramagnetic nature of some

metal ions on the other hand limit the range of potential candidates with respect to the preparation and characterization of these materials. Chiper *et al.* showed that metallo-supramolecular polymers based on [Ni(tpy)<sub>2</sub>]<sup>2+</sup> linkages are stable enough to be investigated by size exclusion chromatography.<sup>44,45</sup> However, NMR spectroscopy cannot be applied for such polymers due to the paramagnetic nature of the Ni<sup>II</sup> ions. In this respect, Fe<sup>II</sup> or Zn<sup>II</sup> ions might be used; however, in particular the latter ions lead to rather weak metal complexes. In the present study, these three metal ions were utilized for the preparation of supramolecular chain-extended polymers {[**(6)**M(**6**)](PF<sub>6</sub>)<sub>2</sub>]<sub>n</sub> (Scheme 3, M = Zn<sup>II</sup>, Fe<sup>II</sup> or Ni<sup>II</sup>). The metallo-polymerization reactions were performed in a chloroform-methanol mixture at a 2 : 1 stoichiometry of macroligand **6d** or **6e** and the corresponding metal M<sup>II</sup> ions. In the case of Fe<sup>II</sup> ions, an equimolar amount of stannous chloride was added to the reaction mixture to prevent oxidation of Fe<sup>II</sup> to the paramagnetic Fe<sup>III</sup>. Subsequent to the anion exchange with PF<sub>6</sub><sup>-</sup>, the polymers {[**(6e)**M(**6e**)](PF<sub>6</sub>)<sub>2</sub>]<sub>n</sub> were characterized by SEC or <sup>1</sup>H NMR spectroscopy (when applicable). The expected significant increase of the molar mass due to the metallo-polymerization of **6** and **7** could not be observed by SEC since the applied polar and protic conditions suppress the formation of UPy dimers. Consequently, only dimers of the type [Ni(**6**)<sub>2</sub>](PF<sub>6</sub>)<sub>2</sub> could be detected – as pointed out above, the kinetic stability of Ni<sup>II</sup> *bis*-terpyridine complexes allows the SEC measurements, while for all other metal ions investigated, dissociation occurs.<sup>44,45</sup> The SEC trace of [Ni(**6d**)<sub>2</sub>](PF<sub>6</sub>)<sub>2</sub> was shifted to a higher molar mass compared to the one obtained for the precursor polymer **6** under the same conditions (Fig. S4†; eluent: DMF containing 0.005 M NH<sub>4</sub>PF<sub>6</sub>). A shoulder at higher molar masses was observed that cannot be explained but has also been reported for other Ni<sup>II</sup>-based systems in the literature.<sup>45</sup> Thus, this shoulder is most likely not caused by any impurity, but rather originates from different solvation, interactions with the column or higher aggregates. The SEC traces recorded with a



**Scheme 3** Schematic representation of the synthesis of supramolecular chain-extended polymers {[**(6)**M(**6**)](PF<sub>6</sub>)<sub>2</sub>]<sub>n</sub> and {[**(7)**M(**7**)](PF<sub>6</sub>)<sub>2</sub>]<sub>n</sub> by metal-to-ligand coordination (SnCl<sub>2</sub> was added to the reaction mixture in order to prevent oxidation of the Fe<sup>II</sup> ion).



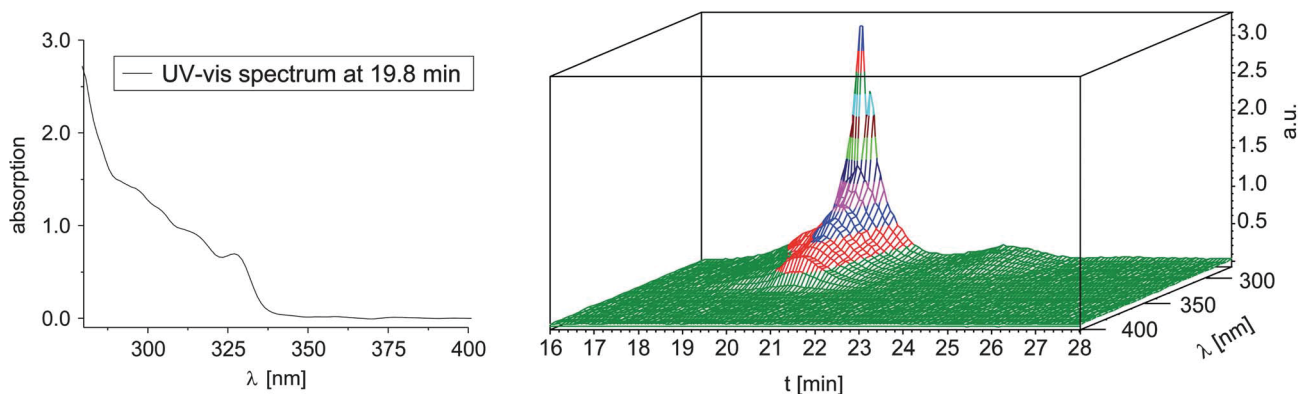


Fig. 8 UV-vis absorption spectrum in DMF (left) and SEC trace (right) of  $[\text{Ni}(\mathbf{6d})_2](\text{PF}_6)_2$  recorded with a PDA detector (eluent: DMF containing 0.005 M  $\text{NH}_4\text{PF}_6$ ).

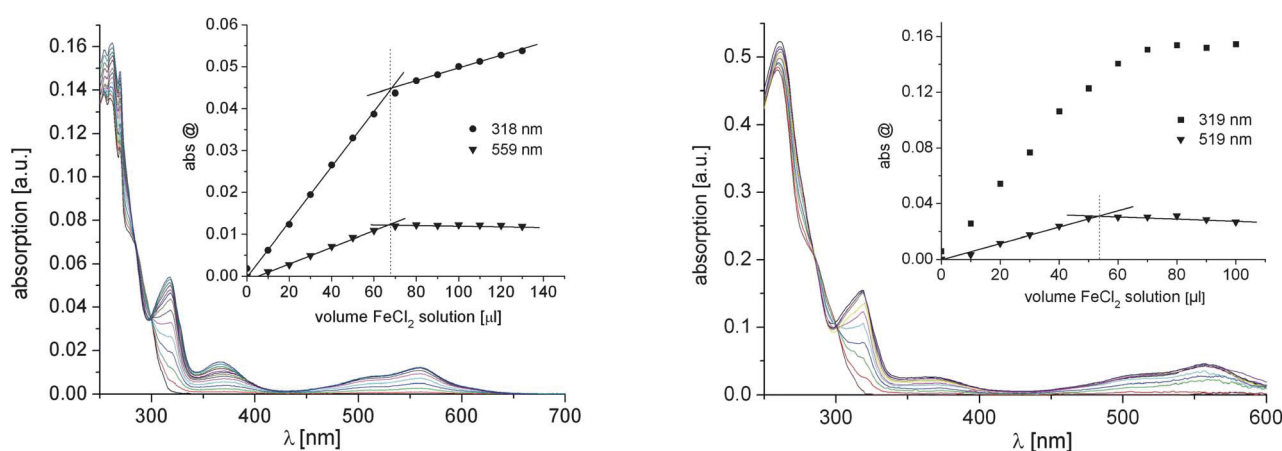


Fig. 9 UV-vis titration curves for the complexation of **6b** (left) and **7** (right) with  $\text{Fe}^{\text{II}}$  ions (solvent: methanol). The insets show the evolution of the LC and MLCT absorption bands as a function of added  $\text{Fe}^{\text{II}}$  ions (the left figure was created from data published in ref. 30).

photodiode array (PDA) detector confirmed the complete shift to lower retention times, *i.e.* higher molar masses (Fig. 8). The corresponding UV-vis absorption spectrum proved the formation of the  $\text{Ni}^{\text{II}}$  *bis*-terpyridine complex by the appearance of the characteristic ligand-centered (LC) bands at 315 and 329 nm.<sup>45</sup>

The formation of the  $\text{M}^{\text{II}}$  *bis*-terpyridine complexes of **6b** and **7** was also monitored by UV-vis titration experiments with  $\text{Fe}^{\text{II}}$  ions (Fig. 9). Since methanol was used as a solvent, the formation of hydrogen bonds between the UPy moieties and, thereby, of the chain-extended polymers does not occur. The evolution of

the LC and the metal-to-ligand charge-transfer (MLCT) absorptions at *ca.* 320 and *ca.* 560 nm, respectively, were plotted as a function of added  $\text{Fe}^{\text{II}}$  ions. The point-of-equivalence indicates the consumption of free tpy sites by complexation at a 2 : 1 ratio of macroligand and  $\text{Fe}^{\text{II}}$  ions (*i.e.* formation of  $[\text{Fe}(\text{tpy})_2]^{2+}$  complexes). From this equivalence point the number average molar mass of the polymers can also be

Table 2 Number average molar masses as determined by SEC measurements,  $^1\text{H}$  NMR spectroscopy and UV-vis titration experiments

Polymer	$M_n$ [ $\text{g mol}^{-1}$ ]		
	SEC <sup>a</sup>	NMR <sup>b</sup>	UV-vis <sup>c</sup>
<b>6b</b>	11 400	13 700	9000
<b>7</b>	10 500	21 500	18 500

<sup>a</sup> A linear polystyrene calibration was used. <sup>b</sup> Determined by comparison of the integrals of the tpy and polystyrene signals. <sup>c</sup> Calculated from the point-of-equivalence in the UV-vis titration experiments.

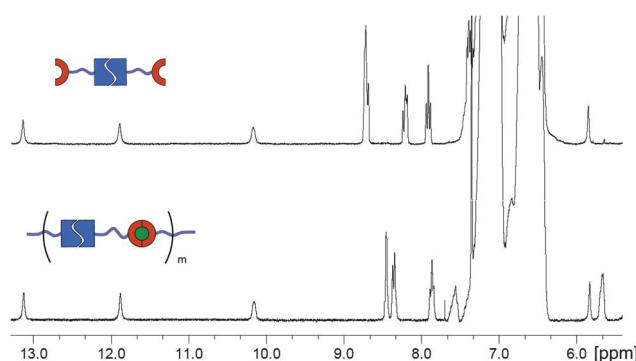
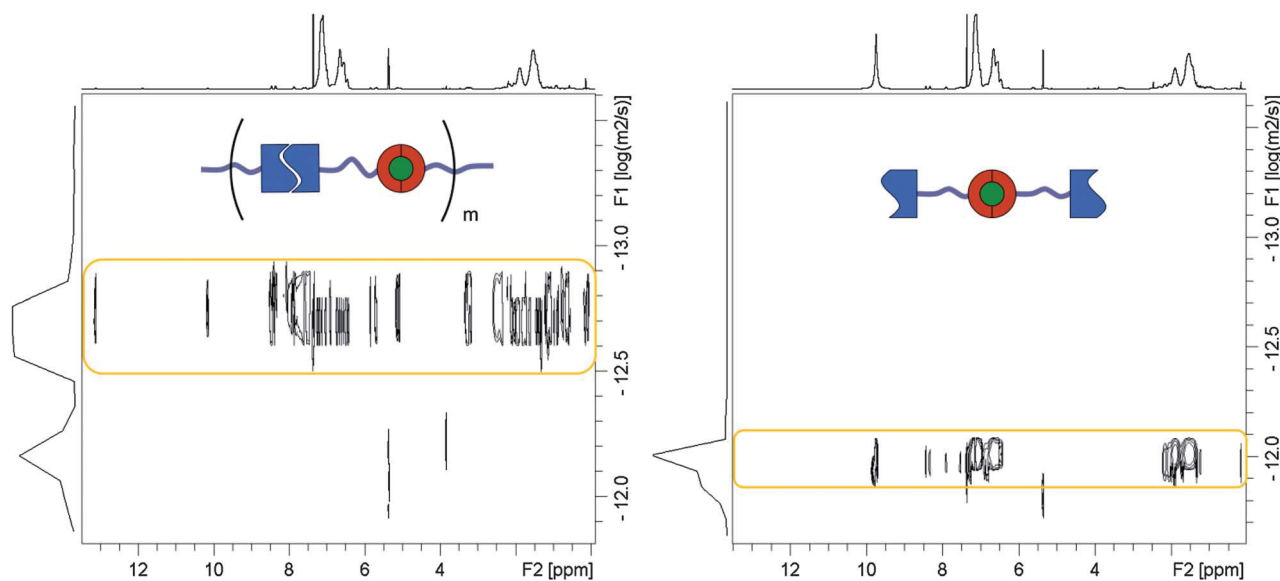


Fig. 10 Zoom into the low-field region of the  $^1\text{H}$  NMR spectra of **(6e)<sub>2</sub>** (top) and  $\{[(\mathbf{6e})\text{Fe}(\mathbf{6e})](\text{PF}_6)_2\}_n$  (bottom). For both spectra: 400 MHz,  $\text{CD}_2\text{Cl}_2$ , 298 K.



**Fig. 11** Left: 2D DOSY spectrum of  $\{[(6e)Fe(6e)](PF_6)_2\}_n$  (400 MHz,  $CD_2Cl_2$ , 298 K) demonstrating the same diffusion coefficients for signals of tpy complex, UPy and polystyrene. Right: 2D DOSY spectrum of  $\{[(6e)Fe(6e)](PF_6)_2\}$  (400 MHz,  $CD_2Cl_2$ , 298 K) after addition of trifluoroacetic acid demonstrates the cleavage of the hydrogen bonding units (diffusion coefficient of dichloromethane was taken as a reference).

calculated (Table 2). For both **6b** and **7**, similar  $M_n$  values as determined by  $^1H$  NMR spectroscopy were obtained. Apparently, the SEC measurements underestimated the  $M_n$  value for **7** due to the unavailability of a suitable calibration.

Due to the diamagnetic character of the  $Fe^{II}$  and  $Zn^{II}$  ions, the respective metallopolymers  $\{[(6e)M(6e)](PF_6)_2\}_n$  could also be investigated by NMR spectroscopy. In the  $^1H$  NMR spectra, the signals of the terpyridine protons were shifted upon complexation, whereas the signals assigned to hydrogen bonding remained unchanged (Fig. 10 and S5<sup>†</sup>). Thus, the formation of a supramolecular polymer based on two different non-covalent interactions in  $CD_2Cl_2$  was demonstrated. The 2D DOSY measurement further confirmed the presence of the two types of supramolecular bonds within the chain-extended polymer: the same relative diffusion coefficients were observed for all tpy, polystyrene and UPy signals of  $\{[(6e)Fe(6e)](PF_6)_2\}_n$  (Fig. 11, left).

In order to study the orthogonal responsiveness of the supramolecular entities, TFA was added to the chain-extended  $Fe^{II}$  polymer. As expected, the quadruple hydrogen bonding of the UPy-dimer was disrupted without affecting the more pH robust metal–ligand binding (Fig. S6<sup>†</sup>). The disappearance of the signals arising from hydrogen bonding in the  $^1H$  NMR spectrum in concert with a significant change in the diffusion behavior confirmed the selective responsiveness (Fig. 11). The comparison of the 2D DOSYs of the polymer  $\{[(6e)Fe(6e)](PF_6)_2\}_n$  and the dimer  $[Fe(6e)_2](PF_6)_2$  clearly shows the influence of the pH value on the molecular structure.

## Conclusion

The one-step preparation of heterotelechelic polymers *via* NMP using an alkoxyamine as inhibitor bearing the desired heterotelechelic end-groups of the resultant polymer was accomplished. The polymerization of styrene was proven to be a controlled

process, while the bulky end-groups, namely tpy and UPy, did not disturb the performance of the initiator. Therefore, the polymeric spacer between the supramolecular binding sites can be easily varied in length by NMP. This approach has a wider scope by means of construction flexibility compared to a postmodification approach for telechelic polymers, as the chain length and composition between the supramolecular binding sites can be varied in less reaction steps and purification can be simply done by precipitation. Therefore, the strategy of functional initiators represents a powerful method for investigating the influence of the polymer spacer between functional groups within supramolecular architectures.

The self-assembly of the prepared building blocks towards linear supramolecular polymers with alternating metal ion complex and hydrogen bonding linkage was investigated in apolar solvents with complexes of zinc(II), iron(II) and nickel(II) metal ions. The selective responsiveness of the system against pH value as an external stimulus was proven where the hydrogen bonding linkage could be switched off while the metal ion complex remained intact.

The presented strategy of functionalized initiators provides a promising strategy for the preparation of various tailor-made supramolecular architectures using polymeric building blocks, with respect to future progress in the field of stimuli-responsive and self-healing materials.

## Experimental section

### Methods and instrumentation

All chemicals were received from Aldrich, Fluka and Acros; solvents were purchased from Biosolve. Unless otherwise stated, the chemicals and solvents were used without further purifications. DMF was dried over molecular sieves (pore size of 4 Å). THF and toluene were dried using a PureSolv-EN<sup>TM</sup> solvent

purification system. Column chromatography was carried out on silica gel 60 and standardized aluminium oxide 90 (Merck). Styrene was freshly purified prior to use by filtration over neutral aluminium oxide 90 (Merck). 1D ( $^1\text{H}$ ,  $^{13}\text{C}$ ) and 2D ( $^1\text{H}$ - $^1\text{H}$ -COSY) nuclear magnetic resonance (NMR) spectra were recorded on a Varian Mercury 400 MHz spectrometer at 298 K, 348 K or 368 K. Chemical shifts are reported in parts per million (ppm) downfield from tetramethylsilane (TMS) and were calibrated to the residual solvent peaks. 2D DOSY experiments were conducted on a Bruker 400 MHz spectrometer at 298 K. Deuterated solvents for NMR spectroscopy were obtained from Cambridge Isotope Laboratories. Two different set-ups for size-exclusion chromatography (SEC) were used: a Shimadzu system equipped with a SCL-10A system controller, a LC-10AD pump, a RID-10A refractive index (RI) detector, an UV-vis absorption detector (250 and 290 nm) and a PSS SDV column utilizing (i) *N,N*-dimethyl acetamide with 2.1 g L $^{-1}$  LiCl or (ii) chloroform/iso-propanol/triethylamine (94/2/4), as eluent. Linear polystyrene was used as the calibration standard. Additionally, SEC was measured on a Waters SEC system consisting of an isocratic pump, solvent degasser, column oven, photodiode array (PDA) detector, RI detector and a Styragel HT-4 SEC column with a precolumn installed. The eluent was DMF containing 0.005 M  $\text{NH}_4\text{PF}_6$  at a flow speed of 0.5 mL min $^{-1}$ . The column temperature was 323 K. Gas chromatographic (GC) measurements were performed on an Interscience Trace GC with a Trace Column RTX-5 connected to a PAL autosampler. UV-vis absorption spectra were recorded in diluted chloroform solutions on a Perkin-Elmer Lambda-45 UV-vis spectrophotometer at room temperature (1 cm cuvettes). Elemental analyses were carried out on a EuroVector EuroEA300 elemental analyzer. GC mass spectrometry was conducted on a Shimadzu GC17A connected to a mass spectrometer. Infrared spectra were recorded on a Bruker IFS55 FT-IR spectrometer. Matrix-assisted laser desorption/ionization time-of-flight mass spectrometry (MALDI-TOF MS) was performed on a Voyager-DE<sup>TM</sup> PRO Biospectrometry<sup>TM</sup> Workstation (Applied Biosystems) time-of-flight mass spectrometer using linear and reflector mode for operation. Dithranol or 2-[(2E)-3-(4-*tert*-butylphenyl)-2-methylprop-2-enylidene]malononitrile (DCTB) were used as matrices and NaI as an additive. The spectra were recorded in the positive ion mode and ionization was performed with a 337 nm pulsed nitrogen laser. The MALDI-TOF mass spectra of polymers were also measured on a Bruker Ultraflex<sup>TM</sup> III TOF/TOF spectrometer.

The following compounds were prepared according to literature procedures: 2,2':6',2''-terpyridin-4'(1'*H*)-one,<sup>46</sup> *N*-(*tert*-butyl)-*O*-(1-(4-(chloromethyl)phenyl)ethyl)-*N*-(2-methyl-1-(4-((tetrahydro-2*H*-pyran-2-yl)oxy)methyl)phenyl)propyl)hydroxylamine (1), *O*-(1-(4-((2,2':6',2''-terpyridin-4'-yloxy)methyl)phenyl)ethyl)-*N*-(*tert*-butyl)-*N*-(2-methyl-1-(4-((tetrahydro-2*H*-pyran-2-yl)oxy)methyl)phenyl)propyl)-hydroxylamine (2),<sup>30</sup> 4-(1-((1-(4-((2,2':6',2''-terpyridin-4'-yloxy)methyl)phenyl)ethoxy)(*tert*-butyl)amino)-2-methylpropyl)phenyl)methanol (3),<sup>30</sup> 1-(6-isocyanato-hexyl)-3-(6-methyl-4-oxo-1,4-dihydro-pyrimidin-2-yl)urea (4)<sup>30</sup> and 4-(1-((1-(4-((2,2':6',2''-terpyridin-4'-yloxy)methyl)phenyl)ethoxy)(*tert*-butyl)amino)-2-methyl-propyl)benzyl (6-(3-(6-methyl-4-oxo-1,4-dihydropyrimidin-2-yl)ureido)hexyl)carbamate (tpy-TIPNO-UPy, 5).<sup>30</sup>

## General polymerization procedure

Styrene monomers were freshly purified by filtration over  $\text{Al}_2\text{O}_3$  prior to use in order to remove the inhibitor. The freshly purified styrene was added to a clear anisole solution of the TIPNO-based initiator in a polymerization vessel. After applying three freeze-pump-thaw-cycles to remove the oxygen, the vessel was purged with argon and immersed in an oil bath at 123 °C for a certain period of time. To remove residual monomer the reaction mixture was precipitated from  $\text{CHCl}_3$  into cold methanol. The monomer conversion was determined by GC measurements (before precipitation), the molar masses (*i.e.*  $M_n$  and  $M_w$ ) and the polydispersity index (PDI) values were determined by SEC, whereas  $^1\text{H}$  NMR spectroscopy was applied for the determination of the end-group functionality (by integration and comparison of the corresponding end-group signals) and  $M_n$  values (by integration of the polymer backbone to the terpyridine signals).

TPY-PS<sub>50</sub>-UPY (6c).  $^1\text{H}$  NMR (400 MHz,  $\text{CD}_2\text{Cl}_2$ ):  $\delta$  = 0.05–2.71 (set of multiplets), 3.11–3.38 (m, 4H), 3.85–4.37 (m, 1H), 4.97–5.22 (m, 2H), 5.26–5.34 (m, 3H), 5.83 (s, 1H), 6.25–7.54 (m, 200H), 7.91 (dt,  $J^3$  = 7.8 Hz,  $J^4$  = 1.6 Hz, 2H), 8.15–8.24 (m, 2H), 8.64–8.76 (m, 4H), 10.14 (s, 1H), 11.88 (s, 1H), 13.12 (s, 1H) ppm. SEC ( $\text{CHCl}_3$ , RI):  $M_n$  = 6800 g mol $^{-1}$ , PDI = 1.07.

TPY-PPFS<sub>100</sub>-UPY (7).  $^1\text{H}$  NMR (400 MHz,  $\text{CD}_2\text{Cl}_2$ ):  $\delta$  = 0.05–2.96 (set of multiplets), 3.13–3.32 (m, 4H), 4.7–4.9 (m, 1H), 5.01–5.16 (m, 2H), 5.18–5.32 (m, 3H), 5.83 (s, 1H), 6.97–7.47 (m, 10H), 7.91 (dt,  $J^3$  = 7.8 Hz,  $J^4$  = 1.6 Hz, 2H), 8.11–8.18 (m, 2H), 8.63–8.76 (m, 4H), 10.14 (s, 1H), 11.86 (s, 1H), 13.13 (s, 1H) ppm. SEC ( $\text{CHCl}_3$ , RI):  $M_n$  = 10 500 g mol $^{-1}$ , PDI = 1.13.

## General procedure for the chain-extension polymerization

The macroinitiator tpy-PS<sub>50</sub>-UPy (6, 70 mg, 0.012 mmol) was dissolved in anisole (200  $\mu\text{L}$ ) and freshly purified styrene. After following the general polymerization procedure (*vide supra*) the reaction was stopped after 6 h.

TPY-PS<sub>212</sub>-UPY (8). The chain-extension polymerization was conducted with a monomer-to-initiator ratio of  $M/I$  = 145 : 1.  $^1\text{H}$  NMR (400 MHz,  $\text{CD}_2\text{Cl}_2$ ):  $\delta$  = 0.05–2.71 (set of multiplets), 3.11–3.38 (m, 4H), 3.85–4.37 (m, 1H), 4.97–5.22 (m, 2H), 5.26–5.34 (m, 3H), 5.83 (s, 1H), 6.25–7.54 (m, 850H), 7.91 (dt,  $J^3$  = 7.8 Hz,  $J^4$  = 1.6 Hz, 2H), 8.15–8.24 (m, 2H), 8.64–8.76 (m, 4H), 10.14 (s, 1H), 11.88 (s, 1H), 13.12 (s, 1H) ppm. SEC (RI):  $M_n$  = 14 600 g mol $^{-1}$ , PDI = 1.18.

## UV-vis titration experiments

The macroligand (6b or 7, 0.852 mg) was dissolved in chloroform (20 mL) and  $\text{FeCl}_2$  (0.913 mg, 0.0072 mmol) was dissolved in methanol (10 mL). The methanol solution was subsequently added to the polymer solution in steps of 10  $\mu\text{L}$  while the formation of  $\text{Fe}^{\text{II}}$  bis-complex 16 was monitored by UV-vis spectroscopy after each addition. The point-of-equivalence and the  $M_n$  value of the macroligand were obtained by plotting the UV-vis absorption intensity at the LC and the MLCT as a function of added  $\text{Fe}^{\text{II}}$  ions.

### Metallo-polymerization of the macroligands

To a solution of macroligand **6** or **7** (0.003 mmol) in chloroform (200  $\mu$ L) was added a solution of  $MCl_2$  ( $M^{II} = Ni^{II}$ ,  $Fe^{II}$  or  $Zn^{II}$ ; 0.002 mmol) in methanol (100  $\mu$ L). For  $Fe^{II}$  complexation  $SnCl_2$  was used stoichiometric to avoid partial oxidation. The resultant clear solution was stirred under an argon atmosphere at 40 °C for 24 h. The chain-extended polymer was precipitated by adding an excess of  $NH_4PF_6$  (ca. 10 eq.).

$\{[(6D)Ni(6D)](PF_6)_2\}_n$ . The material was analyzed without further purification by SEC coupled with a PDA detector to prove the formation of the  $Ni^{II}$  bis-terpyridine complex; SEC (PDA/RI).

$\{[(6E)Fe(6E)](PF_6)_2\}_n$ .  $^1H$  NMR (400 MHz,  $CD_2Cl_2$ ):  $\delta = 0.39$ – $2.58$  (set of multiplets),  $3.13$ – $3.37$  (m, 4H),  $4.05$ – $4.25$  (m, 1H),  $4.97$ – $5.29$  (m, 3H),  $5.59$ – $5.66$  (m, 2H),  $5.79$ – $5.92$  (s, 1H),  $6.28$ – $7.50$  (m, 500 H),  $7.51$ – $7.67$  (m, 2H),  $7.80$ – $7.93$  (m, 2H),  $8.29$ – $8.40$  (m, 2H),  $8.41$ – $8.50$  (m, 2H),  $10.16$  (s, 1H),  $11.88$  (s, 1H),  $13.12$  (s, 1H) ppm.

$\{[(6E)Zn(6E)](PF_6)_2\}_n$ .  $^1H$  NMR (400 MHz,  $CD_2Cl_2$ ):  $\delta = 0.38$ – $2.62$  (set of multiplets),  $3.12$ – $3.38$  (m, 4H),  $4.04$ – $4.31$  (m, 1H),  $4.99$ – $5.21$  (m, 3H),  $5.52$ – $5.62$  (m, 2H),  $5.82$  (s, 1H),  $6.28$ – $7.63$  (m, 760H),  $7.73$ – $7.8$  (m, 2H),  $8.06$ – $8.25$  (m, 4H),  $8.38$ – $8.48$  (m, 2H),  $10.13$  (s, 1H),  $11.86$  (s, 1H),  $13.11$  (s, 1H) ppm.

### Acknowledgements

The authors kindly acknowledge financial support from the Dutch Polymer Institute (DPI, technology area HTE), the Thüringer Ministerium für Bildung, Wissenschaft und Kultur (Grant no. B514-09049: PhotoMic) and the Deutsche Forschungsgemeinschaft (DFG, SPP 1568). Moreover, the authors thank Grit Festag and Anja Baumgaertel for their help with SEC and MALDI-TOF MS measurements, respectively.

### Notes and references

- N. Hadjichristidis, M. Pitsikalis, S. Pispas and H. Iatrou, *Chem. Rev.*, 2001, **101**, 3747–3792.
- K. Matyjaszewski, *Prog. Polym. Sci.*, 2005, **30**, 858–875.
- C. J. Hawker, *Adv. Polym. Sci.*, 1999, **147**, 113–160.
- A. Winter, M. D. Hager and U. S. Schubert, Supramolecular Polymers, in *Polymer Science: A Comprehensive Reference*, ed. M. Möller and K. Matyjaszewski, Elsevier Ltd., Oxford, 2012, vol. 5.
- T. F. A. De Greef, M. M. J. Smulders, M. Wolffs, A. P. H. J. Schenning, R. P. Sijbesma and E. W. Meijer, *Chem. Rev.*, 2009, **109**, 5687–5754.
- C. K. Ober and G. Wegner, *Adv. Mater.*, 1997, **9**, 17–31.
- L. Brunsveld, B. J. B. Folmer, E. W. Meijer and R. P. Sijbesma, *Chem. Rev.*, 2001, **101**, 4071–4098.
- W. H. Binder and R. Zirbs, *Adv. Polym. Sci.*, 2007, **207**, 7–78.
- U. S. Schubert and C. Eschbaumer, *Angew. Chem., Int. Ed.*, 2002, **41**, 2892–2926.
- D. G. Kurth and M. Higuchi, *Soft Matter*, 2006, **2**, 915–927.
- J. D. Fox, *Macromolecules*, 2009, **42**, 6823–6835.
- J.-F. Gohy, B. G. G. Lohmeijer and U. S. Schubert, *Chem.–Eur. J.*, 2003, **9**, 3472–3479.
- J.-F. Gohy, B. G. G. Lohmeijer, A. Alexeev, X.-S. Wang, I. Manners, M. A. Winnik and U. S. Schubert, *Chem.–Eur. J.*, 2004, **10**, 4315–4323.
- C. D. Eisenbach and U. S. Schubert, *Macromolecules*, 1993, **26**, 7372–7374.
- M. D. Hager, P. Greil, C. Leyens, S. van der Zwaag and U. S. Schubert, *Adv. Mater.*, 2010, **22**, 5424–5430.
- R. Shunmugam, G. J. Gabriel, K. A. Aamer and G. N. Tew, *Macromol. Rapid Commun.*, 2010, **31**, 784–793.
- B. Happ, A. Winter, M. D. Hager and U. S. Schubert, *Chem. Soc. Rev.*, 2012, **41**, 2222–2255.
- R. Hoogenboom, D. Fournier and U. S. Schubert, *Chem. Commun.*, 2008, 155–162.
- W. Gerhardt, M. Črne and M. Weck, *Chem.–Eur. J.*, 2004, **10**, 6212–6221.
- H. Hofmeier and U. S. Schubert, *Chem. Commun.*, 2005, 2423–2432.
- J. M. Pollino and M. Weck, *Chem. Soc. Rev.*, 2005, **34**, 193–207.
- T. Aida, E. W. Meijer and S. I. Stupp, *Science*, 2012, **335**, 813–817.
- S.-K. Yang, A. V. Ambade and M. Weck, *Chem. Soc. Rev.*, 2012, **40**, 129–137.
- A. V. Ambade, S.-K. Yang and M. Weck, *Angew. Chem., Int. Ed.*, 2009, **48**, 2894–2898.
- K. P. Nair, V. Breedveld and M. Weck, *Macromolecules*, 2011, **44**, 3346–3357.
- U. S. Schubert, C. Eschbaumer, P. Andres, H. Hofmeier, C. H. Weidl, E. Herdtweck, E. Dulkeith, A. Morteani, N. E. Hecker and J. Feldmann, *Synth. Met.*, 2001, **121**, 1249–1252.
- U. S. Schubert, O. Hien and C. Eschbaumer, *Macromol. Rapid Commun.*, 2000, **21**, 1156–1161.
- U. S. Schubert, C. Eschbaumer and G. Hochwimmer, *Synthesis*, 1999, **5**, 779–782.
- H. Hofmeier, R. Hoogenboom, M. E. L. Wouters and U. S. Schubert, *J. Am. Chem. Soc.*, 2005, **127**, 2913–2921.
- U. Mansfeld, M. D. Hager, R. Hoogenboom, C. Ott, A. Winter and U. S. Schubert, *Chem. Commun.*, 2009, 3386–3388.
- S. Schmatloch, A. M. J. van den Berg, A. S. Alexeev, H. Hofmeier and U. S. Schubert, *Macromolecules*, 2003, **36**, 9943–9949.
- H. Hofmeier, S. Schmatloch, D. Wouters and U. S. Schubert, *Macromol. Chem. Phys.*, 2003, **204**, 2197–2203.
- D. Benoit, V. Chaplinski, R. Braslau and C. J. Hawker, *J. Am. Chem. Soc.*, 2001, **121**, 3904–3920.
- B. G. G. Lohmeijer and U. S. Schubert, *J. Polym. Sci., Part A: Polym. Chem.*, 2004, **42**, 4016–4027.
- M. Heller and U. S. Schubert, *J. Org. Chem.*, 2002, **67**, 8269–8272.
- H. Fischer, *Chem. Rev.*, 2001, **101**, 3581–3610.
- T. Fukuda, T. Terauchi, A. Goto, K. Ohno, Y. Tsuji, T. Miyamoto, S. Kobatake and B. Yamada, *Macromolecules*, 1996, **29**, 6393–6398.
- C. Ott, R. Hoogenboom and U. S. Schubert, *Chem. Commun.*, 2008, 3516–3518.



- 39 C. R. Becer, K. Babiuch, D. Pilz, S. Hornig, T. Heinze, M. Gottschaldt and U. S. Schubert, *Macromolecules*, 2009, **42**, 2387–2394.
- 40 C. Ott, C. Ulbricht, R. Hoogenboom and U. S. Schubert, *Macromol. Rapid Commun.*, 2012, **33**, 556–561.
- 41 W. Dempwolf, S. Flakus and G. Schmidt-Naake, *Macromol. Symp.*, 2007, **259**, 416–420.
- 42 T. Schulte, K. O. Siegenthaler, H. Luftmann, M. Letzel and A. Studer, *Macromolecules*, 2005, **38**, 6833–6840.
- 43 U. S. Schubert, A. Winter and G. R. Newkome, *Terpyridine-based Materials*, Wiley-VCH, Weinheim, 2011.
- 44 M. Chiper, M. A. R. Meier, D. Wouters, S. Hoepfener, C.-A. Fustin, J.-F. Gohy and U. S. Schubert, *Macromolecules*, 2008, **41**, 2771–2777.
- 45 M. Chiper, M. A. R. Meier, J. M. Kranenburg and U. S. Schubert, *Macromol. Chem. Phys.*, 2007, **208**, 679–689.
- 46 E. C. Constable and M. D. Ward, *J. Chem. Soc., Dalton Trans.*, 1990, 1405–1409.





## Supporting Information

to

### **Stimuli-responsive self-assembly of one-step prepared supramolecular heterotelechelic polymers**

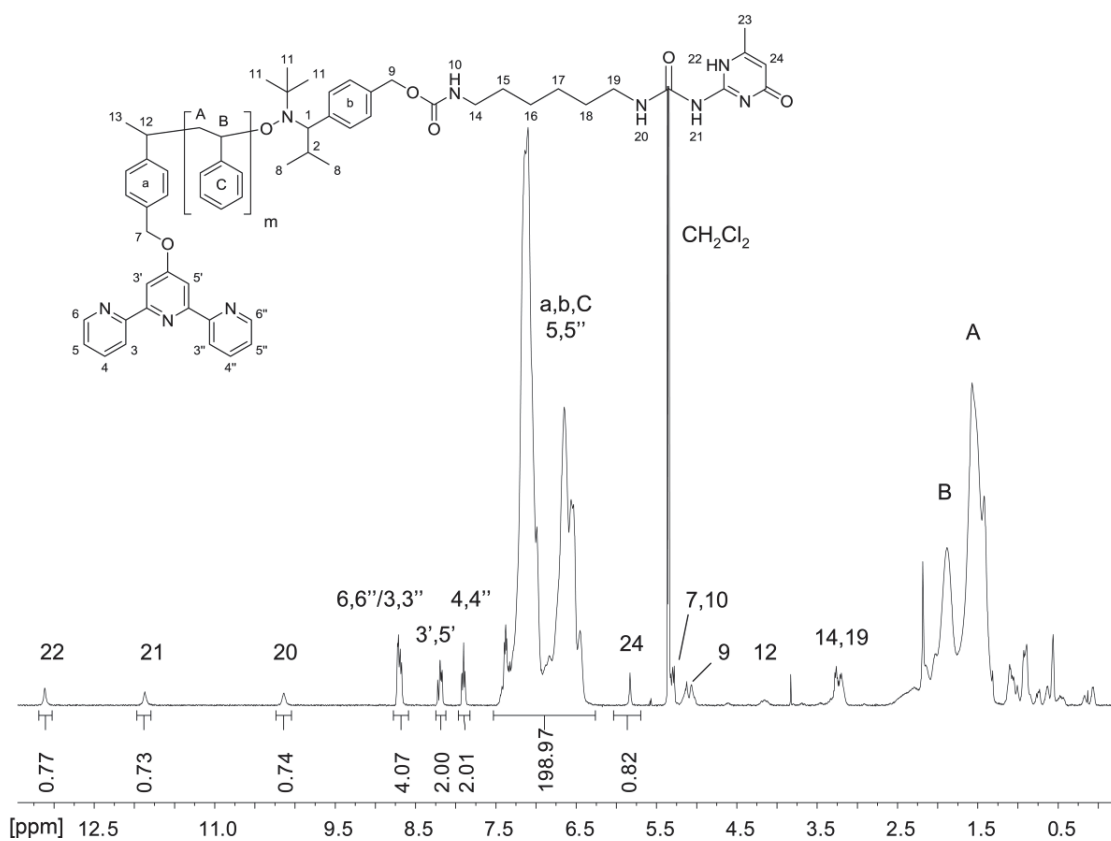
Ulrich Mansfeld,<sup>a,b,c</sup> Andreas Winter,<sup>a,b,c</sup> Martin D. Hager,<sup>a,b,c</sup> Richard Hoogenboom,<sup>d</sup> Wolfgang Günther<sup>a</sup> and Ulrich S. Schubert<sup>\*a,b,c</sup>

<sup>a</sup> *Laboratory of Organic and Macromolecular Chemistry (IOMC), Friedrich-Schiller-University Jena, Humboldtstr. 10, 07743 Jena, Germany. Fax: +49 (0)3641 948202; Tel: +49 (0)3641 948200; E-mail: ulrich.schubert@uni-jena.de; Internet: www.schubert-group.de*

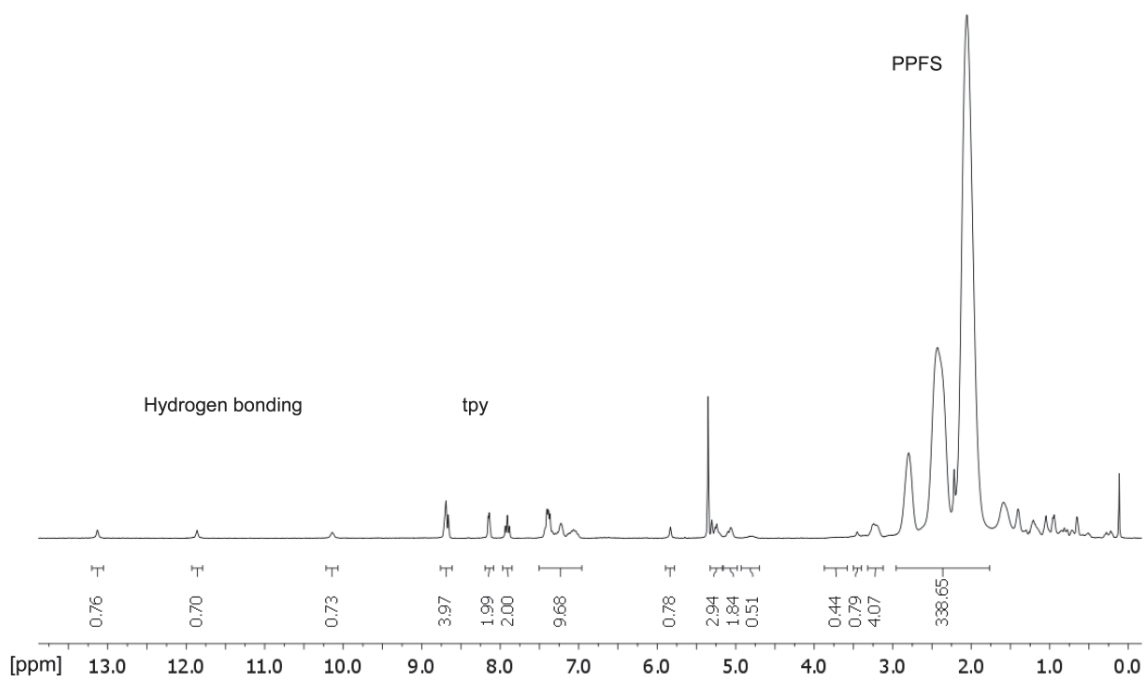
<sup>b</sup> *Jena Center for Soft Matter (JCSM), Friedrich-Schiller-University Jena, Philosophenweg 7, 07743 Jena, Germany*

<sup>c</sup> *Dutch Polymer Institute (DPI), P.O. Box 902, 5600 AX Eindhoven, The Netherlands*

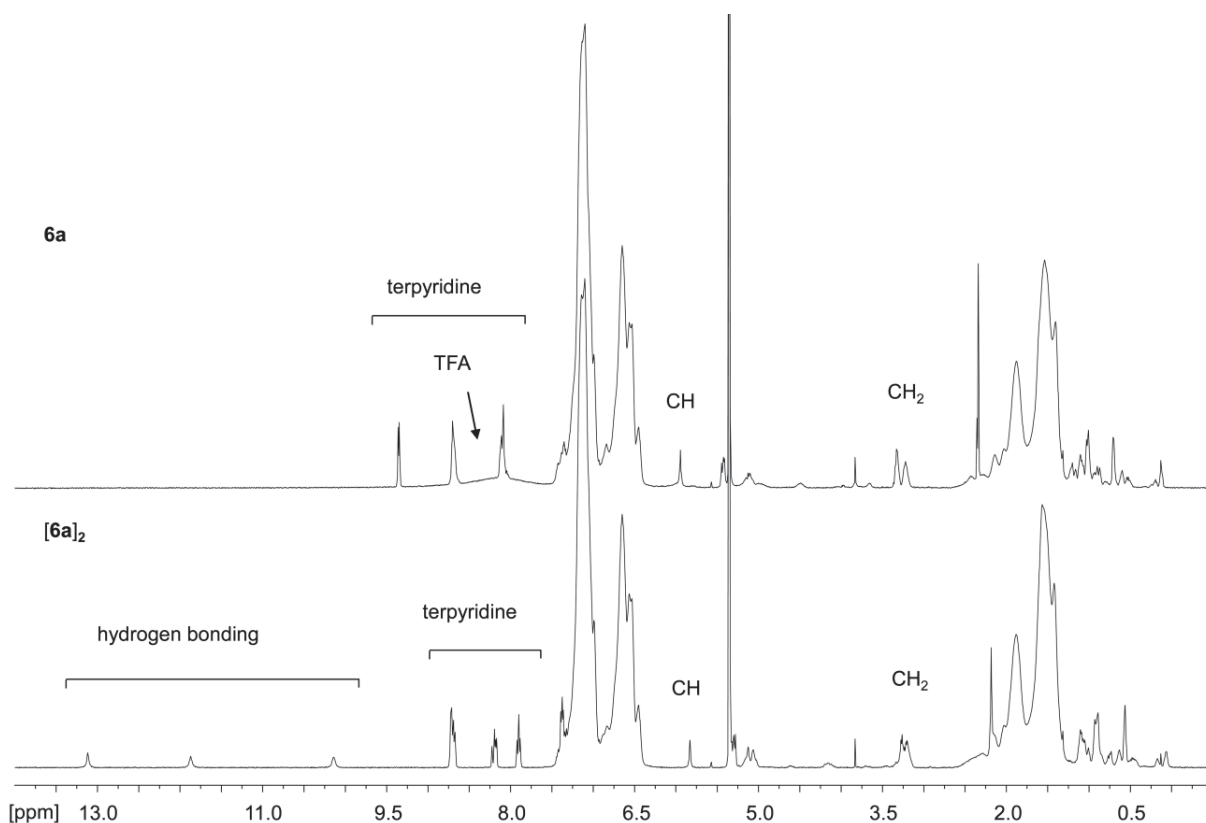
<sup>d</sup> *Department of Organic Chemistry, Ghent University, Krijkslaan 218 S4, 9000 Ghent, Belgium*



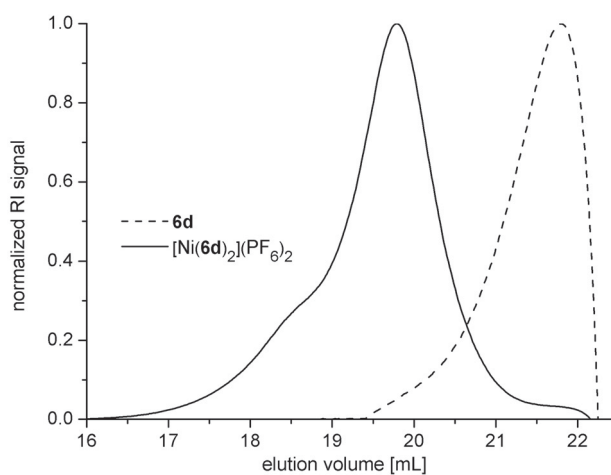
**Figure S1** <sup>1</sup>H NMR spectrum of tpy~PS~UPy **6a** (400 MHz, CD<sub>2</sub>Cl<sub>2</sub>).



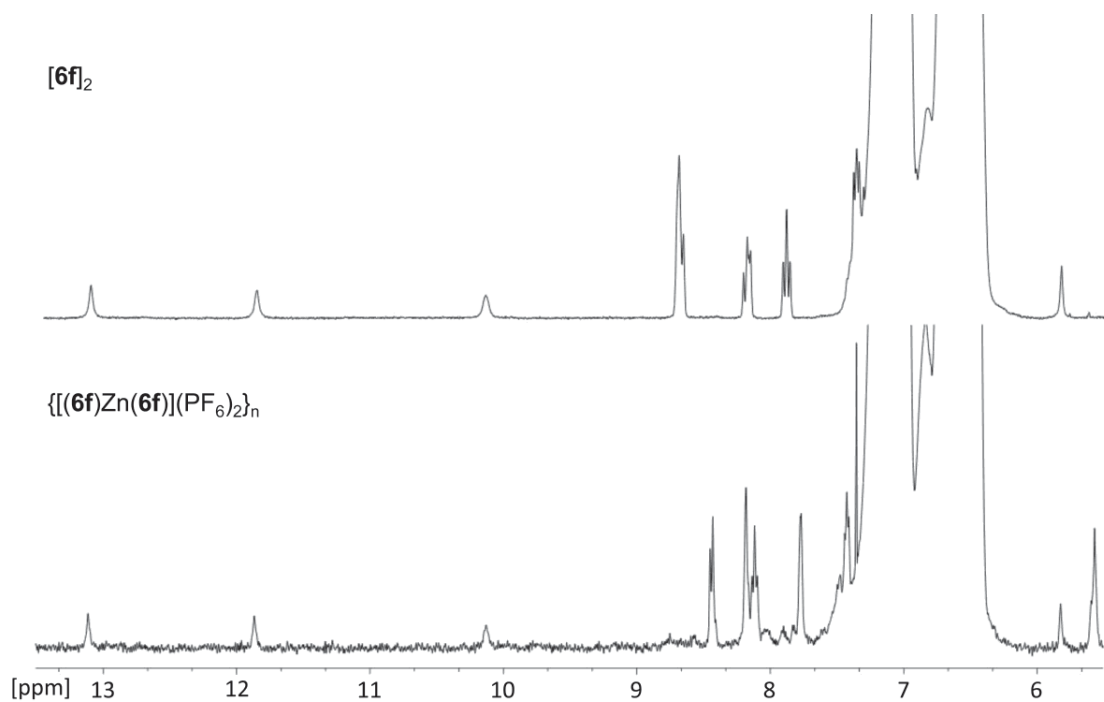
**Figure S2** <sup>1</sup>H NMR spectrum of tpy~PPFS~UPy **7** (400 MHz, CD<sub>2</sub>Cl<sub>2</sub>).



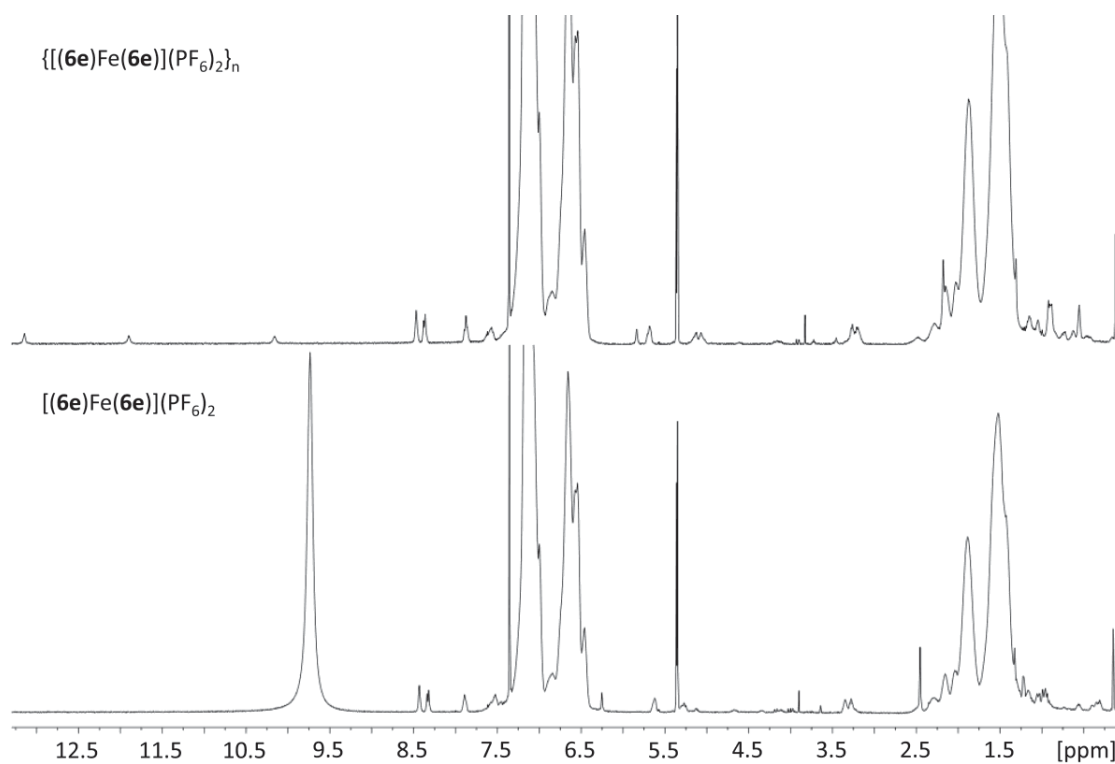
**Figure S3**  $^1\text{H}$  NMR spectra for the monomeric (denoted **6a**) and dimeric (denoted  $[\mathbf{6a}]_2$ ) species of tpy~PS~UPy in  $\text{CD}_2\text{Cl}_2$  (bottom) and  $\text{CD}_2\text{Cl}_2$ -TFA (top) (400 MHz,  $\text{CD}_2\text{Cl}_2$ , 298 K).



**Figure S4** SEC traces (RI signal) of **6** and  $[\text{Ni}(\mathbf{6d})_2](\text{PF}_6)_2$ ; eluent: DMAc containing 0.005 M  $\text{NH}_4\text{PF}_6$  (Figure was created from data published in *Chem. Commun.*, **2009**, 3386-3388).



**Figure S5** Zoom into the low-field region of the <sup>1</sup>H NMR spectra of  $(\mathbf{6f})_2$  (top) and  $\{[(\mathbf{6f})\text{Zn}(\mathbf{6f})](\text{PF}_6)_2\}_n$  (bottom) (400 MHz,  $\text{CD}_2\text{Cl}_2$ , 298 K).



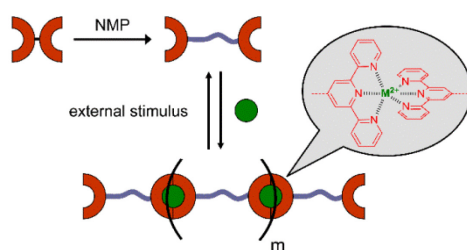
**Figure S6** <sup>1</sup>H NMR spectra of the linear supramolecular polymer  $\{[(\mathbf{6e})\text{Fe}(\mathbf{6e})](\text{PF}_6)_2\}_n$  (in  $\text{CD}_2\text{Cl}_2$ ) and the dimer  $[(\mathbf{6e})_2](\text{PF}_6)_2$  after the *in-situ* addition of TFA (400 MHz,  $\text{CD}_2\text{Cl}_2$ , 298 K).

## Publication P3:

### *A homotelechelic bis-terpyridine macroligand: one-step synthesis and its metallo-supramolecular self-assembly*

U. Mansfeld, A. Winter, M. D. Hager, W. Günther, E. Altuntas and U. S. Schubert

*J. Polym. Sci., Part A: Polym. Chem.* **2013**, *51*, 2006-2015



Reprinted with permission of John Wiley and Sons.  
Copyright © 2013 Wiley Periodicals, Inc.





# A Homotelechelic Bis-terpyridine Macroligand: One-Step Synthesis and Its Metallo-Supramolecular Self-Assembly

Ulrich Mansfeld,<sup>1,2,3</sup> Andreas Winter,<sup>1,2,3</sup> Martin D. Hager,<sup>1,2,3</sup> Wolfgang Günther,<sup>1</sup>  
Esra Altuntaş,<sup>1,2</sup> Ulrich S. Schubert<sup>1,2,3</sup>

<sup>1</sup>Laboratory for Organic and Macromolecular Chemistry (IOMC), Friedrich-Schiller-University Jena, Humboldtstr. 10, 07743 Jena, Germany

<sup>2</sup>Jena Center for Soft Matter (JCSM), Philosophenweg 7, 07743 Jena, Germany

<sup>3</sup>Dutch Polymer Institute (DPI), P.O. Box 902, 5600 AX Eindhoven, The Netherlands

Correspondence to: U. S. Schubert (E-mail: ulrich.schubert@uni-jena.de)

Received 6 November 2012; revised 23 December 2012; accepted 8 January 2013; published online 14 February 2013

DOI: 10.1002/pola.26586

**ABSTRACT:** A homotelechelic macroligand bearing two 2,2':6',2''-terpyridin-4'-yl units, as chain ends, is used as building block for the preparation of a linear metallo-supramolecular chain-extended polymer. The macroligand has been prepared by nitroxide-mediated polymerization (NMP) of styrene using a *bis*-terpyridine-functionalized NMP initiator. The controlled character of the NMP process has been confirmed by detailed characterization of the polymer by size-exclusion chromatography, nuclear magnetic resonance spectroscopy as well as mass spectrometry. Subsequently, the self-assembly with Fe<sup>II</sup> ions

into the chain-extended metallopolymer and the disassembly thereof, in the presence of a strong competitive ligand, has been studied by UV-vis absorption spectroscopy and diffusion-ordered NMR spectroscopy. The reversibility of the formation of the metallo-supramolecular material, when addressed by external stimuli, could be proven. © 2013 Wiley Periodicals, Inc. *J. Polym. Sci., Part A: Polym. Chem.* **2013**, *51*, 2006–2015

**KEYWORDS:** metal-polymer complexes; nitroxide-mediated polymerization; supramolecular structures; telechelic

**INTRODUCTION** The design of functional materials with tailor-made chemical and physical properties meeting the needs of various technology areas is one of the key challenges in today's polymer and material science. In particular, polymers precisely functionalized at their chain ends play an important role in view of potential applications, for example, in the synthesis of block copolymers, thermoplastic elastomers, polymer networks, surfactants, or as macromonomers.<sup>1</sup> Telechelic polymers are defined as polymeric molecules featuring reactive end-groups that have the capacity to enter into further polymerizations or other reactions.<sup>2</sup> Telechelics can be classified as mono-/semi-, di-, tri-, and multifunctional telechelics (i.e., polytelechelics).<sup>3</sup> In polymer science, the term "telechelic" typically refers to a linear polymer having the same functionality at both chain ends ("homotelechelic"); when the polymer chain possesses two different functional groups at its ends, it is called "heterotelechelic."<sup>4</sup> Thereby, the end-groups originate either from the initiator or the terminating agent (or the chain-transfer agents) in the case of polymers prepared by chain-growth reactions. In contrast, the functional groups could originate from monomer(s)

in typical polycondensation and polyaddition reactions, respectively.<sup>5</sup> The end-group modification may also take place in appropriate post-polymerization reactions. Starting from Bayer's and Ureack's pioneering work<sup>6,7</sup> this class of polymeric materials has attracted considerable interest in current research.<sup>4</sup>

The precise control of the polymerization process is crucial for the preparation of well-defined telechelics and other end-functionalized macromolecules.<sup>8</sup> Traditionally, control over the degree-of-functionality, the molar mass as well as the uniformity (i.e., polydispersity) was accomplished using living ionic polymerization techniques.<sup>9</sup> As a drawback, the ionic processes suffer from stringent synthetic requirements and, in some cases, are sensitive to the functional groups to be incorporated. In contrast, free radical polymerization is flexible and less sensitive to the polymerization conditions and tolerates a large variety of functional groups. However, free radical polymerization reactions suffer from poor control over the molar mass and degree-of-functionalization (due to competing coupling, disproportionation reactions

Additional Supporting Information may be found in the online version of this article.

© 2013 Wiley Periodicals, Inc.

and uncontrolled chain transfer). The vast developments in controlled radical polymerization (CRP) nowadays provide access to well-defined telechelic polymers with controlled functionality.<sup>10</sup> In this respect, the atom-transfer radical polymerization,<sup>11,12</sup> the nitroxide-mediated polymerization (NMP),<sup>13</sup> the reversible addition-fragmentation chain-transfer polymerization<sup>14</sup> and others<sup>15–18</sup> have been used for the preparation of telechelic polymers.<sup>4,19</sup> For the most common CRP methods, two main strategies for synthesizing telechelic polymers can be pointed out:<sup>20,21</sup> functionalities can be incorporated onto the initiating and/or the terminating fragment of initiators providing  $\alpha,\omega$ -difunctionalized,  $\alpha$ -functionalized and  $\omega$ -functionalized telechelic polymers, respectively. Moreover, one type or two different types of functionalities can be attached to yield homotelechelic and heterotelechelic polymers, respectively. Alternatively, the functionalization of the chain ends can be achieved by appropriate post-polymerization reactions. However, the former approach has a wider scope by means of construction flexibility compared to a postmodification approach for telechelic polymers, as the chain length and composition between the functionalities can be varied in less reaction steps and purification can be simply performed by precipitation.

In this study, a homodifunctional alkoxyamine based on the TIPNO nitroxide was utilized for the synthesis of a homotelechelic polymer via NMP. Functionalized TIPNO derivatives were initially reported by Hawker and coworkers<sup>22,23</sup> as universal initiators for NMP featuring a high end-group fidelity and a high tolerance toward a broad range of functional groups (TIPNO: 2,2,5-trimethyl-4-phenyl-3-azahexane-3-nitroxide). Schubert and co-workers expanded the scope of functional TIPNOs to the field of terpyridine chemistry by using tpy-TIPNO, as initiator, for the synthesis of terpyridine-functionalized semi-telechelic block copolymers via NMP.<sup>24–27</sup> Later, the utilization of a heterodifunctional TIPNO initiator featuring one terpyridine (tpy) and one 2-ureido-4*H*-pyrimidone (UPy) moiety, as orthogonal supramolecular binding sites, for the NMP of styrenes was reported.<sup>28,29</sup> The heterotelechelic polymers were self-assembled into supramolecular chain-extended polymers exhibiting stimuli-responsive behavior based on the orthogonality of the non-covalent interactions. The homodifunctional initiator bearing two tpy moieties would be a versatile building block for the preparation of metallo-supramolecular chain-extended polymers based on in-chain metal-to-ligand coordinative bonds.<sup>24,30–33</sup> Herein, the synthesis of the initiator, its application in the NMP of styrene and the subsequent reversible formation of a chain-extended polymer via metal-ion complexes is reported.

## EXPERIMENTAL

All chemicals were received from Aldrich, Fluka and Acros; solvents were purchased from Biosolve. Unless otherwise stated, the chemicals and solvents were used without further purifications. DMF was dried over molsieves (pore size of 4 Å). THF and toluene were dried using a PureSolv-EN<sup>TM</sup> solvent purification system. Column chromatography was carried out on silica gel 60 and standardized aluminum oxide 90

(Merck). Styrene was freshly purified prior to use by filtration over neutral aluminum oxide 90 (Merck). 1D (<sup>1</sup>H, <sup>13</sup>C) and 2D (<sup>1</sup>H–<sup>1</sup>H COSY, DOSY) nuclear magnetic resonance (NMR) experiments were conducted on a Bruker 400 MHz spectrometer at 298 K. Chemical shifts are reported in parts per million (ppm) downfield from tetramethylsilane and were calibrated to the residual solvent peaks. Deuterated solvents for NMR spectroscopy were obtained from Cambridge Isotope Laboratories as well as Eurisotop. For size-exclusion chromatography (SEC) an Agilent system equipped with a PSS Degasser, a G1310A Pump, a G1329A AS, a G1362A RID detector and a PSS GRAM guard/1000/30 column was used. Dimethylacetamide (DMA) containing 0.21% LiCl was used as eluent with a flow rate of 1 mL/min at 40 °C. Linear polystyrene was used as the calibration standard. Gas chromatographic (GC) measurements were performed on an Interscience Trace GC with a Trace Column RTX-5 connected to a PAL autosampler. UV-vis absorption spectra were recorded in diluted chloroform solutions on a Perkin-Elmer Lambda-45 UV-vis spectrophotometer at room temperature (1-cm cuvettes). GC mass spectrometry was conducted on a Shimadzu GC17A connected to a mass spectrometer. Infrared spectra were recorded on a Bruker IFS55 FT-IR spectrometer. Matrix-assisted laser desorption/ionization time-of-flight mass spectrometry (MALDI-TOF MS) was performed on a Voyager-DE<sup>TM</sup> PRO Biospectrometry<sup>TM</sup> Workstation (Applied Biosystems) time-of-flight mass spectrometer using linear and reflector mode for operation. Dithranol or 2-[(*ZE*)-3-(4-*tert*-butylphenyl)-2-methylprop-2-enylidene]malononitrile (DCTB) were used as matrices and NaI as additive. The spectra were recorded in the positive ion mode and ionization was performed with a 337 nm pulsed nitrogen laser. The MALDI-TOF mass spectra of polymers were also measured on a Bruker Ultraflex<sup>TM</sup> III TOF/TOF spectrometer. Electrospray ionization time-of-flight (ESI-TOF) mass spectrometric measurements were performed in the positive ion mode with a micrOTOF (Bruker Daltonics) mass spectrometer equipped with an automatic syringe pump which is supplied from KD Scientific for sample injection. The standard ESI source was used to generate the ions. For polymer samples, a concentration of 10  $\mu\text{g mL}^{-1}$  was used (solvent: chloroform/acetonitrile mixtures) and injected at a constant flow of the sample solution (3  $\mu\text{L min}^{-1}$ ). No salt or acid addition prior to analysis was required, ionization occurred readily from the sodium content that is naturally present in the glass or in the polymer sample. The ESI-Q-TOF MS instrument was calibrated in the *m/z* range of 50 to 3000 using a calibration standard which is supplied from Agilent (Tunemix solution). All data were processed via Bruker's data analysis software version 4.0. The ESI mass spectra were deconvoluted to obtain singly charged species, from the deconvoluted spectrum the  $M_n$  value of the polymer was calculated. The following compounds were prepared according to literature procedures: *N*-(*Tert*-butyl)-*O*-(1-(4-(chloromethyl)phenyl)ethyl)-*N*-(2-methyl-1-(4-(((tetrahydro-2*H*-pyran-2-yl)oxy)methyl)phenyl)propyl)hydroxylamine (**1**),<sup>28</sup> 2,2':6',2''-terpyridin-4' (1'*H*)-one (**2**),<sup>34</sup> *O*-(1-(4-(((2,2':6',2''-terpyridin-4'-yloxy)methyl)phenyl)ethyl)-*N*-(*tert*-butyl)-*N*-(2-methyl-1-(4-(((tetrahydro-2*H*-pyran-2-yl)-oxy)methyl)phenyl)propyl)hydroxylamine (**3**)<sup>28</sup> and 4-(1-(((1-(4-(((2,2':6',2''-terpyridin-4'-

xyloxy)methyl]phenyl)ethoxy)(*tert*-butylamino)-2-methylpropyl-phenyl)methanol (**4**).<sup>28</sup>

*N*-(1-(4-((2,2':6',2''-Terpyridin-4'-yloxy)methyl)phenyl)-2-methylpropyl)-*O*-(1-(4-((2,2':6',2''-terpyridin-4'-yloxy)methyl)phenyl)ethyl)-*N*-(*tert*-butyl)hydroxylamine (**tpy-TIPNO-tpy**, **5**). Triphenylphosphine (100 mg, 0.38 mmol), **3** (70 mg, 0.11 mmol) and 2,2':6',2''-terpyridin-4' (1'*H*)-one (35 mg, 0.14 mmol) were dissolved in dry THF (1.5 mL). Diisopropyl azodicarboxylate (DIAD, 77 mg, 0.38 mmol) was added dropwise to the solution. Subsequently, the reaction mixture was stirred overnight at room temperature. The solution was concentrated and subjected to a precolumn (Al<sub>2</sub>O<sub>3</sub>, eluent: heptane-to-chloroform gradient) to remove instable, gas-generating byproducts. The concentrated oil was subsequently purified by column chromatography (Al<sub>2</sub>O<sub>3</sub>; eluent: diethyl ether/pentane, 4:1 ratio) and preparative SEC (BioRad beads S-X8; eluent: dichloromethane) to yield **5** as a colorless amorphous solid (69 mg, 70%, mixture of diastereomers).

<sup>1</sup>H NMR (400 MHz, CD<sub>2</sub>Cl<sub>2</sub>,  $\delta$ , diastereomers a+b): 0.20 (d, *J* = 6.5 Hz, 3H, a), 0.58 (d, *J* = 6.4 Hz, 3H, b), 0.83 (s, 9H, b), 0.95 (d, *J* = 6.2 Hz, 3H, a), 1.09 (s, 9H, a), 1.35 (d, *J* = 6.3 Hz, 3H, b), 1.38–1.51 (m, 1H, a), 1.59 (d, *J* = 6.5 Hz, 3H, a), 1.68 (d, *J* = 5.3 Hz, 3H, b), 2.28–2.49 (m, 1H, b), 3.39 (d, *J* = 10.8 Hz, 1H, a), 3.52 (d, *J* = 10.6 Hz, 1H, b), 4.99 (q, *J* = 6.5 Hz, 2H, a+b), 5.27 (s, 2H, a/b), 5.32 (s, 2H, b), 5.34 (s, 2H, a/b), 5.37 (s, 2H, a), 7.27–7.66 (m, 16H, a+b), 7.27–7.40 (m, 8H, a+b), 7.82–7.94 (m, 8H, a+b), 8.11–8.20 (m, 8H, a+b), 8.58–8.77 (m, 16H, a+b); <sup>13</sup>C NMR (100 MHz, CD<sub>2</sub>Cl<sub>2</sub>,  $\delta$ , diastereomers a+b): 20.6, 20.8, 21.7, 21.8, 22.7, 24.4, 28.0, 28.2, 31.7, 32.0, 53.4, 60.4, 60.5, 69.9, 70.0, 70.1, 70.1, 71.7, 71.8, 82.5, 83.3, 107.4, 107.5, 121.1, 123.9, 126.5, 126.7, 127.4, 127.4, 127.6, 131.2, 131.3, 134.0, 134.3, 134.6, 135.4, 136.7, 142.3, 142.6, 144.9, 145.8, 149.1, 155.9, 156.0, 157.2, 167.0, 167.0, and 167.1; MALDI-TOF MS (*m/z*, matrix: DCTB): 870.46 [(M+Na)<sup>+</sup>]; High resolution ESI-MS: anal. calcd. for [C<sub>54</sub>H<sub>53</sub>N<sub>7</sub>O<sub>3</sub>Na]<sup>+</sup> *m/z* = 870.4102, found: *m/z* = 870.4103.

#### General Procedure for the Polymerization of Styrene

Styrene was freshly purified by filtration over Al<sub>2</sub>O<sub>3</sub> prior to use to remove the inhibitor. Solvents were used as supplied. To a clear solution of the initiator **5** in anisole, freshly purified styrene was added to the polymerization vessel. After applying three freeze-pump-thaw-cycles to remove the oxygen, argon was added and the vessel was immersed in an oil bath at 123 °C for a certain period of time. To remove residual monomer the reaction mixture was precipitated from chloroform into cold methanol. The conversion was determined by GC measurements, the molar masses (*M<sub>n</sub>*, *M<sub>w</sub>*) and the polydispersity index (PDI) were determined by SEC, whereas <sup>1</sup>H NMR spectroscopy was used for the calculation of the end-group functionality (by integration and comparison of the corresponding end-group signals) and *M<sub>n</sub>* values (by the integration of the polymer backbone to the terpyridine signals).

#### tpy-PS-TIPNO-tpy (**6b**)

<sup>1</sup>H NMR (400 MHz, CD<sub>2</sub>Cl<sub>2</sub>):  $\delta$  = 0.05–2.64 (set of multiplets), 3.15–3.41 (m, 1H), 4.03–4.25 (m, 1H), 5.22–5.41 (m,

4H), 6.34–7.54 (m, 550H), 7.90 (m, 4H), 8.11–8.26 (m, 4H), 8.62–8.76 (m, 8H) ppm. SEC (CHCl<sub>3</sub>, RI): *M<sub>n</sub>* = 10,000 g mol<sup>-1</sup>, PDI = 1.17.

#### UV-Vis Titration Experiments

The macroligand (**6b** 0.85 mg) was dissolved in chloroform (20 mL) and FeCl<sub>2</sub> (0.913 mg, 0.0072 mmol) was dissolved in methanol (10 mL). The methanol solution was subsequently added to the polymer solution in steps of 10  $\mu$ L while the formation of the Fe<sup>II</sup> *bis*-complex was monitored by UV-vis absorption spectroscopy after each addition. The point-of-equivalence and the *M<sub>n</sub>* value of the macroligand were obtained by plotting the UV-vis absorption intensity at the LC (319 nm) and the absorption band at 559 nm [mainly ascribed to the metal-to-ligand charge-transfer (MLCT)] as a function of added Fe<sup>II</sup> ions.

#### Metallo-Polymerization of **6b**

A solution of FeCl<sub>2</sub> · 4H<sub>2</sub>O (0.015 mmol) and SnCl<sub>2</sub> · 2H<sub>2</sub>O (0.015 mmol) in methanol (300  $\mu$ L) was added to a solution of **6b** (0.010 mmol) in chloroform (1.2 mL). The resultant clear solution was stirred under an argon atmosphere at 40 °C for 24 h. After cooling to room temperature and adding an excess of NH<sub>4</sub>PF<sub>6</sub> (ca., 15 eq.) the reaction mixture was partitioned between water and dichloromethane. The organic phase was washed three times with water, dried over Na<sub>2</sub>SO<sub>4</sub> and concentrated *in vacuo* to result the chain-extended polymer.

{[Fe(**6b**)<sub>2</sub>](PF<sub>6</sub>)<sub>2</sub>]<sub>*n*</sub>. <sup>1</sup>H NMR (400 MHz, CD<sub>2</sub>Cl<sub>2</sub>):  $\delta$  = 0.46–2.67 (set of multiplets), 3.24–3.51 (m, 1H), 4.12–4.30 (m, 1H), 5.61–5.81 (m, 4H), 6.35–7.48 (m, 570H), 7.50–7.71 (m, 4H) 7.80–7.94 (m, 4H), 8.28–8.54 (m, 8H) ppm.

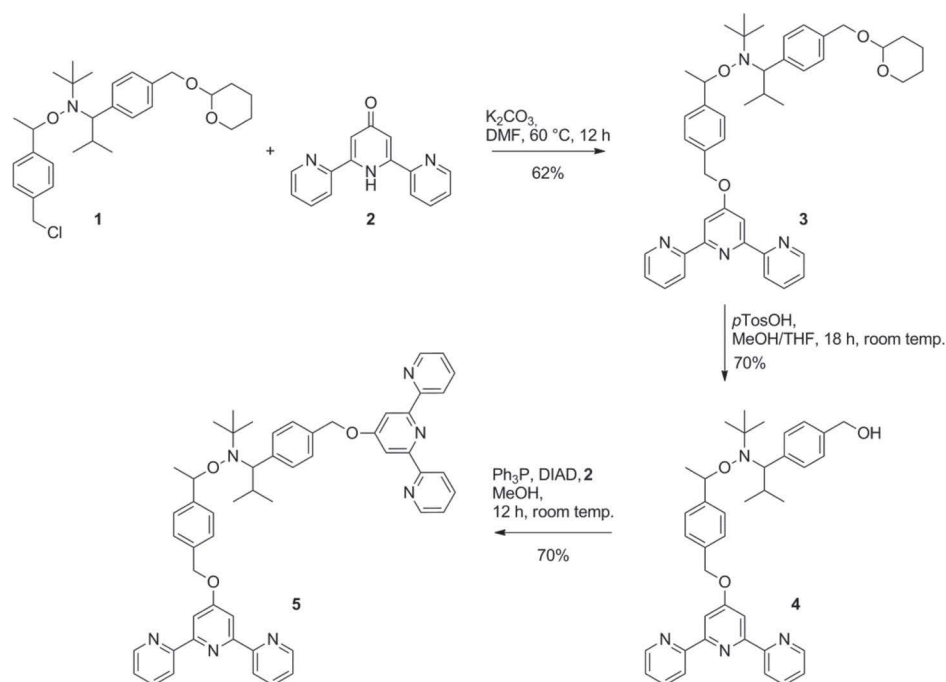
#### DOSY NMR Experiments of {[Fe(**6b**)<sub>2</sub>](PF<sub>6</sub>)<sub>2</sub>]<sub>*n*</sub>

For the DOSY experiment 30 mg of the supra-polymer {[Fe(**6b**)<sub>2</sub>](PF<sub>6</sub>)<sub>2</sub>]<sub>*n*</sub> were dissolved in 1 mL dichloromethane-*d*<sub>2</sub>/methanol-*d*<sub>4</sub> (4:1) and measured at 298 K. For the investigation of the responsiveness, 50  $\mu$ L of an aqueous solution (35%) of HEEDTA was added into the NMR tube and after 10 min the DOSY was measured again.

## RESULTS AND DISCUSSION

The synthesis of the homodifunctional initiator tpy-TIPNO-tpy (**5**) was carried out via stepwise functionalization of the nitroxide derivative **1** (Scheme 1). As reported previously,<sup>28,29</sup> the terpyridine-containing initiator **4**, as key building block, was obtained by nucleophilic substitution reaction of the heterodifunctional alkoxyamine **1** with 2,2':6',2''-terpyridin-4' (1'*H*)-one (**2**) and subsequent cleavage of the THP-protecting group from the intermediate **3** (THP: tetrahydropyrane). Finally, the homodifunctional system **5** could be prepared in high yield via Mitsunobu coupling of **4** with **2**.<sup>35,36</sup>

The telechelic initiator was characterized by NMR spectroscopy and mass spectrometry. The central TIPNO moiety has two stereogenic centers. Thus, **5** was obtained as a mixture of two diastereomers. Consequently, two main sets of signals (in a ca. 1:1 ratio) could be observed in the <sup>1</sup>H and (partially) also in the <sup>13</sup>C NMR spectrum (see Fig. 1 and Supporting



**SCHEME 1** Schematic representation of the synthesis of telechelic **5** via stepwise functionalization.

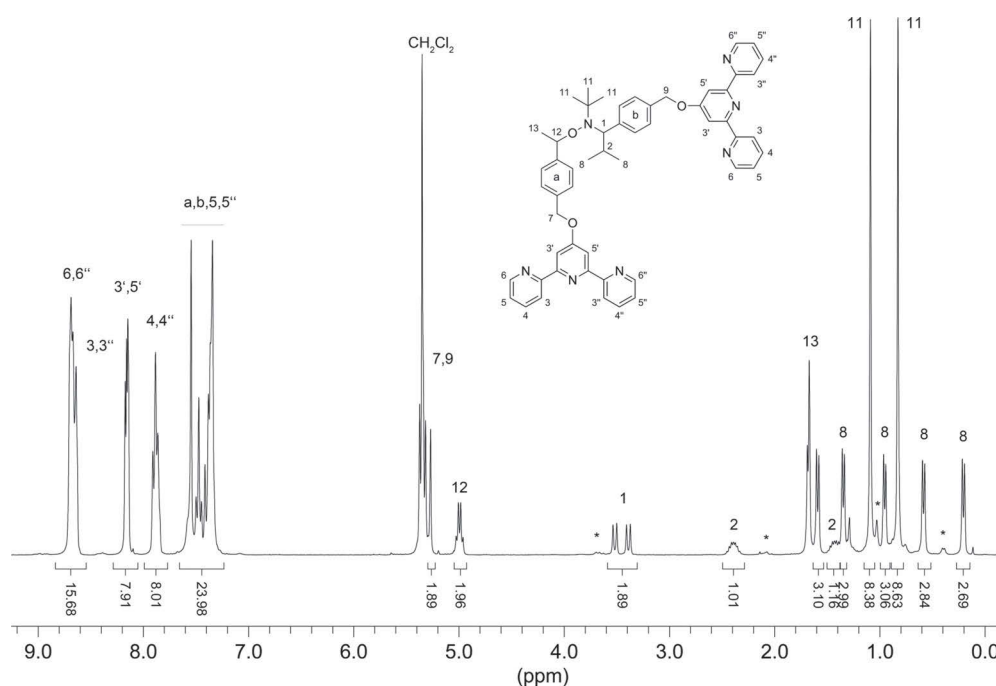
Information Fig. S1). The attachment of the second terpyridine entity was characterized in the  $^1\text{H}$  NMR spectrum by a quantitative shift of the signals for the benzyl group compared to alkoxyamine **4**, that is, for the methylene group **9** (4.5 ppm to 5.4 ppm) and the aromatic protons **b** (7.2–7.5 ppm; Fig. 1). The full assignment of these signals could be carried out unambiguously by 2D NMR experiments. Admittedly, additional signals could be observed in the  $^1\text{H}$  NMR spectra, which are still present after repeated column chromatography as well as preparative SEC purifications of the product. After careful analysis of these signals in the 2D NMR spectra, they show a similar cross peak pattern as the desired structure **5** and, thus, the presence of the analogous *meta*-substituted isomer can be concluded (commercially available 4-chloromethylstyrene, used for the synthesis of **1**, consists of a mixture of *para*- and *meta*-isomers in a about 9:1 ratio, see Supporting Information Fig. S2). In this vein, MALDI-TOF mass spectrometric analysis of **5** showed only the expected  $[\text{M}+\text{H}]^+$  adduct at  $m/z = 870.46$ , the experimental isotopic pattern was in good agreement with the calculated value of  $m/z = 870.41$  (Fig. 2). All additional peaks at lower  $m/z$  values could be assigned to fragments of **5**, as supported by the parent ion peaks from the spectrum in the LIFT mode. The main peaks at  $m/z = 389$  and  $504$  are ascribed to the  $\text{Na}^+$ -adducts of fragments pointing to a fragmentation at the thermally labile  $\text{NO}-\text{C}$  bond of the alkoxyamine entity under the measurement conditions. Alkoxyamine **5** was further confirmed by high resolution ESI-TOF MS measurements, where also the  $\text{Na}^+$  adduct could be experimentally found ( $m/z = 870.4103$ ), deviated by only  $m/z = 0.0001$  from the calculated value ( $m/z = 870.4102$ ; see the isotopic pattern in the Supporting Information Fig. S3).

In view of homotelechelic polymers featuring terpyridine moieties at both chain ends, the NMP initiated by **5** has to meet several criteria: the polymerization has to be of controlled nature (a) and exhibit a high end-group fidelity (b), that is, the functional groups at both chain ends must not be cleaved in course of the polymerization.<sup>4,37</sup>

As a model reaction, the NMP of styrene, initiated by **5**, was investigated (Scheme 2, Table 1): The polymerization process is controlled and oligomers and polymers (up to  $M_n = 10,000 \text{ g mol}^{-1}$ ) with PDI values below 1.2 were obtained (**6a,b**). In the  $^1\text{H}$  NMR spectrum of **6b** (Supporting Information Fig. S4) a high field shift for the protons next to the nitroxide at the position **12** (5.0 ppm to 4.2 ppm) and **1** (3.5 ppm to 3.3 ppm; Fig. 1) could be observed pointing to the insertion of the styrene between the initiating and the mediating fragment. The  $M_n$  values calculated from NMR seem to overestimate the molar mass that was theoretical expected, while the  $M_n$  values obtained from the SEC are in the same range (Table 1). Since low polydispersity index values (PDI) alone are not a stringent evidence for a controlled progress of a polymerization reaction, kinetics investigations were also performed. For this purpose, different reaction vessels were equipped with **5** and styrene (solvent: anisole); after the removal of oxygen, the vessels were subjected to an oil bath (temperature:  $123 \text{ } ^\circ\text{C}$ ) and the reactions were stopped after certain periods of time (up to 5 h).

With increasing polymerization time, the SEC traces of tpy-PS-TIPNO-tpy (**6c-e**) were shifted to shorter elution times corresponding to an increase of the molar mass. For all samples taken narrow, unimodal curves could be observed indicating control over the polymerization (Fig. 3). The kinetic





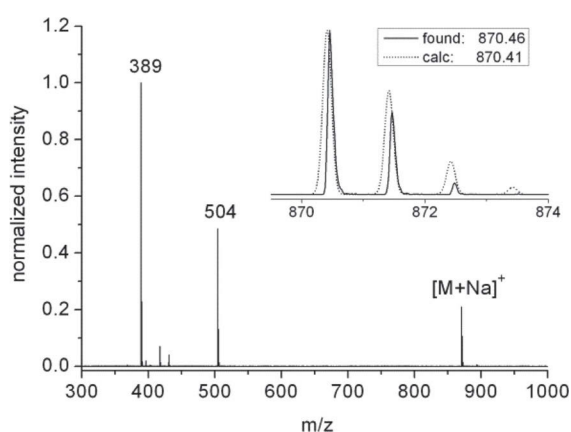
**FIGURE 1**  $^1\text{H}$  NMR spectrum of **5** (400 MHz,  $\text{CD}_2\text{Cl}_2$ , 298 K). The signals arising from the meta-substituted regioisomer are marked with asterisks (see 2D  $^1\text{H}$ - $^1\text{H}$  COSY evaluation in Supporting Information Fig. S2).

plots, that is, the semilogarithmic plot for the polymerization index as a function of time ( $\ln([M_0]/[M])$  vs.  $t$ ) and the plot for the molar mass vs. conversion revealed a linear dependency [Fig. 4(a,b)].

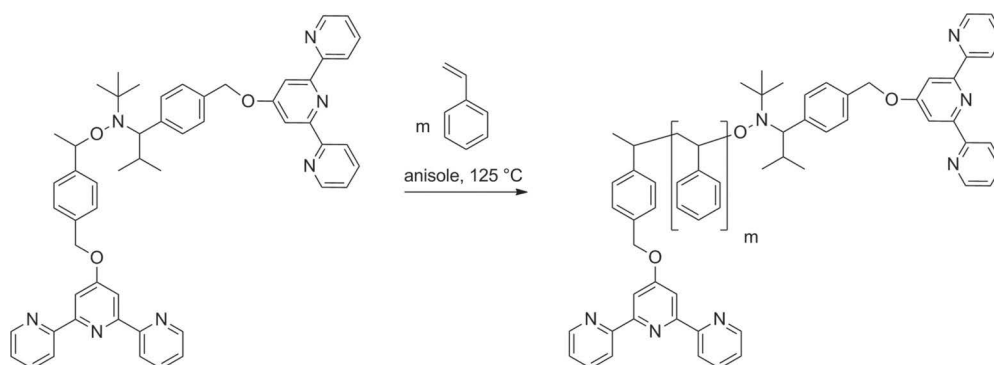
The observed  $M_n$  values were in good agreement with the theoretical ones showing narrow polydispersity index values ( $\text{PDI} < 1.2$ ) (Table 1, Fig. 4). Thus, the homodifunctional initiator **5** enables the polymerization of styrene under the used conditions in a controlled fashion at least up to a con-

version of 40%. In contrast to the heterotelechelic initiator bearing one tpy as well as one UPy moiety no persistent radical effect was observed under the same conditions for the polymerization of styrene.<sup>29</sup>

The purified polymer **6a** was characterized by mass spectrometry, in particular with respect to end-group analysis. However, MALDI-TOF MS was found to be ineligible in this case due to a distinct fragmentation behavior (Supporting Information Fig. S5). As known from literature, the characterization of nitroxide-functionalized polymers by mass spectrometry is often difficult due to the complex fragmentation during the MALDI-process.<sup>38,39</sup> One major distribution, showing peak-to-peak distances of  $m/z = 104$  as it is typical for polystyrene, could be observed; however, the peaks could neither be correlated to the expected telechelic materials nor to reasonable fragmentations, that were found for parent heterotelechelic polystyrenes<sup>29</sup>—independent from the nature of the applied matrix (dithranol, DCTB) or the ionic additive (e.g.,  $\text{Na}^+$ ,  $\text{Ag}^+$ ). In contrast, the ESI-TOF MS using a milder ionization method exhibited in the mass spectrum two main distributions for **6a** corresponding to doubly and triply charged polystyrene species, respectively (Fig. 5). After careful analysis, the main distribution could be assigned to a PS series, where one of the terpyridine units was cleaved off during the ESI-TOF measurement leaving the central TIPNO moiety still intact. The predetermined breaking point is ascribed to the benzylic bond of the terpyridine entity. Due to the assigned fragmentation, only one terpyridine can here directly be proven as end-group. Nonetheless, the main fragmentation promotes the assumption that also the second tpy



**FIGURE 2** MALDI-TOF mass spectrum of **5**; the inset shows the comparison of the experimental and the calculated isotopic pattern for the  $[\text{C}_{54}\text{H}_{53}\text{N}_7\text{O}_3+\text{Na}]^+$  peak. A fragmentation of **5** due to the labile alkoxyamine N—O bond give rise to the additional signals  $m/z = 389$  and 504 (matrix: DCTB).



**SCHEME 2** Schematic representation of the polymerization of styrene using **5** as initiator.

is incorporated into the polymer; since this unusual degradation is most likely caused by the ESI-process and not by thermal degradation during polymerization.

However, the intact telechelic PS bearing both tpy units could be assigned to a sub distribution (Supporting Information Fig. S6). The isotopic pattern as obtained from high-resolution ESI measurements was in good agreement with the calculated one: The calculated pattern for the triply charged species  $[C_{54}H_{53}N_7O_3(C_8H_8)_{63}+3H]^{3+}$  deviated by only  $m/z = 0.0004$  from the experimental found value (Supporting Information Fig. S6) which confirms the incorporation of both tpy units into the polystyrene. The  $M_n$  value of  $8500 \text{ g mol}^{-1}$  for **6a** was derived from the deconvoluted mass spectrum of the singly charged species. The number-averaged molar mass obtained from ESI measurements is in agreement with the one derived from SEC ( $M_n = 7200 \text{ g mol}^{-1}$ ).

More important, 2D ( $^1\text{H}$ – $^1\text{H}$ ) DOSY experiments were carried out to confirm that the terpyridine units (representing small molecules) were attached to polystyrene chains (representing in comparison rather large molecules), which could be recognized by similar relative diffusion coefficients (similar to Fig. 9 right). However, the presence of small amounts of mono- or non-functionalized polystyrene, for example, formed by auto-polymerization of styrene, could not be excluded by this method (this point will be addressed below).

The complexation of the terpyridine sites, in particular by divalent transition metal ions, is of importance—from an

analytic as well as a synthetic point of view. From an analytical point of view, UV-vis titration experiments with  $\text{Fe}^{\text{II}}$  ions were carried out to determine the number-averaged molar mass of **6b** via one further independent method. For this purpose, the evolution of the ligand-centered and the MLCT at related absorptions at 318 and 559 nm, respectively, were plotted as a function of added  $\text{Fe}^{\text{II}}$  ions (Fig. 6). The point-of-equivalence indicates the full consumption of free tpy sites by complexation at a 1:1 ratio of the macroligands and  $\text{Fe}^{\text{II}}$  ions (i.e., formation of  $[\text{Fe}(\text{tpy})_2]^{2+}$  complexes). The  $M_n$  value of  $7500 \text{ g mol}^{-1}$ , as calculated from this experiment, was roughly in the same range as the values derived from the other analytical methods (Table 1) while showing an underestimation as it is reported for the heterotelechelic tpy functionalized PS bearing the 2-ureido-4*H*-pyrimidone (UPy) moiety on the other end.<sup>29</sup>

From a synthetic point of view, the complexation of divalent metal ions is in the present case important, since the complexation with the telechelic polystyrene is the strongest supramolecular driving force that can be used to engineer defined suprapolymeric structures.

The incorporation of **6**, as ditopic macroligand, into a metallo-supramolecular chain-extended polymer can be achieved by complexation with divalent transition metal ions via formation of *bis*-terpyridine complexes of (distorted) octahedral geometry.<sup>24</sup> According to the theory of polyaddition reactions, polymers of maximum molar masses are

**TABLE 1** Overview of the Synthesized Telechelic Polystyrenes using Alkoxyamine **5** as Initiator at 125 °C with a Monomer to Initiator Ratio of 200:1 and a Monomer Concentration of  $3 \text{ mol L}^{-1}$

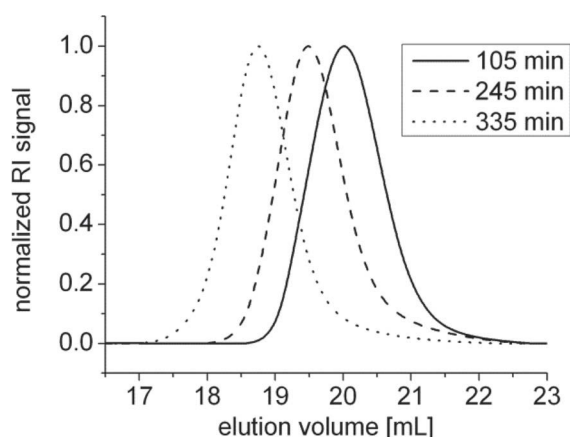
	Time [min]	Conv. [%] (GC)	$M_n$ [ $\text{g mol}^{-1}$ ] (theo.) <sup>a</sup>	$M_n$ [ $\text{g mol}^{-1}$ ] ( $^1\text{H}$ NMR)	$M_n$ [ $\text{g mol}^{-1}$ ] (SEC) <sup>b,c</sup>	PDI (SEC)
<b>6a</b>	320	–	–	9,500	7,200	1.18
<b>6b</b>	380	40	9,300	12,100	10,100	1.17
<b>6c</b>	105	15	4,450	–	4,500	1.15
<b>6d</b>	245	23	6,150	–	6,000	1.18
<b>6e</b>	335	39	10,100	–	9,900	1.16

<sup>a</sup>  $M_n$  (theo.) represents the targeted  $M_n$  with respect to the conversion (GC).

<sup>b</sup> After precipitation of the polymer into methanol.

<sup>c</sup> A linear polystyrene calibration with DMA as eluent was used.





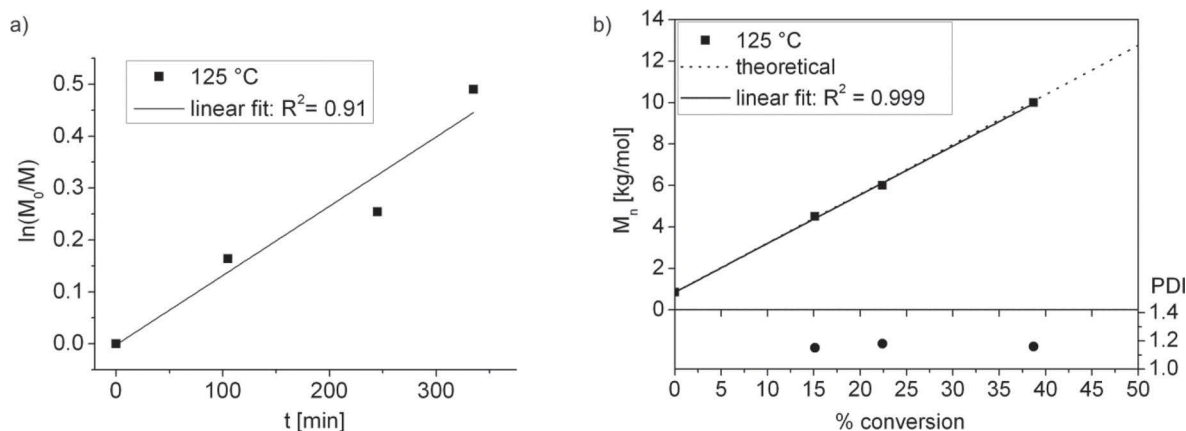
**FIGURE 3** SEC traces of **6c–e** after different polymerization times for the NMP of styrene using alkoxyamine **5** as initiator (eluent: DMA).

formed at an ideal 1:1 ratio of ditopic macroligand and the corresponding metal ions.<sup>40</sup> Among the common used metal ions for *bis*-terpyridine complexes, the iron(II) was chosen as the model ion for the formation of a responsive coordination polymer, since the iron(II) ion shows the tendency of forming *bis*-terpyridine complexes characterized by a high binding constant ( $\log K_2 = 13.8$  in water), while the *mono*-terpyridine complex shows a relative low binding constant ( $\log K_1 = 7.1$  in water).<sup>41</sup> Despite the high complex stability constants the Fe(II) complexes are considered as labile.<sup>42</sup> These two facts ensure the formation of high molar mass coordination polymers and the insensitivity against exceeding the metal-to-ligand ratio of 1:1, which can happen by using macroligands with averaged masses.<sup>43,44</sup> In this vein, the corresponding nickel(II) or cobalt(II) *bis*-complexes are in fact also very stable in water ( $\log K_2 \approx 10$  in water),<sup>41</sup> but since the *mono*-complexes show proximate binding constants, the formation of high molar mass polymers is sensitive against metal-to-ligand ratios exceeding 1:1.<sup>44</sup>

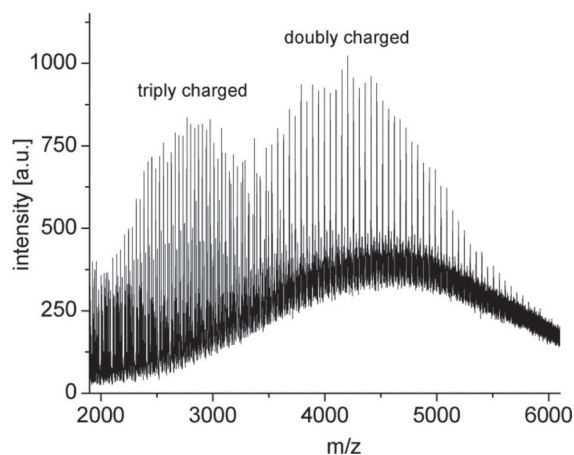
Another disadvantage of using nickel(II) ions for the preparation of responsive polymers is the inert character of the complex against external stimuli as it can be also seen for ruthenium(II) and cobalt(III) *bis*-terpyridine complexes. In contrast the zinc(II) and cadmium(II) *bis*-complexes are sufficiently labile but the formation is weak and for zinc weaker than the formation of the mono-complexes,<sup>41</sup> which would hinder the formation of linear high molar mass coordination polymers.

Following optimized reaction conditions described by Schubert and coworkers,<sup>45–47</sup> the metallopolymer  $\{[\text{Fe}(\mathbf{6b})_2](\text{PF}_6)_2\}_n$  (Fig. 7) was obtained as a purple powder (the color was arising from the MLCT absorption of the Fe<sup>II</sup> *bis*-terpyridine complex related to the absorption at 559 nm, see Supporting Information Fig. S7). An excess of the metal ion was used to ensure the quantitative coordination of the macroligand **6b** as the *bis*-complex is believed to be insensitive against exceeding the metal-to-ligand ratio of 1:1 also in an organic solvent. Moreover, the excess of metal ions suppress the formation of rings, as a ring-chain equilibrium has to be assumed for the flexible polymeric spacer.<sup>48</sup> To prevent oxidation of the Fe<sup>II</sup> ions prior to coordination, stannous chloride was added as reducing agent in stoichiometric amounts. Utilizing  $\text{PF}_6^-$  as counterions, the solubility of the supramolecular polymer in organic solvents could be enhanced. The formation of the chain-extended polymer was also confirmed by <sup>1</sup>H NMR spectroscopy: upon complexation by the Fe<sup>II</sup> ions, the signals of the terpyridine protons were significantly shifted as it was reported for Fe<sup>II</sup> *bis*-terpyridine complexes—in small molecules as well as in macromolecular species [Fig. 8(a,b)].<sup>24,46</sup> In addition, the methylene protons in the benzylic positions of the end-groups are quantitatively low-field shifted upon complexation pointing also to a complete complexation within the sensitivity limits of NMR spectroscopy.

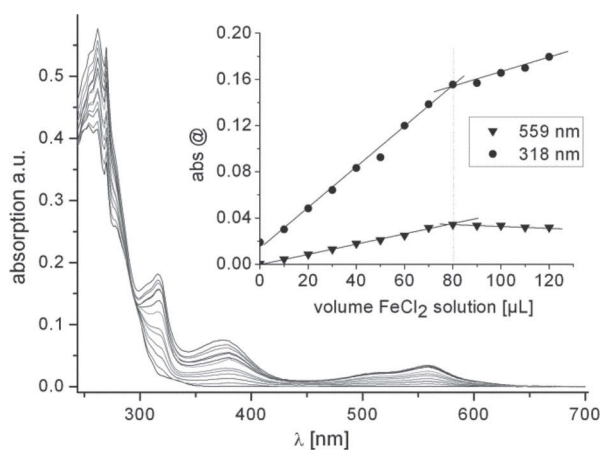
Moreover, 2D DOSY measurements of  $\{[\text{Fe}(\mathbf{6b})_2](\text{PF}_6)_2\}_n$  were carried out. These measurements revealed that all signals (i.e., terpyridine, polystyrene and TIPNO protons)



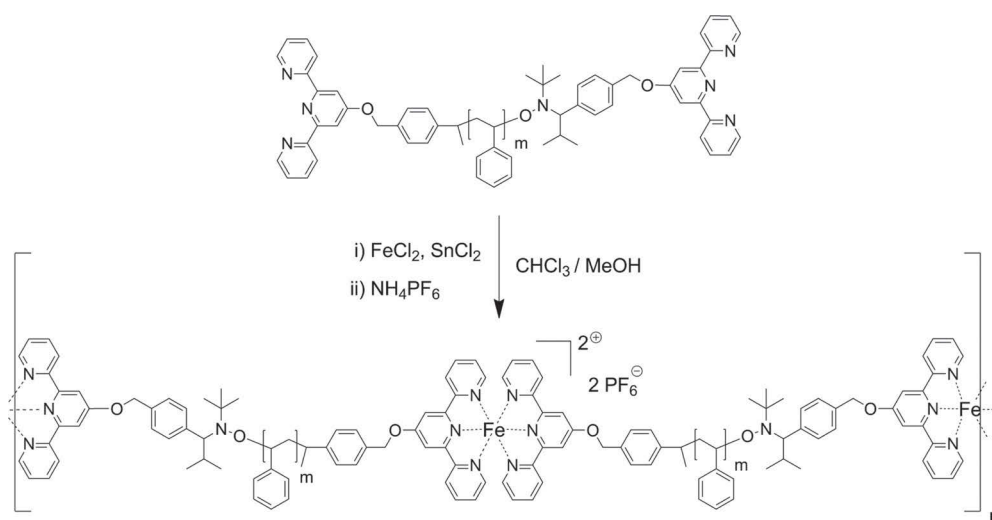
**FIGURE 4** Kinetic plots for the NMP of styrene using alkoxyamine **5**: (a) semilogarithmic plot of monomer conversion vs. polymerization time and (b) molar mass vs. conversion.



**FIGURE 5** ESI-TOF mass spectrum of **6a** reveals different charged distributions.



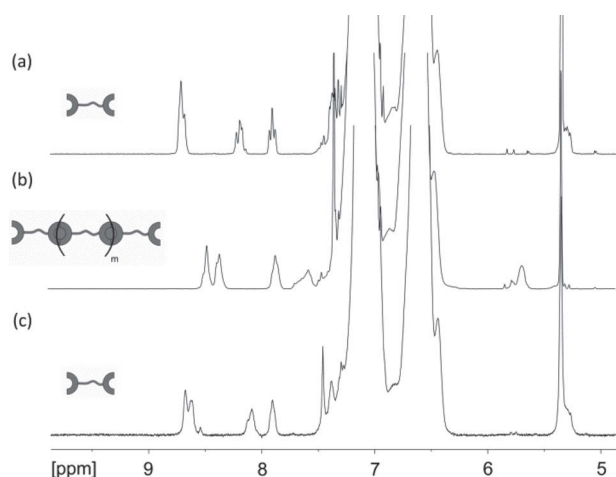
**FIGURE 6** UV-vis absorption titration experiments of **6b** with  $\text{Fe}^{\text{II}}$  ions. The evolution of the absorption bands at 318 and 559 nm, respectively, as a function of added  $\text{Fe}^{\text{II}}$  ions is also shown.



**FIGURE 7** Schematic representation of the synthesis of supramolecular chain-extended polymers  $\{[(\mathbf{6b})\text{M}(\mathbf{6b})](\text{PF}_6)_2\}_n$  by metal-to-ligand coordination ( $\text{SnCl}_2$  was added to the reaction mixture to prevent oxidation of the  $\text{Fe}^{\text{II}}$  ion).

arising from one macromolecular species, due to the same relative diffusion coefficients of all moieties (Fig. 9, left). It can be concluded within the sensitivity limits of  $^1\text{H}$  NMR spectroscopy that both endgroups are attached to the polymer chain and the presence of nonfunctionalized polystyrene or monofunctional tpy-PS can be excluded, as such compounds would reveal a different diffusion coefficient range for the terpyridine and polystyrene signals. To prove the reversibility of the metal-to-ligand coordination, the metallo-polymer was treated *in situ* with  $\text{Na}_3(\text{HEEDTA})$ , as strong competitive ligand (HEEDTA: hydroxy-2-ethylenediaminetriacetic acid). The disassembly of the metallo-polymer was monitored by 2D DOSY measurements (Fig. 9, right).

The tremendous decrease in molar mass due to the decomplexation of  $\{[\text{Fe}(\mathbf{6b})_2](\text{PF}_6)_2\}_n$  toward **6b** could be concluded from the significant differences in the relative diffusion behavior for the tpy and the PS signals of both materials (Fig. 9). This points within the sensitivity of  $^1\text{H}$  NMR spectroscopy to the absence of monomeric or low molar mass coordination polymers of **6b** and, thus, to the predominant formation of the iron(II) *bis*-complex within  $\{[\text{Fe}(\mathbf{6b})_2](\text{PF}_6)_2\}_n$  before the decomplexation. However, no reasonable estimation for the molar mass of  $\{[\text{Fe}(\mathbf{6b})_2](\text{PF}_6)_2\}_n$  could be concluded via the Stokes-Einstein equation. A correlation between diffusion coefficient and molar mass that is valid for the polymeric monomer and for the supramolecular polymer is unknown, since the backbone of the supramolecular polymer is different in nature (as partially ionic) due to the metal complexes giving a different correlation between molar mass and hydrodynamic radius. To the best of our knowledge no example is reported up to now where an estimation of the molar mass for a metallo-polymer via DOSY NMR is given. In addition, since the iron(II) *bis*-terpyridine complex is not stable under the SEC conditions used for polystyrenes, the molar



**FIGURE 8** Zoom into the low-field region of the  $^1\text{H}$  NMR spectra of (a) telechelic polystyrene **6b**, (b) the suprapolymer  $\{[(\mathbf{6b})\text{Fe}(\mathbf{6b})](\text{PF}_6)_2\}_n$  and the telechelic polystyrene **6b** (c) after the addition of HEEDTA as competing ligand. For all spectra: 400 MHz, 298 K with  $\text{CD}_2\text{Cl}_2$  for (a), (b), and  $\text{CD}_2\text{Cl}_2/\text{MeOD}$  for (c) as solvents (see the whole spectrum of  $\{[(\mathbf{6b})\text{Fe}(\mathbf{6b})](\text{PF}_6)_2\}_n$  in the Supporting Information Fig. S8).

mass can also not be determined by this method.<sup>46</sup> A theoretical estimation of the average molar mass of the coordination polymer in solution suggests  $M_n \approx 10^6 \text{ g mol}^{-1}$ , which is based on a ring-chain equilibrium model and binding constants in organic solvents with distinct assumptions (a critical consideration is provided in the supporting information).<sup>48–50</sup>

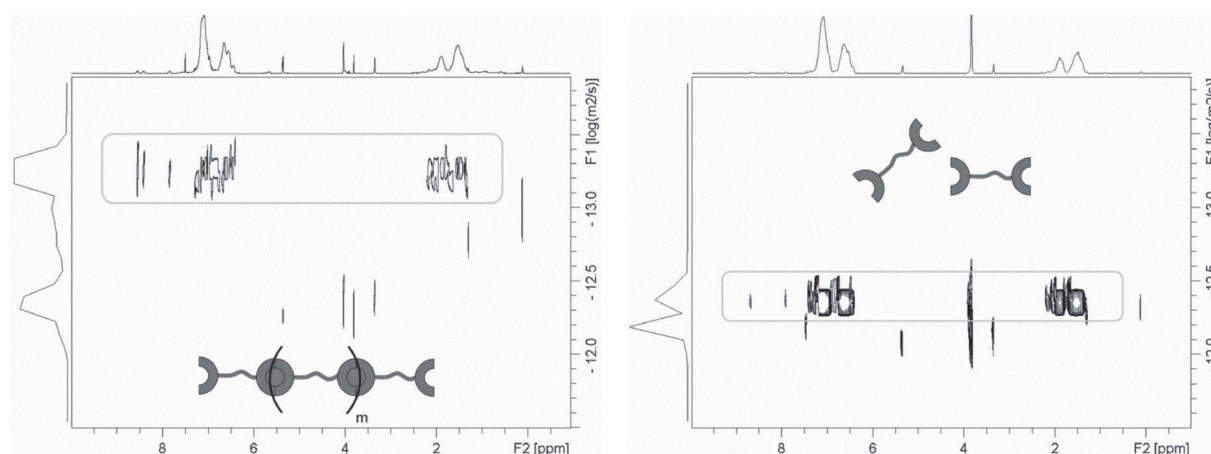
The related  $^1\text{H}$  NMR spectrum shows quantitative backshifts of the tpy signals as well as for the benzylic methylene groups of both end-groups which are similar with that of the initial macroligand **6b** [Fig. 8(a,c)]. The slight difference in

chemical shift for the tpy signals can be explained by the change of the NMR solvent from pure dichloromethane to a mixture of methanol and dichloromethane. Thus, metal-free **6b** could be regenerated quantitatively by addressing the metalpolymer with an external stimulus, that is, a strong competitor for the  $\text{Fe}^{\text{II}}$  ions—a similar behavior is expected for significant changes in the pH value or when applying redox chemistry, that is, oxidizing the metal ions to a +III state which will be investigated in future work.

## CONCLUSIONS

In the present contribution a *bis*-terpyridine functionalized initiator for NMP was synthesized to access  $\alpha,\omega$ -difunctionalized polymers in one-step retaining the terpyridines as end-groups. The polymerization of styrene was proven to be a controlled process, while tpy as substituent of the initiating as well as of the mediating fragment of the alkoxyamine did not disturb the performance of the initiator. This approach has a wider scope by means of construction flexibility compared to a postmodification approach, as the chain length and composition between the supramolecular binding sites can be varied in less reaction steps and purification can be simply done by precipitation. The self-assembly of the prepared building blocks via iron-ion complexation toward linear supramolecular polymers was investigated by UV-vis spectroscopy and DOSY. The reassembly and responsiveness of the system against a competing ligand to the tpy was proven by NMR techniques.

The presented work provides a promising strategy for the construction of metallo-supramolecular architectures in a minimum of steps, which makes it appealing for studying the influence of the polymeric spacer within more reversible architectures (using, for example, zinc complexes) or more complex structure (using, for example, heteroleptic complexes) with respect to the progress of efficient stimuli-responsive and self-healing materials.



**FIGURE 9** Left: 2D  $^1\text{H}$ – $^1\text{H}$  DOSY spectrum of  $\{[(\mathbf{6b})\text{Fe}(\mathbf{6b})](\text{PF}_6)_2\}_n$  demonstrating the same diffusion coefficients for signals of tpy complex and polystyrene. Right: 2D  $^1\text{H}$ – $^1\text{H}$  DOSY spectrum of **6b** after the addition of HEEDTA demonstrating the decomplexation (diffusion coefficient of dichloromethane was taken as reference).

## ACKNOWLEDGMENTS

The authors kindly acknowledge financial support from the Dutch Polymer Institute (DPI, technology area HTE), the Fonds der Chemischen Industrie and the Thuringian Ministry for Education, Science and Culture (grant #B514-09049, PhotoMic).

## REFERENCES AND NOTES

- Handbook of Vinyl Polymers; M. K. Mishra, Y. Yagci, Eds.; CRC Press: Boca Raton, **2009**.
- Y. Yagci, O. Nuyken, V.-M. Graubner, Encyclopedia of Polymer Science and Technology; J. I. Kroschwitz, Ed.; Wiley: New York, **2005**; pp 57–130.
- Telechelic Polymers; E. J. Goethals, Ed.; CRC Press: Boca Raton, **1989**.
- M. A. Tasdelen, M. U. Kahveci, Y. Yagci, *Prog. Polym. Sci.* **2011**, *36*, 455–567.
- Compendium of Polymer Terminology and Nomenclature; R. G. Jones, J. Kahovec, R. Stepto, E. S. Wilks, M. Hess, T. Kitayama, W. V. Metanomski, Eds.; RSC Publishing: Cambridge, **2009**.
- O. Bayer, *Angew. Chem.* **1947**, *59*, 257–272.
- C. A. Uraneck, H. L. Hsieh, O. G. Buck, *J. Polym. Sci.* **1960**, *46*, 535–539.
- Macromolecular Engineering: Precise Synthesis, Materials Properties, Applications; K. Matyjaszewski, Y. Gnanou, L. Leibler, Eds.; Wiley-VCH: Weinheim, **2007**.
- N. Hadjichristidis, M. Pitsikalis, S. Pispas, H. Iatrou, *Chem. Rev.* **2001**, *101*, 3747–3792.
- W. A. Braunecker, K. Matyjaszewski, *Prog. Polym. Sci.* **2007**, *32*, 39–146.
- M. Kamigaito, T. Ando, M. Sawamoto, *Chem. Rev.* **2001**, *101*, 3689–3746.
- K. Matyjaszewski, J.-H. Xia, *Chem. Rev.* **2001**, *101*, 2921–2990.
- C. J. Hawker, A. W. Bosman, E. Harth, *Chem. Rev.* **2001**, *101*, 3661–3688.
- J. Chiefari, Y.-K. B. Chong, F. Ercole, J. Krstina, J. Jeffrey, T. P.-T. Le, R. T. A. Mayadunne, G. F. Meijs, C. L. Moad, G. Moad, E. Rizzardo, S.-H. Thang, *Macromolecules* **1998**, *31*, 5559–5562.
- T. Otsu, *J. Polym. Sci. Part A: Polym. Chem.* **2000**, *38*, 2121–2136.
- G. David, C. Boyer, J. Tonnar, B. Ameduri, P. Lacroix-Desmazes, B. Boutevin, *Chem. Rev.* **2006**, *106*, 3936–3962.
- A. Debuigne, R. Poli, C. Jérôme, R. Jérôme, C. Detrembleur, *Prog. Polym. Sci.* **2009**, *34*, 211–239.
- S. Yamago, *Chem. Rev.* **2009**, *109*, 5051–5068.
- U. Mansfeld, C. Pietsch, R. Hoogenboom, C. R. Becer, U. S. Schubert, *Polym. Chem.* **2010**, *1*, 1560–1598.
- Handbook of Radical Polymerization; K. Matyjaszewski, T. P. Davis, Eds.; Wiley-Interscience: Hoboken, **2002**.
- V. Coessens, T. Pintauer, K. Matyjaszewski, *Prog. Polym. Sci.* **2001**, *26*, 337–377.
- D. Benoit, V. Chaplinski, R. Braslau, C. J. Hawker, *J. Am. Chem. Soc.* **2001**, *121*, 3904–3920.
- M. Rodlert, E. Harth, I. Rees, C. J. Hawker, *J. Polym. Sci. Part A: Polym. Chem.* **2000**, *38*, 4749–4763.
- U. S. Schubert, A. Winter, G. R. Newkome, Terpyridine-Based Materials; Wiley-VCH: Weinheim, **2011**.
- B. G. G. Lohmeijer, U. S. Schubert, *J. Polym. Sci. Part A: Polym. Chem.* **2004**, *42*, 4016–4027.
- C. Ott, B. G. G. Lohmeijer, D. Wouters, U. S. Schubert, *Macromol. Chem. Phys.* **2006**, *207*, 1439–1449.
- J.-F. Gohy, C. Ott, S. Hoepfener, U. S. Schubert, *Chem. Commun.* **2009**, 6038–6040.
- U. Mansfeld, M. D. Hager, R. Hoogenboom, C. Ott, A. Winter, U. S. Schubert, *Chem. Commun.* **2009**, 3386–3388.
- U. Mansfeld, A. Winter, M. D. Hager, R. Hoogenboom, W. Gunther, U. S. Schubert, *Polym. Chem.* **2013**, *4*, 113–123.
- C. D. Eisenbach, U. S. Schubert, *Macromolecules* **1993**, *26*, 7372–7374.
- M. Chiper, R. Hoogenboom, U. S. Schubert, *Macromol. Rapid Commun.* **2009**, *30*, 565–578.
- H. Hofmeier, S. Schmatloch, D. Wouters, U. S. Schubert, *Macromol. Chem. Phys.* **2003**, *204*, 2197–2203.
- S. Schmatloch, A. M. J. van den Berg, A. S. Alexeev, H. Hofmeier, U. S. Schubert, *Macromolecules* **2003**, *36*, 9943–9949.
- E. C. Constable, M. D. Ward, *J. Chem. Soc. Dalton Trans.* **1990**, 1405–1409.
- T. Y.-S. But, P. H. Toy, *Chem. Asian J.* **2007**, *2*, 1340–1355.
- J. Hovinen, *Tetrahedron Lett.* **2004**, *45*, 5707–5709.
- C. J. Hawker, A. W. Bosman, E. Harth, *Chem. Rev.* **2001**, *101*, 3661–3688.
- W. Dempwolf, S. Flakus, G. Schmidt-Naake, *Macromol. Symp.* **2007**, *259*, 416–420.
- T. Schulte, K. O. Siegenthaler, H. Luftmann, M. Letzel, A. Studer, *Macromolecules* **2005**, *38*, 6833–6840.
- A. Winter, M. D. Hager, U. S. Schubert, In *Polymer Science: A Comprehensive Reference*; M. Möller, K. Matyjaszewski, Eds.; Elsevier BV: Amsterdam, **2012**; Vol. 5, pp 269–310.
- R. H. Holyer, C. D. Hubbard, S. F. A. Kettle, R. G. Wilkins, *Inorg. Chem.* **1966**, *5*, 622–625.
- R. Hogg, R. G. Wilkins, *J. Chem. Soc.* **1962**, 341–350.
- R. Dobrawa, F. Würthner, *J. Polym. Sci. Part A: Polym. Chem.* **2005**, *43*, 4981–4995.
- B. G. G. Lohmeijer, PhD-thesis, Eindhoven University of Technology, **2004**, 19–68.
- M. Chiper, M. A. R. Meier, J. M. Kranenburg, U. S. Schubert, *Macromol. Chem. Phys.* **2007**, *208*, 679–689.
- M. Chiper, M. A. R. Meier, D. Wouters, S. Hoepfener, C.-A. Fustin, J.-F. Gohy, U. S. Schubert, *Macromolecules* **2008**, *41*, 2771–2777.
- H. Hofmeier, R. Hoogenboom, M. E. L. Wouters, U. S. Schubert, *J. Am. Chem. Soc.* **2005**, *127*, 2913–2921.
- T. Vermonden, J. van der Gucht, P. de Waard, A. T. M. Marcelis, N. A. M. Besseling, E. J. R. Sudhölter, G. J. Fleer, M. A. Cohen Stuart, *Macromolecules* **2003**, *36*, 7035–7044.
- R. Shunmugam, G. J. Gabriel, K. A. Aamer, G. N. Tew, *Macromol. Rapid Commun.* **2010**, *31*, 784–793.
- D. G. Kurth, *Sci. Technol. Adv. Mater.* **2008**, *9*, 014103.

# **A Homotelechelic Bis-terpyridine Macroligand: One-step Synthesis and its Metallo-supramolecular Self-assembly**

Ulrich Mansfeld,<sup>a,b,c</sup> Andreas Winter,<sup>a,b,c</sup> Martin D. Hager,<sup>a,b,c</sup> Wolfgang Günther,<sup>a</sup> Esra Altuntaş,<sup>a,b</sup>  
Ulrich S. Schubert\*<sup>a,b,c</sup>

<sup>a</sup> Laboratory for Organic and Macromolecular Chemistry (IOMC), Friedrich-Schiller-University Jena, Humboldtstr. 10, 07743 Jena, Germany

<sup>b</sup> Jena Center for Soft Matter (JCSM), Humboldtstr. 10, 07743 Jena, Germany

<sup>c</sup> Dutch Polymer Institute (DPI), P.O. Box 902, 5600 AX Eindhoven, The Netherlands

Correspondence to: Ulrich S. Schubert (E-mail: [ulrich.schubert@uni-jena.de](mailto:ulrich.schubert@uni-jena.de))

## Supporting Information

### Estimation for the average molar mass of $\{[\text{Fe}(\mathbf{6b})_2](\text{PF}_6)_2\}_n$

A valuable theoretical estimation of the molar mass is complicated: The available binding constants are determined in water.<sup>1</sup> The binding constants and kinetic aspects of a metal complex depends essentially on the solvent and on the counterion of the coordination polymer in solution.<sup>2</sup> No specific binding constants are available for the present complex in a mixture of chloroform/methanol or dichloromethane with  $\text{PF}_6^-$  as counterion. Würthner *et al.* reported on lower limits binding constants for Fe(II) bisterpyridine complexes in acetonitrile with  $\text{ClO}_4^-$ , which are more suitable for an organic solvent and are used as a rough estimation neglecting the influence of the counterion. Furthermore, since no rigid spacer between the tpy end groups is present, the simplified isodesmic model<sup>3</sup> cannot be used without the following assumptions as the ring-chain equilibrium has to be taken into account. With the assumption of a high monomer concentrations and a monomer-to-metal ratio larger than 1, the formation of rings will be neglected, although this depends on the ratio of the binding constants.<sup>4</sup> This binding constants ratio is unknown for organic solvents as Würthner *et al.* comment only on the lower limits were  $K_1$  and  $K_2$  are larger than  $10^8 \text{ M}^{-1}$ .<sup>5</sup> In addition, the average degree of polymerization (DP) also depends on the ratio of the binding constants if the monomer-to-metal ratio exceeds 1, which shows the maximum average DP. As we assume  $K_2 \gg K_1$  for the Fe(II) biscomplex also in organic solvents, the deviation from the maximum average DP at the metal-to-ligand ratio of 1:1 is also neglected in our case. With these assumptions the average number of monomers per chain can be roughly estimated according to Vermonden *et al.*:<sup>4</sup>

$$\langle n \rangle \approx (K_2 c)^{1/2} \quad (1)$$

DP is the degree of polymerization,  $K_2$  is the binding constant for the bisterpyridine complex and  $c$  is the overall concentration of the telechelic polystyrene **6b**. Taken the labile character of the Fe(II) bistpy complex into account, the DP of reaction mixture and the DOSY investigation can be estimated:

With  $K_2 = 10^8 \text{ M}^{-1}$ ,  $c^{\text{reaction}} = 7 \cdot 10^{-3} \text{ mol} \cdot \text{L}^{-1}$ ,  $c^{\text{DOSY}} = 4 \cdot 10^{-3} \text{ mol} \cdot \text{L}^{-1}$  and  $M_n(\mathbf{6b}) = 7,200 \text{ g mol}^{-1}$  (1) revealed:

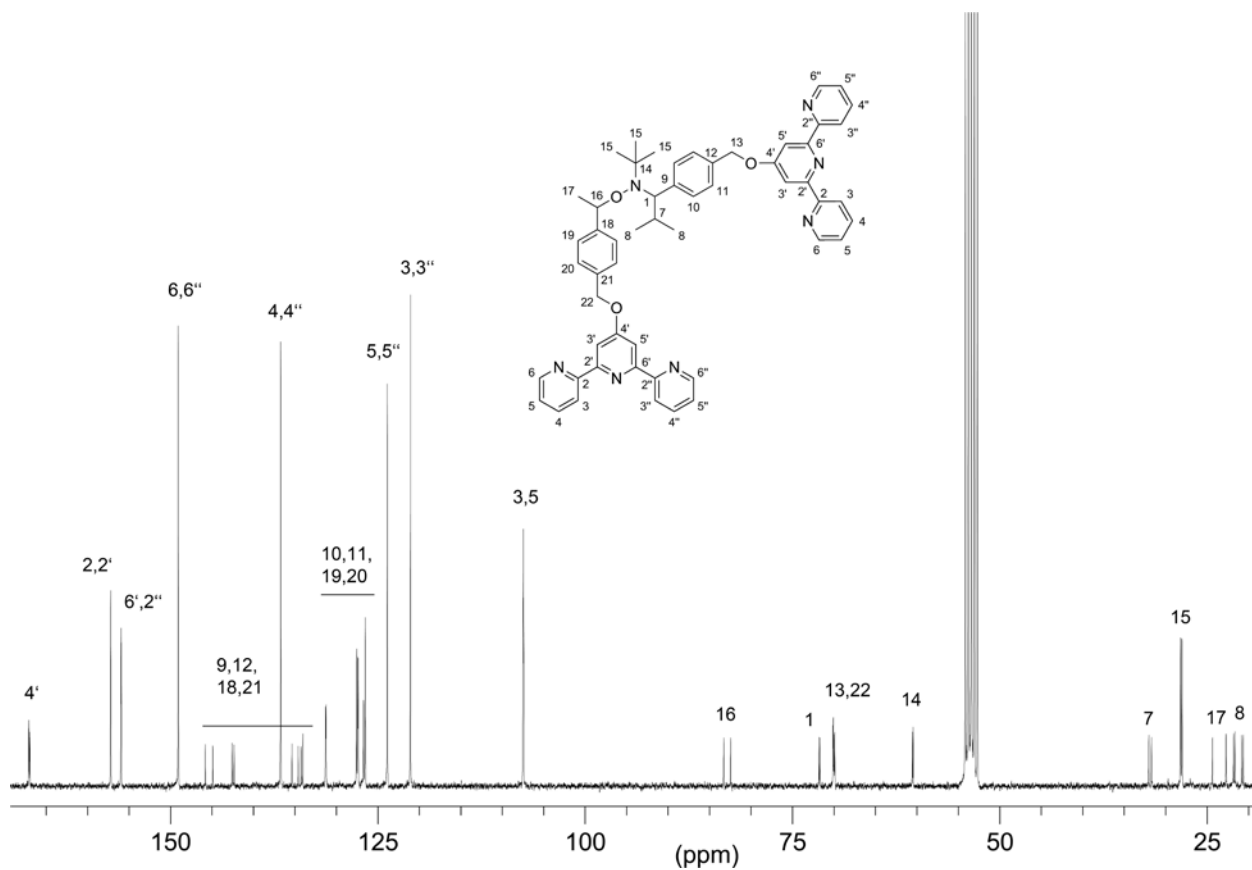
For the assembly reaction solution:

$$\langle n_1 \rangle \approx 800 \text{ and } M_n^{\text{reaction}} \approx 6 \cdot 10^6 \text{ g mol}^{-1}$$

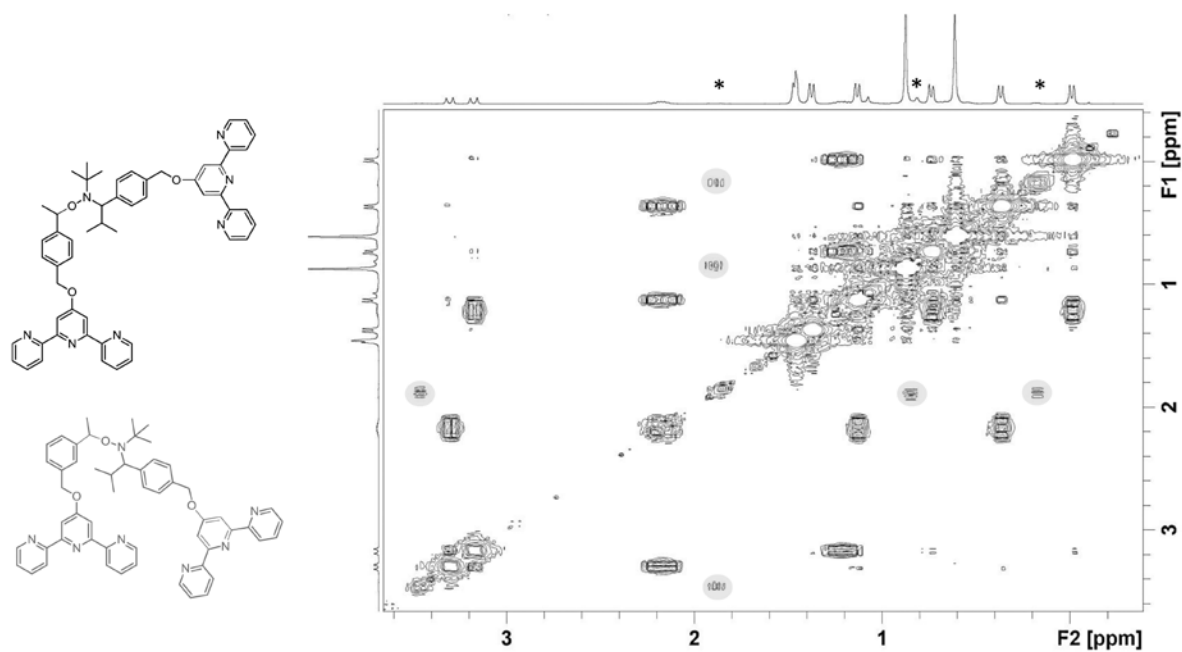
For the DOSY investigation solution:

$$\langle n_2 \rangle \approx 650 \text{ with } M_n^{\text{DOSY}} \approx 4 \cdot 10^6 \text{ g mol}^{-1}$$

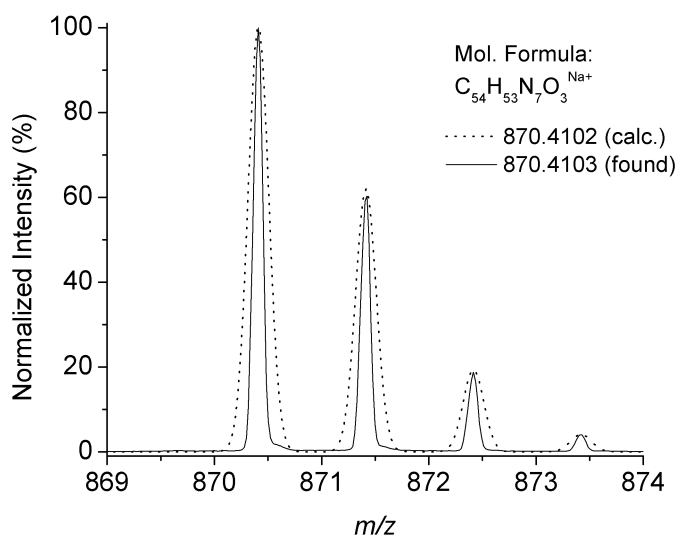




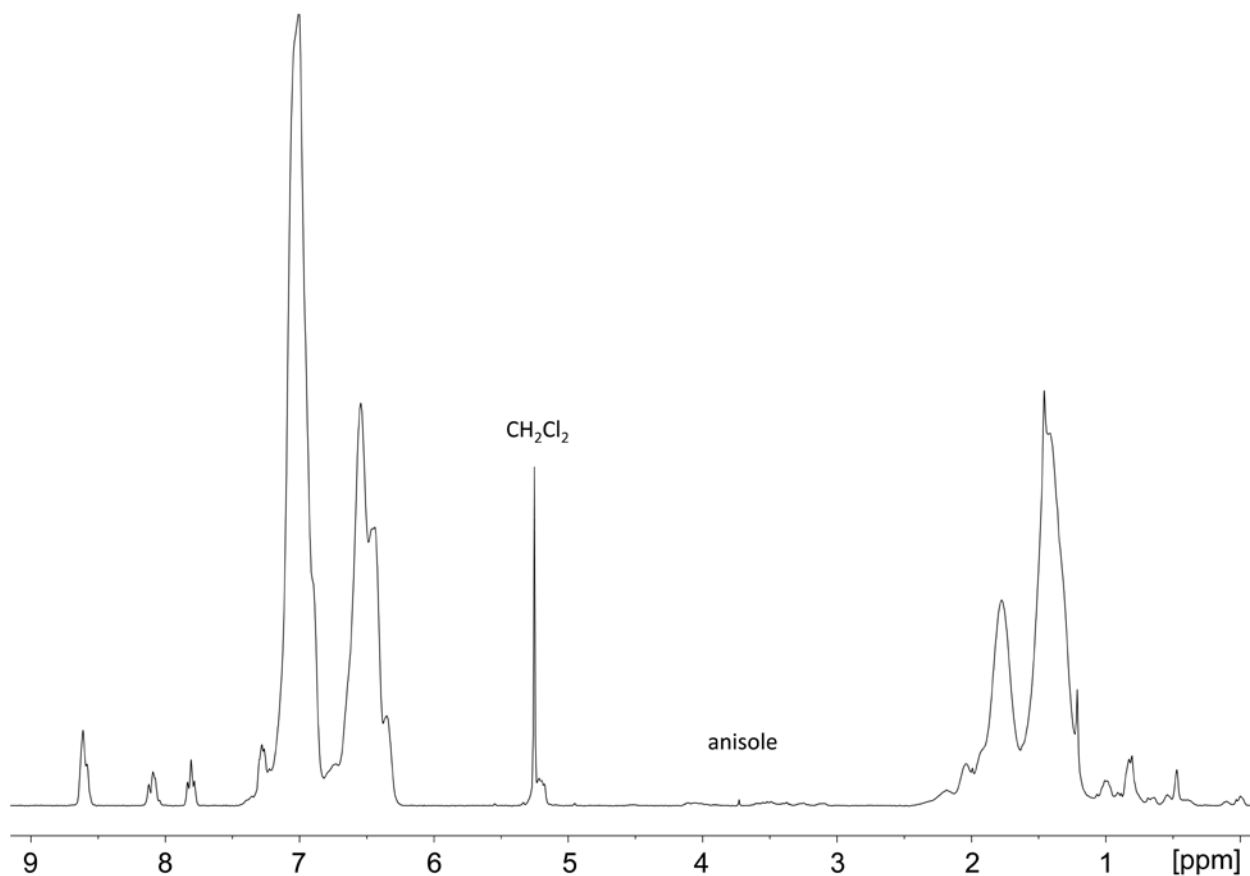
**Figure S1.**  $^{13}\text{C}$  NMR spectrum of *tpy*-TIPNO-*tpy* **5** (100 MHz,  $\text{CD}_2\text{Cl}_2$ , diastereomers a+b).



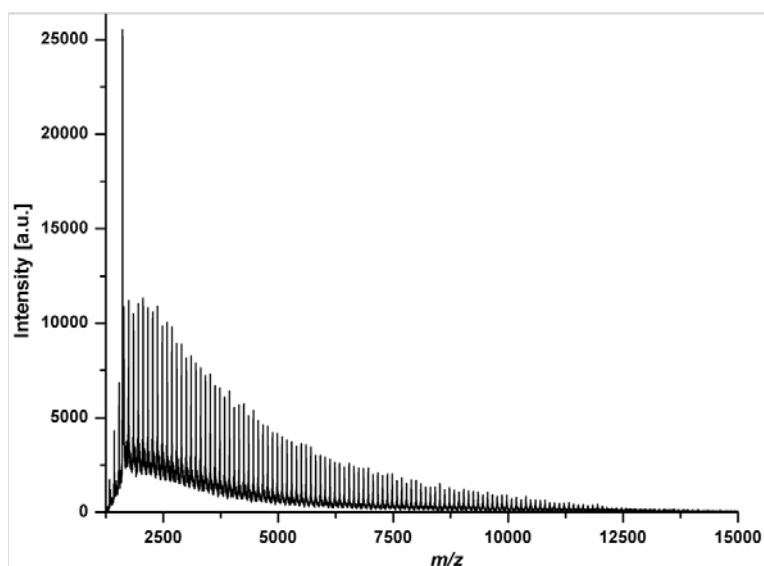
**Figure S2.** 2D  $^1\text{H}$ - $^1\text{H}$  COSY of **5** revealed the meta-substituted isomer with different cross-peak signals (asterisks, marked in grey) compared to the para-substituted isomer (400 MHz,  $\text{CD}_2\text{Cl}_2$ , 298 K).



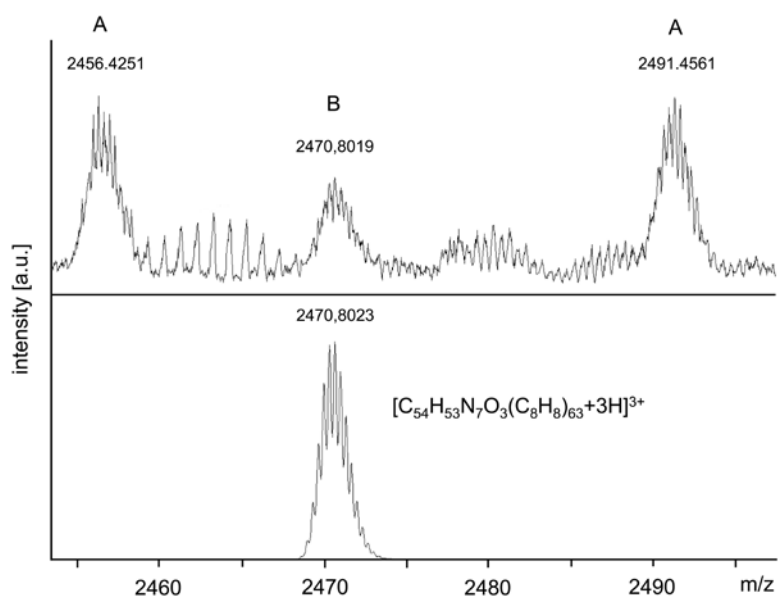
**Figure S3.** Zoom into the high-resolution ESI spectrum of **5** shows the comparison of the calculated/measured isotopic pattern.



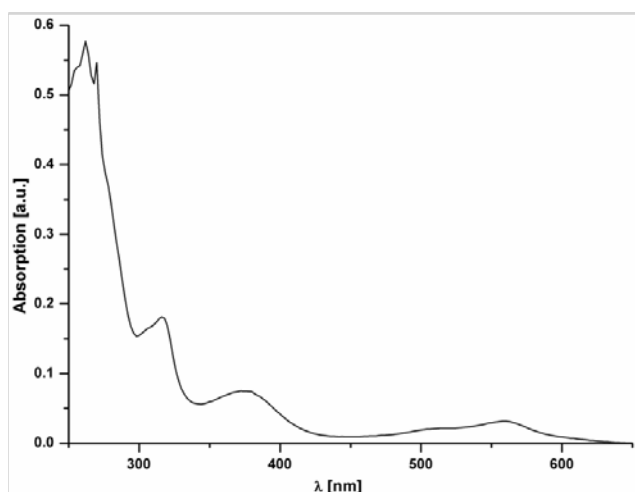
**Figure S4.**  $^1H$  NMR spectrum of **6b** (400 MHz,  $CD_2Cl_2$ , 298 K).



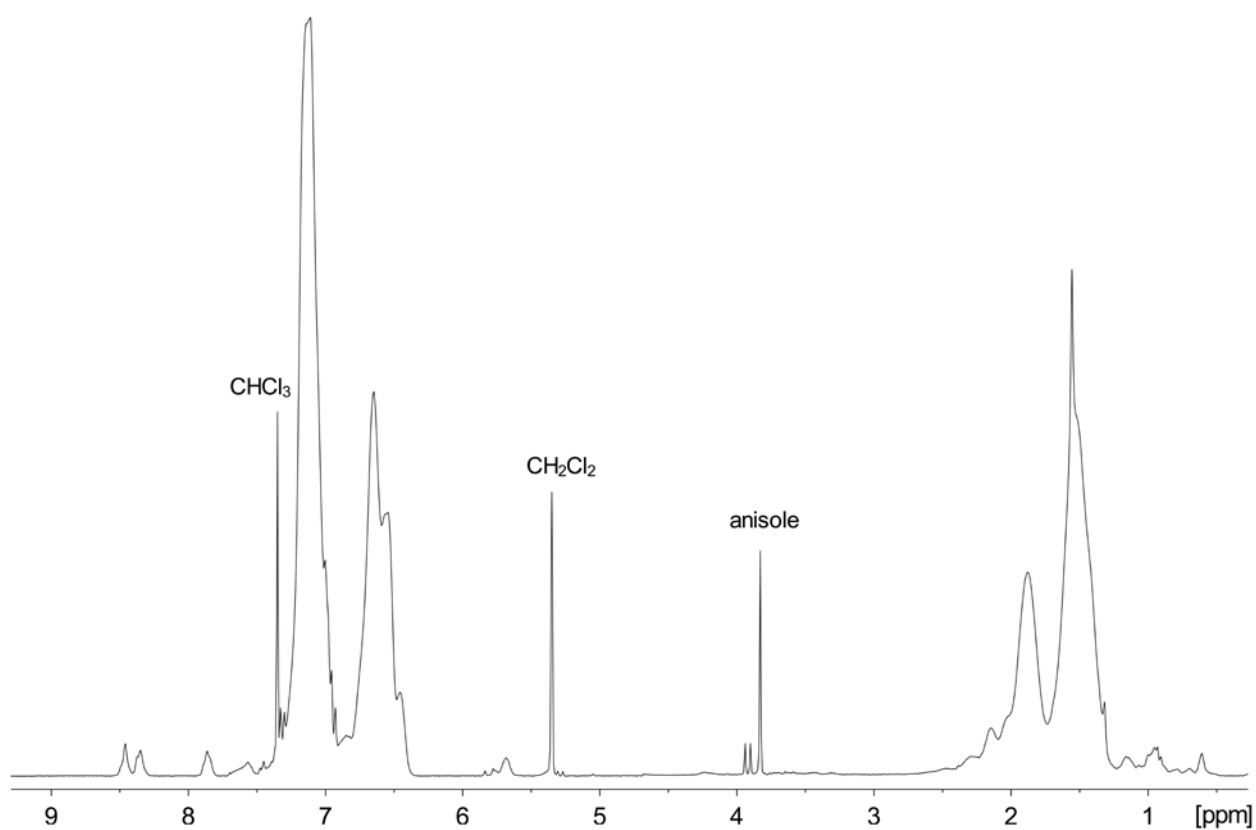
**Figure S5.** MALDI-TOF mass spectrum of tpy-PS-TIPNO-tpy **6a** (matrix DCTB).



**Figure S6.** Zoom into the ESI spectrum of **6a** showing the main distribution A related to a triply-charged polystyrene distribution with a not assignable fragmentation of an end-group ( $\Delta m/z = 35$ ) and the sub distribution B that correlates to the non-fragmented PS with both tpy as end-groups.



**Figure S7.** UVvis spectrum of metallopolymer  $\{[\text{Fe}(\mathbf{6b})_2](\text{PF}_6)_2\}_n$  showing the characteristic MLCT absorption of the  $\text{Fe}^{\text{II}}$  *bis*-terpyridine complex at 559 nm.



**Figure S8.**  $^1\text{H}$  NMR spectrum of  $\{[(\mathbf{6b})\text{Fe}(\mathbf{6b})](\text{PF}_6)_2\}_n$  (400 MHz,  $\text{CD}_2\text{Cl}_2$ , 298 K).

References:

1. Holyer, R. H.; Hubbard, C. D.; Kettle, S. F. A.; Wilkins, R. G. *Inorganic Chemistry* **1966**, *5*, 622-625.

2. Shunmugam, R.; Gabriel, G. J.; Aamer, K. A.; Tew, G. N. *Macromol. Rapid Commun.* **2010**, *31*, 784-793.
3. Martin, R. B. *Chemical Reviews* **1996**, *96*, 3043-3064.
4. Vermonden, T.; van der Gucht, J.; de Waard, P.; Marcelis, A. T. M.; Besseling, N. A. M.; Sudhölter, E. J. R.; Fleer, G. J.; Cohen Stuart, M. A. *Macromolecules* **2003**, *36*, 7035-7044.
5. Dobrawa, R.; Ballester, P.; Saha-Moller, C. R.; Wurthner, F. *Metal-Containing and Metallosupramolecular Polymers and Materials*, (Eds: U. S. Schubert, G. R. Newkome, I. Manners), ACS Symposium Series, Washington, D.C. **2006**, *43*, 4981-4995.



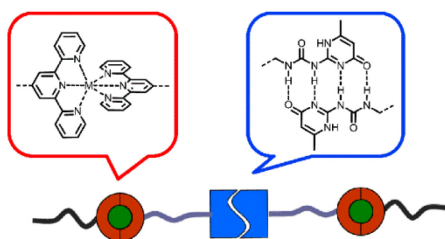


## Publication P4:

### *Amphiphilic supramolecular A(B)<sub>2</sub>A quasi-triblock copolymers*

U. Mansfeld, A. Winter, M. D. Hager, G. Festag, S. Hoepfner and U. S. Schubert

*Polym. Chem.* **2013**, 4, 3177-3181



Reproduced by permission of The Royal Society of Chemistry

<http://dx.doi.org/10.1039/C3PY00216K>



## Amphiphilic supramolecular A(B)<sub>2</sub>A quasi-triblock copolymer†

Cite this: *Polym. Chem.*, 2013, **4**, 3177

Ulrich Mansfeld,<sup>abc</sup> Andreas Winter,<sup>abc</sup> Martin D. Hager,<sup>abc</sup> Grit Festag,<sup>ab</sup> Stephanie Hoepfener<sup>ab</sup> and Ulrich S. Schubert<sup>\*abc</sup>

Received 12th February 2013

Accepted 12th March 2013

DOI: 10.1039/c3py00216k

www.rsc.org/polymers

The efficient synthesis of a responsive amphiphilic supramolecular triblock copolymer A(B)<sub>2</sub>A is described, where the blocks are held together by self-complementary hydrogen bonding at the homojunction (B–B) and by heteroleptic metal complexes at the heterojunction (A–B). The supramolecular copolymer was prepared in a minimum of steps by using heterotelechelic building blocks with orthogonal binding sites polymerized in one step.

Conventional organic polymers have been introduced in a wide range of today's technologies due to their mechanical, thermal and/or electronic properties. Whilst the exclusively covalent nature of some of these polymers results in an intrinsic non-reversible or non-responsive character when addressed by external stimuli, all supramolecular polymer-based materials are inherently stimuli-responsive due to their reversible and/or dynamic non-covalent bonds. The properties of both are merged in supramolecular polymers.<sup>1</sup> This approach enables the construction of a new class of stimuli-responsive polymers with tailor-made functions that have a strong impact on materials science.<sup>2–7</sup> Various types of non-covalent interactions have been utilized for the preparation of supramolecular polymers:  $\pi$ - $\pi$  stacking,<sup>8–11</sup> hydrophobic<sup>12,13</sup> and other non-covalent interactions<sup>14–17</sup> including metal-to-ligand coordination<sup>18–23</sup> and (multiple) hydrogen bonding.<sup>24–26</sup> In particular, the latter two are of interest for the construction of advanced architectures *via* self-assembly processes due to their binding strength, complementarity and directionality.<sup>27</sup> Terpyridine (tpy) bis-complexes are among the most common motifs in metallo-supramolecular

chemistry and have been applied for the synthesis of a wide range of supramolecular polymers: chain-extended polymers, block copolymers, graft copolymer macrocycles and dendrimers.<sup>28,29</sup> The self-complementary 2-ureido-4*H*-pyrimidone (UPy) moiety was introduced by the Meijer group for preparing various types of supramolecular polymers based on quadruple hydrogen bonding.<sup>26</sup> These two systems with orthogonality of the non-covalent interactions were combined by Schubert and coworkers for the preparation of supramolecular polymers based on both interactions.<sup>30–32</sup>

In this contribution, the utilization of a heterotelechelic macroligand tpy-PS-UPy (**1a**) for the orthogonal assembly of amphiphilic supramolecular quasi-triblock copolymers is shown *via* self-complementary hydrogen bonding and heteroleptic metal-ion complexation with a monofunctional tpy-PEG.

It is an established concept in terpyridine chemistry that highly stable heteroleptic Ru<sup>II</sup> tpy bis-complexes can be obtained *via* stepwise self-assembly.<sup>29</sup> Recently, an alternative stepwise one-pot assembly was shown for Ni<sup>II</sup> systems due to the characteristic kinetic stabilities of the mono-complexes.<sup>33a,b</sup> Details on the characteristic stability of the complexes are discussed in the ESI (Fig. S1†).<sup>33c–e</sup> If polymer chains are attached in the 4'-position to the terpyridine units, the formation of block copolymers with metallo-supramolecular linkers at the block junction is enabled.<sup>34</sup> In this respect, by far the most intensively studied system is the AB diblock copolymer [(MPEG-tpy)Ru(tpy-PS)]<sup>2+</sup> (MPEG (A): poly(ethylene glycol) monomethyl ether, PS (B): polystyrene).<sup>29</sup> If the PS block in such an array bears additionally a terminal self-complementary UPy moiety (**1a**), dimerization into an A(B)<sub>2</sub>A quasi-triblock system *via* quadruple hydrogen bonding is expected in apolar aprotic solvents. As a reference, a heterotelechelic tpy-PS-OH (**1b**) bearing a hydroxy group was synthesized that does not assemble *via* hydrogen bonding leading to an AB diblock copolymer in the same environment (for the <sup>1</sup>H NMR spectrum, see Fig. S2†). Compared to a related postmodification example,<sup>35</sup> both heterotelechelic PS blocks were readily polymerized in one step using the strategy of difunctional initiators for the nitroxide-mediated polymerization process

<sup>a</sup>Laboratory of Organic and Macromolecular Chemistry (IOMC), Friedrich Schiller University Jena, Humboldtstr. 10, 07743 Jena, Germany. E-mail: ulrich.schubert@uni-jena.de; Web: <http://www.schubert-group.de>; Fax: +49 (0)3641948202; Tel: +49 (0)3641 948200

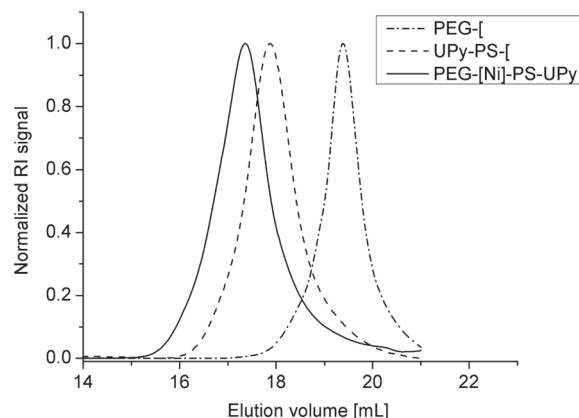
<sup>b</sup>Jena Center for Soft Matter (JCSM), Friedrich Schiller University Jena, Philosophenweg 7, 07743 Jena, Germany

<sup>c</sup>Dutch Polymer Institute (DPI), P.O. Box 902, 5600 AX Eindhoven, The Netherlands

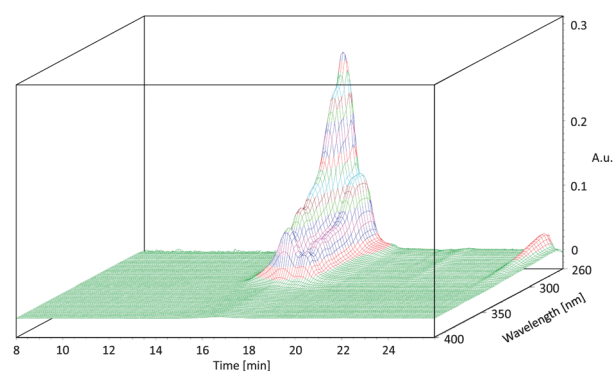
† Electronic supplementary information (ESI) available: See DOI: 10.1039/c3py00216k

(for details see the ESI†).<sup>31,32</sup> In this vein, the UPy or OH moiety is attached to the PS *via* a temperature-responsive alkoxyamine; thus the coordination chemistry of Ru<sup>II</sup> requiring relatively harsh reaction conditions cannot be applied. Therefore, mild complexation of Ni<sup>II</sup> was used to yield [(MPEG-tpy)Ni(**1a**)<sub>2</sub>-Ni(tpy-MPEG)](PF<sub>6</sub>)<sub>n</sub> or [(MPEG-tpy)Ni(**1b**)](PF<sub>6</sub>)<sub>n</sub>. As outlined in Scheme 1, the one-pot, two-step procedure as described by Mugemana *et al.* was utilized.<sup>33a</sup> Starting from the precursor complex nickel(II) chloride hexa(dimethylformamide), the nickel(II) mono-complex was formed instantaneously upon addition of the heterotelechelic PS (**1a** or **1b**)<sup>36</sup> as block B. Subsequently, MPEG<sub>44</sub>-tpy (block A)<sup>37,38</sup> was added and coordinated to the metal center yielding the respective heteroleptic bis-complexes. Anion exchange to PF<sub>6</sub><sup>-</sup> was carried out to guarantee the solubility of the supramolecular assemblies in organic solvents. The crude products were washed with diethyl ether and water to purify the copolymers from non-coordinated PS and PEG, respectively.<sup>33a</sup>

The copolymers were investigated by size exclusion chromatography (SEC). Since *N,N*-dimethylacetamide (DMAc) containing NH<sub>4</sub>PF<sub>6</sub> has to be utilized for metallo-supramolecular polymers as an eluent, the hydrogen bonding *via* the UPy moiety was suppressed under the measurement conditions. Accordingly, only the AB diblock copolymers could be observed in both cases: the monomodal distributions show a distinct shift of the SEC trace (refractive index (RI) detector) to a shorter elution volume when compared to the traces of the metal-free building blocks (Fig. 1 and S3†). SEC coupled to a photodiode array (PDA) detector allows monitoring of the UV-vis absorption spectrum as a function of the elution volume for [(MPEG-tpy)Ni(**1a**)<sup>2+</sup>](Fig. 2). In contrast to the RI traces, besides a main distribution (retention time: 17.5 min) also a low molar mass side distribution becomes visible (18.4 min). Both distributions show the characteristic UV-vis absorption for Ni<sup>II</sup> terpyridine complexes represented by the ligand-centered (LC) bands at 315 and 329 nm (Fig. S4†). Nevertheless, the distributions show differences by comparison of the UV-vis spectra. The main distribution can be related to the desired heteroleptic complex due to an absorption maximum at λ<sub>max</sub> < 270 nm according to the non-complexed PS educt **1a**. The low molar mass distribution is tentatively ascribed to small amounts of the homoleptic complex [Ni(MPEG)<sub>2</sub>]<sup>2+</sup> showing, besides a larger retention time



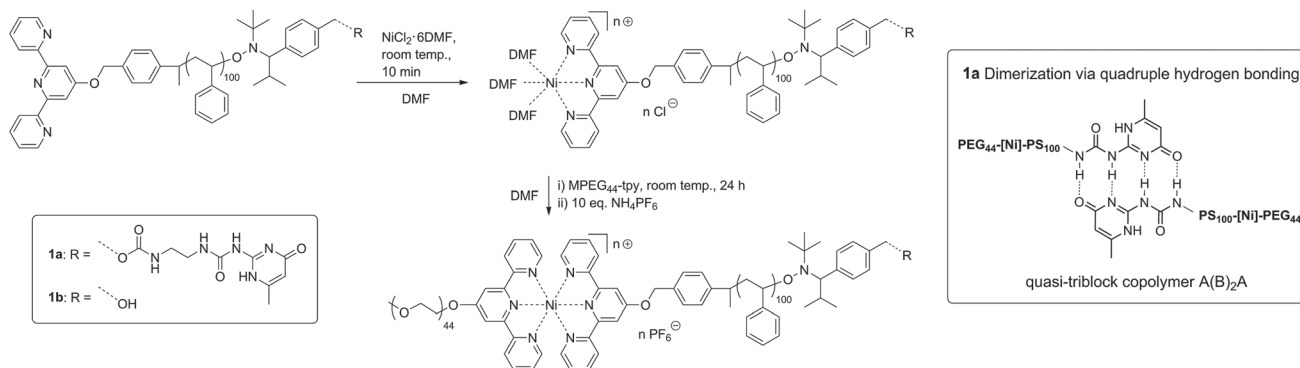
**Fig. 1** SEC traces (RI detector) of the diblock copolymer [(MPEG-tpy)Ni(**1a**)<sup>2+</sup>](solid line) in comparison to those of the building blocks MPEG-tpy (dotted line) and **1a** (dashed line). For all measurements DMAc containing 0.005 M NH<sub>4</sub>PF<sub>6</sub> was used as an eluent.



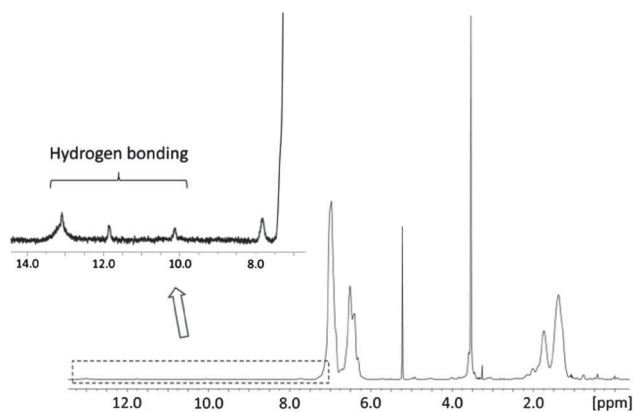
**Fig. 2** 3D-SEC trace of [(MPEG-tpy)Ni(**1a**)<sup>2+</sup>](solid line) as recorded with a PDA detector (eluent: DMAc containing 0.005 M NH<sub>4</sub>PF<sub>6</sub>).

as the PS educt **1a** (retention time: 18.0 min), an absorption maximum at λ<sub>max</sub> = 275 nm according to the tpy-MPEG educt. In this respect, analogous observations were made for [(MPEG<sub>44</sub>-tpy)Ni(**1b**)<sup>2+</sup>](Fig. S5†).

In addition, <sup>1</sup>H NMR spectroscopic investigations were carried out to investigate if (a) both polymeric blocks were linked



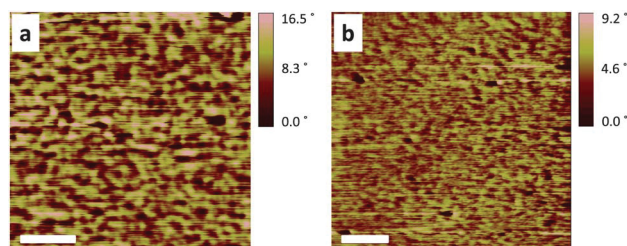
**Scheme 1** Schematic representation of the synthesis of the supramolecular quasi-triblock copolymer A(B)<sub>2</sub>A [(MPEG-tpy)Ni(tpy-PS-UPy)]<sub>2</sub>(PF<sub>6</sub>)<sub>4</sub> and the reference diblock copolymer [(MPEG)Ni(tpy-PS-OH)](PF<sub>6</sub>)<sub>2</sub>.



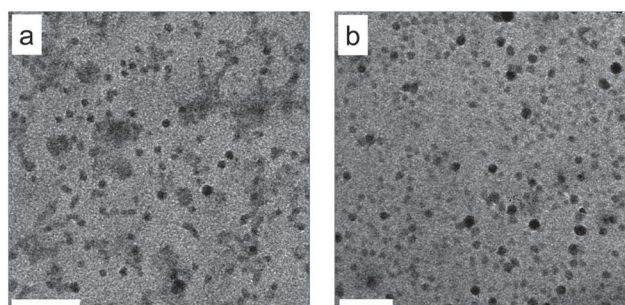
**Fig. 3**  $^1\text{H}$  NMR spectrum (400 MHz,  $\text{CD}_2\text{Cl}_2$ , 298 K) of  $\{[(\text{MPEG-tpy})\text{Ni}(\text{tpy-PS-UPy})]_2\}(\text{PF}_6)_4$ . The inset shows the formation of the related hydrogen bonds.

*via* terpyridine bis-complexes and (b) in the case of  $\{[(\text{MPEG-tpy})\text{Ni}(\text{tpy-PS-UPy})]_2\}(\text{PF}_6)_4$ , dimerization of the AB diblock copolymer *via* hydrogen bonding towards  $\text{A}(\text{B})_2\text{A}$  occurred in dichloromethane as a non-coordinating solvent (Fig. 3). Both blocks are represented by the characteristic signals for PS and PEG, although (a) the signals corresponding to the terpyridine units could not be observed due to the paramagnetic nature of the Ni(II) complex, whereas (b) the signals arising from hydrogen bonding could unambiguously be identified. The hydrogen bonding signal around 13 ppm overlaps with the signals ascribed to a low-field shift of the terpyridine protons caused by the paramagnetic environment (this signal can also be observed for the nonhydrogen-bonded  $[(\text{MPEG})\text{Ni}(\text{tpy-PS-OH})](\text{PF}_6)_2$  (see Fig. S6<sup>†</sup>). The hydrogen bonding can be cleaved by adding an acid to the solution neither affecting the alkoxyamine<sup>31</sup> nor the pH insensitive Ni(II) bis-terpyridine complex.<sup>39</sup> Within the accuracy of NMR integration, the estimated ratio of the degree-of-polymerization (DP) of the PS and PEG blocks was in good agreement with the expected ratio (see ESI<sup>†</sup>). Thus, the formation of the heteroleptic complex as well as the formation of the  $\text{A}(\text{B})_2\text{A}$  quasi-triblock copolymer could be confirmed. The metallopolymers of the quasi-triblock  $\{[(\text{MPEG-tpy})\text{Ni}(\text{tpy-PS-UPy})]_2\}(\text{PF}_6)_4$  ( $\text{A}(\text{B})_2\text{A}$ ) as well as the diblock  $[(\text{MPEG})\text{Ni}(\text{tpy-PS-OH})](\text{PF}_6)_2$  (AB) were also processed into the solid state by spin-coating from a 2 wt% solution of toluene as a nonpolar aprotic solvent allowing self-complementary hydrogen bonding of the UPy moieties.

The morphology of the thin film was investigated by atomic force microscopy (AFM) in the hard tapping mode without prior annealing (see ESI<sup>†</sup> for preparation details). Due to the immiscibility of the incorporated polymer blocks, phase separation occurred in the solid state for the AB diblock copolymer; the same behavior was observed for  $\text{A}(\text{B})_2\text{A}$ , though less well expressed. The AFM images showed areas of hard and soft materials that could be assigned to the PS and PEG blocks, respectively (Fig. 4). Hereon, a phase separation was present, but non-ordered, for the AB copolymer, while for the  $\text{A}(\text{B})_2\text{A}$  only a poorly and non-ordered phase separation with a significantly smaller length scale was observed. In contrast to this, the previously studied non-annealed films of metallo-supramolecular AB diblock copolymers of the general type  $[(\text{MPEG-tpy})$



**Fig. 4** AFM phase image (hard-tapping mode) of Ni(II)-containing copolymer films spin-coated from toluene: (a)  $[(\text{MPEG})\text{Ni}(\mathbf{1b})](\text{PF}_6)_4$  and (b)  $[(\text{MPEG})\text{Ni}(\mathbf{1a})](\text{PF}_6)_2$  (scale bar: 200 nm).



**Fig. 5** TEM images of a DMAC/water solution (2 : 1,  $0.6 \text{ g L}^{-1}$ ) of the AB block copolymers without staining: (a)  $[(\text{MPEG}_{44})\text{Ni}(\text{tpy-PS-OH})](\text{PF}_6)_2$  and (b)  $[(\text{MPEG}_{44})\text{Ni}(\text{tpy-PS-UPy})](\text{PF}_6)_2$  (scale bar: 200 nm).

$\text{Ru}(\text{tpy-PS})](\text{PF}_6)_2$  with different lengths of the PEG and PS blocks showed ordered phase separation and revealed that a change of the counterion has a large impact on the phase separation behavior.<sup>40</sup> It might be speculated that the block lengths of the synthesized block copolymers are too short to achieve an ordered phase separation. However, the difference in the phase separation for the two systems indicated the presence of the multiple hydrogen bonding within  $[(\text{MPEG})\text{Ni}(\mathbf{1a})](\text{PF}_6)_2$  and its influence on the phase separation in the solid state.

As the micellization of amphiphilic block copolymers in a selective solvent has, in the present case of a metal complex at the heterojunction, a stringent evidence for the formation of the heteroleptic Ni(II) complex, DMAC solutions ( $1 \text{ g L}^{-1}$ ) were used for micellization by a cosolvent method with water as the selective solvent for the PEG block. Since this solvent mixture is a strong competitor for hydrogen bonding, only the AB diblock copolymers could be observed in both cases by transmission electron microscopy (TEM) (Fig. 5, left:  $[(\text{MPEG})\text{Ni}(\mathbf{1b})](\text{PF}_6)_2$ , right:  $[(\text{MPEG}_{44})\text{Ni}(\mathbf{1a})](\text{PF}_6)_2$ ). In both cases, spherical micellar assemblies were observed, while the block length cannot be related to the size of the micellar aggregation as for covalently bonded PEG-*b*-PS due to the ionic interactions of the complexes.<sup>41</sup> This indicates the formation of heteroleptic Ni(II) complexes for both heterotelechelic PS blocks.

## Conclusions

The efficient one-pot synthesis of an amphiphilic  $\text{A}(\text{B})_2\text{A}$  supramolecular block copolymer is shown where two



orthogonal non-covalent types of interaction – metal-to-ligand coordination and hydrogen bonding – have been utilized at the heterojunction (A–B) and homojunction (B–B) between the blocks, respectively. The polymeric materials have been characterized by size exclusion chromatography, UV-vis spectroscopy and  $^1\text{H}$  NMR spectroscopy. Furthermore, the assembly of the amphiphilic block copolymers was investigated in solution (TEM) and in the solid state (AFM) proving the heteroleptic complexation and the influence of the hydrogen bonding moiety on the morphology of the films, respectively. In solution, self-complementary hydrogen bonding of the AB diblock metallopolymer  $[(\text{MPEG-tpy})\text{Ni}(\text{tpy-PS-UPy})](\text{PF}_6)_2$  towards the  $\text{A}(\text{B})_2\text{A}$  quasi-triblock copolymer  $\{[(\text{MPEG-tpy})\text{Ni}(\text{tpy-PS-UPy})]_2\}(\text{PF}_6)_4$  was proven in an aprotic solvent by  $^1\text{H}$  NMR studies. Since the stimuli-responsive behavior of the  $\text{Ni}^{\text{II}}$  metallo-supramolecular entities has already been shown elsewhere for amphiphilic metallo-supramolecular AB diblock copolymers,<sup>33a</sup> we conclude that the supramolecular materials can be addressed *via* the nickel complex, but in the present case additionally *via* the hydrogen bonding connection. This expands the range of responsiveness and, thus, the control over the assembly of such supramolecular block copolymers as not only the constitution can be controlled over the metal complex at the heterojunction (PEG–PS), but also the block length by reversible hydrogen bonding representing the homojunction (PS–PS). Thereby, the block junctions can be independently addressed due to the orthogonality of the supramolecular binding sites. The presented approach of combining one-step polymerized telechelic building blocks with one-pot orthogonal assembly of supramolecular binding sites is promising for studying the influence of multiple supramolecular linkages on the self-assembly behavior of amphiphilic copolymers as the polymeric spacers can be varied within a minimum number of steps.

## Acknowledgements

We thank the Dutch Polymer Institute (DPI, technology area HTE) and the Deutsche Forschungsgemeinschaft (DFG, SPP 1568) for financial support.

## Notes and references

- X.-H. Yan, F. Wang, B. Zheng and F.-H. Huang, *Chem. Soc. Rev.*, 2012, **41**, 6042–6065.
- T. F. A. De Greef and E. W. Meijer, *Nature*, 2008, **453**, 171–173.
- O. Ikkala and G. Ten Brinke, *Science*, 2002, **295**, 2407–2409.
- A. Harada, R. Kobayashi, Y. Takashima, A. Hashidzume and H. Yamaguchi, *Nat. Chem.*, 2011, **3**, 34–37.
- H. H. Dam and F. Caruso, *Adv. Mater.*, 2011, **23**, 3026–3029.
- J. Luo, T. Lei, L. Wang, Y. Ma, Y. Cao, J. Wang and J. Pei, *J. Am. Chem. Soc.*, 2009, **131**, 2076–2077.
- D. González-Rodríguez and A. P. H. J. Schenning, *Chem. Mater.*, 2011, **23**, 310–325.
- S. Fuji and J.-M. Lehn, *Angew. Chem., Int. Ed.*, 2009, **48**, 7635–7638.
- C. C. Lee, C. Grenier, E. W. Meijer and A. P. H. J. Schenning, *Chem. Soc. Rev.*, 2009, **38**, 671–683.
- P. Jonkheijm, P. Van der Schoot, A. P. H. J. Schenning and E. W. Meijer, *Science*, 2006, **313**, 80–83.
- F. J. M. Hoeben, P. Jonkheijm, E. W. Meijer and A. P. H. J. Schenning, *Chem. Rev.*, 2005, **105**, 1491–1546.
- A. Ustinov, H. Weissman, E. Shirman, I. Pinkas, X.-B. Zuo and B. Rybtchinski, *J. Am. Chem. Soc.*, 2001, **133**, 16201–16211.
- E. Obert, M. Bellot, L. Bouteiller, F. Andrioletti, C. Lehen-Ferrenbach and F. Boué, *J. Am. Chem. Soc.*, 2007, **129**, 15601–15605.
- H. W. Roesky and M. Andruh, *Coord. Chem. Rev.*, 2003, **236**, 91–119.
- R. Hoogenboom, D. Fournier and U. S. Schubert, *Chem. Commun.*, 2008, 155–162.
- S.-K. Yang, A. V. Ambade and M. Weck, *Chem. Soc. Rev.*, 2011, **40**, 129–137.
- R. Dobrawa and F. Würthner, *J. Polym. Sci., Part A: Polym. Chem.*, 2005, **43**, 4981–4995.
- A. Wild, A. Winter, F. Schlütter and U. S. Schubert, *Chem. Soc. Rev.*, 2011, **40**, 1459–1511.
- G. R. Whittell, M. D. Hager, U. S. Schubert and I. Manners, *Nat. Mater.*, 2011, **10**, 176–188.
- K. A. Williams, A. J. Boydston and C. W. Bielawski, *Chem. Soc. Rev.*, 2007, **36**, 729–744.
- J.-C. Eloi, L. Chabanne, G. R. Whittell and I. Manners, *Mater. Today*, 2008, **11**, 28–36.
- C.-L. Ho and W.-Y. Wong, *Coord. Chem. Rev.*, 2011, **255**, 2469–2502.
- M. Chiper, R. Hoogenboom and U. S. Schubert, *Macromol. Rapid Commun.*, 2009, **30**, 565–578.
- W. H. Binder and R. Zirbs, *Adv. Polym. Sci.*, 2007, **207**, 1–78.
- L. Brunsveld, B. J. B. Folmer, E. W. Meijer and R. P. Sijbesma, *Chem. Rev.*, 2001, **101**, 4071–4097.
- T. F. A. De Greef, M. M. J. Smulders, M. Wolffs, A. P. H. J. Schenning, R. P. Sijbesma and E. W. Meijer, *Chem. Rev.*, 2009, **109**, 5687–5754.
- A. Winter, M. D. Hager and U. S. Schubert, *Supramolecular Polymers in Polymer Science: A Comprehensive Reference*, ed. M. Möller, K. Matyjaszewski, H.-W. Schmidt and M. Ueda, Elsevier BV, Amsterdam, 2012, vol. 5, pp. 269–310.
- U. S. Schubert, C. Eschbaumer, P. Andres, H. Hofmeier, C. H. Weidl, E. Herdtweck, E. Dulkeith, A. Morteani, N. E. Hecker and J. Feldmann, *Synth. Met.*, 2001, **121**, 1249–1252; U. S. Schubert and C. Eschbaumer, *Angew. Chem., Int. Ed.*, 2002, **41**, 2892–2926; H. Hofmeier, S. Schmatloch, D. Wouters and U. S. Schubert, *Macromol. Chem. Phys.*, 2003, **204**, 2197–2203.
- U. S. Schubert, A. Winter and G. R. Newkome, *Terpyridine-based Materials*, Wiley-VCH, Weinheim, 2011.
- H. Hofmeier, A. El-ghayoury, A. P. H. J. Schenning and U. S. Schubert, *Chem. Commun.*, 2004, 318–319; H. Hofmeier, R. Hoogenboom, M. E. L. Wouters and U. S. Schubert, *J. Am. Chem. Soc.*, 2005, **127**, 2913–2921.
- U. Mansfeld, M. D. Hager, R. Hoogenboom, C. Ott, A. Winter and U. S. Schubert, *Chem. Commun.*, 2009, 3386–3388.



- 32 U. Mansfeld, A. Winter, M. D. Hager, R. Hoogenboom, W. Günther and U. S. Schubert, *Polym. Chem.*, 2013, **4**, 113–123.
- 33 (a) C. Mugemana, P. Guillet, S. Hoepfener, U. S. Schubert, C.-A. Fustin and J.-F. Gohy, *Chem. Commun.*, 2010, **46**, 1296–1298; (b) R. Shunmugam, G. J. Gabriel, K. A. Aamer and G. N. Tew, *Macromol. Rapid Commun.*, 2010, **31**, 784–793; (c) R. Hogg and R. G. Wilkins, *J. Chem. Soc.*, 1962, 341–350; (d) R. H. Holyer, C. D. Hubbard, S. F. A. Kettle and R. G. Wilkins, *Inorg. Chem.*, 1966, **5**, 622–625; (e) D. Rablen and G. Gordon, *Inorg. Chem.*, 1969, **8**, 395–397.
- 34 J.-F. Gohy, B. G. G. Lohmeijer and U. S. Schubert, *Chem.–Eur. J.*, 2003, **9**, 3472–3479; J.-F. Gohy, B. G. G. Lohmeijer, A. Alexeev, X.-S. Wang, I. Manners, M. A. Winnik and U. S. Schubert, *Chem.–Eur. J.*, 2004, **10**, 4315–4323.
- 35 B. G. G. Lohmeijer and U. S. Schubert, *J. Polym. Sci., Part A: Polym. Chem.*, 2004, **42**, 4016–4027.
- 36 The heterotelechelic polymers **1a** and **1b** were synthesized using the hetero-functionalized alkoxyamines tpy-TIPNO-UPy and tpy-TIPNO-OH as initiators for the polymerization of styrene (for details see the ESI†).
- 37 M. Chiper, M. A. R. Meier, J. M. Kranenburg and U. S. Schubert, *Macromol. Chem. Phys.*, 2007, **208**, 679–689.
- 38 The degree-of-polymerization of the PEG chain was DP = 44: MeO(CH<sub>2</sub>CH<sub>2</sub>)<sub>44</sub>O-tpy.
- 39 B. G. G. Lohmeijer and U. S. Schubert, *Macromol. Chem. Phys.*, 2003, **204**, 1072–1078.
- 40 M. Al-Hussein, B. G. G. Lohmeijer, U. S. Schubert and W. H. de Jeu, *Macromolecules*, 2003, **36**, 9281–9284; B. G. G. Lohmeijer, D. Wouters, Z.-H. Yin and U. S. Schubert, *Chem. Commun.*, 2004, 2886–2887; M. Al-Hussein, W. H. de Jeu, B. G. G. Lohmeijer and U. S. Schubert, *Macromolecules*, 2005, **38**, 2832–2836.
- 41 P. Guillet, C.-A. Fustin, B. G. G. Lohmeijer, U. S. Schubert and J.-F. Gohy, *Macromolecules*, 2006, **39**, 5484–5488.



## Supporting Information

### Amphiphilic supramolecular A(B)<sub>2</sub>A quasi-triblock copolymers

*Ulrich Mansfeld,<sup>a,b,c</sup> Andreas Winter,<sup>a,b,c</sup> Martin D. Hager,<sup>a,b,c</sup> Grit Festag,<sup>a,b</sup> Stephanie Hoepfener,<sup>a,b</sup> Ulrich S. Schubert<sup>\*a,b,c</sup>*

<sup>a</sup> Laboratory of Organic and Macromolecular Chemistry (IOMC), Friedrich-Schiller-University Jena, Humboldtstr. 10, 07743 Jena, Germany.

<sup>b</sup> Jena Center for Soft Matter (JCSM), Philosophenweg 7, 07743 Jena, Germany.

<sup>c</sup> Dutch Polymer Institute (DPI), P.O. Box 902, 5600 AX Eindhoven, The Netherlands.

## Experimental Details

**Methods and Instrumentation.** All chemicals were received from Aldrich, Fluka and Acros; solvents were purchased from Biosolve. Unless otherwise stated, the chemicals and solvents were used without further purifications. DMF was dried over molsieves (pore size of 4 Å). THF and toluene were dried using a PureSolv-EN<sup>TM</sup> solvent purification system. Styrene was freshly purified prior to use by filtration over neutral aluminium oxide 90 (Merck). 1D (<sup>1</sup>H, <sup>13</sup>C) nuclear magnetic resonance (NMR) spectra were recorded on a Varian Mercury 400 MHz spectrometer at 298 K, 348 K or 368 K. Chemical shifts are reported in parts per million (ppm) downfield from tetramethylsilane (TMS) and were calibrated to the residual solvent peaks. Deuterated solvents for NMR spectroscopy were obtained from Cambridge Isotope Laboratories as well as Eurisotop. Two different set-ups for size-exclusion chromatography (SEC) were used: A Shimadzu system equipped with a SCL-10A system controller, a LC-10AD pump, a RID-10A refractive index (RI) detector, an UV-vis absorption detector (250 and 290 nm) and a PSS SDV column utilizing chloroform/isopropanol/triethylamine [94/2/4] as eluent. The column temperature was 40 °C at a flow rate of 1 mL min<sup>-1</sup>. Linear polystyrene was used as the calibration standard. Additionally, SECs were measured on a Waters SEC system consisting of an isocratic pump (HPLC 1515), a solvent degasser (DG-980-50), a column oven (Column Heater 1500), a photodiode array detector (Detector 2996), a RI detector (2414) and a Phenomenex Phenogel column with a precolumn installed. The eluent was DMAc containing 0.08 % NH<sub>4</sub>PF<sub>6</sub> at a flow rate of 1 mL min<sup>-1</sup>. The column temperature was 50 °C. AFM measurements were performed on a Nanoscope IIIa Multimode.

## Synthesis

tpy-MPEG<sub>44</sub> was synthesized as described elsewhere.<sup>1</sup>

SEC (RI, eluent: CHCl<sub>3</sub>):  $M_n = 2\ 050\ \text{g mol}^{-1}$ , PDI = 1.13. UV-vis (CHCl<sub>3</sub>):  $\lambda_{\text{max}} = 277\ \text{nm}$ .

## General styrene polymerization procedure<sup>2</sup>

Styrene monomers were freshly purified by filtration over Al<sub>2</sub>O<sub>3</sub> prior to use in order to remove the inhibitor. The freshly purified styrene was added to a clear anisole solution of the TIPNO-based initiator in a polymerization vessel. After applying three freeze-pump-thaw-cycles to remove the oxygen, the vessel was purged with argon and immersed in an oilbath at 123 °C for a certain period of time. To remove residual monomer the reaction mixture was precipitated from CHCl<sub>3</sub> into cold methanol. The monomer conversion was determined by GC measurements (before precipitation), the molar masses (*i.e.*  $M_n$  and  $M_w$ ) and the polydispersity index (PDI) values were determined by SEC, whereas <sup>1</sup>H NMR spectroscopy was applied for the determination of the endgroup functionality (by integration and comparison of the corresponding endgroup signals) and  $M_n$  values (by integration of the polymer backbone to the terpyridine signals).

### tpy-PS-UPy, **1a**

The heterotelechelic macroligand **1a** (tpy-PS-UPy) was synthesized by using the initiator tpy-TIPNO-UPy that was synthesized according to literature.<sup>2</sup>

m(tpy-TIPNO-UPy) = 15 mg; m(Styrene) = 350 mg; V(anisole) = 800  $\mu$ L; monomer to initiator ratio: M/I = 200; concentration: c = 3 mol L<sup>-1</sup>; polymerization time: t = 300 min.

<sup>1</sup>H NMR (400 MHz, CD<sub>2</sub>Cl<sub>2</sub>):  $\delta$  = 0.06–2.63 (set of multiplets), 3.05–3.37 (m, 4H), 3.39–3.66 (m, 1H), 3.99–4.24 (m, 1H), 4.95–5.35 (m, 5H), 5.83 (s, 1H), 6.30–7.50 (m, 560H), 7.81 (m, 2H), 8.12–8.22 (m, 2H), 8.61–8.74 (m, 4H), 10.13 (s, 1H), 11.83 (s, 1H), 13.09 (s, 1H) ppm. SEC (CHCl<sub>3</sub>, RI):  $M_n$  = 9,300 g·mol<sup>-1</sup>, PDI = 1.17.

conversion [%] (GC)	$M_n$ [g/mol] theoret.	$M_n$ [g/mol] (SEC)	PDI (SEC)	$M_n$ [g/mol] ( <sup>1</sup> H NMR)
41	9 400	9 300	1.17	12 300

### tpy-PS-OH, **1b**

The heterotelechelic macroligand **1b** (tpy-PS-OH) was synthesized using the initiator tpy-TIPNO-OH that was prepared according to literature.<sup>2</sup>

m(tpy-TIPNO-OH) = 10 mg; m(Styrene) = 350 mg; V(anisole) = 800  $\mu$ L; monomer to initiator ratio: M/I = 200; concentration: c = 3 mol L<sup>-1</sup>; polymerization time: t = 300 min.

<sup>1</sup>H NMR (400 MHz, CD<sub>2</sub>Cl<sub>2</sub>):  $\delta$  = 0.06–2.60 (set of multiplets), 3.07–3.35 (m, 1H), 4.00–4.22 (m, 1H), 4.50–4.72 (m, 2H), 5.20–5.38 (m, 2H), 6.26–7.50 (m, 530H), 7.38–7.94 (m, 2H), 8.10–8.22 (m, 2H), 8.62–8.75 (m, 4H) ppm. SEC (CHCl<sub>3</sub>, RI):  $M_n$  = 9,000 g·mol<sup>-1</sup>, PDI = 1.14.

conversion [%] (GC)	$M_n$ [g/mol] theoret.	$M_n$ [g/mol] (SEC)	PDI (SEC)	$M_n$ [g/mol] ( <sup>1</sup> H NMR)
38	8 900	9 000	1.14	11 400

### {[(MPEG<sub>44</sub>)Ni(**1a**)]<sub>2</sub>}(PF<sub>6</sub>)<sub>4</sub>

The precursor complex of NiCl<sub>2</sub>·6DMF was prepared by stirring of NiCl<sub>2</sub>·6H<sub>2</sub>O (0.83 mg, 3.5  $\mu$ mol) in 1.7 mL of dry DMF for 1 h at room temperature under argon. The polymeric mono-complex was synthesized by addition of tpy-PS<sub>110</sub>-UPy (31 mg, 3.3  $\mu$ mol) in 1.7 mL of DMF. After stirring the solution for 10 min the macroligand tpy-PEG<sub>44</sub> (7.4 mg, 3.3  $\mu$ mol) in 1.7 mL of DMF was added and the solution was stirred under argon overnight at room temperature. An exchange of the counterion was made by addition of an excess of NH<sub>4</sub>PF<sub>6</sub> (10 mg) to the reaction mixture and stirring for 3 h. Subsequently the reaction mixture was concentrated under vacuum and the residue was washed under stirring with diethyl ether (2 days) and with water (1 day). The reaction yield was estimated at 50%.

$^1\text{H}$  NMR (400 MHz,  $\text{CD}_2\text{Cl}_2$ ):  $\delta$  = 0.06–2.65 (set of multiplets), 3.09–3.29 (m, 4H), 3.45–3.89 (m, 140H), 4.02–4.21 (m), 4.52–4.72 (m), 4.95–5.21 (m, 3H), 5.74–5.92 (m), 6.30–7.45 (m, 570H), 7.72–7.97 (m), 10.13 (s, 1H), 11.83 (s, 1H), 12.73–13.42 (m) ppm.

$\{[(\text{MPEG}_{44})\text{Ni}(\mathbf{1b})]\}(\text{PF}_6)_2$

The precursor complex of  $\text{NiCl}_2 \cdot 6\text{DMF}$  was prepared *in situ* by stirring of  $\text{NiCl}_2 \cdot 6\text{H}_2\text{O}$  (0.83 mg, 3.5  $\mu\text{mol}$ ) in 1.7 mL of dry DMF for 1 h at room temperature under argon. The polymeric mono-complex was synthesized by addition of tpy- $\text{PS}_{100}\text{-OH}$  (30 mg, 3.3  $\mu\text{mol}$ ) in 1.7 mL of DMF. After stirring the solution for 10 min, the macroligand tpy- $\text{PEG}_{44}$  (7.4 mg, 3.3  $\mu\text{mol}$ ) in 1.7 mL of DMF was added and the solution was stirred under argon overnight at room temperature. An exchange of the counterion was made by addition of an excess of  $\text{NH}_4\text{PF}_6$  (10 mg) to the reaction mixture and stirring for 3 h. Subsequently the reaction mixture was concentrated under vacuum and the residue was washed under stirring with diethyl ether (2 days) and with water (1 day). The reaction yield was estimated at 35%.

$^1\text{H}$  NMR (400 MHz,  $\text{CD}_2\text{Cl}_2$ ):  $\delta$  = 0.06–2.36 (set of multiplets), 3.07–3.65 (m, 1H), 3.33–4.01 (m, 160), 4.04–4.20 (m), 4.50–4.80 (m), 5.20–5.38 (m, 2H), 6.23–7.41 (m, 530H), 7.70–7.94 (m), 12.81–13.44 (m) ppm.

AFM investigations of the polymer films

100  $\mu\text{L}$  of a solution of  $\{[(\text{MPEG}_{44})\text{Ni}(\mathbf{1b})]\}(\text{PF}_6)_2$  in toluene (2 wt%) was spin-coated on a silicon wafer (500 rpm, 30 s) and the resulting polymeric films were allowed to dry for 24 h and were subsequently investigated by AFM without further temperature annealing. The samples were investigated by light and hard tapping mode.

### **Theoretical aspects on the selective formation of heteroleptic nickel(II) *bis*-terpyridine complexes in a one-pot reaction.**

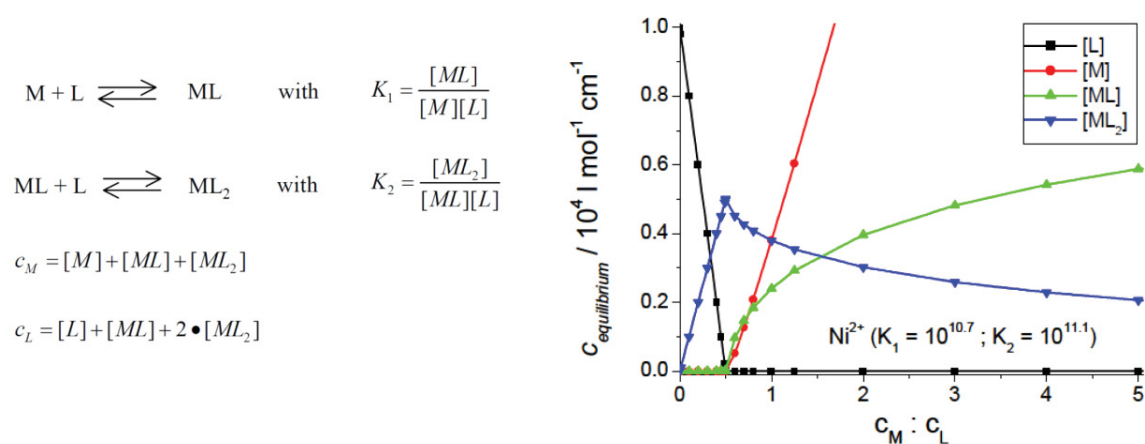
Considering only the thermodynamic stability of the Ni(II) complex the selectivity for the heteroleptic complex formation cannot be explained for the present one-pot strategy:

Both the *mono*- as well as the *bis*-terpyridine complex of Ni(II) have high stability constants compared to other transition metal ions:  $\lg K_1 = 10.7$  and  $\lg K_2 = 11.1$  (in water at 25 °C) as determined by Wilkins and coworkers.<sup>3</sup> In contrast to iron(II), the stability of the *mono*-complex is only slightly lower compared to the stability of the *bis*-complex: This results in the formation of comparable equilibrium concentrations of both complexes at the metal-to-ligand ratio of 1:1 that is visualized in Figure S1. But as this ratio has to be ensured for the stoichiometric formation of the *mono*-complex within the stepwise one-pot complexation, kinetic considerations have to be taken into account to understand the A-B selectivity: The *mono*-terpyridine complex of Ni(II) is of unique inertness indicated by a high stability against

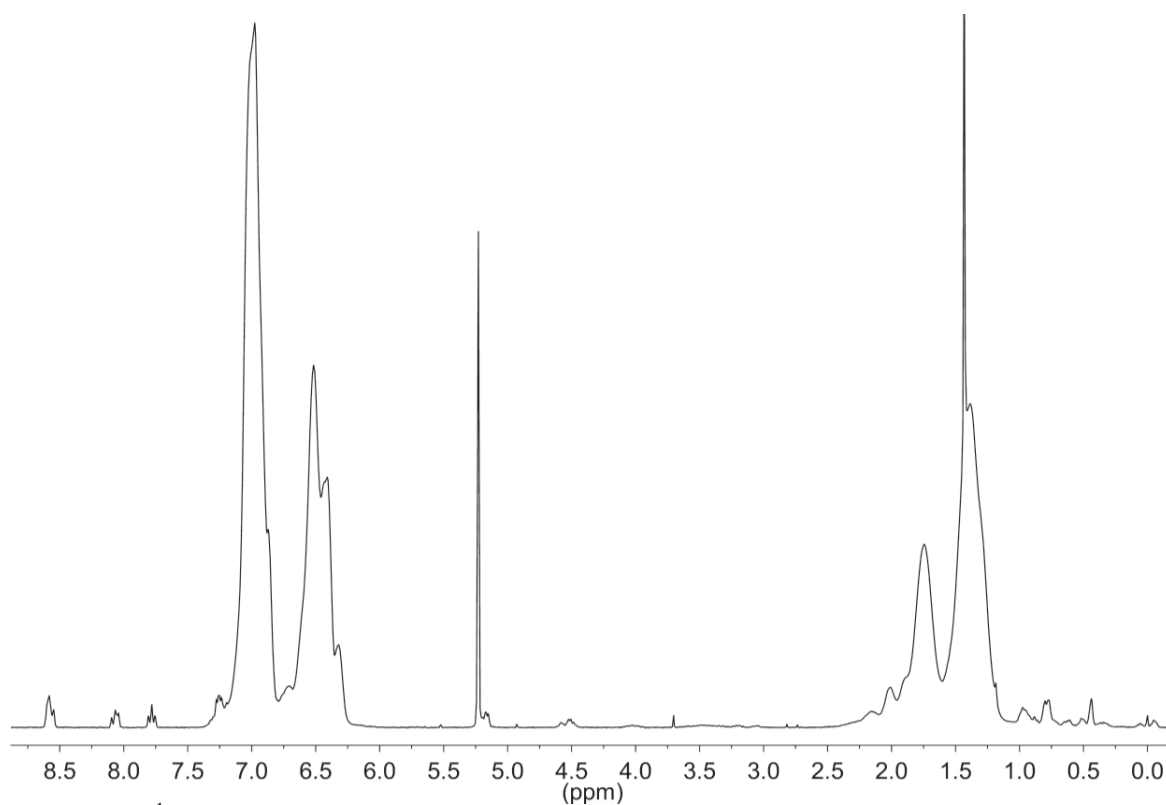


disproportionation<sup>4</sup> and due to the fact that the *bis*-complex formation is not enhanced as it was observed for other transition metals.<sup>5</sup> Furthermore, by using DMF as solvent the kinetic stability of the *mono*-complex is tentatively enhanced as the formation rates of the *bis*- as well as the *mono*-complex are significantly decreased changing the solvent from water<sup>3</sup> to DMSO<sup>6</sup> due to the higher coordination rate of the solvent.

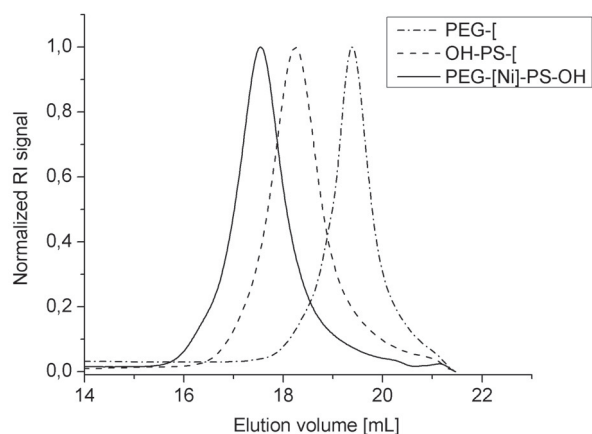
The addition of the second ligand after a short period of time guarantees the kinetic control for the first step with non-equilibrium concentrations pronouncing the formation of the *mono*-complex as precursor at a metal-to-ligand ratio of 1:1 before the addition. The metal-to-ligand ratio of 1:2 after addition of the second ligand ensures the formation of the heteroleptic *bis*-complex under thermodynamic control with equilibrium concentrations (visualized in Figure S1) as the reaction mixture was allowed to stir overnight. The inert character of the *bis*-terpyridine Ni(II) complex maintains the heteroleptic complex and thus allows the integrity of the A-B formation.<sup>4,7</sup>



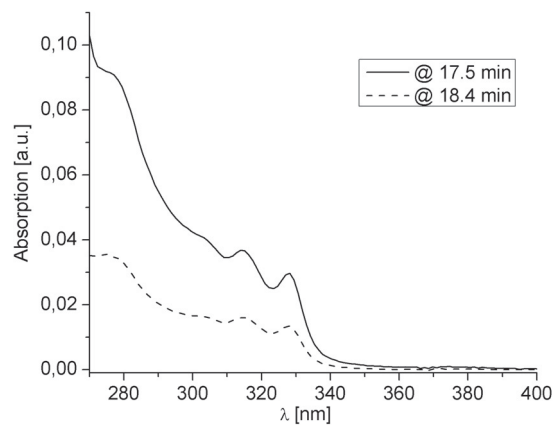
**Figure S1.** Modeling of the equilibrium concentrations of ligand [L], metal ion [M], mono-complex [ML] and *bis*-complex [ML<sub>2</sub>] as a function of the initial ratio of metal to ligand  $c_M:c_L$  using the equilibrium constants  $\lg K_1=10.7$  and  $\lg K_2=11.1$  for Ni<sup>II</sup> in water at 25 °C as determined by Wilkins and coworkers<sup>3</sup> (image was reprinted from literature<sup>8</sup>).



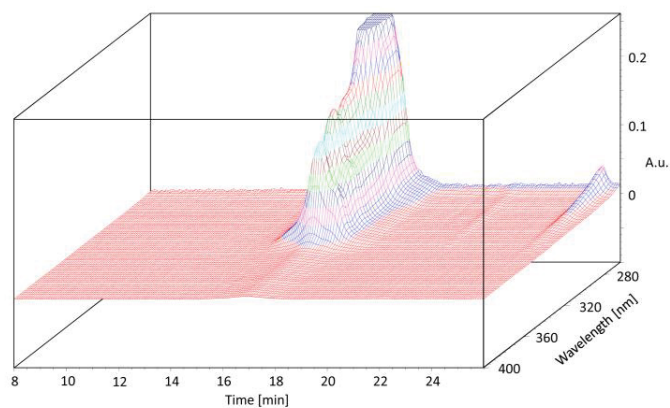
**Figure S2.** <sup>1</sup>H NMR spectrum of tpy-PS-OH, **1b** (400 MHz, CD<sub>2</sub>Cl<sub>2</sub>, 298 K).



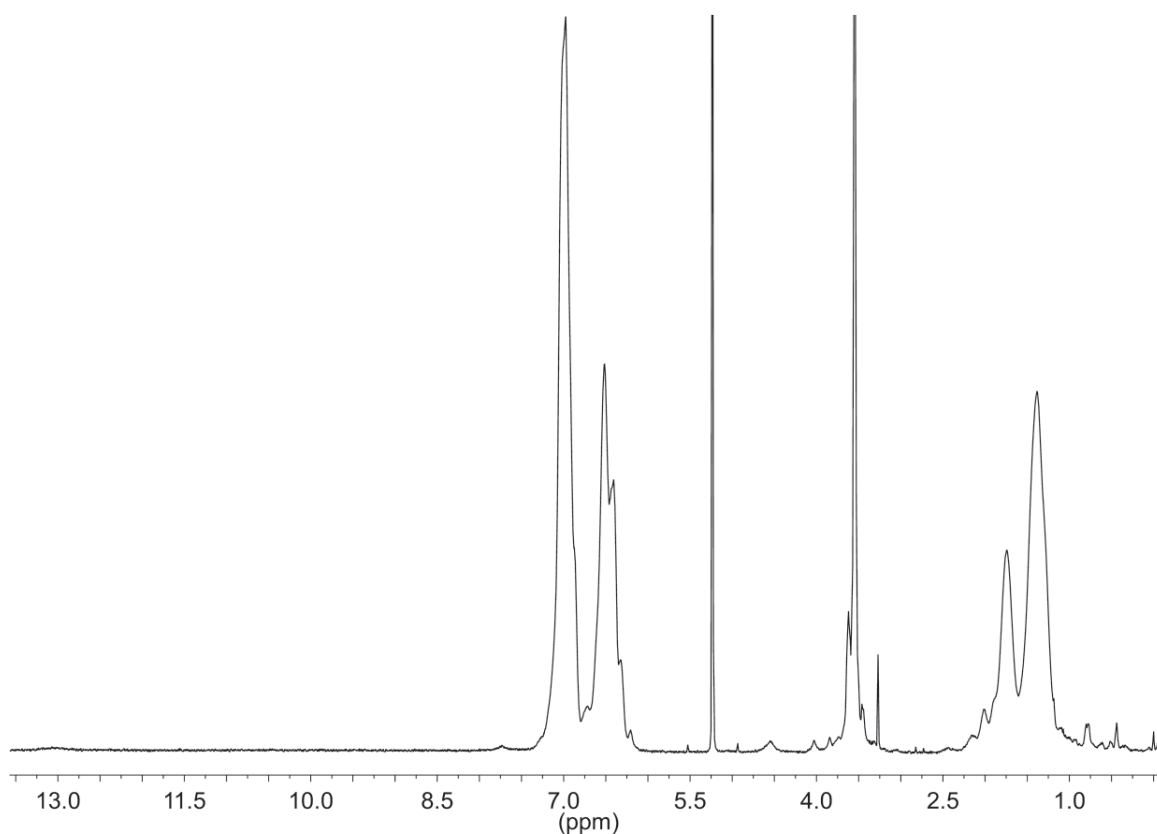
**Figure S3.** SEC traces (RI detector) of the diblock copolymer [(MPEG-tpy)Ni(**1b**)]<sup>2+</sup> (solid line) in comparison to those of the building blocks MPEG-tpy (dotted line) and **1b** (dashed line). For all measurements: DMAc containing 0.005 M NH<sub>4</sub>PF<sub>6</sub> as eluent.



**Figure S4.** UV-vis absorption spectra of  $[(\text{MPEG-tpy})\text{Ni}(\mathbf{1a})]^{2+}$  as recorded with a PDA detector at 17.5 min and 18.4 min (solvent: DMAc containing 0.005 M  $\text{NH}_4\text{PF}_6$ ).



**Figure S5.** 3D-SEC trace of  $[(\text{MPEG})\text{Ni}(\mathbf{1b})]^{2+}$  as recorded with a PDA detector showing the formation of the Ni(II) *bis*-terpyridine complex with the characteristic ligand-centered bands at 329 nm and 315 nm. A small shoulder at low molar masses represents the formation of  $[(\text{MPEG})_2\text{Ni}]^{2+}$  (eluent: DMAc containing 0.005 M  $\text{NH}_4\text{PF}_6$ ).



**Figure S6.**  $^1\text{H}$  NMR spectrum of  $\{(\text{MPEG})\text{Ni}(\mathbf{1b})\}(\text{PF}_6)_2$  (400 MHz,  $\text{CD}_2\text{Cl}_2$ , 298 K).

## References

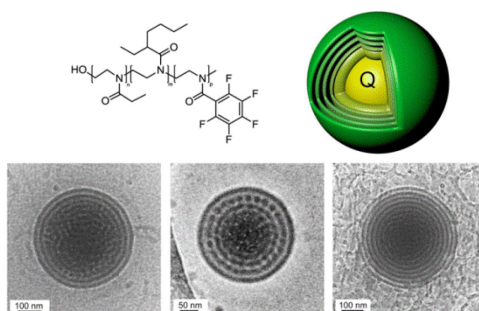
- [1] M. Chiper, M. A. R. Meier, J. M. Kranenburg, and U. S. Schubert, *Macromol. Chem. Phys.*, 2007, **208**, 679-689.
- [2] U. Mansfeld, M. D. Hager, R. Hoogenboom, C. Ott, A. Winter and U. S. Schubert, *Chem. Commun.*, 2009, 3386-3388.
- [3] R. H. Holyer, C. D. Hubbard, S. F. A. Kettle and R. G. Wilkins, *Inorg. Chem.*, 1966, **5**, 622-625.
- [4] R. Hogg and R. G. Wilkins, *J. Chem. Soc.*, 1962, 341-350.
- [5] D. Rablen and G. Gordon, *Inorganic Chemistry*, 1969, **8**, 395-397.
- [6] P. A. Cock, C. E. Cottrell and R. K. Boyd, *Can. J. Chem.*, 1972, **50**, 402-411.
- [7] R. Shunmugam, G. J. Gabriel, K. A. Aamer and G. N. Tew, *Macromol. Rapid Commun.* 2010, **31**, 784-793.
- [8] B. G. G Lohmeijer, *Playing LEGO with macromolecules*, PhD Thesis, Eindhoven University of Technology, The Netherlands, **2005**.

## Publication P5:

### *Tuning the morphology of triblock terpoly(2-oxazoline)s containing a 2-phenyl-2-oxazoline block with varying fluorine content*

U. Mansfeld, S. Hoepfener, K. Kempe, J.-M. Schumers, J.-F. Gohy and U. S. Schubert

*Soft Matter* **2013**, *9*, 5966-5974



Reproduced by permission of The Royal Society of Chemistry

<http://dx.doi.org/10.1039/C3SM50159K>





## Tuning the morphology of triblock terpoly(2-oxazoline)s containing a 2-phenyl-2-oxazoline block with varying fluorine content†

Cite this: *Soft Matter*, 2013, 9, 5966

Ulrich Mansfeld,<sup>ab</sup> Stephanie Hoepfener,<sup>\*ac</sup> Kristian Kempe,<sup>ab</sup> Jean-Marc Schumers,<sup>d</sup> Jean-François Gohy<sup>d</sup> and Ulrich S. Schubert<sup>abc</sup>

The formation of nanostructures in triblock terpolymers consisting of poly[2-ethyl-2-oxazoline-*block*-2-(1-ethylpentyl)-2-oxazoline-*block*-2-(X-fluorophenyl)-2-oxazoline] (X = di, tri, tetra and penta) was investigated in water. For this purpose a gradually increasing degree of fluorination was introduced in the molecular structures and its influence on the self-assembly was studied. It can be demonstrated that the basic form of aggregation of these systems resembles rod-like micelles, which tend, upon introduction of fluorinated blocks, to aggregate first into 2-dimensional and later into 3-dimensional super-aggregates. In the case of di- and pentafluorinated terpolymers well-defined structures were observed, which represent likely intermediate, stable transient structures formed during an assumed rod-to-vesicle transition. DLS and cryo-TEM were utilized to analyze the structural features of these nanostructures and a model for their further assembly into super-structures was developed.

Received 14th January 2013

Accepted 11th April 2013

DOI: 10.1039/c3sm50159k

[www.rsc.org/softmatter](http://www.rsc.org/softmatter)

### Introduction

Recently, increasing research interest has been focused on the utilization of block copolymers as building blocks for the formation of functional nanostructures in solution. Potential applications for these structures are found, *e.g.*, in biology, drug delivery, templating and catalysis.<sup>1–4</sup> A major advantage of the utilization of block copolymers is the virtually unlimited possibility to combine a large diversity of different functionalities within a single macromolecule. While most of the studies have been devoted to the control of morphologies formed by diblock copolymers, the utilization of triblock terpolymers promises a larger variability of the formed nanostructures.<sup>5</sup> In this context, several previous studies have demonstrated that, besides the conventionally observed micellar and vesicular structures, more complex structures can also be obtained due to the facile interplay of different inter- and intramolecular forces exerted between the individual blocks of the terpolymers and between these blocks and the solvent. These additional driving forces can lead to the formation of, *e.g.*,

multicompartmentalized features,<sup>6–9</sup> which are superimposed on the basic structure of the formed aggregates, *i.e.*, raspberry-like micelles,<sup>8,10</sup> bicontinuous micelles,<sup>11,12</sup> lamellar<sup>13</sup> or tube-walled vesicles.<sup>14</sup> Moreover, those structures can further self-assemble to more complex super-aggregates due to secondary interactions, *e.g.* hexagonally packed hollow hoops (HHHs), as reported by Eisenberg and coworkers.<sup>15</sup> Müller *et al.* recently introduced comprehensive guidelines for the controlled hierarchical self-assembly of multicompartment micelles.<sup>16</sup> The authors discussed different considerations for the design of triblock terpolymers (*e.g.* poly[styrene-*b*-butadiene-*b*-(methyl methacrylate)s]) and controlled the self-assembly by a stepwise formation of intermediate, pre-assembled structures. This process leads to a gradual reduction of the degree of freedom during the self-assembly process and enables the precisely controlled formation of complex multicompartment micellar systems, in particular, regarding their size, geometry, patchiness and number of sub-units.

In general, molecular building blocks for copolymer nanostructures can consist of side-chain functionalized blocks with lipophilic, hydrophilic, fluorophilic, hard or soft properties. Fluorinated polymers are of increasing interest due to their oil and water repellence, low refractive index, low dielectric constant, low permittivity and low surface energy.<sup>17,18</sup> A general strategy to improve the poor processability of fluoropolymers is their integration into copolymer structures. Structural investigations by means of transmission electron microscopy (TEM) and cryo-TEM of such systems in solution have been performed<sup>19</sup> and frequently complex organized nanostructures with a multicompartment segmentation were found. Examples for the large

<sup>a</sup>Laboratory of Organic and Macromolecular Chemistry (IOMC), Friedrich Schiller University Jena, Humboldtstr. 10, 07743 Jena, Germany. E-mail: s.hoepfener@uni-jena.de; Fax: +49 3641 948202; Tel: +49 3641 948261

<sup>b</sup>Dutch Polymer Institute (DPI), P.O. Box 902, 5600 AX Eindhoven, The Netherlands  
<sup>c</sup>Jena Center for Soft Matter (JCSM), Friedrich Schiller University Jena, Philosophenweg 7, 07743 Jena, Germany

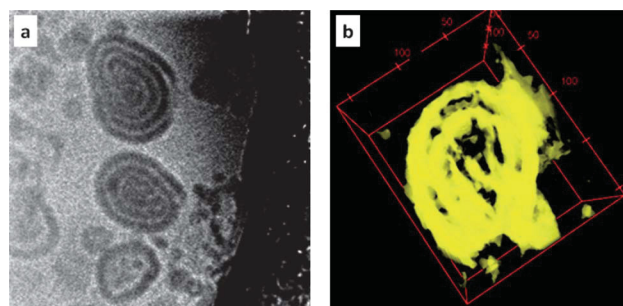
<sup>d</sup>Bio and Soft Matter (BSMA), Institute of Condensed Matter and Nanoscience (IMCN), Université Catholique de Louvain, Place L. Pasteur 1, 1348 Louvain-la-Neuve, Belgium

† Electronic supplementary information (ESI) available: SEC traces of the terpolymers and corresponding <sup>1</sup>H NMR spectra. See DOI: 10.1039/c3sm50159k

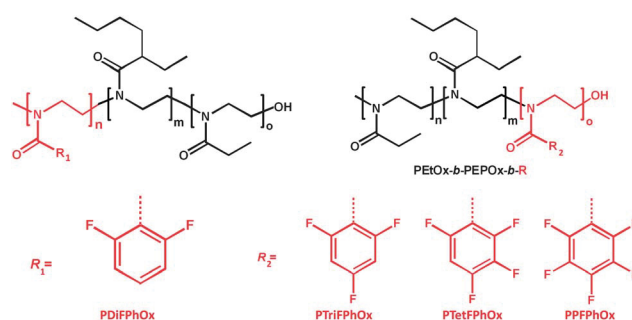
diversity of structures, which can be obtained, include the work of Tong *et al.* The authors described the self-assembly of perfluorocyclobutyl aryl ether-based amphiphilic ABA triblock copolymers containing a hydrophilic poly(ethylene glycol) segment as the middle block and reported a transition from spherical to cylindrical micelles with increasing content of the hydrophobic block.<sup>20</sup> Von Berlepsch *et al.* studied the self-assembly of poly[2-ethylhexyl acrylate-*b*-(oligoethylene glycol monomethyl ether) acrylate-*b*-1*H*,1*H*,2*H*,2*H*-perfluorodecyl acrylate],<sup>21</sup> which formed raspberry-like micelles. Kubowicz *et al.* investigated the self-assembly of poly[4-methyl-4-(4-vinylbenzyl) morpholin-4-ium chloride-*b*-styrene-*b*-pentafluorophenyl-4-vinylbenzyl ether] and found a core which is segregated into nanometer-sized compartments in which fluorocarbon-rich domains coexist with a continuous hydrocarbon region.<sup>22</sup> Lodge *et al.* studied the structural morphologies of miktoarm star terpolymers with varying composition of the copolymers.<sup>10,23–26</sup> The authors observed ‘hamburger’-like micelles, segmented worms, bilayers and vesicles, among others, by varying the length of the hydrophilic block. Segmented ribbons and bilayers were observed at low fluoropolymer contents. Large fluorine contents on the other hand, where the length of the fluorinated block exceeds the length of the hydrocarbon block, induced a ‘double frustration’ and further increased the structural variability, including well-defined segmented worms, raspberry-like micelles, and multicompartimentalized worms.<sup>19</sup>

In general also poly(2-oxazoline)s represent a well-suited class of functional polymers that can merge different (complementary) properties. The living character of the cationic ring-opening polymerization of 2-oxazolines allows, under optimized reaction conditions, to prepare well-defined polymers with tailored polymer architectures.<sup>27–30</sup> In particular fluorinated sub-units can be introduced.<sup>31</sup> Komenda and Jordan demonstrated the synthesis of a triblock terpolymer consisting of a fluorinated 2-oxazoline, a 2-methyl-2-oxazoline, and 2-nonyl-2-oxazoline.<sup>32</sup> An example of a fluorinated poly(2-oxazoline) block copolymer recently reported by our group demonstrated the formation of spiral disk-like structures which were formed by a linear ABC terpoly(2-oxazoline) containing 2-ethyl-2-oxazoline (EtOx), 2-(1-ethylpentyl)-2-oxazoline (EPOx) and 2-(2,6-difluorophenyl)-2-oxazoline (DiFPhOx) blocks (PDiFPhOx-*b*-PEPOx-*b*-PETOx) (Fig. 1a and Scheme 1, R<sub>1</sub>).<sup>33</sup>

The formation of these structures was attributed to the presence of not only one water soluble and an insoluble block but also to the integration of an additional fluorinated block, which is not miscible with the hydrophobic hydrocarbon block. The formation of distinct compartmentalized structures within the polymer aggregates resulted in the formation of unique spiral structures. Those spiral structures were evidenced as transient structures that can be seen as intermediates between rod-like micelles and vesicles. In the classical phase diagram of surfactants the increase in the concentration of amphiphiles results in a phase transition from spherical micelles to rod-like micelles and finally to unilamellar (vesicles) or multilamellar structures (“onions”). This sequence of morphological transitions can be additionally triggered by changing the hydrophilic–hydrophobic composition of the



**Fig. 1** (a) Cryo-TEM image of a spiral-like structure formed by PDiFPhOx-*b*-PEPOx-*b*-PETox. (b) Back-projected tomogram of a tilt series of individual spirals.



**Scheme 1** Schematic representation of the chemical structures of the investigated triblock terpoly(2-oxazoline)s.

surfactants; this can be parameterized by the so-called packing parameter, as introduced by Israelachvili *et al.*<sup>34</sup> The rod-to-vesicle transition is generally assumed to happen *via* a lateral packing of rod-like micelles that further merge into a lamella. In the case of spiral-like aggregates, we found that a single rod-like micelle rolled-up instead of overlapping laterally with other rod-like micelles. This could be attributed to the fact that spiral-like aggregates were prepared in a rather dilute solution and have only a few opportunities to gather with other rod-like micelles. The predominating two-dimensional character of the nanostructures can further be demonstrated by TEM tomography data as represented in Fig. 1b. Besides the spiral-like aggregates, classical vesicular structures were also observed as a coexisting structure, confirming the hypothesis that the utilized triblock terpolymer had the correct characteristic features to ultimately lead to vesicles.

Based on the promising structural features of the assembly in solution which can be introduced by the presence of the fluorinated blocks in such triblock terpolymers, further investigations were performed. In the present study the influence of the fluorophilic character on the formation of triblock terpolymer aggregates was investigated. For this purpose, a series of block copolymers was synthesized which consist of a poly[2-ethyl-2-oxazoline-*block*-2-(1-ethylpentyl)-2-oxazoline-*block*-2-(Xfluorophenyl)-2-oxazoline] (PETox-*b*-PEPOx-*b*-PXFFPhOx) structure (X = tri, tetra, penta). The increasing number of F substituents is expected to gradually increase the fluorophilic character of the terpolymer and, moreover, can potentially affect the steric

conformation inside the polymer chain. Additionally, the increasing fluorine content will influence the interaction parameters between the different blocks and between the fluorinated block and the solvent. The chemical structures of the synthesized triblock terpolymers are summarized in Scheme 1.

## Experimental section

### Materials

Chemicals were purchased from Sigma-Aldrich and were used as received if not otherwise mentioned. Methyl tosylate and 2-ethyl-2-oxazoline (EtOx) were obtained from Acros and were distilled prior to use and stored under argon. 2-(2,4,6-Trifluorophenyl)-2-oxazoline (TriFPhOx), 2-(2,3,4,6-tetrafluorophenyl)-2-oxazoline (TetFPhOx) and 2-(2,3,4,5,6-pentafluorophenyl)-2-oxazoline (PFPhOx) were prepared as described in the literature.<sup>31</sup> 2-(1-Ethylpentyl)-2-oxazoline (EPOx) was synthesized according to a literature procedure.<sup>35</sup> The synthesis of the difluorinated block copolymers was performed according to literature procedures.<sup>33</sup>

### General methods and instrumentation

The Initiator Sixty single-mode microwave synthesizer from Biotage, equipped with a noninvasive IR sensor (accuracy:  $\pm 2\%$ ), was chosen for the polymerizations under microwave irradiation. Microwave vials were heated to 110 °C overnight, allowed to cool to room temperature and filled with argon before use. All polymerization reactions were carried out with temperature control. Gas chromatography (GC) was conducted on an Interscience Trace gas chromatograph with a Trace Column RTX-5 connected to a PAL autosampler. Size exclusion chromatography (SEC) measurements were performed on an Agilent system equipped with a diode array detector and a refractive index detector. Two PSS SDV (5  $\mu\text{m}$  pore size) columns were placed in series. DMA with 5 mmol of LiCl was used as an eluent at 1 mL  $\text{min}^{-1}$  flow rate, and the column oven was set to 50 °C. Molar masses were calculated against polystyrene standards. For preparative SEC, Bio-Beads SX1 (crosslinked polystyrene polymers) from Bio-Rad were used.  $^1\text{H}$  NMR spectra were recorded on a Bruker AC 250 MHz spectrometer at room temperature, with  $\text{CDCl}_3$  as a solvent. The chemical shifts are given in ppm relative to the signal from the residual non-deuterated solvent. All samples have been

characterized by means of size exclusion chromatography (SEC),  $^1\text{H}$  NMR spectroscopy, DLS (Table 1), and cryo-TEM. DLS measurements were performed on a Malvern CGS-3 apparatus equipped with a He-Ne laser with a wavelength of emission at 632.8 nm. The DLS data were analyzed using either the cumulants or CONTIN method, which is based on an inverse-Laplace transformation of the data and gives access to a size distribution histogram for the analyzed micellar solutions. The polydispersity index (PDI) of the micelles was estimated from the  $\Gamma_2$ - $\Gamma_{12}$  ratio in which  $\Gamma_1$  and  $\Gamma_2$  represent the first and second cumulants, respectively.

Cryo-TEM investigations were conducted on a Philips CM-120. Samples were vitrified in a home-built blotting device in liquid ethane. Samples were transferred in a liquid nitrogen environment into the Gatan 626 holder at temperatures lower than  $-180$  °C and were imaged at low electron doses.

### Microwave-assisted polymerizations: triblock terpolymer synthesis

In order to synthesize triblock terpolymers a stock solution of the first monomer (EtOx), initiator (MeOTs) and solvent (nitromethane) was prepared and divided over five polymerization vials. All five vials were exposed to microwave radiation for a pre-calculated time to obtain near-quantitative conversion ( $\ln[M]_0/[M]_t = 4$ ). For control purposes, in one vial the polymerization was stopped by addition of 50  $\mu\text{L}$  water. Subsequently, the second monomer (EPOx) was transferred *via* a syringe to the other vials. Analogous to the first step, all four samples were subjected to microwave irradiation. 50  $\mu\text{L}$  of water were added to one of the vials in order to terminate the polymerization and to obtain the precursor diblock copolymer. The three different fluorinated monomers were added to the three remaining polymerization vials which again were subjected to microwave irradiation in order to obtain the respective triblock terpolymers.  $^1\text{H}$  NMR spectroscopy was used to confirm the absence of residual monomer as well as to investigate the polymer composition. Full conversion of each monomer as well as the molar mass distribution after each polymerization step was investigated using GC and SEC, respectively. The obtained diblock copolymer and triblock terpolymers were purified either by selective precipitation or preparative size exclusion chromatography, respectively.

**Table 1** Molecular characteristic features of the different block copolymers synthesized in this study (SEC traces and  $^1\text{H}$  NMR spectra can be seen in the ESI)

Copolymer	$M_n^a$ [ $\text{g mol}^{-1}$ ]	PDI <sup>a</sup>	Molecular composition <sup>b</sup> (EtOx/EPOx/FlOx) [mol%]		$R_h^c$ [nm]	PDI <sup>c</sup>
			Theor.	Exp.		
PetOx- <i>b</i> -PEPOx	11 440	1.14	66/33/0	69/31/0	72	0.35
PDiFPhOx- <i>b</i> -PEPOx- <i>b</i> -PEtOx	7 990	1.12	25/25/50	23/28/49	—	—
PETox- <i>b</i> -PEPOx- <i>b</i> -PTriFPhOx	14 930	1.15	50/25/25	52/34/14	209	0.21
PETox- <i>b</i> -PEPOx- <i>b</i> -PTetFPhOx	15 620	1.15	50/25/25	55/24/21	219	0.22
PETox- <i>b</i> -PEPOx- <i>b</i> -PPFPhOx	12 930	1.14	50/25/25	57/34/9	69/440	—/—

<sup>a</sup> SEC results (eluent: *N,N*-dimethylacetamide with 2.1 g  $\text{L}^{-1}$  LiCl; PS standards). <sup>b</sup> Determined using  $^1\text{H}$  NMR spectroscopy. <sup>c</sup> From DLS measurements.



## Results and discussion

The aim of this study was to investigate systems with different degrees of fluorination in the pFOx block. The characteristic length and compositions of the different samples are listed in Table 1. In order to study the aggregation behavior of the PEtOx-*b*-PEPOx subunit, the corresponding diblock copolymer was also investigated as a reference indicating that the changes in assembly in the solution rely on the subsequently introduced fluorinated block.

It has to be mentioned here that a direct comparison of the non-fluorinated diblock structures as well as the fluorinated terpolymers has to be critically evaluated: all investigated systems have different overall lengths and slightly different lengths of the fluorinated block. Therefore, the observed differences in assembly behavior cannot be exclusively related to the degree of fluorination. Moreover, the influence of the different fluorinated block on the solubility of the system is completely neglected.

### PEtOx-*b*-PEPOx diblock copolymer

In a first investigation the characteristic structure of the precursor diblock PEtOx-*b*-PEPOx was determined. The synthesized diblock copolymer was efficiently purified by precipitation and a diblock copolymer with a molar mass ( $M_n$ ) of 11 400 g mol<sup>-1</sup> and a PDI value of 1.14 was obtained. The composition was estimated by <sup>1</sup>H NMR analysis and showed a mol% ratio of 66 : 33. These polymers were used to form nanostructures by direct dissolution of the copolymers in water. The respective DLS measurements provided a hydrodynamic radius of 72 nm with a PDI value of 0.35. These solutions were subsequently investigated by cryo-TEM to reveal the structure of the polymer aggregates (Fig. 2).

Cryo-TEM showed the presence of spherical and cylindrical micelles as the predominating structures in solution. In some of the investigated areas the cylindrical micelles tend to arrange in a lamellar fashion, which allowed estimation of the overall dimensions of the individual fibers, assuming that in the organized areas a close packing of the cylindrical micelles is reached. The typical fiber periodicity in these areas is 32 ± 2 nm. These dimensions fit well with the expected length of the individual polymer chain. The typical thickness of the dark core area, which is supposed to be composed of the hydrophobic PEPOx blocks, is 19 nm ± 1 nm and is separated by bright areas

of a thickness of 13 nm ± 1 nm. These dimensions suggest that the diblock copolymers are forming classical rod-like micelle architectures; however, the corona of the aggregates seems to be not completely stretched. This could be caused by a collapse of the corona or by partial entanglements of the coronal chains of neighboring cylindrical micelles.

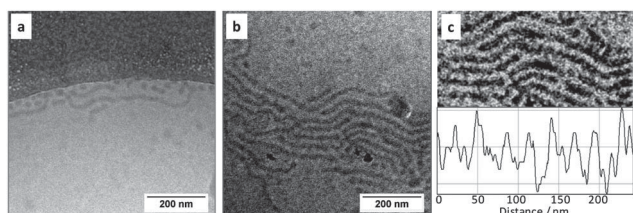
### PEtOx-*b*-PEPOx-*b*-PXFPPhOx triblock terpolymers

The influence of the fluorinated block is the subject of the investigations performed on the terpolymer systems. In this case the variation of the degree of fluorination of the phenyl-oxazoline is studied.

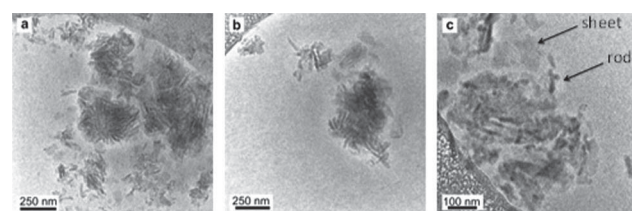
The structural analysis of PEtOx-*b*-PEPOx-*b*-PTriFPhOx with a trifluorophenyl oxazoline block was performed by means of cryo-TEM investigation and the aggregation behavior was further analyzed by DLS (Table 1). Fig. 3 depicts the typical aggregates which are formed by the trifluorophenyl-2-oxazoline (TriFPhOx) terpolymers. It can be observed that the extended aggregates are apparently formed by parallel rod- or sheet-like (Fig. 3c) features. Their assembly might be caused by a strong segregation introduced by the fluorinated block which causes the interfacial tension to be the predominant driving force for the self-assembly.<sup>36</sup>

To further decrease the surface tension, the assemblies tend to stack, resulting in aggregates with sizes in the range of 200 nm, which correlates well with the obtained DLS values of 209 nm.

Careful analysis of the features reveals a dark core region, most likely consisting of the densely packed fluorinated block, with a typical thickness of 6 nm, surrounded by a corona which is presumably formed by the PEPOx blocks. The typical distances of parallel-aligned sheets are 20 ± 2 nm. These dimensions indicate that a different model for the structure formation has to be applied compared to the previously investigated diblock nanostructures. Since the length of the fluorinated block is assumed to be 5 nm, the dark part of the core area can be formed only by a single fluorinated molecule or by strongly entangled fluorinated units/blocks. A possible formation mechanism might be an assembly of molecules, which is induced due to the strong hydrophobic character of the PTriOx block and the stacking of the fluorinated phenyl rings due to dipole-dipole interactions between C-F bonds<sup>37</sup> resulting in the formation of the rod- and sheet-like structures. In analogy to the observations for the spiral-like assemblies formed by the PDiFPhOx-*b*-PEPOx-*b*-PETOx terpolymer the PETOx block is



**Fig. 2** (a and b) Cryo-TEM images of the PEtOx-*b*-PEPOx system: rod-like micelles are identified as the major form of aggregation. (c) The densely packed area of rod-like micelles allows the determination of typical core and corona dimensions.



**Fig. 3** Typical nanostructures formed by the PEtOx-*b*-PEPOx-*b*-PTriFOx triblock terpolymer in water as observed by cryo-TEM.

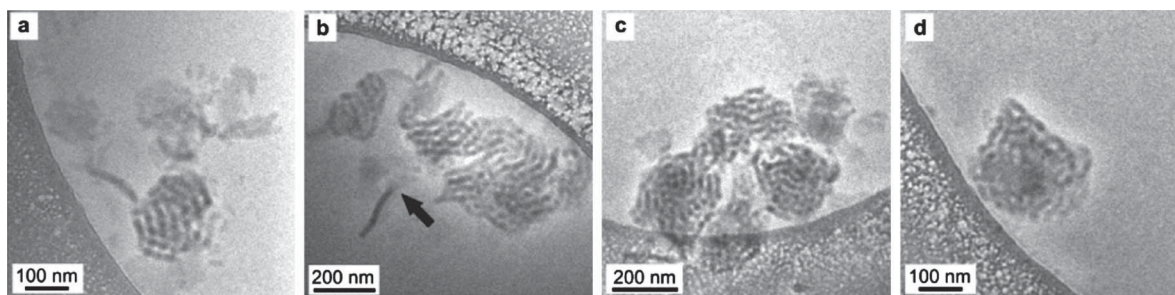


Fig. 4 TEM images of nanostructures formed by the PEtOx-*b*-PEPOx-*b*-PTetFPhOx triblock terpolymer in water as observed by cryo-TEM.

apparently squeezed out of the water insoluble domains – both the hydrophobic and fluorophilic parts – and is utilized to stabilize the structures in water.

Increasing the degree of fluorine substitution of the 2-oxazoline block from PTriOx to PTetFPhOx does result in more defined overall shapes (Fig. 4) revealing for PEtOx-*b*-PEPOx-*b*-PTetFPhOx, besides the presence of few separated sheet-like features (Fig. 4a), an assembly of either parallel aligned or entangled rod-like features. A transition between sheet-like and rod-like features might be seen in Fig. 4b on the bottom left of the structure as indicated by the arrow. The average size of the super-aggregates formed by the PEtOx-*b*-PEPOx-*b*-PTetFPhOx sample (Fig. 4c) is in roughly the same range as noted before for the PEtOx-*b*-PEPOx-*b*-PTriFPhOx system, and can be confirmed by means of DLS, where an average hydrodynamic volume of 219 nm with a PDI value of 0.22 was determined. An analysis of the structural features of the aggregates shows the tendency to form more organized and defined structures compared to the PTriPhOx block containing terpolymer. The internal structure of the objects resembles a complex folding and entanglement of the individual rod-like structures (Fig. 4d). The dark areas have a typical diameter of  $16 \pm 1$  nm. This corresponds well with the

typical length of the PEPOx-*b*-PTetFPhOx blocks. In contrast to the structures obtained from the TriFPhOx terpolymer, the structures formed by the TetFPhOx terpolymer show the presence of distinct PEtOx-areas within the structure. These are represented by brighter areas in between the darker structures with a typical distance of  $12 \pm 1$  nm. They are assigned to a collapsed and/or entangled PEtOx-corona since, theoretically, for a completely stretched chain a length of  $\sim 20$  nm is predicted.

In a next step the fluorine content of the third block was further increased by the synthesis of a pentafluorophenyl-2-oxazoline containing terpolymer (PEtOx-*b*-PEPOx-*b*-PPFPhOx) (see Table 1). In this case, well-defined nanostructures were obtained in the form of perfectly round-shaped 'super-aggregates'. Fig. 5a depicts a cryo-TEM image of a densely populated area, where a large number of these round-shaped aggregates can be observed. Next to these structures a large amount of rod-like micelles are also found. This is again supported by the corresponding DLS investigations, which postulate the presence of two populations of nanostructures with hydrodynamic radii of 69 and 440 nm, respectively. The large spherical structures were not present in the corresponding diblock

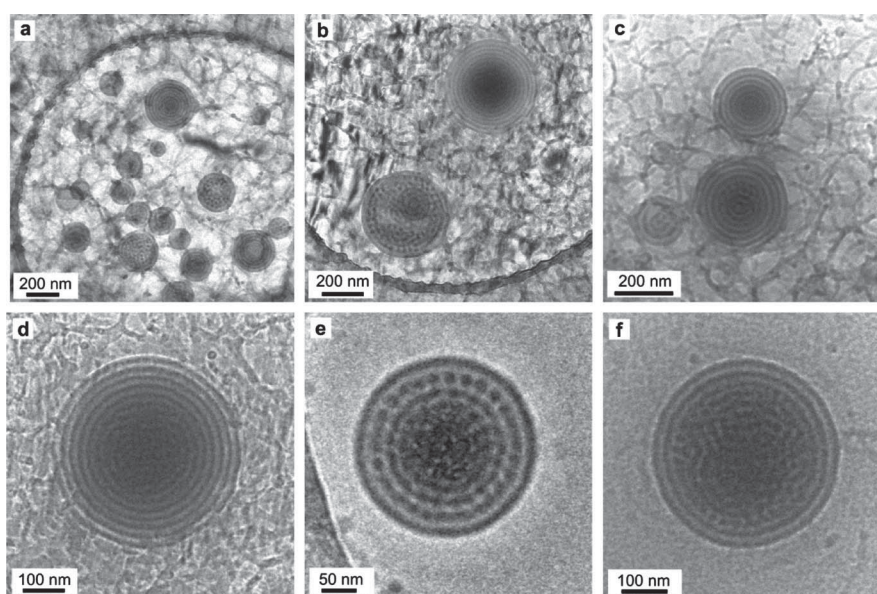


Fig. 5 Representative nanostructures formed by the PEtOx-*b*-PEPOx-*b*-PPFPhOx triblock terpolymer in water as observed by cryo-TEM.



PEtOx-*b*-PEPOx copolymer, which shows a comparable molar mass to the PPhOx terpolymer. The presence of these spherical structures clearly points out the influence of the fluorinated block during the assembly process. The successful fluorination was confirmed by the monomodal shape of the SEC traces (see ESI†), the low PDI index as well as the quantitative shift of the traces towards larger elution volumes.

A closer investigation of the structure of the round-shaped aggregates reveals characteristic features inside the super-aggregates. These features resemble either “onion-like” multi-lamellar vesicle structures (Fig. 5b–d) or perfectly segregated concentric lamellar features, which consist themselves of an arrangement of round dots (Fig. 5e). Also other structures can be observed, which show a reduced degree of symmetry but still suggest a highly ordered segregation of the polymer assemblies inside the super-structure (Fig. 5f). A full characterization *via* the 3D structure of the super-aggregates would require the acquisition of a tomography series and subsequent reconstruction of the volume structure by back-projection algorithms. However, it was observed that the stability of the features was rather limited due to strong beam damage effects (see, *e.g.*, the interior of the structure depicted in Fig. 5e), which did not permit the acquisition of a respective tilt series. Thus, a careful analysis of a large number of individual structures was performed to extract the characteristic features of the formed aggregates. Since practically, only round-shaped structures are observed, it can be assumed that only spherical aggregates are formed (Fig. 5a). Therefore, the formation of cylindrical, disk-like or elliptical super-structures is unlikely and can be excluded. The characteristic diameter of the observed dots within the spherical structures is  $16 \text{ nm} \pm 1 \text{ nm}$  and the individual layers are separated by 11 nm. The dot diameter is slightly larger than the expected length of the hydrophobic blocks of the investigated terpolymer.

A simple explanation for the observation of the two distinct super-aggregate structures can be found taking into account the projection-determined image formation during TEM imaging. Here, contrast is mainly generated by electron-opaque structures, which provide the contrast of the resulting images. Thus, imaging of a structure which consists of rods, which are *e.g.* assembled according to a ‘ball of yarn’ with a preferential winding direction, will result in a concentric dot pattern if the roll-up direction of the rods is parallel to the electron beam. On the other hand, a perpendicular orientation would result in images which look similar to multi-lamellar vesicle structures. Such an explanation would suggest also a strong influence of the orientation of the nanostructures in the ice film, which is in fact frequently observed. This is supported also by the analysis of the structural features of the multilamellar vesicles, which show a periodicity of  $22 \text{ nm} \pm 2 \text{ nm}$  and consist of a dark stripe with a thickness of 12 nm separated by a bright lamella with a diameter of 10 nm. In particular the thickness of the bright stripe is in agreement with the dimension of the bright separation layer which was found inside the dotted band structure. Another possible explanation targets the assembly of super-aggregates by the formation of micellar bicontinuous structures or a coexistence of lamellar and bicontinuous phases within the confined

nanostructures. A bicontinuous assembly of the rod-like micelles can be potentially caused by the formation of a network of the rods which are separated by regions which are enriched by the hydrophilic, hydrated PEtOx blocks. Examples of such bicontinuous micelles have only rarely been reported until recently in the literature, despite the fact that their existence was theoretically predicted by Fraaije and Sevink<sup>38</sup> by self-consistent-field simulation of dispersed droplets of surfactant molecules. Wooley *et al.* observed bicontinuous micelle structure formation for a poly(acrylic acid-*b*-methyl acrylate-*b*-styrene) (PAA<sub>99</sub>-*b*-PMA<sub>73</sub>-*b*-PS<sub>203</sub>) block terpolymer, which was complexed with 2,2'-(ethylenedioxy)diethylamine in THF–water mixtures.<sup>11</sup> Despite the fact that PAA-*b*-PMA-*b*-PS is a widely studied system and a large variety of weight fractions of the individual blocks and THF–water mixtures were investigated (which led to the formation of spherical, disk-like or segmented cylindrical stacks of disk-like micelles,<sup>39</sup> toroidal,<sup>40,41</sup> *etc.*) the presence of bicontinuous structures was only found for PAA<sub>99</sub>-*b*-PMA<sub>73</sub>-*b*-PS<sub>203</sub>. This suggests that the formation of bicontinuous phases requires a facile interplay of the packing parameters.<sup>42</sup> Recently, Sommerdijk *et al.* succeeded in the detailed structural analysis of quasi-triblock amphiphilic polynorbornene-based copolymers with comb-like structures of oligo(ethylene glycol)methyl ether (OEG) and a tripeptide sequence forming bicontinuous nanostructures by cryo-electron tomography, and a strong influence on the chosen tripeptide units was found.<sup>12</sup> The authors also studied the aggregation behavior of a semicrystalline comb-like quasi triblock system consisting of a poly(ethylene oxide-*b*-octadecyl methacrylate) (PEO<sub>36</sub>-*b*-PODMA<sub>17</sub>) copolymer at different temperatures.<sup>13</sup> The semicrystalline character of this block copolymer suggests that the formed structures are polymeric analogues of cubosomes, which are normally formed by low molar mass compounds, often in the presence of additional surfactants.<sup>43</sup>

The nanostructures found for PEtOx-*b*-PEPOx-*b*-PPPhOx could resemble an analogue of such bicontinuous structures. Next to concentric multilamellar vesicles (Fig. 5c and d) many of the super-aggregates show a perfectly symmetric and organized segregation pattern (Fig. 5e) of nano-phase separated bands which consist of round-shaped dots. The two distinct kinds of super-aggregates formed might be the result of the coexistence of different states of aggregation within the sample. Similar to the spiral structures found for PDiFPhOx-*b*-PEPOx-*b*-PEtOx these nanostructures are considered as intermediate ‘transient’ structures towards the formation of vesicles, which are supposed to be the thermodynamically ultimate morphology as expected from the triblock composition. A comparable tendency to form such transient structures was also observed by Eisenberg *et al.* The authors reported the formation of tube-walled vesicles<sup>14</sup> and hexagonally packed hollow hoops<sup>15</sup> which were formed by poly[styrene-*b*-ethylene oxide] (PS<sub>100</sub>-*b*-PEO<sub>43</sub>) and poly[styrene-*b*-acrylic acid] (PS<sub>410</sub>-*b*-PAA<sub>13</sub>) diblock copolymers, respectively. In this case different stages of structure formation are observed indicating the presence of intermediate transient structures, which are involved in the formation of the final aggregates. Evolution steps involve the formation of individual vesicles, which fuse into large compound vesicles upon addition

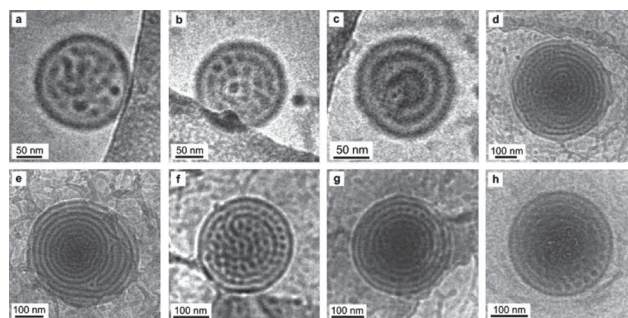


of sodium chloride. The following intermediate structures are triggered by slow diffusion and show first a short range order. The aggregates gradually grow due to coalescence of smaller aggregates and at a later stage an increase in order moving towards the interior is observed.

In the present case we suggest the coexistence of multilamellar vesicles and a cubic phase (Fig. 5b), which is practically<sup>13,44</sup> rarely reported but theoretically<sup>45–47</sup> predicted in the literature for block copolymers in solution. Considering a large number of TEM images, there are different spherical states observed for the assembly of PETox-*b*-PEPOx-*b*-PPFPhOx ranging from complete multilamellar vesicles to bicontinuous phases surrounded by vesicles (Fig. 5d–f). The morphology between the interior bicontinuous phase and the surrounding shell is often represented by segregated dotted bands, which could be attributed to a transition between lamellar and bicontinuous morphologies.<sup>48–51</sup> In many multilamellar vesicles (Fig. 5c and d) a different morphology is found in the very center area, which points either to a water content dependent morphology<sup>52</sup> and/or to a dependence of the morphology on curvature. In the latter case the curvature for a bilayer increases towards the center. To minimize the frustration of the high curvature, the system decreases the interfacial tension by minimizing its surfaces. The transition can result *e.g.* in the formation of cubic phases, which generally lead to bicontinuous morphologies.<sup>53,54</sup> This was theoretically described for a small amphiphile by Conn *et al.* showing that this cubic phase transition acts as a seed for the formation of bicontinuous phases. The authors expect the coexistence of bilayer and lamellar structures for multilamellar vesicles in solution.<sup>48</sup> Furthermore, the avoidance of frustration by high curvature in the lamellar system can be supported, since the formation of multilamellar vesicles is not observed for aggregates with a diameter below 200 nm (Fig. 6a–c). In some examples the observed assembly pattern changes from the highly ordered structures to non-regular structures as can be seen in Fig. 6d–f which represent either the transition between both structures or changes in the orientation of the phases. As such some of the segregated lamellae within the structures are changed, *i.e.*, some of the structures reveal the partial appearance of a segregated dotted band within a multilamellar vesicle structure (Fig. 6g and h).

The analysis of the outer shell of the super-aggregates deserves special consideration. All structures are surrounded by an envelope layer which never shows the segregation into dot-like features, even in highly symmetric systems. A careful analysis of the characteristic dimensions of these envelope structures reveals a similar thickness to the dot diameter. In this case the stabilizing PETox blocks can completely point out of the structure and are not influenced by the presence of hydrophobic blocks, which might result in the formation of a closed, vesicle-like envelope layer. The formation of such an envelope layer is in agreement with the predictions of Fraaije and Sevink<sup>38</sup> where the formation of the vesicular surrounding is suggested as a thermodynamically driven reduction of the interfacial tension of the hydrophobic block to the solution.

Since the given explanation of the super-structures relies on thermodynamically non-equilibrium conditions and, thus,



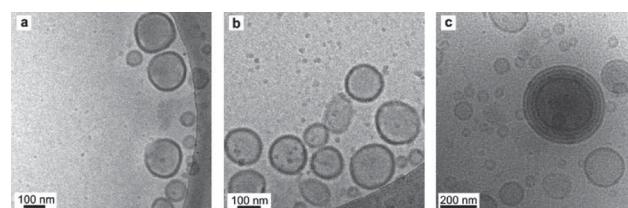
**Fig. 6** Less-ordered nanostructures formed by the PETox-*b*-PEPOx-*b*-PPFPhOx triblock terpolymer in water as observed by cryo-TEM.

the formation of transient structures, samples were further prepared from a solution which was heated up to 70 °C for 2 days. The elevated temperature is supposed to support the formation of the thermodynamically most favorable structures and the expected predominant formation of vesicular structures was observed (Fig. 7).

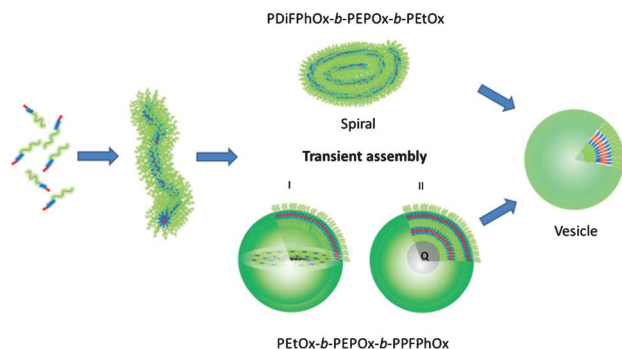
Besides predominant unilamellar vesicles with a large size distribution a few larger multilamellar vesicles but no rod-like structures could be observed. This behavior suggests the transient nature of the segregated vesicular structures as well as the vesicular structure of the terpolymer as the ultimate equilibrium state of aggregation. Based on these considerations the following scheme of the phase transition behavior of the di- and pentafluorinated terpolymers can be developed (Fig. 8).

The formation of the spiral-like and bicontinuous phases as observed for PDiFPhOx-*b*-PEPOx-*b*-PETox and PETox-*b*-PEPOx-*b*-PPFPhOx, respectively, can be summarized in the following model: both structures are formed by the organization of rod-like micelles. If a fluorinated block is present additional interactions have to be taken into account and, in particular, the differences in solubility of the blocks are increased.

These additional interactions promote the self-assembly of the rod-like structures into super-aggregates. When the amount of fluorine is low (PETox-*b*-PEPOx-*b*-PDiFPhOx) the rod-like micelles are forced to roll-up to form planar spiral structures. Higher fluorine contents on the other hand favor the formation of 3D nanostructures, which might be caused by a stronger interaction among the fluorinated domains. These structures can be seen as a 3D analogue of the spiral-like structures which were formed by the difluorophenyl-functionalized and represent super-aggregates consisting of a bicontinuous phase where



**Fig. 7** TEM images of the assembly of the PETox-*b*-PEPOx-*b*-PPFPhOx terpolymer in water preheated for two days at 70 °C prior to the cryo-TEM investigation.



**Fig. 8** Schematic representation of the structural evolution of the rod-to-vesicle transformation of di- and pentafluorophenyl triblock terpoly(2-oxazoline)s in aqueous solution: the PETox block is shown in green, the PEPOx block in blue and PDI/PPHox or PPFPhOx in red. The transient assembly for the difluorophenyl-functionalized terpolymer is a spiral structure, while the transient assembly for the pentafluorophenyl-functionalized terpolymer can be explained by a coexistence of lamellar and cubic phases within one spherical aggregate.

multilamellar and cubic phases coexist. For both systems an ultimate transition to the most favorable structure of a vesicle is observed.

## Conclusions

The current study represents an investigation of the influence of the degree of fluorination of the PXFPhOx block on the resulting structure of triblock super-aggregates. Only in the case of di- and penta-fluorination of the XFPhOx blocks well-defined supramolecular structures were observed, which in both cases showed a high complexity. The structure formation was attributed to the coexistence of bicontinuous and lamellar phases, which were demonstrated to form non-equilibrium super-aggregates as transient structures towards the formation of vesicular structures. The ultimate thermodynamically stable aggregate structure was determined by temperature-induced equilibrium conditions. Structural analysis enabled the development of a preliminary model for the structure as well as for the transformation of the aggregates and introduced the degree of fluorination of such systems as an additional parameter for consideration for the future design of complex supramolecular intermediate transient structures. Even though the structure formation cannot exactly be explained at this stage of investigation the studied system represents an interesting example of the emerging possibilities which arise from the concept of incorporating fluorinated blocks into the architecture of multiblock copolymer structures to further increase the complexity of multi-compartmentalized supramolecular aggregates. Further investigations will target, *e.g.*, the influence of the block order within the triblock copolymer chains and the influence of the length of the individual subunits.

## Acknowledgements

The authors kindly acknowledge the financial support of the Dutch Polymer Institute (DPI, technology area High-throughput experimentation (HTE)). We also thank Prof. Richard

Hoogenboom for his contribution to the development of the synthetic methodology.

## Notes and references

- 1 A. Blanazs, S. P. Armes and A. J. Ryan, *Macromol. Rapid Commun.*, 2009, **30**, 267–277.
- 2 Z. L. Tyrrell, Y. Shen and M. Radosz, *Prog. Polym. Sci.*, 2010, **35**, 1128–1143.
- 3 T. Lohmüller, D. Aydin, M. Schwieder, C. Morhard, I. Louban, C. Pacholski and J. P. Spatz, *Biointerphases*, 2011, **6**, 1–12.
- 4 R. K. O'Reilly, *Philos. Trans. R. Soc., A*, 2007, **35**, 2863–2878.
- 5 J. F. Gohy, *Adv. Polym. Sci.*, 2005, **190**, 65–136.
- 6 A. O. Moughton, M. A. Hillmyer and T. P. Lodge, *Macromolecules*, 2011, **45**, 2–19.
- 7 J.-F. Gohy, C. Ott, S. Hoepener and U. S. Schubert, *Chem. Commun.*, 2009, 6038–6040.
- 8 J. F. Lutz and A. Laschewsky, *Macromol. Chem. Phys.*, 2005, **206**, 813–817.
- 9 A. Laschewsky, *Curr. Opin. Colloid Interface Sci.*, 2003, **8**, 274–281.
- 10 Z. Li, M. A. Hillmyer and T. P. Lodge, *Langmuir*, 2006, **22**, 9409–9417.
- 11 K. Hales, Z. Chen, K. L. Wooley and D. J. Pochan, *Nano Lett.*, 2008, **8**, 2023–2026.
- 12 A. L. Parry, P. H. H. Bomans, S. J. Holder, N. Sommerdijk and S. C. G. Biagini, *Angew. Chem., Int. Ed.*, 2008, **47**, 8859–8862.
- 13 B. E. McKenzie, F. Nudelman, P. H. H. Bomans, S. J. Holder and N. Sommerdijk, *J. Am. Chem. Soc.*, 2010, **132**, 10256–10259.
- 14 K. Yu, C. Bartels and A. Eisenberg, *Langmuir*, 1998, **31**, 9399–9402.
- 15 L. Zhang, C. Bartels, Y. Yu, H. Chen and A. Eisenberg, *Phys. Rev. Lett.*, 1997, **79**, 5034–5037.
- 16 A. H. Gröschel, F. H. Schacher, H. Schmalz, O. V. Borisov, E. B. Zhulina, A. Walther and A. H. E. Müller, *Nat. Commun.*, 2012, **3**, 710.
- 17 K. Jankova and S. Hvilsted, *J. Fluorine Chem.*, 2005, **126**, 241–250.
- 18 M. Antonietti and S. Oestreich, *Topics Appl. Chem.*, 2002, **1**, 151–166.
- 19 J. Mao, P. Ni, Y. Mai and D. Yan, *Langmuir*, 2007, **23**, 5127–5134.
- 20 L. Tong, Z. Shen, D. Yang, S. Chen, Y. Li, J. Hu, G. Lu and X. Huang, *Polymer*, 2009, **50**, 2341–2348.
- 21 H. v. Berlepsch, C. Bottcher, K. Skrabania and A. Laschewsky, *Chem. Commun.*, 2009, 2290–2292.
- 22 S. Kubowicz, J.-F. Baussard, J. F. Lutz, A. F. Thünemann, H. v. Berlepsch and A. Laschewsky, *Angew. Chem., Int. Ed.*, 2005, **44**, 5262–5265.
- 23 Z. Li, E. Kesselman, Y. Talmon, M. A. Hillmyer and T. P. Lodge, *Science*, 2004, **306**, 98–101.
- 24 Z. Li, M. A. Hillmyer and T. P. Lodge, *Macromolecules*, 2004, **37**, 8933–8940.
- 25 Z. Li, M. A. Hillmyer and T. P. Lodge, *Macromolecules*, 2005, **39**, 765–771.

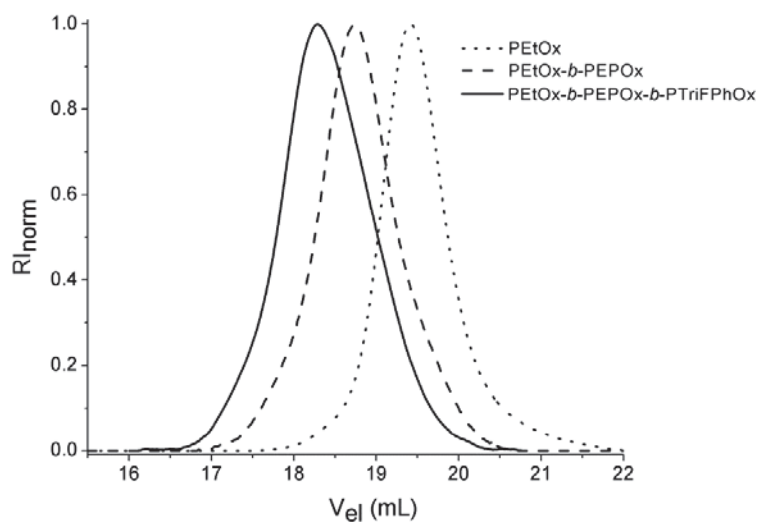
- 26 Z. Li, M. A. Hillmyer and T. P. Lodge, *Nano Lett.*, 2006, **6**, 1245–1249.
- 27 N. Adams and U. S. Schubert, *Adv. Drug Delivery Rev.*, 2007, **59**, 1504–1520.
- 28 R. Hoogenboom and H. Schlaad, *Polymers*, 2011, **3**, 467–488.
- 29 A. Makino and S. Kobayashi, *J. Polym. Sci., Part A: Polym. Chem.*, 2010, **48**, 1251–1270.
- 30 H. Schlaad, C. Diehl, A. Gress, M. Meyer, A. L. Demirel, Y. Nur and A. Bertin, *Macromol. Rapid Commun.*, 2010, **31**, 511–525.
- 31 M. Lobert, H. M. L. Thijs, T. Erdmenger, R. Eckardt, C. Ulbricht, R. Hoogenboom and U. S. Schubert, *Chem.–Eur. J.*, 2008, **14**, 10396–10407.
- 32 T. Komenda and R. Jordan, *Abstr. Pap. Am. Chem. Soc.*, 2003, **225**, U573.
- 33 K. Kempe, R. Hoogenboom, S. Hoepfener, C.-A. Fustin, J.-F. Gohy and U. S. Schubert, *Chem. Commun.*, 2010, **46**, 6455–6457.
- 34 J. N. Israelachvili, D. J. Mitchell and B. W. Ninham, *J. Chem. Soc., Faraday Trans. 2*, 1976, **72**, 1525–1568.
- 35 K. Kempe, A. Baumgaertel, R. Hoogenboom and U. S. Schubert, *J. Polym. Sci., Part A: Polym. Chem.*, 2010, **48**, 5100–5108.
- 36 M. A. Hillmyer and T. P. Lodge, *J. Polym. Sci., Part A: Polym. Chem.*, 2002, **40**, 1–8.
- 37 M. D. Blanchard, R. P. Hughes, T. E. Concolino and A. L. Rheingold, *Chem. Mater.*, 2000, **12**, 1604–1610.
- 38 J. G. E. M. Fraaije and G. J. A. Sevink, *Macromolecules*, 2003, **36**, 7891–7893.
- 39 H. G. Cui, Z. Y. Chen, S. Zhong, K. L. Wooley and D. J. Pochan, *Science*, 2007, **317**, 647–650.
- 40 H. G. Cui, Z. Y. Chen, K. L. Wooley and D. J. Pochan, *Soft Matter*, 2009, **5**, 1269–1278.
- 41 D. J. Pochan, Z. Y. Chen, H. G. Cui, K. Hales, K. Yi and K. L. Wooley, *Science*, 2004, **306**, 94–97.
- 42 S. J. Holder and N. Sommerdijk, *Polym. Chem.*, 2011, **2**, 1018–1028.
- 43 M. Thadanki, P. S. Kumari and K. S. Prabha, *Int. J. Res. Pharm. Chem.*, 2011, **1**, 535–541.
- 44 S. Qin, W. Z. Yuan, H. Li and Y. Zhang, *Soft Matter*, 2012, **8**, 8405–8412.
- 45 X. D. Guo, J. P. K. Tan, L. J. Zhang, M. Khan, S. Q. Liu, Y. Y. Yang and Y. Qian, *Chem. Phys. Lett.*, 2009, **473**, 336–342.
- 46 B. Yu, B. Li, P. Sun, T. Chen, Q. Jin, D. Ding and A.-C. Shi, *J. Chem. Phys.*, 2005, **123**, 234902–234908.
- 47 P. Chen, H. Liang and A.-C. Shi, *Macromolecules*, 2008, **41**, 8938–8943.
- 48 C. E. Conn, O. Ces, X. Mulet, S. Finet, R. Winter, J. M. Seddon and R. H. Templer, *Phys. Rev. Lett.*, 2006, **96**, 108102.
- 49 L. J. Ellison, D. J. Michel, F. Barmes and D. J. Cleaver, *Phys. Rev. Lett.*, 2006, **97**, 237801.
- 50 L. V. Chernomordik and M. M. Kozlov, *Annu. Rev. Biochem.*, 2003, **72**, 175–207.
- 51 L. Yang and H. W. Huang, *Science*, 2002, **297**, 1877–1879.
- 52 V. Percec, D. A. Wilson, P. Leowanawat, C. J. Wilson, A. D. Hughes, M. S. Kaucher, D. A. Hammer, D. H. Levine, A. J. Kim, F. S. Bates, K. P. Davis, T. P. Lodge, M. L. Klein, R. H. DeVane, E. Aqad, B. M. Rosen, A. O. Argintaru, M. J. Sienkowska, K. Rissanen, S. Nummelin and J. Ropponen, *Science*, 2010, **328**, 1009–1014.
- 53 K. Kita-Tokarczyk, J. Grumelard, T. Haefele and W. Meier, *Polymer*, 2005, **46**, 3540–3563.
- 54 M. Almgren, *J. Dispersion Sci. Technol.*, 2007, **28**, 43–54.



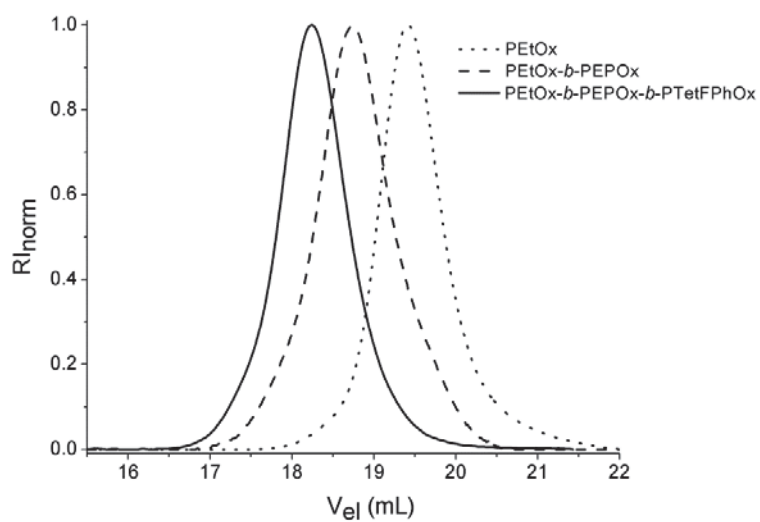
# **Tuning the morphology of triblock terpoly(2-oxazoline)s containing a 2-phenyl-2-oxazoline block with varying fluorine content**

Ulrich Mansfeld,<sup>1,2</sup> Stephanie Hoepfner,<sup>1,3\*</sup> Kristian Kempe,<sup>1,2</sup> Jean-Marc Schumers,<sup>4</sup> Jean-Francois Gohy,<sup>4</sup> Ulrich S. Schubert<sup>1,2,3</sup>

## **Supporting Information**

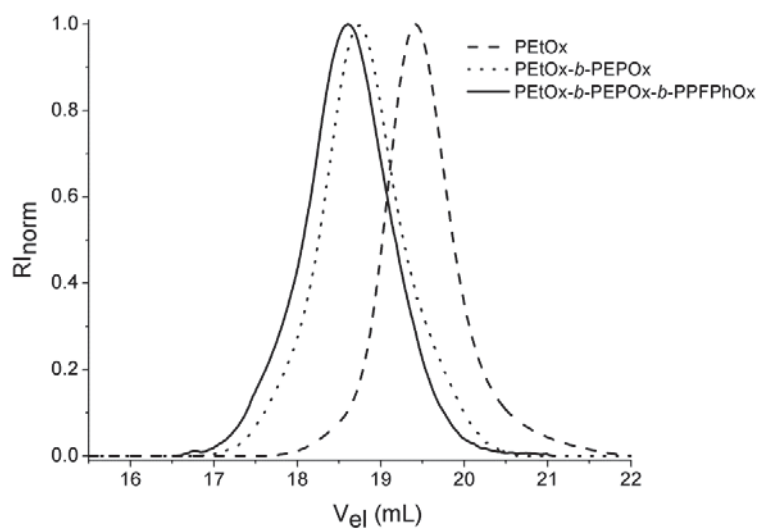


**Figure S1.** SEC traces of PETox-*b*-PEPOx-*b*-PTriFPhOx (solid line) and prepolymers (eluent: *N,N*-dimethyl acetamide (DMA) with LiCl ( $2.1 \text{ g L}^{-1}$ )).

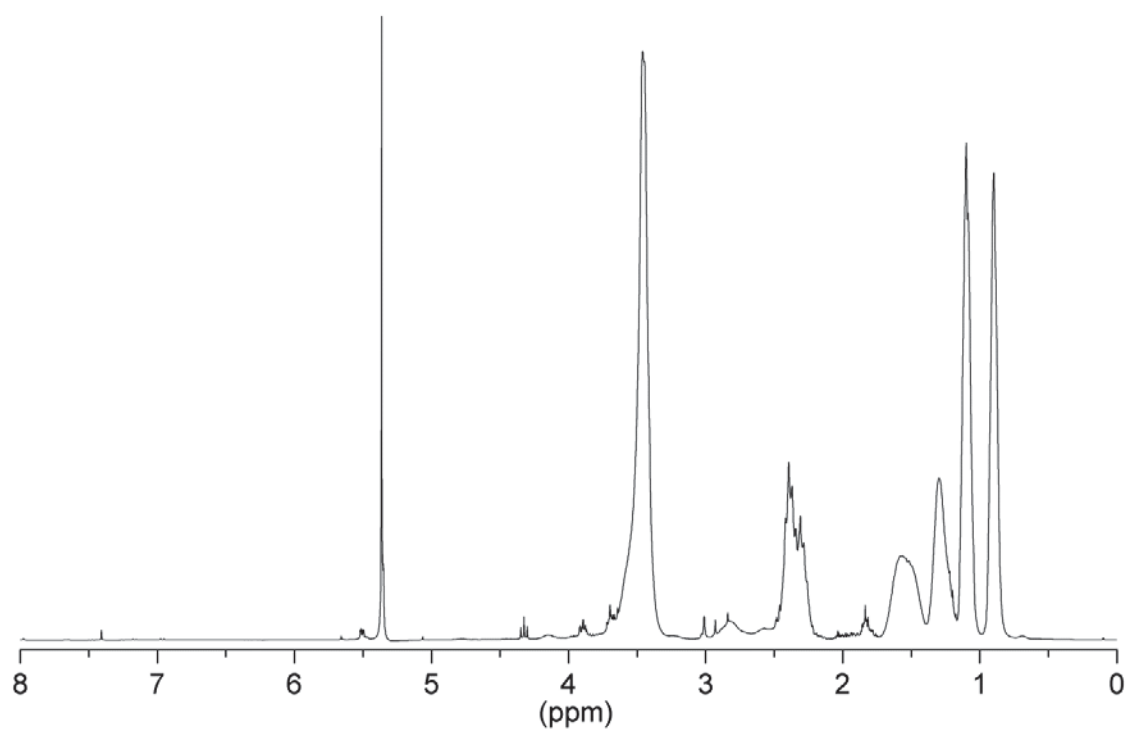


**Figure S2.** SEC traces of PETox-*b*-PEPOx-*b*-PTetFPhOx (solid line) and prepolymers (eluent: *N,N*-dimethyl acetamide (DMA) with LiCl ( $2.1 \text{ g L}^{-1}$ )).

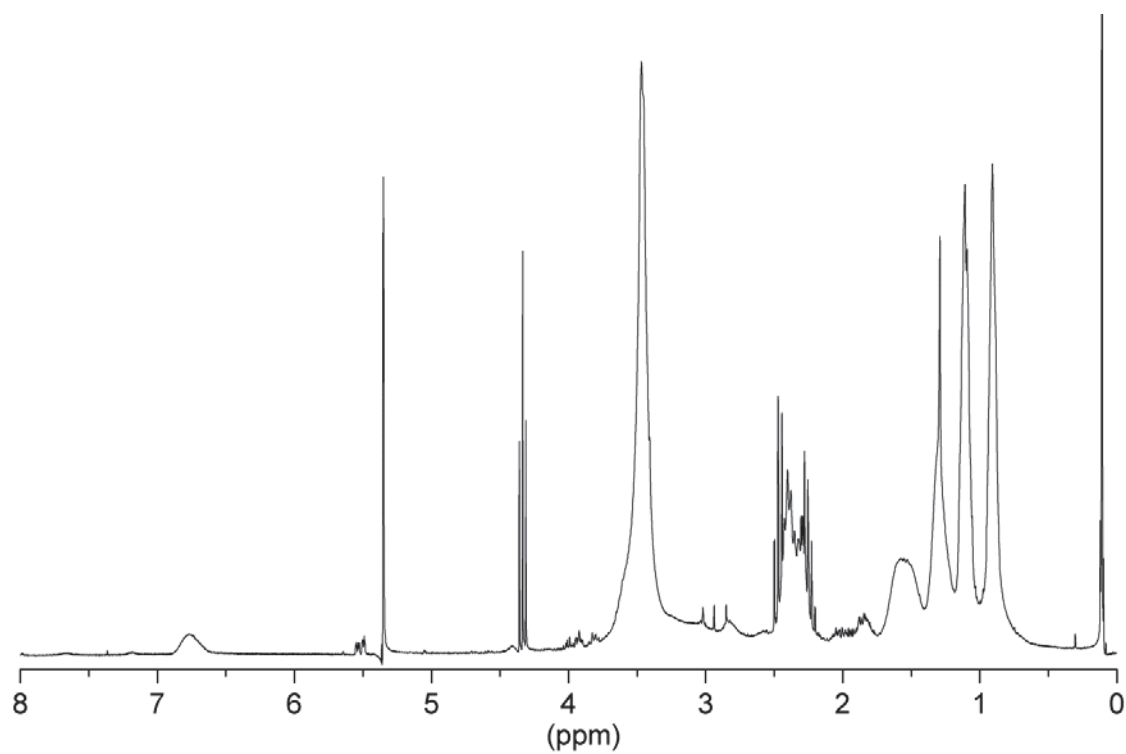




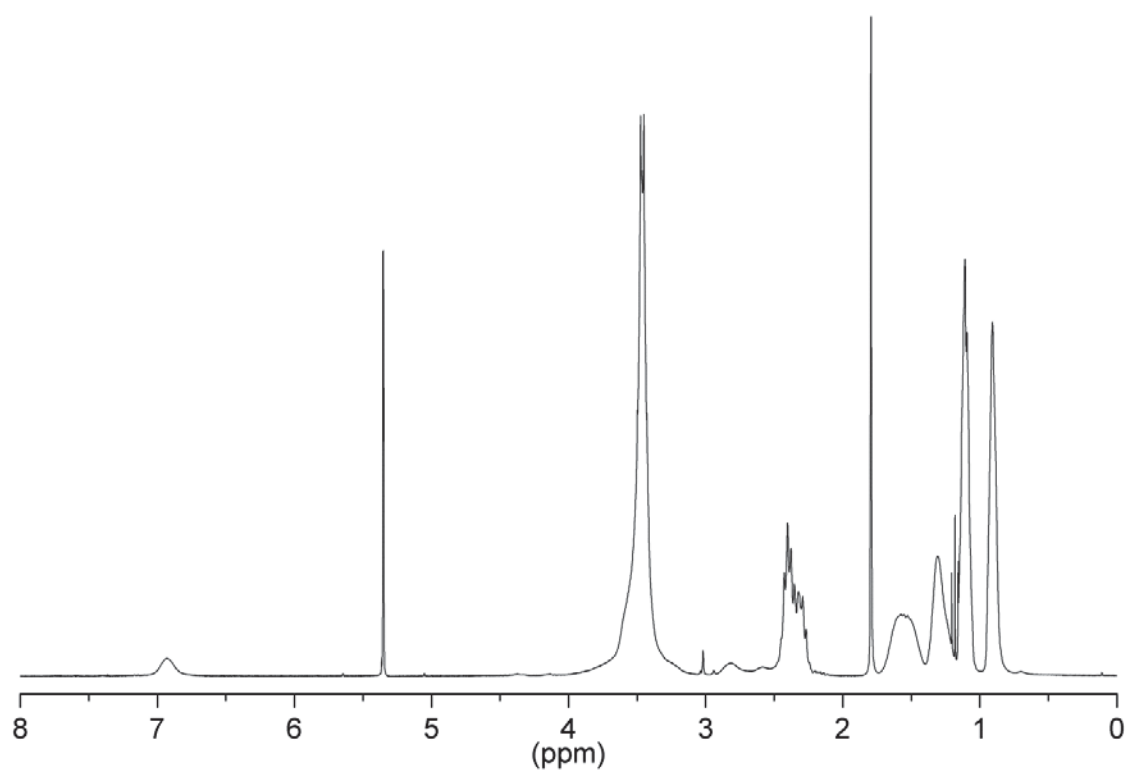
**Figure S3.** SEC traces of PEtOx-*b*-PEPOx-*b*-PPFPhOx (solid line) and prepolymers (eluent: *N,N*-dimethyl acetamide (DMA) with LiCl (2.1 g L<sup>-1</sup>)).



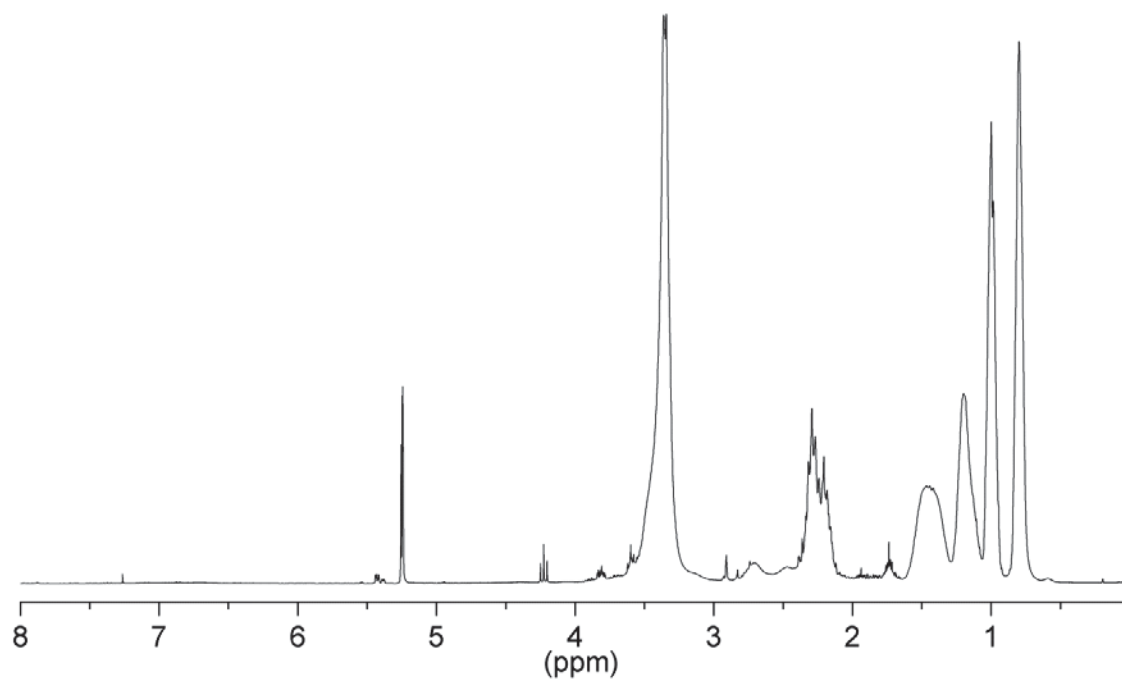
**Figure S4.** <sup>1</sup>H NMR spectrum of PEtOx-*b*-PEPOx (250 MHz, CDCl<sub>3</sub>).



**Figure S5.** <sup>1</sup>H NMR spectrum of PEtOx-*b*-PEPOx-*b*-PTriFPhOx (250 MHz, CDCl<sub>3</sub>).



**Figure S6.** <sup>1</sup>H NMR spectrum of PEtOx-*b*-PEPOx-*b*-PTetFPhOx (250 MHz, CDCl<sub>3</sub>).



**Figure S7.** <sup>1</sup>H NMR spectrum of PEtOx-*b*-PEPOx-*b*-PPFPhOx (250 MHz, CDCl<sub>3</sub>).

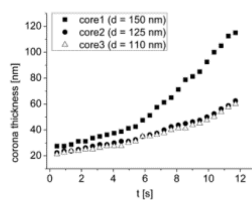
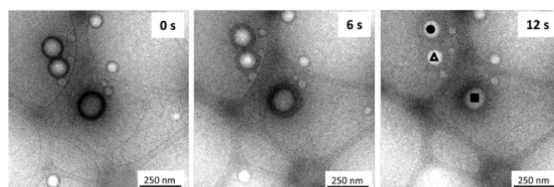


## Publication P6:

### *Polymer nanostructures in ionic liquids: From staining to motion*

U. Mansfeld, S. Hoepfener, C. Guerrero-Sanchez, J.-F. Gohy and U. S. Schubert,

*Microscopy and Microanalysis* **2013**, submitted







## **Polymer nanostructures in ionic liquids: From staining to motion**

Ulrich Mansfeld,<sup>1,2</sup> Stephanie Hoepfener,<sup>1,2\*</sup> Carlos Guerrero-Sanchez,<sup>1,3</sup> Jean-François Gohy,<sup>4</sup>

Ulrich S. Schubert<sup>1,2,5</sup>

- 1 Laboratory of Organic and Macromolecular Chemistry (IOMC), Friedrich Schiller University Jena, Humboldtstr. 10, 07743 Jena
- 2 Jena Center for Soft Matter (JCSM), Friedrich Schiller University Jena, Philosophenweg 7, 07743 Jena, Germany
- 3 CSIRO - Materials Science and Engineering, Ian Wark Laboratory, Bayview Av., Clayton, Victoria, 3168, Australia
- 4 Bio and Soft Matter (BSMA), Institute of Condensed Matter and Nanoscience (IMCN), Université catholique de Louvain, Place Louis Pasteur, 1348 Louvain-la-Neuve, Belgium
- 5 Dutch Polymer Institute (DPI), P.O. Box 513, 5600 MB Eindhoven, The Netherlands

**Corresponding author:** Dr. Stephanie Hoepfener, Jena Center of Soft Matter (JCSM), Philosophenweg 7, 07743 Jena, Germany, Tel.: +49 (0)3641 948 261, Fax: +49 (0)3641 948 202, e-mail: s.hoepfener@uni-jena.de

### **Abstract**

The utilization of ionic liquids (IL) as alternative staining agents and as a liquid support media to investigate the motion of block copolymer nanoparticle assemblies is introduced. Based on the fact that ILs provide a number of surpassing advantages their utilization in Transmission Electron Microscopy (TEM) is demonstrated here by presenting a number of selected examples. The utilization of ILs in TEM introduces benefits for the structural characterization and morphology of polymer aggregates due to enhanced contrast effects. Furthermore, up to now the investigation of dynamic processes possess special challenges on the experimental set-up and frequently the information on this kind of processes is based on a number of snap-shot images, which have to be interpreted to finally

conclude on the dynamic faith of individual nanostructures. The utilization of ILs for TEM imaging was recently demonstrated to provide an elegant approach to observe also the motion of individual nanoparticles in a liquid support film. We present in this contribution an overview of the emerging possibilities by introducing ILs to visualize different aspects of diblock copolymer nanoparticles by TEM.

**Keywords:** Transmission Electron Microscopy, Polymer Nanostructures, Ionic Liquids, Staining, Aggregate Motion

## **Introduction**

The visualization of polymer nanostructures, in particular, self-organized nanoparticle aggregates, by Transmission Electron Microscopy (TEM) encounters several challenges. Issues like the nanostructure stability with respect to the electron beam as well as a proper sample preparation that preserves the native structure of the polymer nanostructures are essential requirements for their investigation. As polymers are moreover frequently composed of only very few, mainly carbon containing subunits with only a very limited variety of other elements with usually low atomic numbers the issue of contrast generation is of special importance. This is in particular true if block copolymers are utilized as building blocks for self-organized polymeric nanostructures and an unambiguous identification of the individual copolymer blocks is to be achieved (Michler, 2008). The utilization of these TEM techniques mainly targets, *e.g.*, the investigation of self-assembled block copolymer micelles and vesicles (Wang *et al.*, 2007; Pochan *et al.*, 2004; Li *et al.*, 2004; Lutz *et al.*, 2004). Due to the small differences in the electron scattering properties of the atoms, polymer samples exhibit frequently low contrast provoking that the determination of their nanostructural conformation remains a challenge. This problem is generally addressed by utilizing positive and/or negative stains (O'Reilly *et al.*, 2006; Fang *et al.*, 2009). While negative stains preferentially absorb on the support film of the TEM grid, positive staining require the preferential absorption of the staining material specifically onto the polymer itself; preferentially only to one of the copolymer blocks. Staining artifacts (Jackson *et al.*, 1998; Wittemann *et al.*, 2005) represent a common problem as they may change the chemical nature

of the samples and might induce also alterations of the self-assembled nanostructures. Even more critical is the fact that staining is mainly performed on samples which are prepared in the dry state simply by blotting the solution onto a TEM grid. In this case the polymer nanostructure is not present any more in its native state, meaning that, *e.g.*, the structure loses its hydration shell, which can cause serious alterations of the structure of the nanoparticles. Also flattening processes of the nanostructures might occur due to the presence of the support film. These problems can be avoided by utilizing cryo-TEM preparation methods (Cui *et al.*, 2007; Zhen *et al.*; 1999; Won *et al.*; 2002; Lutz *et al.*, 2005), where the sample is investigated in a vitrified solution and is not in contact with adhering surfaces. The observed shapes are in this case regarded in a first approximation as the true shape of the solvated molecular aggregates in the solution. These investigations suffer frequently from a low signal-to-noise ratio and only a weak contrast. A major experimental challenge is in this case the formation of a suitable vitrified iced layer, which, *e.g.*, does not show ice crystals and which has to provide a suitable thickness to host the nanostructures and it should remain at the same time transparent for the electron beam. A combination of cryo-TEM investigations and staining techniques is found only in relatively few examples in the literature (Alfredsson *et al.*, 2005; Ludwig *et al.*, 2003). The most critical drawback of cryo-TEM as well as of blotting approaches is the lack of mobility of the nanostructures during their observation. Therefore, particle motion as well as the ability to investigate changes of the structure of nano-objects, *e.g.*, induced by temperature triggers is not accessible by conventional TEM investigations.

These drawbacks motivated the investigation of an alternative approach, which utilizes the advantages of ionic liquids (ILs) as alternative stain substances as well as support media for the investigation of the dynamic behavior of block copolymer nanostructure in a solution-like state.

ILs are substances entirely composed of ions, which remain in the liquid state below 100 °C (Deetlefs & Seddon, 2006). Unlike conventional solvents these liquids do not exhibit a measurable vapor pressure, which potentially makes them compatible with ultra-high vacuum techniques (Kuwabata *et al.*, 2010). Moreover, these ILs inherently provide ions with high *Z* values originating mainly from their inorganic anions and their properties can be tuned over a wide range. In contrast to conventional

solvents, the properties of ILs, *i.e.*, their solubility, electrical conductivity or melting point can be tailored by simply varying the composition of their ions.

The applicability of ILs is well-documented in the literature by a considerable number of ILs are now commercially available (Winterton, 2006; Guerrero-Sanchez *et al.*, 2007). These cover a wide range of properties for specific applications and are frequently characterized by their outstanding chemical and physical stabilities in a broad range of temperatures. In particular the solubility of ILs can be optimized for specific polymers, which opens appealing possibilities to utilize them for the preparation of self-assembled block copolymer micelles in ILs. This approach was pioneered by studies of Lodge *et al.* The authors introduced for the first time the TEM investigation of poly(1,2-butadiene-*block*-ethylene glycol) and poly(styrene-*block*-methyl methacrylate) diblock copolymers (He *et al.*, 2006; Simone & Lodge, 2007) with different chain lengths and block compositions in the hydrophobic IL 1-butyl-3-methylimidazolium hexafluorophosphate (BMIM-PF<sub>6</sub>). BMIM-PF<sub>6</sub> acts as thermodynamically good solvent for the butadiene and styrene blocks, whereas as a bad solvent for the ethylene oxide and methyl methacrylate blocks, respectively. The authors conducted cryo-preparation for these systems and observed the presence of worm-like micelles as well as of vesicles. While the authors pointed out the advantages of this approach, namely, the easy preparation of amorphous support layers and the fact that intrinsic staining can be observed, other appealing applications emerge from the utilization of ILs for the investigation of polymeric nanostructures (Guerrero-Sanchez *et al.*, 2011). These approaches are discussed in this contribution.

## Materials and Methods

BMIM-PF<sub>6</sub> was kindly provided by Solvent-Innovation GmbH. The IL was of synthesis grade and was dried in vacuum at 40 °C at least 3 days before use. 1-Ethyl-3-methylimidazolium ethylsulfate (99%) (EMIm-EtOSO<sub>3</sub>) and 1-butyl-3-methylimidazolium triflate (99%) were purchased from Iolitec and were used without further purification. Poly(styrene-*b*-(2-vinyl pyridine)) ( $M_n$  [kg mol<sup>-1</sup>] = PS<sub>440</sub>-*b*-P2VP<sub>353</sub>), polydispersity index (PDI) = 1.19) was purchased from Polymer Source. Poly(styrene-*b*-(ethylene oxide)) ( $M_n$  [kg mol<sup>-1</sup>] = PS<sub>100</sub>-*b*-PEO<sub>34</sub>) was synthesized according to standard procedures. CH<sub>2</sub>Cl<sub>2</sub> (99,8%) was purchased from Aldrich and was used without further purification.

### **Synthesis of PS-*b*-PMMA**

The diblock copolymers were synthesized by sequential anionic polymerization, as described elsewhere (Guerrero-Sanchez *et al.*, 2005; Hoogenboom *et al.*, 2009; Simone & Lodge, 2007). The polymer showed narrow monomodal molar mass distributions as revealed by size exclusion chromatography (SEC). Proton nuclear magnetic resonance (<sup>1</sup>H NMR) spectroscopy in combination with SEC measurements was utilized for calculating the chain lengths composition of the different block copolymers.

### **Preparation of block copolymer micelles in ILs**

#### **PS-*b*-PMMA**

Self-assembled micelles of the investigated block copolymers were prepared utilizing the co-solvent method. Bulk copolymers were dissolved in a thermodynamically good solvent for both blocks (in tetrahydrofuran at room temperature for PS-*b*-PMMA diblock copolymers) at a concentration of 10 wt%. Subsequently, BMIM-PF<sub>6</sub> IL was gradually added into the polymeric solutions as selective precipitant for the blocks composed of styrene under vigorous stirring in order to reach a concentration of 0.5 wt% for the polymeric materials. The removal of the co-solvent from the micelle dispersion was achieved by placing the vial in a vacuum oven at 40 °C for at least 1 day.

#### **PS-*b*-P2VP**

To prepare a stock solution the polymer (10 mg) was dissolved in dichloromethane (400 μL). EMIm-EtOSO<sub>3</sub> (40 μL) was slowly added into the diluted solution (20 μL of polymer solution and 100 μL of dichloromethane) and the dichloromethane was subsequently evaporated at 70 °C.

### **Characterization techniques**

Dynamic light scattering (DLS) measurements were performed at 25 °C at 90° on a Malvern CGS-3 apparatus equipped with a 633 nm laser. The value of refractive index for BMIM-PF<sub>6</sub>, used during the analysis, was 1.41; whereas the used value of viscosity for BMIM-PF<sub>6</sub> were 196 mPa s. Hydrodynamic radii and polydispersity indices of the micelles were calculated from a cumulant

analysis. The distribution of the hydrodynamic radius was obtained by a deconvolution of the data with the CONTIN algorithm.

SEC measurements of the PS-*b*-PMMA diblock copolymers were performed on a Shimadzu system with a RID-6A refractive index detector and a Mixed-B (Polymer Labs) column utilizing tetrahydrofuran as an eluent at a flow rate of 1 mL min<sup>-1</sup> and a column temperature of 20 °C. The molar masses were calculated against poly(methyl methacrylate) standards. <sup>1</sup>H NMR spectra were recorded on a Varian Gemini 400 MHz spectrometer at room temperature using deuterated chloroform (CDCl<sub>3</sub>).

(Cryogenic) transmission electron microscopy (cryo-TEM) images of the micelle systems were recorded on two different systems:

(I) The PS-*b*-PMMA was investigated on a Technai G<sup>2</sup> Sphera (FEI) Transmission Electron Microscope using an acceleration voltage of 200 kV. Samples for cryo-TEM were prepared using a FEI Vitrobot preparation chamber at a temperature of 65 °C to decrease the viscosity of the IL. Samples were rapidly transferred into liquid ethane and the preparation was performed on an open TEM grid (Hex 700, thin bar) purchased from Agar Scientific.

(II) The PS-*b*-P2VP system was examined on a Phillips CM-120 Transmission Electron Microscope, operated at 80 or 120 kV. The lacey carbon-coated TEM copper grids (Mesh 400) were purchased from Agar Scientific and were plasma-cleaned prior to use for 1 minute. A drop of the polymer solution was placed on the grid, manually blotted for 10 seconds and subsequently plunged into a cryogen reservoir containing liquid ethane by using an in-house built controlled environment vitrification system (CEVS). After preparation the sample were stored and measured at a temperature of approximately -180 °C. Particle motion was investigated in non-vitrified films, prepared by adding a drop of the IL solution onto a lacey carbon grid and subsequent manual blotting for 10 seconds. The images were recorded with a bottom-mounted 1k × 1k charge-coupled-device (CCD) camera from TVIPS. Specimens were investigated using a sample holder from Gatan (626-DH).



## Results and Discussion

### 1. Cryo-TEM in Ionic Liquids

In a first set of experiments amphiphilic poly(styrene-*block*-methacrylate) (PS<sub>73</sub>-*b*-PMMA<sub>66</sub>) diblock copolymers (**Figure 1**) were investigated following the previously introduced approach by Lodge *et al.* (He *et al.*, 2006; Simone & Lodge, 2007). The block copolymer consists of a hydrophobic PS part and a more hydrophilic PMMA block.

The length of the individual blocks of the polymers is indicated as average number of monomer units incorporated into the block copolymer. This system can self-assemble into spherical micelles which spontaneously form in a selective solvent for one of the two blocks (Riess, 2003). Such solvents can be conventional solvents but also ionic liquids (Simone & Lodge, 2007). In the present study BMIM-PF<sub>6</sub> acts as a thermodynamically good solvent for the PMMA block, whereas the PS block remains insoluble in BMIM-PF<sub>6</sub> (Simone & Lodge, 2007). The formed micellar solution was first characterized by means of dynamic light scattering (DLS) performed in the IL. A hydrodynamic radius ( $R_h$ ) of 85 nm was found for the micelles with a relatively broad polydispersity index (PDI) of 0.65. A dilution series resulted in similar  $R_h$  values, thus, it can be concluded that the population of micelles is present in a kinetically frozen state. As a consequence the size of the micellar systems is most likely strongly dependent on the applied preparation protocol (Xu *et al.*, 1991). Next to the knowledge of the overall hydrodynamic radius of the micelles in particular the core-corona morphology is of special interest in such kind of diblock copolymer assemblies. However, this information is not directly accessible by means of DLS. Therefore, in many cases accompanying TEM investigations are performed. We first performed cryo-TEM studies, where the samples were directly prepared from the micelle/IL solution. As a major advantage of this approach it can be highlighted that performing the cryo-preparation is very straight forward. Indeed, ILs easily freeze without the formation of crystalline structures of the IL itself, since the non-crystalline nature of the IL supports the formation of amorphous films. Therefore, no advanced vitrification conditions have to be matched and also the temperature requirements are less strict during sample handling compared to the vitrification of aqueous samples during normal cryo-TEM preparation.

**Figure 2** shows typical cryo-TEM images of the PS-*b*-PMMA micelles formed in BMIM-PF<sub>6</sub>. It can be observed that the spherical micelles appear with a bright contrast on a significantly darker background. This background is formed by the IL, which consists of BMIM and the associated PF<sub>6</sub><sup>-</sup> counter ions, which provide a dark contrast in TEM imaging due to their rather high fluorine content. Interestingly, the films could be even prepared on non-supported open TEM grids (Mesh 700, hexagonal grid) due to the high viscosity of the IL which forms even under these conditions stable films with a sufficiently small thickness. The evaluation of the diameter of the bright structures revealed an average size of 16 nm ± 2 nm, which is associated to the core diameter of the micelles. Obviously, the corona cannot be visualized in this case, while the IL provides an intrinsic negative staining effect.

## ***2. Utilization of ILs as selective staining agents***

In particular to access information on the corona morphology additional possibilities emerge from the utilization of the IL as staining agents for conventional TEM imaging at room temperature. Here the miscibility/immiscibility properties of the IL and the micelle system as well as with other conventional solvents can be utilized as a key feature to investigate the individual block dimensions. For this purpose, the micelle dispersion dissolved in the IL was applied onto a TEM grid, followed by a careful rinsing of the grid with a suitable conventional volatile solvent to remove the IL while preserving the micellar structures on the grid. The following requirements should be matched by the chosen solvents; first it is necessary that the solvent dissolves the IL to facilitate its removal from the grid. Moreover, the solvent has to be thermodynamically incompatible with the corona-forming polymer chains to avoid dissolution. These requirements would enable the partial removal of the IL, while the structural integrity of the micelles is supposed to be maintained. The conventional solvent can be easily removed afterwards, *e.g.*, by vacuum drying, before the micelles are investigated by means of TEM. In the case of PS-*b*-PMMA block copolymer micelles in BMIM-PF<sub>6</sub> acetonitrile can be utilized to remove the IL due to its miscibility. On the other hand, acetonitrile is a poor solvent for the PMMA block (Groele *et al.*, 2003; González-Benito & Koenig, 2006) and it can be assumed that the micellar structure is not altered by the washing step; however, it is well suitable to remove the BMIM-PF<sub>6</sub> from the TEM grid.

Thus, the structure of the micelles is assumed to remain unaltered. The TEM investigations can be subsequently carried out at room temperature by standard TEM imaging conditions.

**Figure 3** shows TEM micrographs of the dried samples. It can be observed that the overall micelle size increases to  $35 \text{ nm} \pm 4 \text{ nm}$ , in contrast to a size of  $16 \pm 2 \text{ nm}$  that was observed for the cryo-TEM samples in the IL. The broader size distribution compared to the cryo-TEM investigations might be a result of the drying process of the micelles. A closer look at the individual micelles reveals a sub-structure within the micelles. They consist of a dark rim with a width of  $9 \text{ nm} \pm 1 \text{ nm}$  that surrounds a brighter core region, with a diameter of  $16 \text{ nm} \pm 2 \text{ nm}$ . A comparison with cryo-TEM suggests that these bright areas in the center of the micelles are associated to the region of the micelle core in agreement with the previous investigations. The dark rim around the core represents the corona of the micelles, which is visible because residues of the IL remain within the corona shell and are not washed off during the rinsing step with acetonitrile. As a consequence of the staining properties of the IL a good contrast is obtained for this part of the micelle and can be therefore directly visualized by TEM imaging. As a further confirmation of this assumption the thickness of the rim was analyzed in the frame of the cryo-TEM investigations in particular in quasi-hexagonally ordered domains of the micelles. Here the distance between the cores is regarded as a measure for the coronal dimensions of the micelles, even though the corona is not directly visible (Hwang *et al.*, 2005). The average distance of closely packed micelles in the cryo-TEM images obtained in the IL solution was found to be 7 to 9 nm. As a consequence, IL could be used here to selectively stain the corona of the micelle simply by utilizing the solvation properties of the micelle/IL system. Moreover, a comparison of cryo-TEM in IL and the selective washing process suggests the collapse of the PMMA corona block. These complementary preparation techniques allow the selective positive and negative staining of the specimens and provide a general and straightforward method to determine core and corona sizes of micellar systems. Therefore, the miscibility/immiscibility properties of the IL with the polymer blocks as well as the intrinsic staining properties can be used to facilitate the characterization of the micellar systems by TEM.

### ***3. Direct visualization of the core and corona of block copolymer micelles in IL***

While both approaches are suitable to visualize the morphology of micelle systems and demonstrate the capabilities of IL liquids in terms of negative and positive staining, a recently introduced approach to utilize IL as free standing liquid support media for the observation of block copolymer nanoparticles opens new ways to investigate polymer nanostructures also in a liquid-like state (Mansfeld *et al.*, 2013). This approach takes advantage of the negligible vapor pressure of the ILs which renders them compatible with the UHV conditions required by TEM. It could be demonstrated that the intrinsic negative staining as well as the liquid properties over a wide temperature range of the ILs can be utilized to investigate not only the morphology but also the movement of polymer nanoparticles. This approach was applied here to a fairly large block copolymer system, namely, polystyrene-*block*-poly-2-vinylpyridine (PS<sub>440K</sub>-*b*-P2VP<sub>353K</sub>) as a model amphiphilic diblock copolymer containing hydrophobic PS as an insoluble block and P2VP as a more hydrophilic polymer that can be dissolved by common polar ionic liquids (Ueki & Watanabe, 2012). This system forms also spherical micelles in ILs and provides, in contrast to the previously discussed example, a thicker corona structure. TEM images of the system prepared by the co-solvent method in EMIm-EtOSO<sub>3</sub>, an aprotic, polar ionic liquid that shows a high electron density, due to the sulfur within the counterion resulted in an increased image contrast and a negative staining for the polymer assemblies.

**Figure 4a** depicts a TEM image acquired in the liquid IL film at an elevated temperature of 92 °C (see also the movie file in the Supplementary Information). The clearly visible nanostructures are also observable at room temperature but as it was previously pointed out the higher temperatures facilitate a more rapid movement of the nanostructures due to the decreased viscosity of the IL (Mansfeld *et al.*, 2013). The trajectories of the individual particles during the measurement are depicted in **Figure 4a**. It can be clearly observed that the individual structures consist of a bright inner core, presumably consisting of the insoluble PS blocks and a diffuse corona which is formed by the P2VP chains. The dark contrast in the corona area is supposed to be formed due to a concentration of higher atom number elements (S of the anion) within the corona caused by the interactions of the IL with the P2VP units. As such, the hydrogen atom of the imidazolium cation of the ionic liquid can interact in a supramolecular fashion either as a hydrogen bonding donor (Dong *et al.*, 2006; Lee *et al.*, 2012; Hunt,

2006) or by cation- $\pi$  interactions between the imidazolium cation and the aromatic pyridine ring (Ma & Dougherty, 1997; Ueki & Watanabe, 2008). The hydrogen bonding of polymers with the imidazolium cations of IL was first described by Lodge *et al.* explaining the unusual LCST behavior of PEG in EMIm BF<sub>4</sub> (Lee *et al.*, 2012).

As a consequence of the hydrogen bonding a positive charging of the corona takes place which causes the anion to be attracted to the positively charged corona (Hoarfrost *et al.*, 2012, Hou *et al.*, 2011). The electron-dense anion EtOSO<sub>3</sub><sup>-</sup> increases the electron density in the area of the corona due to the presence of sulfur and, thus, generates contrast. Investigations on charged corona assemblies in ionic liquids are not reported so far, but are frequently reported in conventional solvents (Zhulina & Borisov, 2012; Förster *et al.*, 2004). One of the results of these investigations is that the charging can lead, *e.g.* by increasing the salt concentration, to a contraction of the charged corona. A contraction of the corona is also observed in the present case of the IL, which is in fact a pure salt. In addition, Förster *et al.* found that the polyelectrolyte corona can phase-separate upon addition of salt in a densely packed inner part and a diluted outer part, resulting in an interior densely packed corona which is clearly visible in TEM with a dark contrast compared to the surrounding environment (Förster *et al.*, 2002). Interestingly, it was frequently observed in the present case that a freshly prepared solution of particles does not immediately exhibit a clearly visible corona structure but aging of the solution could improve the visibility of the corona. This points to a relatively low charging rate of the P2VP corona chains by the interaction with the IL and/or to slow contraction of the charged corona blocks. However, the kinetically frozen PS cores remain unaffected either way.

Next to the generated contrast and the possibility to follow the motion of the individual particles also changes in the corona structure can be observed. In this context a significant increase of the corona thickness could be observed during the imaging process (**Figure 4c-e**). Moreover, next to the thickness increase a significant decrease of the obtainable contrast took place pointing to the expansion of the previously collapsed corona blocks.

The presence of the corona could be furthermore confirmed by comparative cryo-TEM investigations in different ILs. The frozen IL films are relatively sensitive to beam damage and a clear alteration of

the support film morphology could be observed upon prolonged intense electron beam exposure (**Figure 5**).

In the course of cryo-TEM investigations it could be observed that at higher electron doses and/or at longer irradiation times the frozen IL films of BMIm-TfO and EMIm-EtOSO<sub>3</sub> “melt” in a heterogenic way while maintaining the PS-*b*-P2VP assemblies (**Figure 6**). Such a visualization of the shell dimension was recently described by Talmon for P4VP-*b*-PS in DMF to enhance the corona contrast by radiation damage of the surrounding film (Oss-Ronen *et al.*, 2012). Careful analysis shows no alteration of the PS core diameter upon electron irradiation.

For EMIm-EtOSO<sub>3</sub>, the corona is (i) already visible in the non-irradiated cryogenic films and (ii) of comparable thickness to the contracted corona in the liquid film (**Figure 4c**), while for BMIm-TfO only the PS core is visible (**Figure 6a,c**). After longer irradiation times, the corona is visible in both ILs, because the corona areas are less affected upon irradiation in contrast to the surrounding IL films that “melt” in a heterogenic way (**Figure 6b,d**). Thereby, for both ILs the core dimensions remain unaltered. Furthermore, no corona thickness alteration was observed in EMIm-EtOSO<sub>3</sub> (**Figure 6c,d**), which makes this “melting” method suitable for the determination of the corona thickness in cryo-TEM films. In both cases the corona thickness can be clearly determined for aggregates that have a diameter close to the film thickness, while for rather small assemblies the corona is overlaid by the molten ionic liquid film. The corona thickness is determined to be 15 to 30 nm with an average thickness of 23 nm in both liquids, whereas the corona thickness is slightly increased in BMIm-TfO compared to EMIm-EtOSO<sub>3</sub>.

## Conclusion

We demonstrated several different methods where the utilization of IL can be employed to enhance the contrast of polymeric systems to facilitate their structural investigation. The applied methods include cryo-TEM investigations of polymer systems prepared in ILs, the utilization of miscibility/immiscibility properties of IL with polymers and common solvents as well as the investigation of block copolymer micelles in free-standing liquid films of IL. Each of these methods might be directly applicable in certain cases and reveals details of the polymer structure that are not



evidently accessible by conventional TEM imaging conditions. It can frequently avoid the utilization of demanding and time consuming staining approaches. The ultimate goal of these investigations relates to the *in-situ* investigation of changes on the polymer nanostructures responding to external stimuli, *e.g.* temperature changes. Therefore, the dynamic behavior of the system should be maintained during the investigations, which was demonstrated in the present study. In a series of images the movement of the individual nanostructures could be followed and also slight changes in the thickness of the corona thicknesses were observed. These are most likely predominately related at the moment in the investigated systems to charging phenomena, but the general possibility to observe structural changes in the polymer nanostructure becomes evident. Further investigations will focus on temperature-responsive block copolymer systems elucidating new possibilities for the investigation of stimuli-responsive systems.

### **Acknowledgements**

This research forms part of the research program of the Dutch Polymer Institute (DPI), project #401 and #620. The authors thank the Fonds der Chemischen Industrie for financial support and appreciate the collaboration of Solvent Innovation GmbH and Merck KGaA during the realization of this work. This research has been carried out partially with the support of the Soft Matter CryoTEM Research Unit, Department of Chemical Engineering and Chemistry, Eindhoven University of Technology and the Electron Microscopy Center, University of Jena. Dr. F. Steiniger is kindly acknowledged for his valuable support and fruitful discussions.

## References

- ALFEDSSON, V. (2005). Cryo-TEM studies of DNA and DNA-lipid structures. *Curr. Op. Interf. Sci.* **10**, 269-273.
- CUI, H., HODGDON, T.K., KALER, E.W., ABEZGAUZ, L., DANINO, D., LUBOVSKY, M., TALMON, Y. & POCHAN, D.J. (2007). Elucidating the assembled structure of amphiphiles in solution via cryogenic transmission electron microscopy. *Soft Matter* **3**, 945-955.
- DEETLEFS, M. & SEDDON, K.R. (2006). Ionic liquids: fact and fiction. *Chim. Oggi* **24**, 16-23.
- DONG, K., ZHANG, S., WANG, D. & YAO, X. (2006). Hydrogen bonds in imidazolium ionic liquids. *J. Phys. Chem. A* **110**, 9775-9782.
- FANG, B., WALTHER, A.; WOLF, A., Xu, Y., YUAN, J. & MÜLLER, A.H.E. (2009). Undulated multicompartiment cylinders by the controlled and directed stacking of polymer micelles with a compartmentalized corona. *Angew. Chem. Int. Ed.* **48**, 2877-2880.
- FÖRSTER, S., HERMSDORF, N., BÖTTCHER, C. & LINDNER, P. (2002). Structure of polyelectrolyte block copolymer micelles. *Macromolecules* **35**, 4096-4105.
- FÖRSTER, S., ABETZ, V. & MÜLLER, A.H.E. (2004) in *Polyelectrolytes with Defined Molecular Architecture II*, ed. M. Schmidt, Springer Berlin Heidelberg, 2004, vol. 166, pp. 173-210.
- GONZÁLEZ-BENITO, J. & KOENIG, J.L. (2006). Nature of PMMA dissolution process by mixtures of acetonitrile/alcohol (poor solvent/nonsolvent) monitored by FTIR-imaging. *Polymer* **47**, 3065-3072.
- GROELE, R.J., KRASICKY, P.D., CHUN, S.W., SULLIVAN, J. & RODRIGUEZ, F. (1991). Dissolution rates of poly(methyl methacrylate) in mixtures of nonsolvents. *Journal of Applied Polymer Science* **42**, 3-8.
- GUERRERO-SANCHEZ, C., ABELN, C. & SCHUBERT, U.S. (2005). Automated parallel anionic polymerizations: Enhancing the possibilities of a widely used technique in polymer synthesis. *J. Polym. Sci., Part A: Polym. Chem.* **43**, 4141-4160.
- GUERRERO-SANCHEZ, C., LARA-CENICEROS, T., JIMENEY-REGALADO, E., RASA, M. & SCHUBERT, U.S. (2007). Magnetorheological fluids based on ionic liquids. *Adv. Mater.* **19**, 1740-1747.

GUERRERO-SANCHEZ, C., WOUTES, D., HOEPPENER, S., HOOGENBOOM, R. & SCHUBERT, S. (2011). Micellar dye shuttle between water and an ionic liquid. *Soft Matter* **7**, 3827-3831.

HE, Y., SIMONE, P.M. & LODGE, T.P. (2006). Self-assembly of block copolymer micelles in an ionic liquid. *J. Am. Chem. Soc.* **128**, 2745-2750.

HOARFROST, M.L., TYAGI, M.S., SEGALMAN, R.A. & REIMER, J.A. (2012). Effect of confinement on proton transport mechanisms in block copolymer/ionic liquid membranes. *Macromolecules* **45**, 3112-3120.

HOOGENBOOM, R., ROGERS, S., CAN, A., BECER, C.R., GUERRERO-SANCHEZ, C., WOUTERS, D., HOEPPENER, S. & SCHUBERT, U.S. (2009). Self-assembly of double hydrophobic block copolymer mixtures: from micelles to thermoresponsive micelles. *Chem. Commun.*, 5582-5583.

HOU, J., ZHANG, Z. & MADSEN, L.A. (2011). Cation/anion associations in ionic liquids modulated by hydration and ionic medium. *J. Phys. Chem. B* **115**, 4576-4582.

HUNT, P.A., KIRCHNER, B. & WELTON, T. (2006). Characterizing the electronic structure of ionic liquids: An examination of the 1-butyl-3-methylimidazolium chloride ion pair. *Chem. Eur. J.* **12**, 6762-6775.

HWANG, W., HAM, M.H., SOHN, B.H., HUH, J., KANG, Y.S., JEONG, W., MYOUNG, J. & PARK, C. (2005). Micropatterning of block copolymer micelle thin films using solvent capillary contact printing. *Nanotechnology* **16**, 2897-2902.

JACKSON, C.L., CHANZY, H.D., BOY, F.P., DRAKE, B.J., TOMALIA, D.A., BAUER, B.J. & AMIS, E.J. (1998). Visualization of dendrimer molecules by transmission electron microscopy (TEM): Staining methods and cryo-TEM of vitrified Solutions. *Macromolecules* **31**, 6259-6265.

KUWABATA, S., TSUDA, T. & TORIMOTO, T. (2010). Room-temperature ionic liquid. A new medium for material production and analyses under vacuum conditions. *J. Phys. Chem. Lett.* **1**, 3177-3188.

LEE, H.-N., NEWELL, N., BAI, Z. & LODGE, T.P. (2012). Unusual lower critical solution phase behavior of poly(ethylene oxide) in ionic liquids *Macromolecules* **45**, 3627- 3633.

LI, Z., KESSELMANN, E., TALMON, Y., HILLMYER, M.A. & LODGE, T. (2004). Multicompartment micelles from ABC miktoarm stars in water. *Science* **306**, 98-101.

LUDWIG, K., YAN, S., FAN, H., REUTER, W. & BÖTTCHER, C. (2003). The 3D structure of rat DPPIV/CD26 as obtained by cryoTEM and single particle analysis. *Biophys. Res. Commun.* **304**, 73-77.

LUTZ, J.-F. & LASCHEWSKY, A. (2005). Multicompartment micelles: Has the long-standing dream become a reality? *Chem. Phys.* **206**, 813-817.

LUTZ, J.-F., GEFFROY, S., VON BERLEPSCH, H., BÖTTCHER, C., GARNIER, S. & LASCHEWSKY, A. (2007). Investigation of a dual set of driving forces (hydrophobic + electrostatic) for the two-step fabrication of defined block copolymer micelles. *Soft Matter* **3**, 694-698.

MA, J.C. & Dougherty, D.A. (1997). The cation- $\pi$  interaction. *Chem. Rev.* **97**, 1303-1324.

MANSFELD, U., HOEPPENER, S. & SCHUBERT, U.S. (2013). Investigating the motion of diblock copolymer assemblies in ionic liquids by in situ electron microscopy. *Adv. Mater.* **25**, 761-765.

MICHLER, G.H. (2008) Contrast enhancement. In *Electron Microscopy of Polymers*, Michler, G.H. (Ed.), pp. 243-259, Springer Berlin Heidelberg.

O'REILLY, R.K., JORALEMON, M.J., HAWKER, C.J. & WOOLEY, K.L. (2006). Facile syntheses of surface-functionalized micelles and shell cross-linked nanoparticles. *J. Polym. Sci., Part A.: Polym. Chem.* **44**, 5203-5217.

OSS-RONEN, L., SCHMIDT, J., ABETZ, V., RADULESCU, A., COHEN, Y. & TALMON, Y. (2012). Characterization of block copolymer self-assembly: From solution to nanoporous membranes. *Macromolecules* **45**, 9631-9642.

POCHAN, D.J., CHEN, Z., CUI, H., HALES, K., QI, K. & WOOLEY, K.L. (2004). Toroidal triblock copolymer assemblies. *Science* **306**, 94-97.

RIESS, G. (2003). Micellization of block copolymers. *Prog. Polym. Sci.* **28**, 1107-1170.

SIMONE, P. & LODGE, T.P. (2007). Micellization of PS-PMMA diblock copolymers in an ionic liquid. *Macromol. Chem. Phys.* **208**, 339-348.

UEKI, T. & WATANABE, M. (2008). Macromolecules in ionic liquids: Progress, challenges, and opportunities. *Macromolecules* **41**, 3739-3749.

- UEKI, T. & WATANABE, M. (2012). Polymers in ionic liquids: Dawn of neoteric solvents and innovative materials. *Bull. Chem. Soc. Jap.* **85**, 33-50.
- WANG, X., GUERIN, G., WANG, H., WANG, Y., MANNERS, I. & WINNIK, M.A. (2007). Cylindrical block copolymer micelles and co-micelles of controlled length and architecture. *Science* **317**, 644-647.
- WINTERTON, N.J. (2006). Solubilization of polymers by ionic liquids. *J. Mater. Chem.* **16**, 4281-4293.
- WITTEMANN, A., DRECHSLER, M., TALMON, Y. & BALLAUF, M. (2005). High elongation of polyelectrolyte chains in the osmotic limit of spherical polyelectrolyte brushes: a study by cryogenic transmission electron microscopy. *J. Am. Chem. Soc.* **127**, 9688-9689.
- WON, Y.-Y., BRANNAN, A.K., DAVIS, H.T. & BATES, F.S. (2002). Cryogenic transmission electron microscopy (cryoTEM) of micelles and vesicles formed in water by poly(ethylene oxide)-based block copolymer. *J. Phys. Chem. B* **106**, 3354-3364.
- XU, W., WINNIK, M.A., HALLETT, F.R., RIESS, G. & CROUCHER, M.D. (1991). Light-scattering study of the association behavior of styrene-ethylene oxide block copolymers in aqueous solution. *Macromolecules* **24**, 87-93.
- ZHEN, Y., WON, Y.-Y., BATES, F.S., DAVIS, H.T., SCRIVEN, L.E. & TALMON, Y. (1999). Directly resolved core-corona structure of block copolymer micelles by cryo-transmission electron microscopy. *J. Phys. Chem. B* **103**, 10331-10334.
- ZHULINA, E.B. & BORISOV, O.V. (2012). Theory of block polymer micelles: Recent advances and current challenges. *Macromolecules* **45**, 4429-4440.

## Figure Legends

**Figure 1:** Schematic representation of the chemical structure of the block copolymer system PS-*b*-PMMA (a), and chemical composition of the ionic liquid BMIM-PF<sub>6</sub> (b), which is used as selective solvent to prepare micellar systems (c).

**Figure 2:** a,b) Transmission electron micrograph of self-assembled PS-*b*-PMMA block copolymer micelles in the hydrophobic ionic liquid 1-butyl-3-methylimidazolium hexafluorophosphate recorded under cryogenic conditions. c) Histogram of the core diameter.

**Figure 3:** a,b) Transmission electron micrographs of self-assembled PS-*b*-PMMA block copolymer micelles after the removal of the hydrophobic ionic liquid 1-butyl-3-methylimidazolium hexafluorophosphate with acetonitrile recorded at room temperature conditions. c) Histogram of the micelle diameters.

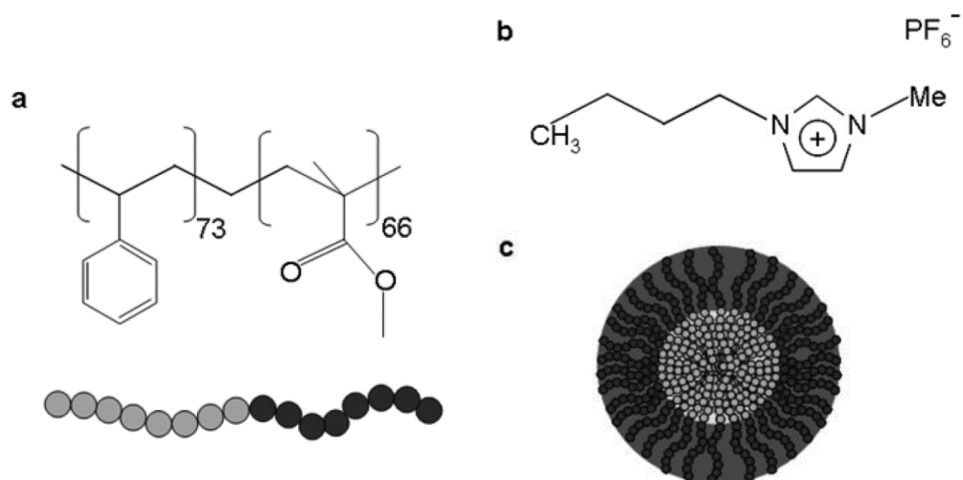
**Figure 4:** Beside the movement of the individual block copolymer nanostructures (indicated by the trajectories highlights in yellow and see MOVIE ( a), an expansion of the corona is observed (b). c-e) Series of images acquired during the expansion process. The initially compact corona starts to continuously open up. This is associated with a decrease of the contrast.

**Figure 5:** Cryo-TEM images (a to c) showing the heterogenic melting evolution of a neat EMIm EtOSO<sub>3</sub> film upon electron radiation (scale bar 200 nm).

**Figure 6:** Cryo-TEM images of PS-*b*-P2VP in BMIM-TfO (a) show contrast for the corona after electron irradiation (b). The already visible corona of PS-*b*-P2VP in EMIm-EtOSO<sub>3</sub> in cryo-TEM (c) was confirmed after electron irradiation (d) (scale bar: 200 nm).

## Figures

### Figure 1



### Figure 2

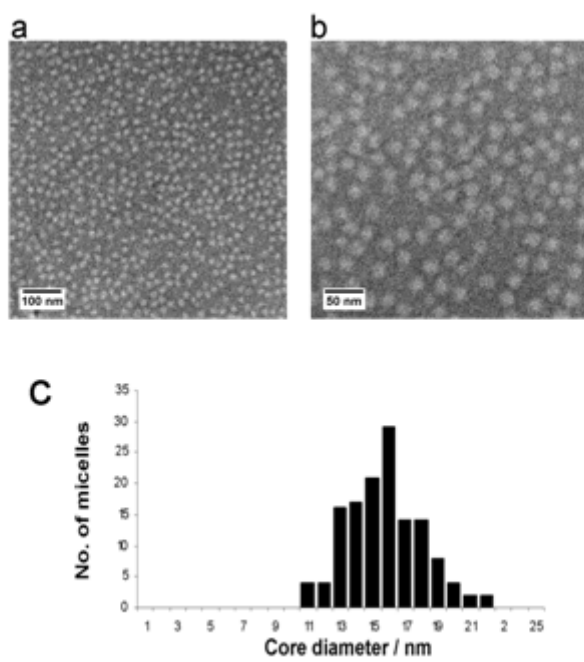




Figure 3

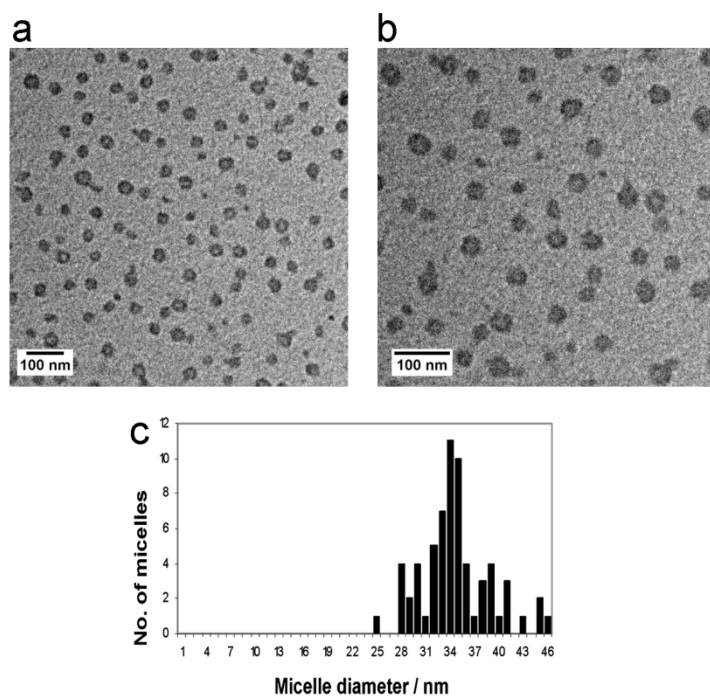
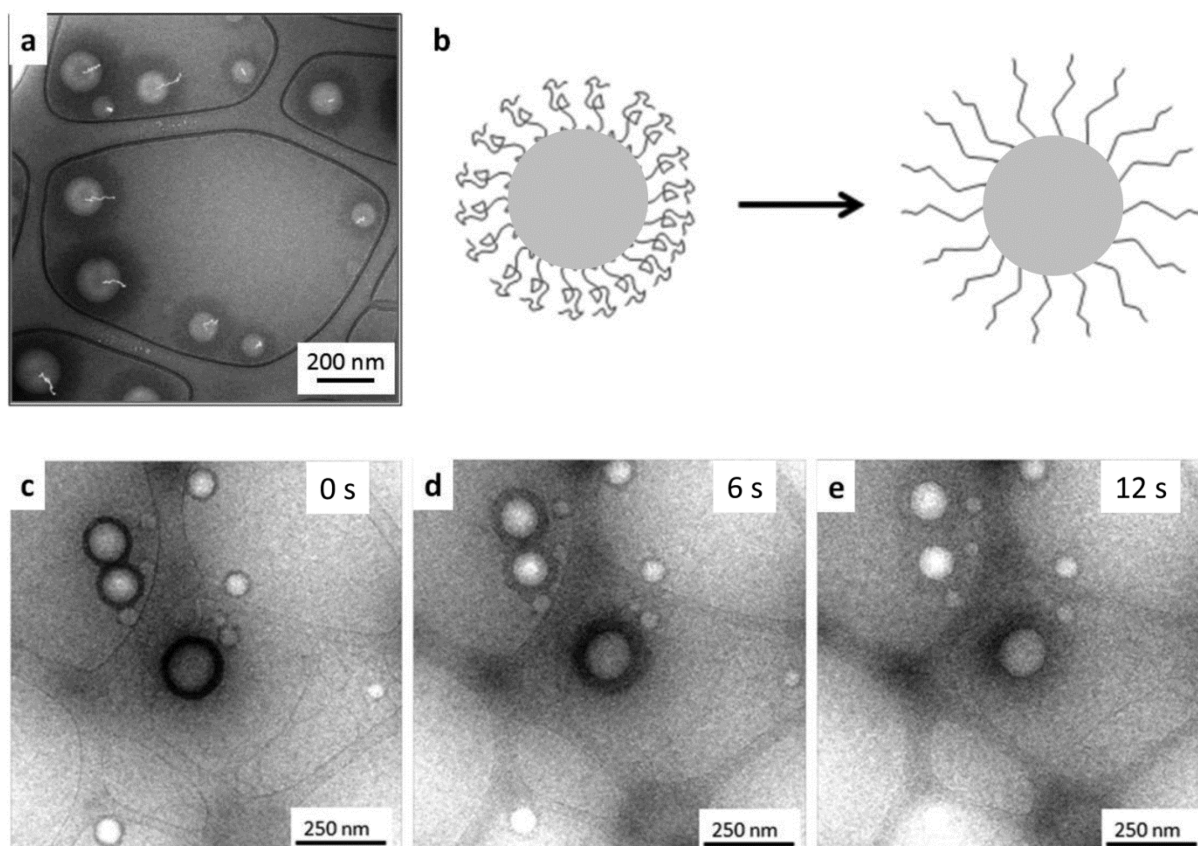
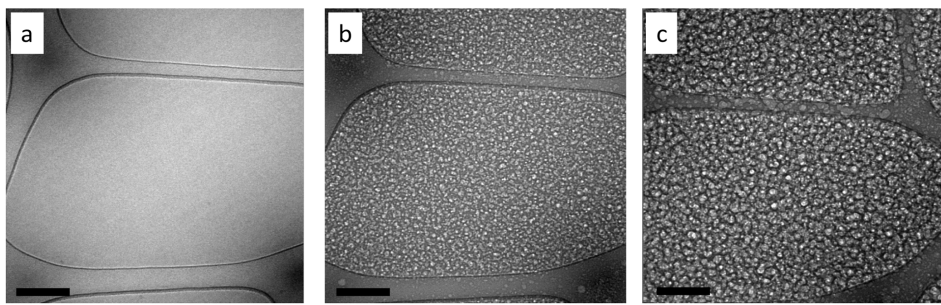


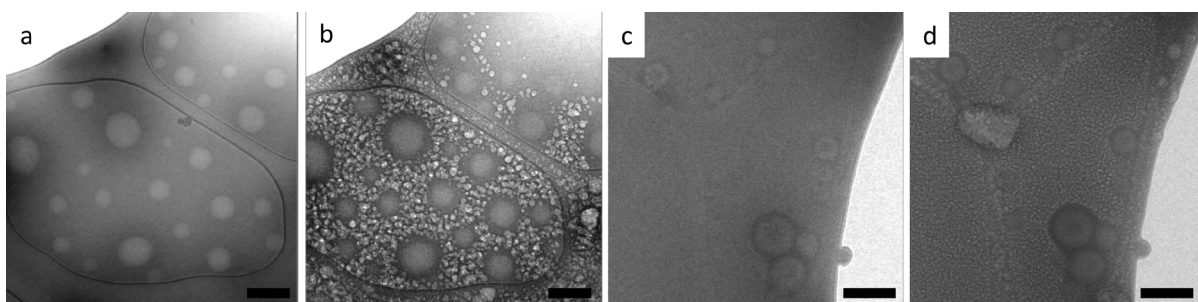
Figure 4



**Figure 5**



**Figure 6**



**Movie Title**

Dynamic investigation of micelles in the IL

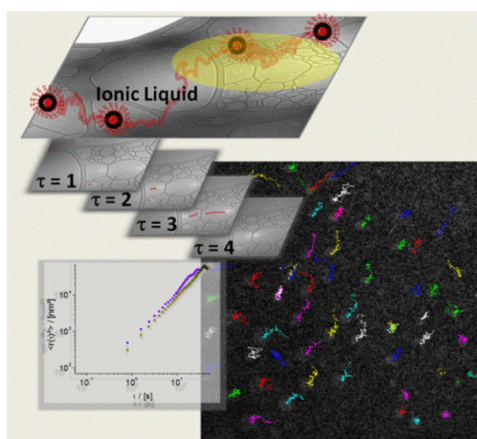


## Publication P7

*Investigating the motion of diblock copolymer assemblies in ionic liquids by in-situ electron microscopy*

U. Mansfeld, S. Hoepfner and U. S. Schubert

*Adv. Mater.* **2013**, 25, 761-765



Reprinted with permission of John Wiley and Sons.

Copyright © 2012 Wiley Periodicals, Inc.



# Investigating the Motion of Diblock Copolymer Assemblies in Ionic Liquids by In Situ Electron Microscopy

Ulrich Mansfeld, Stephanie Hoepfener,\* and Ulrich S. Schubert

The movement of individual supramolecular aggregates and nanoparticles and their behavior in liquids represents a key question in many biological and technological processes. Drug-delivery processes, among many others, rely on conformational changes and transport kinetics, which are generally only observable by techniques that investigate a large number of objects at the same time. Thus, the desire for a direct, high-resolution observation technique (i.e., transmission electron microscopy in liquid environments) is evident. Here we introduce a study that utilizes free-standing thin films of ionic liquids as a fluid support medium for investigating the motion of individual supramolecular assemblies of diblock copolymers. The high-resolution tracking of particle trajectories at different temperatures allows the analysis of their motional characteristics and represents the first direct observation of individual moving supramolecular assemblies with nanometer resolution.

Dynamic processes on the nanometer scale are important phenomena in liquids and fluids. Examples include processes in biological systems,<sup>[1,2]</sup> transport phenomena for drug delivery,<sup>[3]</sup> and the assembly of natural and synthetic molecules into supramolecular structures,<sup>[4,5]</sup> among others. The investigation of these processes in liquids is restricted by a number of experimental difficulties, which makes a direct observation of the dynamics on the level of individual nano-objects challenging. Most studies apply NMR spectroscopy<sup>[6]</sup> and scattering techniques (i.e., static and dynamic light scattering, small- and wide-angle X-ray scattering and small-angle neutron scattering). However, these techniques only provide average information concerning a large number of structures and, thus, allow only statistical insights into dynamic processes of nano-objects. Here, we introduce an approach that permits the high-resolution investigation of individual nanoparticles moving within an ionic liquid (IL) to demonstrate the capability of following the motion of individual supramolecular aggregates of diblock copolymers. It will be demonstrated that supramolecular

aggregates perform motional processes in the ionic liquid at different temperatures and single-particle tracking will be used to identify the nature of the movement. This study represents to the best of our knowledge the first in situ observation of moving copolymer nano-objects in solution. It may potentially open new avenues for the investigation of dynamic processes with high resolution and the visualization of structural changes on the level of supramolecular assemblies. While common imaging techniques, such as transmission electron microscopy (TEM), provide access to information on individual nanostructures, preparations are involved that prohibit a direct investigation of the systems in their liquid environment. As a consequence, the systems are affected by the presence of surfaces and/or drying effects, which limit the possibilities for unperturbed investigations of dynamic processes with high spatial resolution. Recently, tailor-made TEM liquid cells were employed to provide a sealed environment for liquid samples to circumvent these limitations.<sup>[7]</sup> Generally, cryo-TEM is presently regarded as the method of choice to investigate individual systems in a solution-like state. However, the required vitrification of the solution makes an investigation of dynamic processes impossible: images represent only 'snapshots' of the state of the liquid sample in the moment of vitrification. These restrictions, which are mainly based on the requirement of ultrahigh vacuum (UHV) conditions for TEM operation, represent one of the major limitations on the high-resolution investigation of dynamics of individual nanostructures.

In the present study, we propose an approach to overcome most of the restrictions described above by the utilization of ionic liquids (IL) as alternative solvents. These solvents represent promising liquid media, due to their high electrochemical stability, their electroconductivity, and, in particular, their negligible vapor pressure, which makes them compatible with UHV conditions.<sup>[8]</sup> Ionic liquids consist of ions and are, by definition, liquid below 100 °C; many of them being liquid already at room temperature.<sup>[9]</sup> They can be utilized, among other applications,<sup>[10–12]</sup> as selective solvents for copolymer systems, and the formation of micelles and vesicles was observed in various ionic liquids.<sup>[13,14]</sup> Pioneering work concerning this issue was conducted by Lodge and co-workers who investigated micellar and vesicular systems in ionic liquids under cryo-TEM conditions.<sup>[15]</sup> However, up to now, the investigation of motional processes of such systems has not been reported.

In the present contribution, we describe a series of experiments that demonstrate the capability of TEM of investigating the motion of individual nanosized supramolecular aggregates in ionic liquids. For this purpose, supramolecular assemblies consisting of polystyrene (PS) diblock copolymers with poly(2-vinyl pyridine) (P2VP) or poly(ethylene oxide) (PEO) as soluble blocks were prepared in selective ionic liquids, such

U. Mansfeld, Dr. S. Hoepfener, Prof. U. S. Schubert  
Laboratory of Organic and Macromolecular Chemistry  
(IOMC)

Humboldtstr. 10, 07743 Jena, Germany  
E-mail: s.hoepfener@uni-jena.de

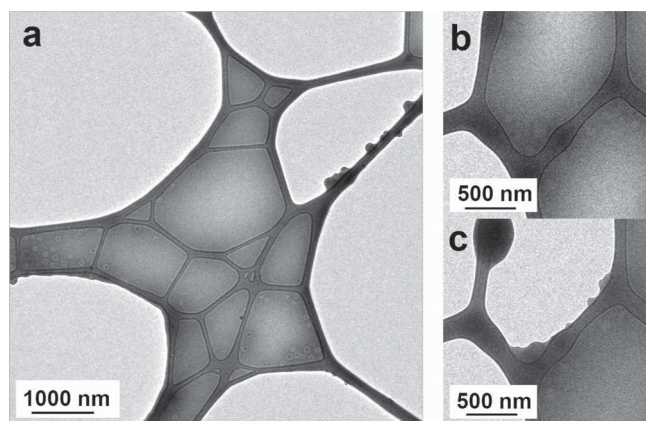
Dr. S. Hoepfener, Prof. U. S. Schubert  
Jena Center for Soft Matter (JCSM)

Humboldtstr. 10, 07743 Jena, Germany

U. Mansfeld, Prof. U. S. Schubert  
Dutch Polymer Institute, 5612 AX Eindhoven  
The Netherlands



DOI: 10.1002/adma.201203423

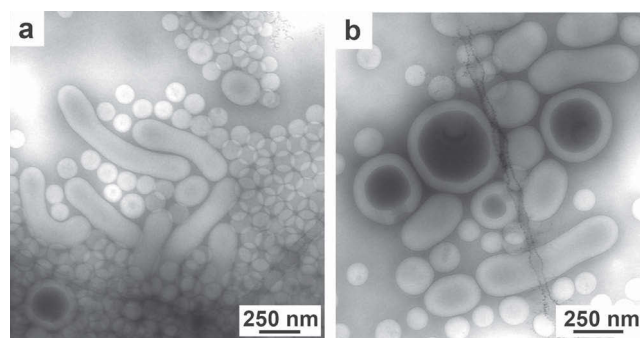


**Figure 1.** a) Free-standing ionic liquid films of [EMIm][EtOSO<sub>3</sub>] on a lacey carbon coated copper grid. b,c) Film bursting and drop formation during electron-beam irradiation points to the liquid state of the ionic liquid in the film (see Supporting Information, Movie SI-1).

as 1-ethyl-3-methylimidazolium ethylsulfate [EMIm][EtOSO<sub>3</sub>] or 1-butyl-3-methyl-imidazolium tetrafluoroborate [BMIm][BF<sub>4</sub>] by the co-solvent method.<sup>[15]</sup>

Ionic liquids can form, due to their characteristic surface tension,<sup>[9]</sup> stable free-standing films over different length scales.<sup>[16]</sup> In TEM in particular, the film thickness is seen as a limiting factor with respect to the obtainable resolution of the imaging process.<sup>[7]</sup> Thus, sufficiently thin films must be prepared, and preferentially no continuous support materials should be required. The most straightforward approach for the formation of free-standing liquid films is their preparation onto lacey carbon grids, which provide open-hole structures with typical dimensions of 200 nm up to micrometers. Free-standing IL films can be prepared by a standard blotting process, whereby the blotting times are in the range of tens of seconds, strongly depending also on the viscosity of the IL. Depending on the open spaces, different film thicknesses can be obtained. **Figure 1a** shows an example of the homogeneous thin films that can be generated. These films span the net-like structures of the lacey carbon support and are found to be stable under common TEM irradiation conditions. The liquid character becomes evident at sufficiently high electron doses and temperatures which make some films – in particular those films formed in large holes – burst. This bursting is a fast process, and drops of the IL are subsequently attached to the lacey carbon support (**Figure 1b,c**; Supporting Information, Movie SI-1). In general, the liquid character of the IL does not impair the quality of the UHV of the TEM; therefore measurements could be conducted over time scales as long as several hours – some samples were even kept in the UHV environment overnight.

With these free-standing IL films, a suitable liquid media is at hand to investigate the supramolecular structure of block copolymers in an ionic liquid. **Figure 2** shows illustrative examples of vesicles and worm-like assemblies of P2VP<sub>350k</sub>-*b*-PS<sub>440k</sub> in [EMIm][EtOSO<sub>3</sub>]. The systems can be well resolved by TEM and a good contrast can be achieved. This is mainly due to the composition of the ionic liquids, containing anions with a high electron density (e.g., I<sup>-</sup>, PF<sub>6</sub><sup>-</sup> and EtOSO<sub>3</sub><sup>-</sup>).<sup>[15]</sup> This intrinsic negative staining represents an advantage compared with



**Figure 2.** High-resolution TEM images of assemblies of PS<sub>440k</sub>-*b*-P2VP<sub>350k</sub> in [EMIm][EtOSO<sub>3</sub>].

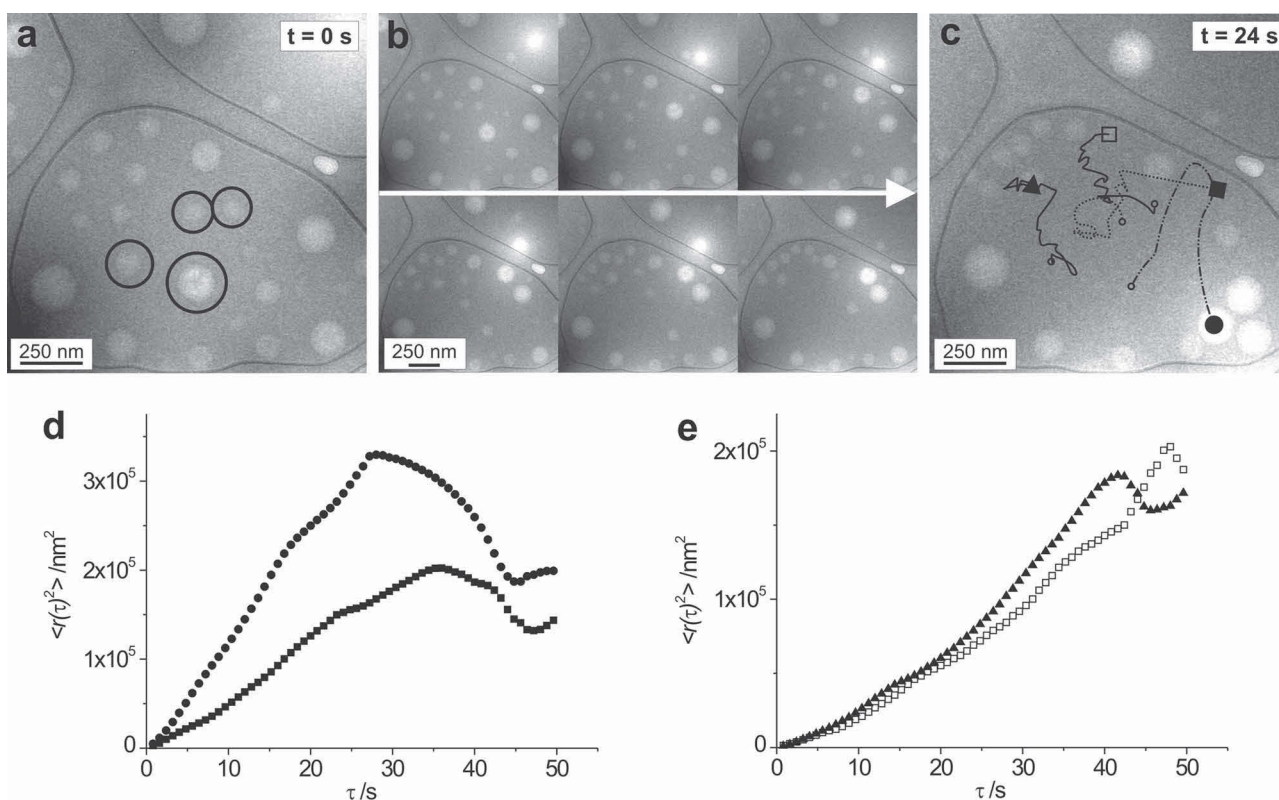
classical cryo-TEM investigations, where, mostly, a rather poor contrast is generated due to the presence of the vitrified ice film. The stability of the free-standing film is another issue where ionic liquids provide improved performance, as the polymer assemblies can be imaged at relative high electron doses or a large number of imaging processes can be applied with minor beam damage of the structures in comparison with cryo-TEM.

For the visualization of the motion of supramolecular nanostructures in ILs, relatively low electron doses had to be applied, as it was observed that high electron doses can result in an inhibition of the particle movement. At sufficiently low electron doses, particle movement could be followed over an image sequence of up to 140 measurements (Supporting Information, Movie SI-4). The motion of the individual supramolecular assemblies depends on the viscosity of the ILs. Thus, heating the samples within a temperature range of 20 to 92 °C allowed the variation of the velocity of the movement of individual nanoparticles.

**Figure 3** summarizes a sequence of images that were acquired with a recording time of 800 ms per frame, showing the movement of PS<sub>440k</sub>-*b*-P2VP<sub>350k</sub> assemblies in [EMIm][EtOSO<sub>3</sub>] at 92 °C. The continuously recorded sequence of TEM images depicts the movement of individual particles along different pathways within the free-standing IL films (Supporting Information, Movie SI-2).

The encircled vesicles show movement in independent directions and exhibit different velocities. The displacement of the supramolecular assemblies can be analyzed by mean-square-displacement (MSD) calculations, which resemble the characteristic features of the particle movement. The corresponding MSD plots (**Figure 3 d,e**) reflect the non-continuous motion of the square-labeled aggregate (■) and, in particular, of the circle-labeled particle (●), which at some stage performs a large directed displacement, represented by the deviation of the slope. In contrast, the two other curves (□, ▲) resemble a more-linear relationship of the MSD values along the time intervals. The characteristic shape of these plots suggests a partially confined random-walk model for the particle movement. The coexistence of all of these movements in a small sample area points to individual movements of the nano-objects within the IL film, rather than an entirely passive motion due to the movement (e.g., convective flow) of the IL film. In general, different driving forces can result in





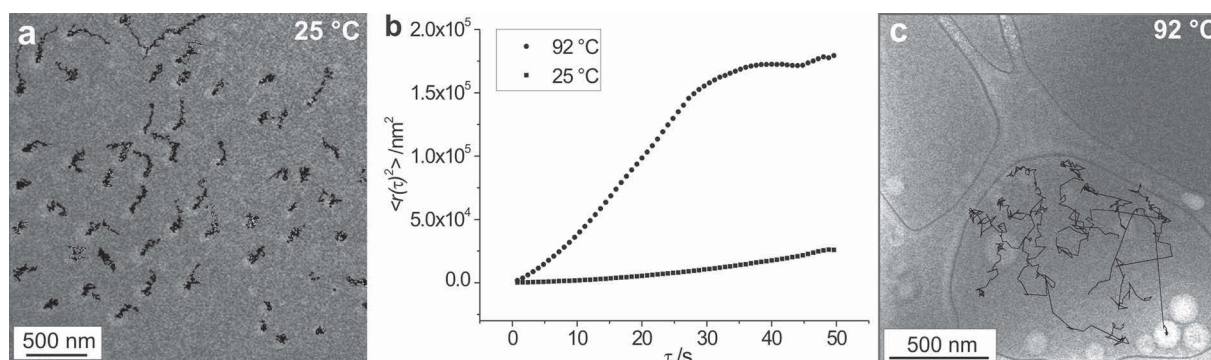
**Figure 3.** Image sequence of PS<sub>440k</sub>-*b*-P2VP<sub>350k</sub> vesicles in [EMIm][EtOSO<sub>3</sub>] at 92 °C showing different dynamic pathways: a) the initial positions of the encircled vesicles, b) an image sequence in the interim, and c) the later position of the encircled vesicles and the related individual trajectories within 24 s. (For detailed movies see Supporting Information, SI-2). d,e) The motion is analyzed by mean-square-displacement (MSD) calculations.

various kinds of motion: i) convection (Supporting Information, Movie SI-3), ii) Brownian motion and diffusion (Supporting Information, Movie SI-4) and iii) oscillation (Supporting Information, Movie SI-5).

**Figure 4** depicts the analysis of a series of images where the motion of a number of individual vesicles is displayed. Due to the characteristic viscosity of the IL at different temperatures, the motion of the particles appears to be temperature-dependent. Thus, the motion of PS<sub>440k</sub>-*b*-P2VP<sub>350k</sub> assemblies in [EMIm][EtOSO<sub>3</sub>] was investigated at two different temperatures by means of MSD analysis (Figure 4). The corresponding individual particle traces are depicted in Figure 4a,c. At a temperature of 92 °C the linear increase of the MSD by time is larger compared with that at 25 °C; hence, a faster diffusion of the supramolecular aggregates is observed. At longer time intervals the MSD plot shows a depletion of the slope (Figure 4b). This behavior is characteristic for a confined random-walk behavior of the aggregates and might be influenced by the film dimensions, adhesion of the particles to the bars of the lacey carbon, additional charging effects, and/or by interactions with other particles. At 25 °C, the linear dependence of the MSD over time corresponds to a preferential Brownian motion of the aggregates. However, with increasing time, an increase in the diffusion coefficient is observed, which might be a result of the heating of the IL under the influence of the electron beam.

Since the chosen diblock copolymers contain a PS block, the assemblies appear to be very stable and no deformation of moving objects, no changes in their structure and no fission or fusion processes could be observed. Instead, the objects seem to represent kinetically trapped, non-equilibrium structures as depicted in Figure 2.<sup>[17,18]</sup> This is assumed to be caused by the rigidity of the PS blocks of the utilized copolymer systems, which are in a glassy state below a temperature of 100 °C. It is expected that transition states might be observed for systems containing more-flexible block structures or by applying higher temperatures in future experiments.

These illustrative examples, derived from initial experiments, allow the conclusion that the utilization of ionic liquids for the investigation of supramolecular assemblies or other nano-objects (i.e., nanoparticles), in free-standing liquid support films offers new possibilities in elucidating the motion of individual objects in a liquid environment on the nanometer scale. The range of specimen systems benefits from the versatile properties of ionic liquids that can be designed by an appropriate cation-anion combination. Moreover, the possibility of adjusting the temperature of the solution in situ offers attractive possibilities for studies on temperature-triggered events on the level of individual nanostructures and to adjust the diffusion velocity of the objects. However, fundamental studies on the influence of the IL on the dynamic behavior of the system, as well as effects that might be attributed to



**Figure 4.** Temperature-dependent analysis of the motion of PS<sub>440k</sub>-*b*-P2VP<sub>350k</sub> vesicles in [EMIm][EtOSO<sub>3</sub>] by means of the mean-square displacement (MSD): a) the tracking lines of particle motion at 25 °C; b) the averaged MSD at the different temperatures (25 °C bottom curve, 92 °C top curve), revealing a significant increase in diffusion of the particles at the higher temperature; c) the tracking lines of particle motion at 92 °C.

electron-beam interactions, have to be conducted in follow-up experiments.

The introduced method could thus be a valuable addition to existing investigation tools, since it potentially offers temperature- and time-dependent studies on dynamic systems on the nanometer scale. In particular, the dynamics of supramolecular assemblies under solution-like conditions might be elucidated, such as phase transitions of thermoresponsive copolymers<sup>[19,20]</sup> and membrane fusion and fission processes (e.g., of polymerosomes<sup>[21]</sup> or liposomes,<sup>[22,23]</sup> among others).

## Experimental Section

**Materials:** 1-Ethyl-3-methylimidazolium ethyl sulfate (99%) and 1-butyl-3-methylimidazolium tetrafluoroborate (99%) were purchased from Iolitec and were used without further purification. Poly(styrene-*block*-(2-vinyl pyridine)) ( $M_n$  (kg mol<sup>-1</sup>) = PS<sub>440</sub>-*b*-P2VP<sub>353</sub>), polydispersity index (PDI) = 1.19) was purchased from Polymer Source. Poly(styrene-*block*-(ethylene oxide)) ( $M_n$  (kg mol<sup>-1</sup>) = PS<sub>100</sub>-*b*-PEO<sub>34</sub>) was synthesized following standard procedures. The lacey carbon coated TEM copper grids (Mesh 400) were purchased from Agar Scientific and were plasma-cleaned prior to use, for 1 minute. The TEM samples were examined using a Phillips CM-120 transmission electron microscope, operated at 80 and 120 kV. Specimens were investigated using a sample holder (Gatan 626-DH) at 20 °C up to 92 °C. The images were recorded with a bottom-mounted 1000 × 1000 pixel charge-coupled-device (CCD) camera from TVIPS.

**General Preparation of Polymeric Assemblies in Ionic Liquids:** To prepare a stock solution, the polymer (10 mg) was dissolved in dichloromethane (400 μL). The ionic liquid (40 μL) was slowly added into the diluted solution (20 μL of polymer solution and 100 μL dichloromethane) and the dichloromethane was subsequently evaporated at 60 °C while flushing the sample with air.

**Preparation of the Free-Standing Liquid Films:** A small droplet of the ionic liquid solution was placed at ambient conditions onto a lacey carbon coated TEM grid that was subsequently blotted with a filter paper on both sides for several seconds. The remaining traces of the co-solvent were removed during the sample-transfer process to the TEM in the prevacuum pumping cycle.

**Imaging Conditions:** For the movie image sequences with a spatial resolution of 800 ms (300 ms acquisition time and 500 ms read-out time), up to 450 ms (300 ms acquisition time and 150 ms read-out time) were recorded.

**Movies of the Motional Processes:** Selected movies of particle movement are available in the Supporting Information.

## Supporting Information

Supporting Information is available from the Wiley Online Library or from the author.

## Acknowledgements

This work was carried out in the framework of the Dutch Polymer Institute (DPI project #620, technology area HTE) and the BMBF project "Photonische Nanomaterialien (PhoNa)". Prof. D. Schubert is gratefully acknowledged for suggestions and discussion. We thank Dr. C. Höppener for valuable input on the single-particle analysis. Dr. F. Steiniger (Electron Microscopy Center, University of Jena) is kindly acknowledged for technical support.

Received: August 17, 2012  
Published online: November 9, 2012

- [1] K. Lippincott-Schwartz, E. Snapp, A. Kenworthy, *Nat. Rev. Mol. Cell Biol.* **2001**, 2, 444.
- [2] P. Mereghetti, D. Kokh, J. A. McCammon, R. Wade, *BMC Biophys.* **2011**, 4, 2.
- [3] K. Sugano, M. Kansy, P. Artursson, A. Avdeef, S. Vendels, L. Di, G. F. Ecker, B. Faller, H. Fischer, G. Gerebtzoff, H. Lennernaes, F. Senner, *Nat. Rev. Drug Discovery* **2010**, 9, 597.
- [4] C. Bohne, *Langmuir* **2006**, 22, 9100.
- [5] H. W. Spiess, *Macromolecules* **2010**, 43, 5479.
- [6] J. R. Bothe, E. N. Nikolova, C. D. Eichhorn, J. Chugh, A. L. Hansen, H. M. Al-Hashimi, *Nat. Methods* **2011**, 8, 919.
- [7] N. de Jonge, F. M. Ross, *Nat. Nanotechnol.* **2011**, 6, 695.
- [8] S. Kuwabata, T. Tsuda, T. Torimoto, *J. Phys. Chem. Lett.* **2010**, 1, 3177.
- [9] H. Weingärtner, *Angew. Chem. Int. Ed.* **2008**, 47, 654.
- [10] T. P. Lodge, *Science* **2008**, 321, 50.
- [11] T. Torimoto, T. Tsuda, K. Okazaki, S. Kuwabata, *Adv. Mater.* **2010**, 22, 1196.
- [12] K. Ueno, M. Watanabe, *Langmuir* **2011**, 27, 9105.
- [13] T. Ueki, M. Watanabe, *Macromolecules* **2008**, 41, 3739.
- [14] H.-N. Lee, T. P. Lodge, *J. Phys. Chem. B* **2011**, 115, 1971.
- [15] Y. He, Z. Li, *J. Am. Chem. Soc.* **2006**, 128, 2745.
- [16] S. Chen, K. Kobayashi, R. Kitaura, Y. Miyata, H. Shinohara, *ACS Nano* **2011**, 5, 4902.

- [17] P. M. Simone, T. P. Lodge, *Macromol. Chem. Phys.* **2007**, *208*, 339.
- [18] K. T. Kim, J. Zhu, S. A. Meeuwissen, J. J. L. M. Cornelissen, D. J. Pochan, R. J. M. Nolte, J. C. M. van Hest, *J. Am. Chem. Soc.* **2010**, *132*, 12522.
- [19] K. Kodama, R. Tsuda, K. Niitsuma, T. Tamura, T. Ueka, H. Kukubo, M. Watanabe, *Polym. J.* **2011**, *43*, 242.
- [20] H.-N. Lee, Z. Bai, N. Newell, T. P. Lodge, *Macromolecules* **2010**, *43*, 9522.
- [21] D. E. Discher, A. Eisenberg, *Science* **2002**, *297*, 967.
- [22] T. L. Greaves, C. J. Drummond, *Chem. Soc. Rev.* **2008**, *37*, 1709.
- [23] F. Gayet, J.-D. Marty, A. Brûlet, N. L. Viguier, *Langmuir* **2011**, *27*, 9706.
-



Copyright WILEY-VCH Verlag GmbH & Co. KGaA, 69469 Weinheim, Germany, 2012.

# ADVANCED MATERIALS

## Supporting Information

for *Adv. Mater.*, DOI: 10.1002/adma.201203423

Investigating the Motion of Diblock Copolymer Assemblies in  
Ionic Liquids by In Situ Electron Microscopy

*Ulrich Mansfeld, Stephanie Hoepfener,\* and Ulrich S.  
Schubert*

DOI: 10.1002/adma.((201203423))

**Investigating the Motion of Diblock Copolymer Assemblies in Ionic Liquids by In-situ Electron Microscopy**

By *Ulrich Mansfeld, Stephanie Hoepfener\** and *Ulrich S. Schubert*

[\*] U. Mansfeld, Dr. S. Hoepfener (Corresponding-Author), Prof. U.S. Schubert  
Laboratory of Organic and Macromolecular Chemistry (IOMC)  
Humboldtstr. 10, 07743 Jena, Germany  
e-mail: s.hoepfene@uni-jena.de  
Dr. S. Hoepfener, Prof. Ulrich S. Schubert  
Jena Center for Soft Matter (JCSM)  
Humboldtstr. 10, 07743 Jena, Germany  
U. Mansfeld, Prof. Ulrich S. Schubert  
Dutch Polymer Institute  
5612 AX Eindhoven, The Netherlands

## **Supporting Information**

**Movies of the motional processes**

Selected movies of particle movement showing:

- Free-standing ionic liquid films on lacey carbon grids.
- Motion of diblock copolymer micelles in ionic liquid films.
- Convection driven movement of micelles.
- Mobility of the ionic liquids with higher time resolution.
- Rapid oscillation of vesicles in a liquid support film.

The recording conditions are given in the SI-Figure captions. The speed of the movies was increased to a frame rate of 7 images/sec to minimize the file size.

This material is available free of charge at:

[http://www.schubert-group.de/index.php?option=com\\_content&view=article&id=118](http://www.schubert-group.de/index.php?option=com_content&view=article&id=118).

Movie files can be viewed in the Internet browser utilizing Adobe Flash Player.

**Movie captions****Movie SI-1**

Free-standing ionic liquid films on lacey carbon grids.

PS<sub>440K</sub>-*b*-P2VP<sub>350K</sub> in [EMIm][EtOSO<sub>3</sub>] Recording duration: t = 51 s with 800 ms/frame (300 ms accumulation, 500 ms read-out); 10 fps frame rate, 120 kV TEM voltage, 92 °C specimen temperature.

**Movie SI-2**

Motion of diblock copolymer micelles in ionic liquid films.

PS<sub>440K</sub>-*b*-P2VP<sub>350K</sub> in [EMIm][EtOSO<sub>3</sub>] Recording duration: t = 32 s with 800 ms/frame (300 ms accumulation, 500 ms read-out); 250 nm scale bar, 10 fps frame rate, 120 kV TEM voltage, 92 °C specimen temperature.



**Movie SI-3**

Convection driven movement of micelles.

PS<sub>440K</sub>-*b*-P2VP<sub>350K</sub> in [EMIm][EtOSO<sub>3</sub>] Recording duration: t = 51 s with 800 ms/frame (300 ms accumulation, 500 ms read-out); 250 nm scale bar, 20 fps frame rate, 120 kV TEM voltage, 92 °C specimen temperature.

**Movie SI-4**

Mobility of the ionic liquids with higher time resolution.

PS<sub>440K</sub>-*b*-P2VP<sub>350K</sub> in [EMIm][EtOSO<sub>3</sub>] Recording duration: t = 60 s with 450 ms/frame (300 ms accumulation, 150 ms read-out); 250 nm scale bar, 8 fps frame rate, 120 kV TEM voltage, 92 °C specimen temperature.

**Movie SI-5**

Rapid oscillation of vesicles in a liquid support film.

PS<sub>100K</sub>-*b*-PEO<sub>34K</sub> in [BMIm][BF<sub>4</sub>] Recording duration: t = 51 s with 800 ms/frame (300 ms accumulation, 500 ms read-out); 250 nm scale bar, 20 fps frame rate, 80 kV TEM voltage, 92 °C specimen temperature.